



HAL
open science

Selective arene and polyarene hydrogenation catalysed by ruthenium nanoparticles

Emma Bresó-Femenia

► **To cite this version:**

Emma Bresó-Femenia. Selective arene and polyarene hydrogenation catalysed by ruthenium nanoparticles. Other. INSA de Toulouse; Universitat Rovira i Virgili (Tarragona, Espana), 2015. English. NNT : 2015ISAT0002 . tel-01179583

HAL Id: tel-01179583

<https://theses.hal.science/tel-01179583>

Submitted on 23 Jul 2015

HAL is a multi-disciplinary open access archive for the deposit and dissemination of scientific research documents, whether they are published or not. The documents may come from teaching and research institutions in France or abroad, or from public or private research centers.

L'archive ouverte pluridisciplinaire **HAL**, est destinée au dépôt et à la diffusion de documents scientifiques de niveau recherche, publiés ou non, émanant des établissements d'enseignement et de recherche français ou étrangers, des laboratoires publics ou privés.

EMMA BRESÓ FEMENIA

**SELECTIVE ARENE AND POLYARENE
HYDROGENATION CATALYSED BY
RUTHENIUM NANOPARTICLES**

DOCTORAL THESIS

Supervised by

Prof. Sergio Castellón Miranda and Prof. Bruno Chaudret

Departament de Química Analítica i Química Orgànica

and

Laboratoire de Physique et Chimie des Nano-Objets



UNIVERSITAT ROVIRA I VIRGILI



Tarragona, 2015



Departament de Química Analítica i Química Orgànica
Facultat de Química
C/ Marcel·lí Domingo, s/n
43007, Tarragona

Els sotasignants Sergio Castellón Miranda, Catedràtic d'Universitat, del Departament de Química Analítica i Química Orgànica de la Universitat Rovira i Virgili, i Bruno Chaudret, Director del Laboratoire de Physique et Chimie des Nano-Objets de l'Institut National des Sciences Appliquées de Toulouse.

FEM CONSTAR que aquesta memòria, titulada “*Selective Arene and Polyarene Hydrogenation Catalysed by Ruthenium Nanoparticles*”, que presenta Emma Bresó Femenia, opta al grau de Doctor en Química per la Universitat Rovira i Virgili i per l'Institut National des Sciences Appliquées i ha estat realitzada sota la nostra direcció al Departament de Química Analítica i Química Orgànica de la Universitat Rovira i Virgili i al Laboratoire de Physique et Chimie des Nano-Objets de l'Institut National des Sciences Appliquées, i que compleix els requeriments per poder optar a la Menció Europea.

Tarragona, 18 de Desembre de 2014

Prof. Sergio Castellón Miranda

Prof. Bruno Chaudret

La present memòria de Tesi Doctoral s'ha dut a terme gràcies al *Programa de Formación del Profesorado Universitario (Ayudas FPU)* (referència: AP2010-5152), finançat pel Ministerio de Ciencia e Innovación. La realització d'aquesta Tesi Doctoral ha estat possible gràcies al finançament dels següents projectes d'investigació:

- *Diseño de Catalizadores para una Química Sostenible: Una Aproximación Integrada. Consolider Ingenio 2010 – Proyecto INTECAT (CSD2006-0003).*
- *Glycolipids and carbohydrates. New synthetic methods and biological applications (CTQ2011-22872).*



Consolider Ingenio 2010
CSD2006-0003

Diseño de Catalizadores
para una Química Sostenible:
una Aproximación Integrada





Université
de Toulouse

THÈSE

En vue de l'obtention du
DOCTORAT DE L'UNIVERSITÉ DE TOULOUSE

Délivré par :

Institut National des Sciences Appliquées de Toulouse (INSA Toulouse)

Discipline ou spécialité :

Nanophysique

Présentée et soutenue par :

Emma Bresó Femenia

le : mercredi 21 janvier 2015

Titre :

Selective Arene and Polyarene Hydrogenation Catalysed by Ruthenium
Nanoparticles

Ecole doctorale :

Sciences de la Matière (SDM)

Unité de recherche :

UMR 5215-LPCNO-IRSAMC-Laboratoire de Physique et Chimie des Nano-Objets

Directeur(s) de Thèse :

Sergio Castellón Miranda

Bruno Chaudret

Rapporteurs :

Jairton Dupont

Roberto Sánchez Delgado

Catherine Santini

Membre(s) du jury :

Piet Van Leeuwen

Montserrat Gómez

Catherine Santini

AGRAÏMENTS

Portar a terme aquesta tesi doctoral ha estat un etapa molt bonica i intensa que m'ha donat la oportunitat d'aprendre, de compartir i de treballar amb persones excepcionals. És per això, que volia dedicar unes línies i agrair a tots aquells que heu estat al meu costat durant aquest darrers anys.

En primer lugar me gustaría agradecer al Prof. Sergio Castellón por darme la oportunidad de realizar esta tesis doctoral bajo su dirección. Gracias por tus consejos, por transmitirme tu pasión por la química, por ser siempre tan cercano, por tu empatía y por estar siempre disponible para hablar y ayudarme en todas las situaciones que se han presentado a lo largo de estos años. Je voudrais également remercier mon co-directeur de thèse, Bruno Chaudret, par m'avoir donné la chance de réaliser cette thèse en cotutelle avec l'INSA. Je vous remercie pour vos conseils pendant toutes ces années, votre optimisme, votre charisme et votre sens de l'humour. A les professores Maribel Matheu i Yolanda Díaz i al Dr. Omar Boutureira, gràcies pels vostres consells i comentaris a les reunions de grup i per estar sempre disposats a donar un cop de mà.

Vull agrair a tots els professors de l'àrea de química orgànica i química inorgànica per la seva disposició a ajudar en qualsevol moment, en especial a la Prof. Carmen Claver i al Dr. Cyril Godard, por ayudarme tantísimo a resolver todas mis dudas y por siempre darme tan buenos consejos en relación a las nanopartículas. Te deseo lo mejor Cyril en esta nueva etapa paternal que comienzas. A les secretàries del departament (Avelina, Dúnia, Olga), gràcies per ajudar-me amb els tràmits administratius, als tècnics del departament i a la Raquel d'inorgànica per ser tan summament eficient i ajudar en tot el que pot i més. També vull agrair a totes les persones que treballen en el Servei de Recursos Científics, molt especialment al Ramón, la Rita, la Irene i el Francesc per estar sempre disponibles per ajudar en el que faci falta.

Aquesta tesi en cotutela m'ha permès la oportunitat de realitzar part del projecte a l'INSA a Toulouse. Volia agrair a tots els que va fer que l'estada fos una experiència inoblidable i als que va ajudar a fer-me sentir com a casa en tot moment. I would like to thank all the members of the group, particularly to Vinciane, Benoît, Nikos and Sangeetha for all the help. I want to especially thank Charbel for being the kindest person I have ever met and for his inexhaustible source of smiles. Gracias a Sergio, Eva, Teresa y Félix por no dejarme ni un segundo sola, por las cervecillas y por hacer que los fines de semana pasaran volando. Gracias a Nuria, Miguel, Patri i Tugce por las horas y horas de risas, por el almax y el robbing, por hacerme sentir una más des del primer día y por ser tan buena gente, os merecéis lo mejor.

Durant la tesis he treballat més hores a la Caixa seca i a la sala de reactors que al 328 i és per aquest motiu que volia donar les gràcies als companys d'inorgànica per acollir-me tan bé des del primer dia i fer-me sentir com una més del grup. Gràcies als més veterans, els que ja són doctors (Angélica, Cris S., Mercè, Vero) per donar-me ànims i consells en l'inici, als que esteu en el procés (Alberto, Carlota, Fran, Jèssica M., Nanette, Marc Magre), als que acabeu de començar la tesi (Enrico, Toni, Marc, Maria, Núria), als companys del CTQC (Bianca, Dolores, Mónica, Jordi Colavida, Jorge, Stefano) i els post-docs (Ana, Bernabé, Itziar, Jamin), vull agrair-vos per tots els bons moments que he compartit amb vosaltres i per rebrem sempre amb un somriure. Un agraïment especial a la Jessi, per la seva simpatia desbordant, per estar sempre disponible a petar la xerradeta i per totes les hores de caixa seca compartides. Moltes sort en aquesta nova etapa que comences, segur que brillaràs tan com sempre. I a la Eli, perquè va ser una gran sort coincidir amb tu al màster. Per tenir sempre un somriure i una paraula bonica que t'alegra el dia, per ajudar-me tantíssim durant tots aquests anys i per tenir sempre un momentet per escoltar i fer veure el costat positiu de les coses.

També voldria agrair a la Idoia, pel seu somriure etern i per l'alegria que transmet. Trobo molt a faltar el teu positivisme contagiós i el bon rollo que desprems a cada pas.

Arriba el moment de donar les gràcies als companys del grup, els que han estat diàriament al meu costat durant tots aquests anys. Espero que el agraïments estiguin a l'alçada de gent tan increïble com vosaltres. Com no, el primer al que li he de donar les gràcies és a mi niño, Isidro! Per ser una de les millors persones que he conegut mai, per estar sempre disposat a ajudar-me, per seguir valorando mi frescor decadente, per ensenyar-me les coses i el vocabulari importants per a la vida moderna i per fer-me riure tantíssim a cada instant. Ja fa molts dies que vas decidir volar cap a terres llunyanes però no hi ha dia que tu niña\$ no et trobi a faltar! A la Míriam D., gràcies per la teva alegria, per ser tan autèntica, per estar sempre disposada a ajudar i escoltar i pels mil moments feliços que vam compartir al 328. Com tu em vas escriure fa un parell d'anys a la teva tesis, jo si que ara puc dir que sé segur que ets i seràs una mare fabulosa! A l'Isma, l'insubstituïble, per totes les hores i hores de xerrades, ajuda, consells i confidències, per aixecar-me la moral quan publicàvem a *Racemic Letters*, per fer-me riure tantíssim amb les frases made in Isma i per ser realment una passada de persona. Sé que puc comptar amb tu pel que sigui, espero que tornem a coincidir ben aviat.

Gràcies al Joan, el meu etern company de viatge. Això no hagués estat el mateix sense tu! Ja saps que ets autèntic, que em fas riure cada cop que obres la boca i que em tens aquí per tot el que necessitis. Em sap molt greu que estiguis de picos pardos quan presenti la tesis però sé que estaràs en esperit

(esperit Juanito). Espero que seguim mantenint l'amistat i que em segueixis invitant a xupitos durant molts anys! Molta sort a la recta final nen!

Gràcies al Collado i al Yordi, per ser l'alegria del 329! Sou molt molons i *graciosos* i ho sabeu. Per fer-nos riure tant a tots amb els vostres sorollets, frases, vídeos i imitacions. No oblidaré mai els mesos compartits amb vosaltres. Ara a gaudir de la millor etapa de la tesis! A Macarena, por tu energía desbordante y por tu risa contagiosa. Ya verás como todo irá genial. Ha sido una suerte compartir estos meses contigo en el laboratorio! A l'Adrià, el prefe, ojalá haguessis arribat abans! Perquè ets com jo però en versió varonil, ens hem entès a la perfecció des del primer dia i m'has fet riure com ningú. Gràcies per les teves bromes, per les classes de moto i per haver animat tantíssim el cotarro aquest últims mesos de tesis. A Xochitl, espero que te lles un buen recuerdo de estos meses en Tarragona y ojalá volvamos a coincidir en un futuro.

Agrair també als que, malauradament, hem coincidit menys temps al laboratori. Gràcies Pep, Irene, Xavi, Mariam, Isa, Sebas, Araceli, Otti i Jenny per tota l'ajuda, consells i suport en les diferents etapes d'aquesta tesis. Ha estat una gran sort compartir aquesta experiència al vostre costat.

Finalment a la meva Míriam, la persona amb la que més he compartit tant dins com fora del laboratori. Perquè tot i ser tan diferents, vam encaixar a la perfecció des del primer dia. Gràcies per escoltar els meus rotllos matinals, per donar sempre els millors consells, per saber tranquil·litzar-me en els moments d'estrès, per ser tan bona, sincera i fantàstica, per ser la millor companya de vitrina, de bomba, de zumba i d'aventures. En definitiva, gràcies pel teu suport incondicional durant aquest 3 anys. Per què després de tantes hores juntes, amb una mirada ja ens entenem. Molta sort en l'etapa final miniM, aquí estaré pel que necessitis, que res ni ningú et faci deixar mai de brillar!

Agrair als companys de polímers per tots els moments compartits pels passadissos, esmorzars, sopars i hores de festa. Especialment a la Maryluz por ser la persona más buena i dulce que he conocido. Estoy segura que la vida te devolverá en felicidad toda tu bondad infinita. Al Camilín, por tu risa contagiosa y por tu pachorrismo. Gracias por hacerme reír tantísimo, por tus sustos y por ser siempre tan amable. A l'Alev i a la Zeynep, gracias por ser tan divertidas y estar siempre disponibles para compartir las penas y alegrías de estos 4 años. Ánimo, esto ya lo tenemos hecho! A l'Asta, la Cristina i al Munti, por ser tan bona gent i estar sempre disposats a donar un cop de mà.

També voldria donar les gràcies a lo millor que em vaig emportar del màster, la Yolanda. Gracias por seguir estando aquí siempre dispuesta a desconectar, tomar un café, ponernos al día y arreglar el mundo en un segundo.

Finalment donar les gràcies als que no tenen res a veure amb la química però que han estat al meu costat en tot moment. A la colla, els amics de veritat, els de tota la vida: Anton, Carles, Elies, Fisco, Ketku, Marcos, Marta, Nachete, Pauli, Sai i Uri. Per totes les aventures viscudes, pels nostres sopars setmanals, perquè tot i que passin els anys res canvia, perquè amb vosaltres ja fa dècades que sobren les paraules i, per sobre de tot, perquè sé que sempre sereu els que no fallen mai. Especialment a la Uli, el meu servei d'assistència 24h/365. Per estar present en tots els moments feliços de la meua vida i treure'm un somriure en els pitjors. Per ser la definició personificada del concepte amistat.

Al Josep, per aparèixer per art de màgia i fer-me somriure tantíssim.

A les meves nenes Laura, Ohiane, Palomi i Sofi per portar tantíssims anys al meu costat mimant-me i fent-me tant feliç. Per tots els ratets, sopars i xerrades eternes. Per ser tant iguals i al mateix temps tan diferents, per tenir sempre la frase que t'ajuda a tirar endavant amb un somriure, per ser tant infinitament especials. Al vostre costat la vida sempre serà un Carnaval.

A la Blanki, que em va caure de cel un estiu envoltat de màgia. Perquè *lo que hemos vivido* mai ens ho prendrà ningú, per estar sempre present i fer que la distància sigui inexistent. Has estat, ets i seràs un pilar fonamental a la meua vida.

A la family de la uni: Anna, Cerra, Glò, Gómes, Joan Carles, Jonathan, Marc, Porràs i Racio per seguir estant aquí al costat tot i el pas dels anys i fer que qualsevol moment al vostre costat sigui una festa. Especialment a les nenes Est, Lau i Marteta per estar sempre al *pie del cañón* diposades a viure la vida i a repartir felicitat. Pels nostres sopars de menú amb skype, per tots els viatges, perquè on dormen 2 hi dormen 4, per ser les persones més objectives del planeta i fer-me tan feliç amb les petites coses de la vida que realment són les importants.

Al Marc, l'Imma, al Pedro, al iaio Joan i a tots els roqueteros. Per tots els anys d'estimació i felicitat.

Finalment voldria agrair a la meua gran família per tot el suport rebut durant aquests anys, sobretot a la tieta Rosa i a la Padrina, per mimar-me i estimar-me com una filla més.

A la iaia, per ser la personeta més bona i que més em mima de tot el planeta. A la Nur, per ser la que mai falla, la que més em coneix, per aguantar com ningú els meus rampells d'impulsivitat, per ser molt més que una amiga. En definitiva, per ser la millor germana del món. Finalment, als meus pares, els que m'han donat tot en aquesta vida sense esperar res a canvi. Per estimar-me i mimar-me infinitament, per l'educació, la moral i els valors que m'heu transmès. Per ser tan fantàstics i moderns, per saber amb una mirada tot el que em passa pel cap, per estar sempre disposats a escoltar i per donar sempre els millors consells.

Sé que us ho hauria de recordar més sovint als quatre però ja ho sabeu, sou la gran sort de la meua vida i el que més m'estimo en aquest món.

Moltes Gràcies/ Muchas Gracias/ Merci Beaucoup/ Thank you

Emma

*Hem estat a dalt de tot
i hem tornat a baixar
des del primer dia
hem rigut i hem plorat
n'hem passat de totes
i això encara no ha acabat.*

*Tot el que hem fet
mai caurà en l'oblit
per més que ho intentin
ningú ens mourà d'aquí.*

Ningú ens mourà d'aquí-Sau

TABLE OF CONTENTS

Abbreviations and Acronyms	1
Summary	5
Resum	7
Résumé	9
Résumé étendu	11

CHAPTER 1

1.1. Introduction to nanoparticles	41
1.2. Synthesis and stabilisation of metal nanoparticles	42
1.3. Characterization of nanoparticles	44
1.4. General applications of metal nanoparticles in catalysis	47
1.4.1. Nanoparticles in C-C coupling reactions	48
1.4.2. Nanoparticles in hydroformylation reactions	50
1.4.3. Nanoparticles in hydrogen transfer reactions	51
1.4.4. Nanoparticles in hydrogenation reactions	53
1.5. Arene hydrogenation	55
1.5.1. Partial arene hydrogenation	57
1.5.2. <i>cis/trans</i> Selectivity in arene hydrogenation	60
1.5.3. Arene hydrogenation vs. other functional groups. Chemoselectivity	62
1.6. References	63

CHAPTER 2

2. Objectives	71
---------------	----

CHAPTER 3

3.1. Introduction to the selective hydrogenation of aromatic ketones	75
--	----

3.1.1. Acetophenone hydrogenation	75
3.1.2. Hydrogenation of non-conjugated aromatic ketones	78
3.3. Outlook and objectives of this chapter	80
3.4. Results and discussion	81
3.3.1. Synthesis, stabilisation and characterization of ruthenium and rhodium nanoparticles	81
3.3.2. Acetophenone hydrogenation	90
3.3.3. Hydrogenation of acetophenone using Ru/C and Rh/C	99
3.3.4. Hydrogenation of non-conjugated aryl ketones	101
3.3.5. Hydrogenation of substituted acetophenones using ruthenium nanoparticles	104
3.3.6. Hydrogenation of substituted acetophenones using rhodium nanoparticles	106
3.5. Conclusions	109
3.6. Experimental Part	111
3.7. References	117

CHAPTER 4

4.1. Introduction to the hydrogenation of polycyclic aromatic hydrocarbons	121
4.1.1. Hydrogenation of naphthalene	123
4.1.2. Hydrogenation of polycyclic aromatic hydrocarbons containing more than two fused arenes	124
4.1.3. Hydrogenation of heteroatomic compounds and substituted naphthalenes	128
4.2. Outlook and objectives of this chapter	131
4.3. Results and discussion	132
4.3.1. Synthesis, stabilisation and characterization of ruthenium nanoparticles	132
4.3.2. Hydrogenation of naphthalenes and polyaromatic substrates	135
4.3.3. Chemoselectivity. Hydrogenation of substituted naphthalenes vs. other functionalities	147
4.3.3.1. Hydrogenation of substituted naphthalenes	147
4.3.3.2. Hydrogenation of aromatic ring vs. ketone	153
4.4. Conclusions	156

4.5. Experimental Part	159
4.6. References	165

CHAPTER 5

5.1. Introduction to the asymmetric hydrogenation of arenes	171
5.2. Outlook and objectives of this chapter	176
5.3. Results and discussion	178
5.3.1. Design and synthesis of the target chiral phosphine ligand	178
5.3.2. Synthesis and stabilization of chiral metal nanoparticles	183
5.3.3. Hydrogenation of disubstituted aromatic compounds using chiral nanoparticles	187
5.3.4. Hydrogenation of aromatic ketones using chiral nanoparticles	192
5.3.5. Deuteration studies	196
5.3.5.1. Deuteration of triphenylphosphine	197
5.3.5.2. Deuteration of triphenylphosphine oxide and triphenylphosphite	204
5.4. Conclusions	208
5.5. Experimental Part	209
5.6. References	222

CHAPTER 6

6. General conclusions	227
------------------------	-----

ABBREVIATIONS AND ACRONYMS**A**

atm	atmosphere
Ac	acetyl
acac	acetylacetonate

B

BINAP	(2,2'-bis(diphenylphosphino)-1,1'-binaphthyl)
BMI	1- <i>n</i> -butyl-3-methyl-imidazolium
bs	broad signal
BT-CF	black tannin grafted collagen fibers

C

<i>ca</i>	approximately
CNT	carbon nanotube
COD	1,5-cyclooctadiene
COT	1,3,5-cyclooctatriene
conv.	conversion

D

d	doublet
DB18C6	dibenzo-18-crown-6-ether
dba	dibenzylideneacetone
DET	diethyl tartrate
DIPT	(-)-diisopropyl D-tartrate
DOCEA	dioctylcyclohexyl-1-ethylamine
DPEN	(<i>R,R</i>)-1,2-diphenylethylenediamine
dppb	1,2-bis(diphenylphosphino)butane

E

E	entry
EA	elemental analysis
ee	enantioselectivity
equiv.	equivalent(s)
ESI-TOF	electrospray ionization- time-of-flight resolution spectrometry

	F	
FWHM		full width at half maximum
FG		functional group
	G	
g		gram(s)
GC-MS		gas chromatography-mass spectrometry
	H	
h		hour(s)
hcp		hexagonal close packing
HP		high pressure
HPLC		high performance liquid chromatography
HPS		hypercross-linked polystyrene
HRTEM		high-resolution transmission electronmicroscopy
Hz		hertz(s)
	I	
IR		infrared
	J	
J		coupling constant
	L	
L		ligand
	M	
m (in NMR)		multiplet
M		metal
m/z		mass under charge
min		minute(s)
MS		mass spectrometry
MTBE		methyl <i>tert</i> -butyl ether
MWNTs		multiwalled carbon nanotubes
	N	
NHC		N-heterocyclic carbene
nm		nanometer(s)
NMR		nuclear magnetic resonance

NPs	nanoparticles
Ns	total number of atoms on the surface
Nt	total number of atoms

P

P	pressure
ppm	parts per million
PAHs	polyaromatic hydrocarbons
PVP	polyvinylpyrrolidone

R

rT	room temperature
----	------------------

S

s (in NMR)	singlet
SEM	scanning electron microscope
S _r	superdelocalizability

T

T	temperature
THF	tetrahydrofuran
TBHP	<i>tert</i> -butyl hydroperoxide
TEM	transmission electron microscopy
TGA	thermogravimetric analysis
TOAG	tetraoctylammonium glycolate

U

UHV	ultra-high vacuum
UV	ultra-violet

V

ν	reaction rate
vs	versus

W

WAXS	wide-angle X-ray scattering
------	-----------------------------

X

XRD	X-ray diffraction
XPS	X-ray photoelectron spectroscopy

SUMMARY

Transition metal nanoparticles have generated considerable attention in recent years as a result of their potential catalytic activity and selectivity. They are at the frontier between homogeneous and heterogeneous catalysis and combine the advantages of both. For this reason, nanoparticles emerged as promising catalyst for different reactions such as for the hydrogenation of arenes. The final goal of this thesis is the synthesis and characterization of ruthenium nanoparticles to explore their performance in arene and polyarene hydrogenation reactions.

Chapter 1 contains a general introduction to the synthesis, characterization and application of nanoparticles in catalysis. Chapter 2 sets out the general objectives of this thesis.

The research in Chapter 3 describes the synthesis and characterization of ruthenium and rhodium nanoparticles stabilized by phosphine donor ligands and their application in a comparative study in the reduction of a wide range of substituted phenyl, benzyl and phenethyl ketones.

In the case of arylketones, ruthenium nanoparticles were found to be more selective than the rhodium ones towards the hydrogenation of the aryl group. Interestingly, only rhodium nanoparticles provided hydrogenolysis products. Concerning the non-conjugated aryl ketones, both metals were found to be really selective towards arene hydrogenation.

The research in Chapter 4 describes the use of ruthenium nanoparticles stabilised by triphenylphosphine in the hydrogenation of polyaromatic substrates under mild reaction conditions. Systems containing 2, 3 or more fused benzene rings are reduced obtaining high selectivities

towards the partial hydrogenation. The recovering of the total hydrogenated product is only achieved for the less hindered substrates like naphthalene and anthracene. Moreover, the influence on the hydrogenation of naphthalenes containing a substituent (reducible or not) is also studied.

The research in [Chapter 5](#) explores the synthesis of a new chiral phosphine ligand, which is obtained in good yield and with 97% optical purity. Then, this phosphine and commercial cinchonidine (Figure 1) are used as stabilizing agents for the synthesis of chiral nanoparticles.

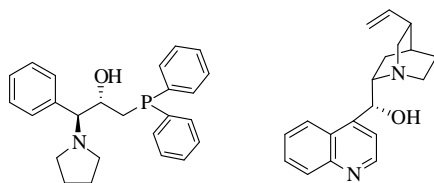


Figure 1. Phosphine and cinchonidine ligands.

These nanoparticles are tested in the asymmetric hydrogenation of different substituted arenes but unsuccessful results in terms of enantioselectivity are obtained. Moreover, deuteration studies to elucidate the coordination of the different substrates to the nanoparticles surface are performed.

[Chapter 6](#) presents the final remarks and conclusions extracted from the results obtained in this thesis.

RESUM

Les nanopartícules metàl·liques han esdevingut un tema de recent actualitat degut al seu potencial catalític i a la seva capacitat de generar elevades selectivitats. Es troben a la frontera entre la catàlisi homogènia i heterogènia i combinen les avantatges d'ambdues. Per aquest motiu, les nanopartícules han emergit com a catalitzadors molt prometedors en diferents reaccions, per exemple, en la hidrogenació d'arens. L'objectiu principal d'aquesta tesi és la síntesi i la caracterització de nanopartícules de ruteni i la seva aplicació en reaccions d'hidrogenació d'arens i poliarens.

En el Capítol 1 es fa una descripció general de la síntesi, caracterització i aplicació de les nanopartícules en catàlisi. En el Capítol 2 s'estableixen els objectius generals d'aquesta tesi.

La recerca en el Capítol 3 es centra en la síntesi i en la caracterització de nanopartícules de ruteni i de rodi, estabilitzades per lligands fosfina i en la seva aplicació en un estudi comparatiu de reducció d'una gran varietat de cetones aromàtiques.

En el cas de les arilcetones, les nanopartícules de ruteni es mostren més selectives respecte la hidrogenació del grup aril que les nanopartícules de rodi. Curiosament, només amb les nanopartícules de rodi s'obtenen productes d'hidrogenòlisi. En relació a les arilcetones no conjugades, els dos metalls són selectius cap a la hidrogenació de l'arè.

La recerca en el Capítol 4 descriu l'ús de nanopartícules de ruteni estabilitzades per trifenilfosfina, en la hidrogenació de sistemes poliaromàtics en condicions suaus de reacció. Diferents sistemes amb 2, 3 o més anells aromàtics conjugats són reduïts en elevades selectivitats cap a la hidrogenació parcial. L'obtenció dels productes totalment hidrogenats només s'assoleix

pels substrats més impeditos estèricament, tals com el naftalè o l'antracè. A més, també s'estudiarà la influència en la hidrogenació dels naftalens que contenen grups funcionals (reduïbles o no).

La recerca en el Capítol 5 explora la síntesi d'un nou lligand fosfina quiral, el qual és obtingut en bons rendiments i amb una pureza òptica del 97%. Posteriorment, aquesta fosfina i el lligand cinconidina comercial (Figura 1) s'utilitzaran com agents d'estabilització per la síntesi de nanopartícules quirals.

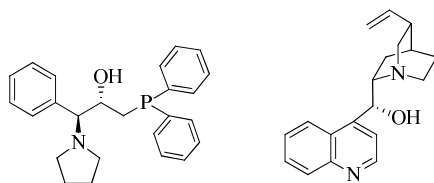


Figura 1. Lligands fosfina i cinconidina.

Aquestes nanopartícules són provades en reaccions d'hidrogenació asimètrica de diferents arens disubstituïts però, malauradament, no s'obté en cap cas enantioselectivitat. D'altra banda, també s'han dut a terme estudis de deuteració per deduir la coordinació dels diferents substrats a la superfície de les nanopartícules.

El Capítol 6 presenta les observacions finals i les conclusions extretes dels resultats obtinguts en aquesta tesi.

RÉSUMÉ

Les nanoparticules de métaux de transition ont suscité une attention considérable au cours des dernières années en raison de leur activité catalytique et sélectivité. Elles sont à la frontière entre la catalyse homogène et hétérogène et combinent les avantages des deux. Pour cette raison, les nanoparticules ont émergé en tant que catalyseurs pour différentes réactions telles que l'hydrogénation d'arènes. L'objectif final de cette thèse est la synthèse et la caractérisation de nanoparticules de ruthénium et l'exploration de leur performance catalytique en réactions d'hydrogénation d'arènes et polyarènes.

Le Chapitre 1 contient une introduction générale à la synthèse, la caractérisation et l'application des nanoparticules en catalyse. Le Chapitre 2 définit les objectifs généraux de cette thèse.

Le Chapitre 3 décrit la synthèse et la caractérisation de nanoparticules de ruthénium et de rhodium stabilisées par des ligands de type phosphine et leur application dans une étude comparative concernant la réduction d'une large gamme de phényles substitués, benzyle et de phénéthyle cétones.

Dans le cas des cétones d'aryle, des nanoparticules de ruthénium ont démontré être plus sélectives pour l'hydrogénation du groupe aryle que celles de rhodium. Par contre, les nanoparticules de rhodium fournissent des produits d'hydrogénolyse. En ce qui concerne les arylcétones non conjuguées, les deux métaux sont très sélectifs envers l'hydrogénation du groupe aryle.

Le Chapitre 4 décrit l'utilisation de nanoparticules de ruthénium stabilisées par la triphénylphosphine pour l'hydrogénation de substrats polycycliques aromatiques dans des conditions réactionnelles douces. Les systèmes contenant deux, trois ou plusieurs cycles aromatiques condensés

sont réduites et montrent une haute sélectivité pour l'hydrogénation partielle. Le produit d'hydrogénation totale est uniquement obtenu pour les substrats moins encombrés, tels que le naphthalène et l'anthracène. L'influence d'un substituant (réductible ou non) sur l'hydrogénation du naphthalène est également étudiée.

La recherche dans le Chapitre 5 explore la synthèse d'un nouveau ligand de type phosphine chirale, qui est obtenu avec un bon rendement et avec une pureté optique de 97%. Ensuite, cette phosphine et la cinchonidine commercial (Figure 2) sont utilisées comme agents de stabilisation pour la synthèse de nanoparticules chirales.

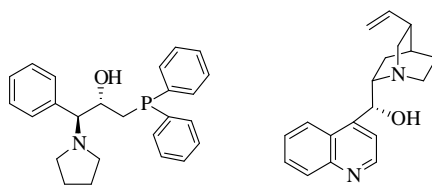


Figure 2. Ligands phosphine et cinchonidine.

Ces nanoparticules ont été testées dans l'hydrogénation asymétrique de différents arènes disubstitués mais en terme d'énantiosélectivité, les résultats n'ont pas été bons. Une étude de deutération a été effectuée pour élucider la coordination des différents substrats à la surface de nanoparticules.

Le Chapitre 6 présente les observations finales et les conclusions de cette thèse.

RÉSUMÉ ÉTENDU

CHAPITRE 1. INTRODUCTION AUX NANOPARTICULES

La nanochimie est un champ de recherche exponentiellement croissant en science et implique la synthèse et l'application de nanoparticules de différentes tailles, formes, activité et sélectivité.¹

Les nanoagrégats modernes de métaux de transition appelés également nanoparticules (NPs), sont dans la gamme 1-10 nm de diamètre, plus petits que les colloïdes classiques (typiquement >10 nm de diamètre). Ils sont isolables et solubles dans les solvants organiques (les colloïdes classiques ont été généralement utilisés dans des systèmes aqueux) et sont bien définis en termes de composition. Les nanoparticules ont des distributions de taille étroites, des surfaces propres et la synthèse et l'activité sont reproductibles.

Les nanoparticules métalliques solubles sont à la frontière de la catalyse homogène et hétérogène et combinent les avantages des deux. Elles sont actives dans des conditions douces, plus sélectives que les systèmes hétérogènes et en raison de leur solubilité, différentes techniques d'analyse permettent d'étudier leur comportement. Ces systèmes sont libres de rotation et ont trois dimensions dans les systèmes de réaction, ce qui améliore l'accessibilité aux sites actifs des surfaces.² Cependant, les nanoparticules présentent aussi quelques inconvénients comme leur tendance à l'agglomération et leur relativement faible stabilité thermique.³

Les propriétés des nanoparticules sont dépendantes de leur taille, ce qui peut affecter leur activité et sélectivité.¹ Chaudret *et al.*⁴ ont développé l'utilisation d'un précurseur organométallique qui peut être décomposé en

présence d'un gaz réducteur (H_2 ou CO), pour obtenir la réduction du métal. Le précurseur idéal doit être un complexe oléfinique avec valence zéro comme $[Ru(COD)(COT)]$, dans lequel les ligands organiques peuvent être facilement déplacés dans des conditions douces afin d'obtenir une surface non contaminée.⁵

Des agents stabilisateurs sont nécessaires pour éviter l'agglomération des nanoparticules. Solvants, polymères, agents de surface ioniques et ligands ont été utilisés pour stabiliser des nanoparticules.⁶

Applications générales des nanoparticules de métal en catalyse

Les nanoparticules ont été beaucoup utilisées comme catalyseurs dans plusieurs réactions telles que oxydation, réaction de couplage, hydroformylation et hydrogénation entre autres.⁷ L'application la plus importante de la réaction d'hydrogénation est la réduction du benzène en cyclohexène pour la production d'acide adipique (précurseur du nylon).⁸

L'hydrogénation des arènes est beaucoup plus difficile que l'hydrogénation des oléfines simples, en raison de l'énergie de stabilisation de résonance qui est perdue lors de l'hydrogénation. Traditionnellement, le Rh/Al_2O_3 , les sulfures métalliques et le Nickel de RaneyTM ont été les catalyseurs de choix pour l'hydrogénation des arènes monocycliques. Néanmoins, des conditions drastiques en termes de température et/ou de pression sont nécessaires.⁹ Pour cette raison, les nanoparticules apparaissent comme une solution pour développer l'hydrogénation d'arène dans des conditions douces.

Le mécanisme généralement accepté pour l'hydrogénation des arènes a été proposé en 1974.¹⁰ Ce mécanisme peut être appliqué aux arènes qui

interagissent avec plus d'un centre métallique comme c'est le cas pour des clusters, nanoparticules ou surfaces métalliques.¹¹

Un mode de coordination commun en chimie de cluster et sur les surfaces métalliques est le $\mu_3\text{-}\eta^2\text{:}\eta^2\text{:}\eta^2$ (Schéma 1). L'addition d'hydrogène sur une seule double liaison conduit à un $\mu_3\text{-}\eta^2\text{:}\eta^2$ -diène et l'hydrogénation d'une double liaison supplémentaire se traduit par la production d'un monoène.¹² La libération des produits diène et monoène peut avoir lieu à travers le remplacement du produit partiellement hydrogéné par un nouveau substrat.¹¹

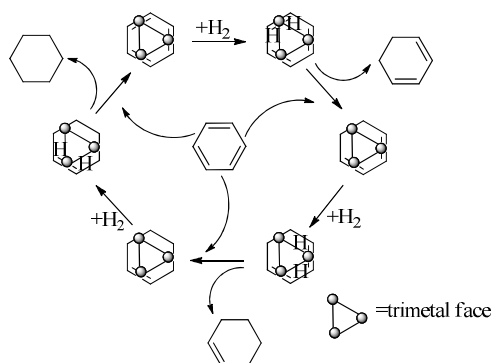


Schéma 1. Mécanisme d'échange d'arènes proposé pour un catalyseur hétérogène.

Hydrogénation partielle d'arènes

La réduction partielle des arènes à diènes cycliques ou monoènes représente une réaction utile en raison de la simple formation de cyclohexanol par hydratation. Cette réduction est généralement réalisée avec des réactifs stœchiométriques comme dans la réduction de Birch.¹³

Les nanoparticules représentent une nouvelle opportunité pour l'hydrogénation partielle des arènes. Cependant, il y a quelques obstacles à surmonter en raison de la réduction facile des dernières doubles liaisons, une

fois l'aromaticité perdue. En outre, l'élimination d'un diène coordonné ou chimisorbé au métal est une tâche difficile.¹⁴

En ce qui concerne l'hydrogénation partielle des arènes substitués, différents exemples ont été rapportés.¹⁵ Par exemple, Chaudret et van Leeuwen ont rapporté l'utilisation de carbènes NHC pour stabiliser les nanoparticules de ruthénium et leur utilisation dans l'hydrogénation d'arènes. À 393 K et 20 % de conversion, environ 60 % d'hydrogénation partielle a été obtenue dans le cas du *o*-méthylanisole.¹⁶

Sélectivité *cis/trans* dans l'hydrogénation d'arènes

Les substituants sur les composés aromatiques disubstitués ont un effet important non seulement sur la vitesse de la réaction, mais aussi sur la sélectivité *cis/trans*. La sélectivité envers le stéréoisomère *cis* est rationalisée par une addition continue d'hydrogène sur une seule face de l'arène, et le stéréoisomère *trans* se forme lorsqu'un intermédiaire partiellement hydrogéné se dissocie de la surface des nanoparticules et réassocie par la face opposée avant hydrogénation supplémentaire (Schéma 2).³

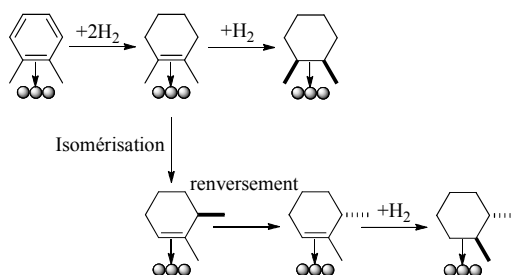


Schéma 2. Mécanisme proposé pour l'hydrogénation des arènes disubstitués sur des surfaces métalliques.

Les arènes disubstitués comme les méthylanisoles ou les xylènes ont été généralement utilisés pour étudier la sélectivité *cis/trans* dans les réactions d'hydrogénation par NPs.¹⁷ Il est intéressant de souligner que le produit *trans*

a été principalement obtenu (taux de 19:1) lorsque des Ru-NPs stabilisées par des monooxazolines chiraux ont été utilisées comme catalyseurs.¹⁸

CHAPITRE 3. HYDROGÈNATION SÉLECTIVE DES CÉTONES AROMATIQUES

Introduction

L'hydrogénation chimiosélective de cycles aromatiques de substrats contenant d'autres groupes fonctionnels réductibles comme des cétones représente toujours un défi. Quelques exemples d'hydrogénation chimiosélective d'arènes ont été rapportés avec des catalyseurs hétérogènes et, en général, des mélanges de produits sont obtenus.¹⁹ Pour cette raison, les nanoparticules sont apparues comme une solution prometteuse pour surmonter ce problème.

L'acétophénone est, en général, le substrat de référence utilisé dans l'étude de l'hydrogénation sélective d'un arène vs. un groupe carbonyle utilisant des nanoparticules. Différents exemples ont été signalés.²⁰ Par exemple, van Leeuwen et ses collaborateurs ont utilisé des carbènes N-hétérocycliques (ItBu et IPr) pour stabiliser des NPs de Ru qui catalysent l'hydrogénation de l'acétophénone. Des sélectivités jusqu'à près de 60 % ont été obtenues pour l'hydrogénation de l'arène en utilisant les nanoparticules stabilisées par IPr.¹⁶

De meilleurs résultats en termes de sélectivité ont été obtenus dans la réduction de cétones aromatiques non conjuguées. Ainsi, par exemple, en 2004, Dupont *et al.* ont réduit la phénylacétone en utilisant des nanoparticules d'iridium. L'hydrogénation de l'arène a été réalisée avec 92 % de sélectivité à 97 % de conversion et dans des conditions de réaction douces (4 atm et 75° C) (Schéma 3).²¹

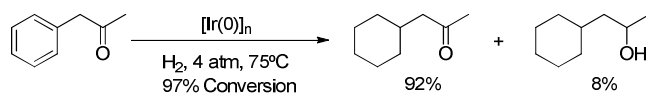


Schéma 3. Hydrogénation sélective de phénylacétone utilisant Ir Nps stabilisées par ILs.²¹

Résultats et Discussion

L'objectif de ce chapitre est la comparaison du comportement catalytique des nanoparticules de Ru et Rh dans l'hydrogénation de l'arène vs. la fonction cétone. L'effet de la nature du métal, de l'agent stabilisant et l'influence de la structure du substrat ont été étudiés.

Des NPs de Ru et Rh stabilisées par les ligands PPh₃ et dppb (P:Ru / Rh= 0,4) ont été synthétisées par décomposition des précurseurs organométalliques [Ru(COD)(COT)] et [Rh(η³-C₃H₅)₃], respectivement, dans le THF et sous pression d'H₂ (Schéma 4). Les NPs ont été isolées comme des poudres noires après précipitation avec pentane et ont été entièrement caractérisées.

Les micrographies du TEM de ces NPs ont révélé, dans tous les cas, la formation de petites nanoparticules de forme sphérique, avec une distribution de la taille étroite et le même diamètre (environ 1.5 nm). Des pics diffus ont été observés dans le spectre XRD de ces NPs, comme prévu pour une répartition homogène de particules très petites avec une structure hexagonale compacte (hc). L'analyse thermogravimétrique des systèmes **Ru1-2** a montré que ces NPs contiennent environ 2 % de solvant, 25 % de ligands phosphines et 70 % de ruthénium.

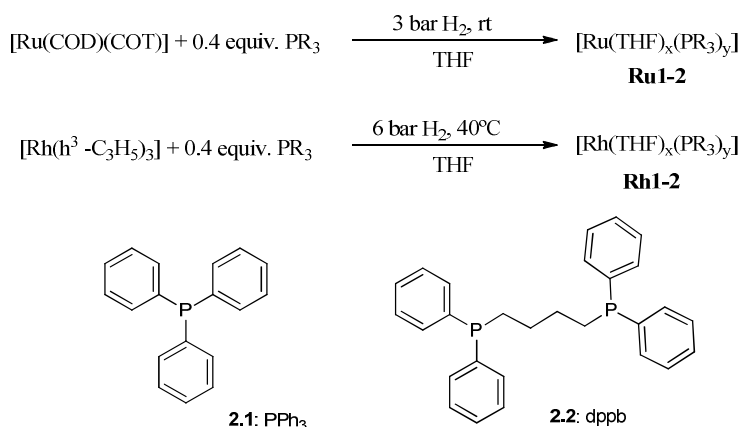


Schéma 4. Synthèse de NPs de Ru et Rh stabilisées avec PPh₃ et dppb.

Des résultats similaires ont déjà été signalés pour les systèmes de Rh.^{15e} Dans le cas de nanoparticules de Rh, les micrographies TEM ont révélé la formation de petites nanoparticules de forme sphérique (environ 1.6 nm). Des pics diffus ont été observés dans le spectre XRD de ces NPs, comme prévu pour une répartition homogène de particules très petites avec une structure cubique à faces centrées (cfc). Aucune réflexion due à l'oxyde de rhodium n'a été observée. L'analyse thermogravimétrique des systèmes **Rh1-2** a montré que ces NPs contiennent 1 % de solvant, 29 % de ligands phosphines et 70 % de Rh.

L'acétophénone **2.3** a été utilisée pour évaluer la sélectivité de l'hydrogénation (groupe aryle *vs.* groupe cétone) en utilisant les nanoparticules **Ru1-2** et **Rh1-2**.

De grandes différences ont été observées selon le métal et les agents stabilisants. Les nanoparticules de ruthénium favorisent la réduction du cycle aromatique par rapport à la réduction du groupe cétonique (on obtient une sélectivité jusqu'à 60%) et elles sont également capables de réduire **2.3a** pour

produire **2.3c**. Toutefois, avec ces catalyseurs, **2.3b** est réduit très lentement (Schéma 5). En outre, la sélectivité est influencée par le ligand stabilisateur.

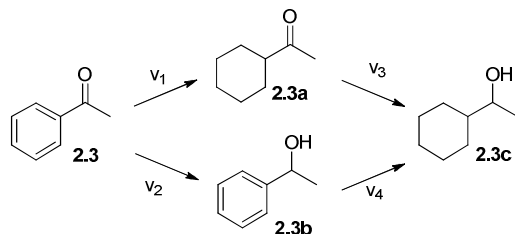


Schéma 5. Chemins de réaction d'hydrogénation de l'acétophénone **2.3** utilisant des nanoparticules **Ru1**.

Cependant, les NPs de rhodium favorisent la réduction du groupe cétone pour produire 1-phényléthanol **2.3b**, qui est de nouveau hydrogéné pour former **2.3c** ou hydrogéné et forme **2.3d** exclusivement lorsque **Rh1** est utilisé comme catalyseur. Fait intéressant, les Rh-NPs ne réduisent pas la cyclohexylcétone **2.3a** (Schéma 6).

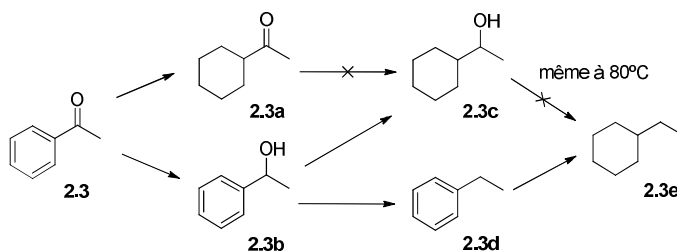


Schéma 6. Voie de réaction d'hydrogénation de l'acétophénone **2.3** utilisant des nanoparticules **Rh1**.

Ces résultats nous ont amenés à étudier le comportement de ces nanocatalyseurs dans l'hydrogénation des aryle cétones non conjuguées (Schéma 7). La réduction d'aryle cétones non conjuguées et l'influence de la longueur de la chaîne alkyle entre le phényle et les groupes cétone (substrats **2.4** et **2.5**) ont été étudiées en utilisant **Ru1-2** et **Rh1-2** comme catalyseurs.

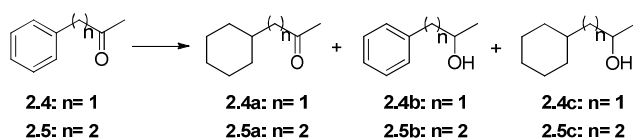


Schéma 7. Hydrogénation des aryle cétones non conjuguées.

Pour les deux métaux, la réduction de l'arène a été principalement observée mais des sélectivités plus élevées ont été observées quand des nanoparticules de Rh ont été utilisées. Dans le cas de la réduction du substrat **2.5** avec des NPs de Rh, ce processus est pratiquement exclusif. La sélectivité pour la réduction de l'arène augmente quand la distance entre l'arène et le groupe cétone augmente. Pour les deux systèmes de rhodium, des sélectivités semblables ont été obtenues, alors que dans le cas de ruthénium, une valeur plus élevée pour la réduction de l'arène a été obtenue avec **Ru1** (jusqu'à 74 %).

Enfin, il a été décidé d'élargir l'étude à la réduction des dérivés d'acétophénone. Les composés **2.6-2.11** contenant différents substituants dans les fractions d'alkyle et de phényle ont été hydrogénés (Schéma 8).

En général, des activités faibles à modérées ont été observées en utilisant les nanoparticules **Ru1-2**. Des conversions inférieures ont été obtenues quand il y avait une augmentation de la substitution de la chaîne alkyle ou dans le cycle aromatique, particulièrement lorsque les substituants sont situés en position *ortho*. La sélectivité pour l'hydrogénation de l'arène est affectée négativement par la présence de substituants sur le cycle aromatique.

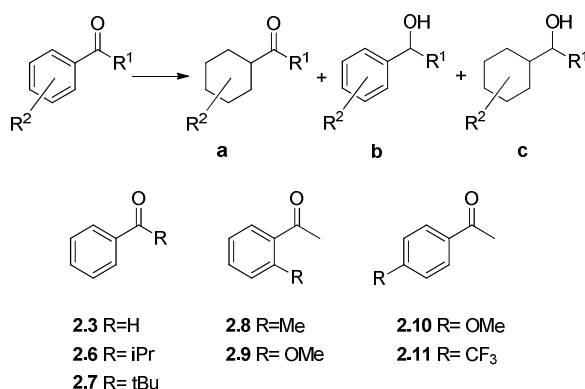


Schéma 8. Hydrogénation des dérivés d'acétophénone.

Dans le cas des nanoparticules **Rh1-2**, l'activité de ces catalyseurs est significativement affectée par l'effet stérique des substituants alkyles de la cétone. Toutefois, lorsque les substituants sont sur le cycle aromatique, ils ont peu d'influence et une activité élevée est obtenue dans tous les cas. En ce qui concerne la sélectivité, dans tous le cas, les produits préférablement obtenus sont ceux qui proviennent de la réduction du groupe cétone (>70 %).

En outre, l'hydrogénolyse des dérivés de 1-phényléthanol a été observée seulement avec les nanoparticules **Rh1** stabilisées avec PPh₃. Il convient de noter que le processus d'hydrogénolyse est interrompu lorsque l'effet stérique de la chaîne allylique augmente, mais pas quand les substituants sont présents en position *ortho* ou *para* du cycle aromatique.

CHAPITRE 4. HYDROGÉNATION SÉLECTIVE D'ARÈNES POLYCYCLIQUES EN UTILISANT DES NANOPARTICULES DE RUTHENIUM

Introduction

Les hydrocarbures aromatiques polycycliques (HAPs) sont une classe de composés organiques formés par deux ou plusieurs cycles

benzéniques fusionnés avec différents arrangements structuraux.²² Les HAPs ont gagné une attention considérable en raison de leurs effets toxiques, cancérigènes et tératogènes.²³ Différentes méthodes ont été proposées pour l'assainissement des HAPs, comme le traitement thermique, bio-remédiation, photodégradation, oxydation chimique, etc. mais ce sont encore des procédés lents qui impliquent des techniques complexes avec une forte consommation d'énergie.²⁴

Comme il a été commenté auparavant, les nanoparticules ont été utilisées dans une grande variété de réactions. En particulier, plusieurs études ont porté sur l'hydrogénation des composés aromatiques mais peu d'études ont été publiées concernant l'hydrogénation de substrats polyaromatiques dans des conditions douces catalysées par des nanoparticules.²⁵

Le naphthalène a été probablement le système polycyclique aromatique le plus étudié dans les réactions d'hydrogénation (Schéma 9).²⁶ L'un des premiers exemples concernant l'utilisation de nanoparticules dans l'hydrogénation de naphthalène a été signalé en 2002. Dans cet article, le naphthalène a été réduit en utilisant des nanoparticules de rhodium dans une microémulsion de CO₂ supercritique dans l'eau et, après une heure, 96% de conversion a été obtenu et la tétraline a été obtenue comme produit unique.²⁷ En général, la décaline est rarement obtenue.

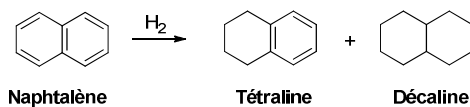


Schéma 9. Produits formés dans l'hydrogénation du naphthalène.

L'hydrogénation des naphthalènes est connue pour avoir lieu dans des conditions de réaction douces en utilisant une variété de catalyseurs. Néanmoins, la réduction des arènes polycycliques (Figure 1) requière plus de

température et de pression et un mélange de produits est en général obtenu (sélectivité faible).²⁸

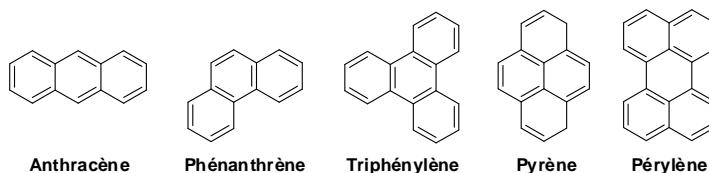


Figure 1. Structures d'hydrocarbures aromatiques polycycliques sélectionnées.

Des nanoparticules ont aussi été utilisées comme catalyseurs pour l'hydrogénation d'hydrocarbures polycycliques aromatiques, avec plus de deux cycles conjugués. Néanmoins, des produits qui viennent de l'hydrogénation totale sont rarement obtenus.²⁹ Par exemple, en 2007, Park *et al.* ont synthétisé des nanoparticules de Rh et Ir prises au piège dans des nanofibres d'oxyde d'hydroxyde aluminium, qui ont été appliquées dans des réactions d'hydrogénation d'arènes. Des rendements et sélectivités élevés furent obtenus pour l'hydrogénation de composés aromatiques bicycliques et tricycliques. Le naphthalène était réduit à tétraline et l'anthracène à 9,10-dihydroanthracène à température ambiante avec un ballon à hydrogène (1 atm, Schéma 10). Cependant, de longs temps de réaction étaient nécessaires pour obtenir des produits totalement hydrogénés et une charge élevée de catalyseur dans le cas de l'anthracène.^{20h}

Quelques exemples d'hydrogénation chimiosélective des arènes ont été signalés à l'aide de catalyseurs hétérogènes et, en général, on a obtenu des mélanges de produits.¹⁹

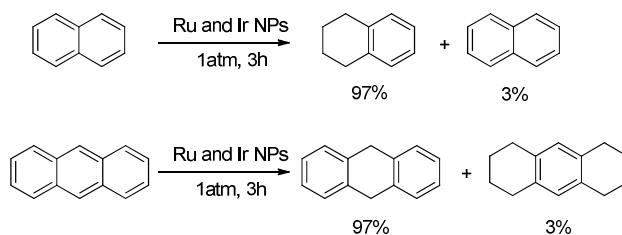


Schéma 10. Hydrogénation du naphthalène et d'anthracène sous 1 atm et à température ambiante pendant 3h.

Résultats et Discussion

L'objectif de ce travail était de réaliser une étude de l'hydrogénation de différents arènes polycycliques dans des conditions douces en utilisant des nanoparticules de ruthénium. L'étude se concentre sur la sélectivité pour l'hydrogénation partielle des polyarènes, mais vise également à savoir s'il est possible d'atteindre la réduction totale de polyarènes dans des conditions douces. En outre, l'hydrogénation des naphthalènes contenant des substituants en différentes positions du cycle aromatique a été tentée.

Dans ce chapitre, des nanoparticules stabilisées avec 0.2 et 0.4 équivalent de PPh_3 (**Ru3** et **Ru1**) ont été préparées, caractérisées et utilisées comme catalyseurs dans l'hydrogénation de différents hydrocarbures polycycliques aromatiques. En comparant les nanoparticules **Ru3** et **Ru1**, on peut conclure que les NPs **Ru3** sont légèrement plus grosses que **Ru1**. Les nanoparticules présentent une structure hexagonale compacte et aucune oxydation n'est détectée. Quantitativement, elles contiennent environ 70 % de Ru et 30 % de PPh_3 .

Le naphthalène était initialement utilisé comme substrat modèle pour évaluer la sélectivité envers l'hydrogénation partiel et totale. On peut conclure que la sélectivité dépend fortement de la pression et l'obtention du naphthalène hydrogéné partiellement ou totalement peut être facilement ajusté. Des

sélectivités jusqu'à 93% pour la formation de la tétraline à 70% de conversion (3 bar de H₂, 10 h) et une sélectivité jusqu'à 84 % de la *cis*-décaline à conversion complète (20 bar de H₂, 16 h) ont été atteintes.

Puis, des systèmes polycycliques aromatiques contenant trois arènes conjugués ont été hydrogénés (Schéma 11). L'objectif de cette partie était la réduction sélective d'une arène. Bien qu'ayant le même nombre d'arènes, un comportement très différent a été observé pour l'anthracène et le phénanthrène. Dans le cas de l'anthracène, le cycle externe A a été initialement hydrogénée et le produit **4.2a** a été sélectivement obtenu à 44% de conversion dans les conditions de réaction optimisées (20 bar pression H₂ et 30°C). Après un temps de réaction de 9h, on obtient le produit **4.2c** avec une sélectivité de 96 % à conversion complète.

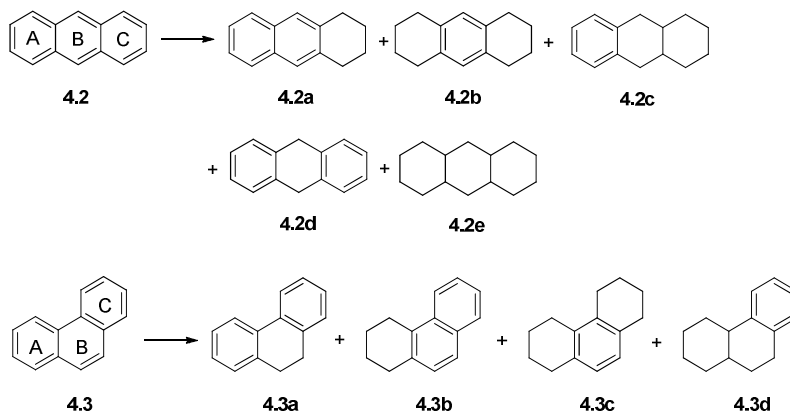


Schéma 11. Produits obtenus dans l'hydrogénation de l'anthracène et du phénanthrène.

L'hydrogénation du phénanthrène donne des mélanges de produits dès le début de la réaction. Le produit totalement hydrogéné n'est pas observé. Dans ce cas le cycle B est préférentiellement réduit, mais le cycle A est réduit avec une sélectivité proche de celle de l'anneau B. Une fois que l'anneau A

est réduit, l'anneau C semble être aussi facilement réduit, et les composés **4.3b** et **4.3c** sont obtenus avec un pourcentage similaire (~ 30 %).

L'hydrogénation de polyaromatiques contenant 4 arènes conjugués ou plus a aussi été tentée (Schéma 12). Le triphénylène **4.4** a été réduite à 20 bar et 30°C pendant 16h et 61% de conversion ont été obtenus. Le produit **4.4a**, qui a seulement un cycle hydrogéné, a été obtenu avec une sélectivité jusqu'à 53% à 61% de conversion. Le composé **4.4b** (2 anneaux extérieurs hydrogénés) a été obtenu avec 12% de sélectivité et le produit **4.4c** (3 anneaux externes hydrogénés) avec 35%. C'est clair que la réduction des anneaux externes est facile et le produit totalement hydrogéné n'est pas observé. Lorsque la température est augmentée à 80°C, 100% de sélectivité envers le produit **4.4c** est obtenue.

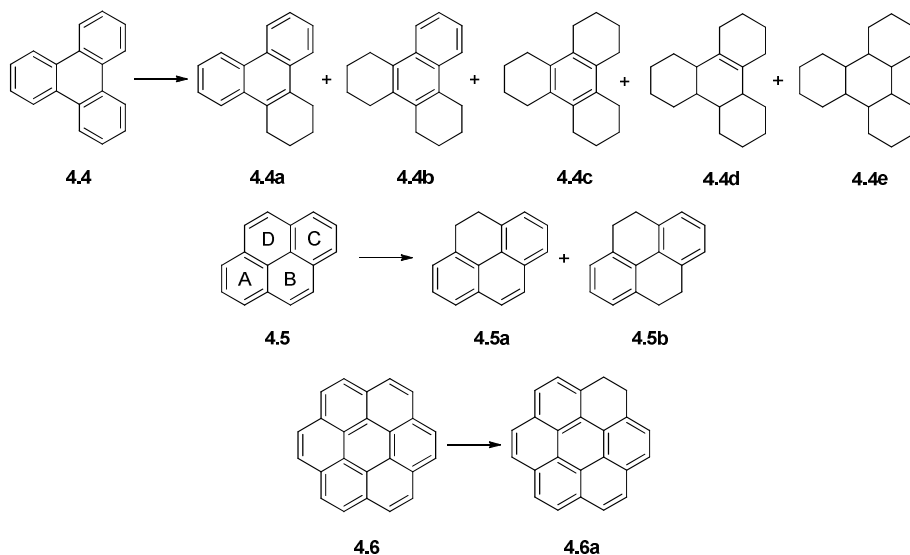


Schéma 12. Produits obtenus dans l'hydrogénation de polyaromatiques contenant 4 arènes conjugués ou plus.

Dans le cas du pyrène **4.5**, la température a un effet important sur l'activité. 60 heures de réaction à 80°C ont été nécessaires pour atteindre 86%

de sélectivité vers le produit **4.5a** et 45% de conversion. Quand la réaction a été effectuée avec les nanoparticules **Ru3**, la sélectivité s'est élevée à 100%, mais la conversion était très basse (7 %). L'hydrogénation du coronène n'a pas été possible.

Les résultats obtenus dans l'hydrogénation de tous ces composés polycycliques aromatiques démontrent que, lorsque le nombre de cycle benzénique augmente, l'hydrogénation devient plus difficile.

Enfin, une étude sur l'effet de la substitution sur la sélectivité de l'hydrogénation de polyarènes, ainsi que la réduction sélective de polyarènes *vs.* autres groupes fonctionnels a aussi été réalisée. Les naphthalènes substitués en positions α (position 1) et β (position 2) avec des substituants donneurs et accepteurs, ainsi qu'avec des substituants qui pourraient être réduits de façon compétitive, ont été sélectionnés.

Au départ, des naphthalènes avec différents substituants en position 2 ont été hydrogénés (Schéma 13). Lorsque l'effet stérique est augmenté par rapport au naphthalène, la réaction devient plus lente et la sélectivité est influencée par le type de substituant (donneur ou accepteur). Dans tous les cas, l'hydrogénation de l'arène qui ne contient pas de substituant est préférable. Des sélectivités d'environ 80% ont été obtenues pour le substrat **4.7a**. Toutefois, de très faibles conversions ont été obtenues pour les substrats **4.8** et **4.9**.

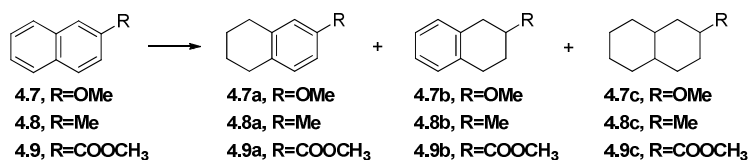


Schéma 13. Hydrogénation des naphthalènes substitués en position 2.

L'étude a été poursuivie en réduisant des naphthalènes contenant un substituant dans la position la plus proche à l'arène vicinaux, position 1 (Schéma 14). Quand un groupe méthoxy se trouve en position 1, la réaction devient plus lente et 40 % de conversion est obtenue bien que la sélectivité reste inchangée (85 % de **4.10a**). La présence d'un groupe accepteur comme le -CF₃, en comparaison avec les groupes donneurs, la réduction du cycle plus substitué était légèrement favorable. Quand une amine est présente dans le substrat comme pour **4.12**, la conversion diminue considérablement (même après plusieurs heures). La faible réactivité des anilines et en général d'aminoarènes a été déjà observée.³⁰

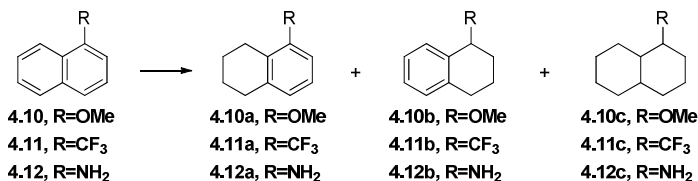


Schéma 14. Hydrogénation des naphthalènes substitués en position 1.

La position du substituant a plus d'influence sur la conversion que sur la sélectivité. Lorsque le substituant est en position 1, les conversions sont plus faibles, probablement en raison de l'effet stérique plus important qui rend plus difficile l'approche du substrat à la surface. Néanmoins, la sélectivité n'est pas significativement affectée et l'arène qui ne contient pas de substituants est toujours celui qui est favorablement hydrogéné.

Comme dernier objectif de ce chapitre, en relation avec le chapitre précédent, nous étions intéressés dans l'étude de la réduction des naphthalènes qui contiennent des cétones. De des résultats obtenus, on peut conclure qu'aussi dans ce cas, il y a une compétition importante entre la réduction de l'arène vs. la cétone et qu'elle est influencée par la position du groupe cétonique.

Ainsi, lorsque le groupe cétonique est en position 2, la réduction du cycle aromatique le moins substitué a lieu principalement, bien qu'on observe également une réduction significative du carbonyle. Si le groupe cétonique est en position 1, l'observation la plus pertinente est le fait que le cycle le plus substitué est également réduit. Le fait que les groupes électroaccepteurs activent l'hydrogénation du cycle voisin a déjà été observé dans le cas du dérivé trifluorométhyle (4.11), mais maintenant, nous pouvons conclure que cet effet est plus important lorsque le substituant est en position 1.

CHAPITRE 5. VERS L'HYDROGÉNATION ENANTIOSELECTIVE DES ARÈNES UTILISANT DES NANOPARTICULES DE RUTHENIUM CHIRAUX

Introduction

L'important développement de la catalyse énantiosélective en systèmes homogènes a augmenté l'intérêt pour les propriétés et le développement de surfaces chirales et leur application en catalyse asymétrique.

Différents mécanismes et modes de coordination ont été proposés pour l'adsorption du substrat et du modificateur sur la surface métallique. Toutefois, il est généralement admis que les responsables de

l'énantiosélection sont des interactions modificateur-substrat à la surface métallique.³¹

Le premier exemple de catalyse énantiosélective avec des nanoparticules métalliques a été publié en 1994 par Lemaire, Gallezot *et al.* sur l'hydrogénation de cycles aromatiques disubstitués utilisant des nanoparticules de Rh à l'aide de l'amine chirale DOCEA comme ligand. Toutefois, un excès énantiomérique très modeste de 10% avait été observé (Schéma 15).^{17b}

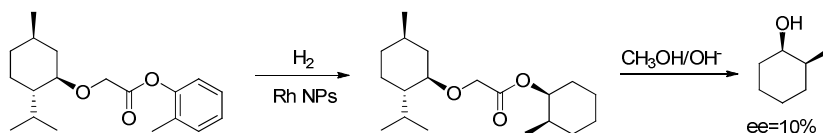


Schéma 15. Hydrogénation diastéréosélective utilisant des Rh NPs et DOCEA.^{17b}

Par la suite, plusieurs réactions asymétriques utilisant des nanoparticules ont été tentées. La plus étudiée est l'hydrogénation des α -cétotoesters comme pyruvate d'éthyle et des énantiosélectivités jusqu'à 98 % à conversion complète ont été obtenues en utilisant des nanoparticules de Pt stabilisées par des dérivés de quinine (Schéma 16).³² En général, dans tous ces exemples, des ligands chiraux s'ajoutent au cours de la catalyse afin d'obtenir des ee élevés. Cette exigence est attribuée à l'épuisement du modificateur de la surface du métal en raison de l'hydrogénation.³³ Dans certains cas, on suppose qu'il existe une déplétion des ligands à la surface des nanoparticules et des complexes chiraux homogènes peuvent être formés in situ et deviennent le véritable catalyseur.

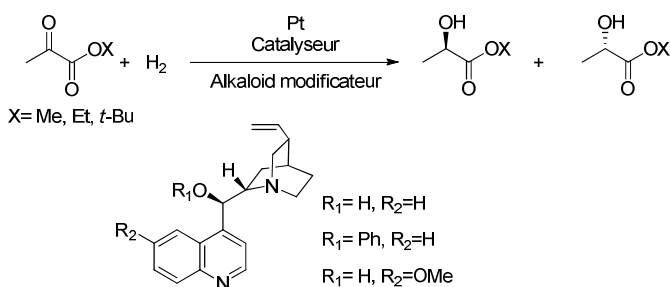


Schéma 16. Hydrogénation énantiosélective de pyruvates en utilisant des NPs de Pt.³⁴

Plusieurs exemples d'hydrogénation asymétrique de différents groupes fonctionnels et de transfert d'hydrogène à l'aide de NPs recouvertes de ligands chiraux ont été publiés.³⁵ Néanmoins, en général, l'obtention d'énantiosélectivité dans des réactions d'hydrogénation d'arènes est toujours une tâche très difficile.

Seuls quelques exemples ont été signalés et les énantiosélectivités obtenues ont été inférieures à 10%. Des nanoparticules de rhodium stabilisées par des amines chirales ont été utilisées dans l'hydrogénation des *o*-méthylanisole et *o*-méthyl-*O*-triméthylsilyl-benzène. Une bonne sélectivité *cis/trans* a été obtenue, mais les excès énantiomériques n'ont pas dépassé les 6%.^{17b,36}

En 2009, Claver *et al.* ont rapporté la synthèse de nanoparticules de Ru, Rh et Ir stabilisées par des ligands diphosphite chiraux pour l'hydrogénation d'arènes monocycliques. De bonnes activités sous des conditions douces et des résultats intéressants en termes de sélectivité *cis* ont été obtenus. Cependant, seule une énantiosélectivité très faible a été atteinte (jusqu'à 6%).³⁷

Résultats et Discussion

Le but de ce travail était de synthétiser et utiliser des ligands chiraux phosphine et cinchonidine pour stabiliser des nanoparticules de ruthénium pour l'hydrogénation asymétrique d'arènes. L'hypothèse était basée sur l'interaction supramoléculaire entre le ligand et le substrat qui pourrait induire un produit énantiomériquement enrichi.

Dans le cadre de cette étude, nous avons réalisé que nous avons besoin d'informations sur l'interaction du ligand avec la nanoparticule pour la conception du ligand. Des études de deutération de ligands simples ont été effectuées afin de comprendre comment les agents stabilisants peuvent interagir avec la surface des nanoparticules.

La conception des agents stabilisants pour nanoparticules est une étape importante afin d'obtenir de bons résultats en termes de sélectivité et d'activité en nanocatalyse. Notre hypothèse était de synthétiser une phosphine avec des groupes fonctionnels supplémentaires avec de faibles propriétés acides et basiques. Par conséquent, la phosphine **5.13** a été synthétisée en 4 étapes et utilisée avec la cinchonidine comme stabilisateurs de nanoparticules de ruthénium (Schéma 17).

Les NPs **Ru4** ont un diamètre de 1.61 ± 0.35 nm, sont hautement cristallines avec une structure hexagonale compacte et aucune oxydation ne fut détectée. Quantitativement, ils contiennent 79 % du Ru et 21 % de ligand **5.13**. En comparant les deux nanoparticules stabilisées par cinchonidine, on peut déduire que les plus petites sont obtenues quand une plus grande proportion de ligand est utilisée pour les stabiliser (**Ru6** sont plus petites que **Ru5**). Aucune différence appréciable de la proportion de ruthénium vs. proportion de ligand n'est observée.

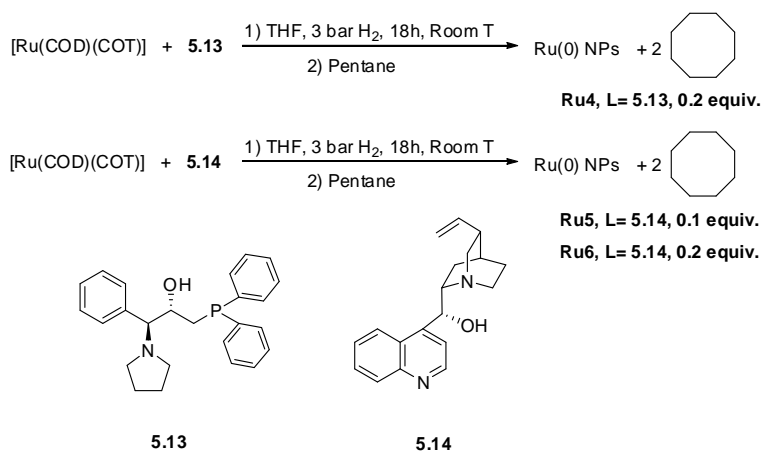


Schéma 17. Synthèse de nanoparticules de ruthénium stabilisés par des ligands chiraux.

Au départ, nous avons sélectionné les amides **5.15** et **5.16**, 2-pyridinemethanol (**5.17**) et le 2-methoxyphenylmethanol (**5.18**) comme substrats en raison de la possibilité de créer des interactions acide-base avec le ligand **5.13**. La chiralité des fonctions acide-base du ligand devrait déterminer l'interaction avec le substrat (Figure 2).

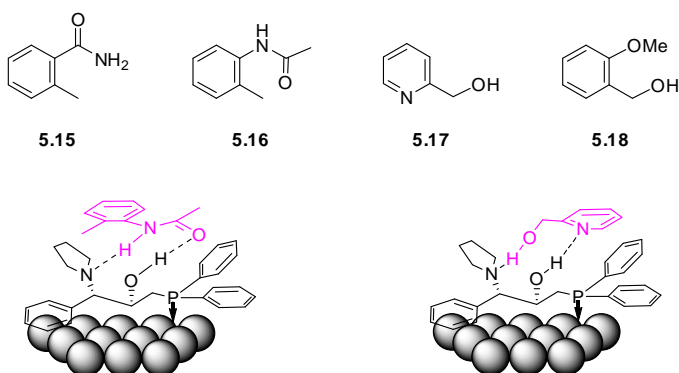


Figure 2. Des interactions proposées entre le ligand **5.13** et des substrats disubstitués.

Nous avons entrepris l'étude en réduisant **5.15** et **5.16** en utilisant des nanoparticules **Ru4** et **Ru6**. Malgré les similitudes entre les deux substrats,

des différences importantes ont été observées. Dans le cas de **5.15**, seulement le produit *cis* totalement hydrogéné a été observé, indiquant que les deux substrats ont un mode de coordination différent à la surface des nanoparticules, ce qui, dans le cas de **5.16**, permet la formation du produit *trans*. Sans doute, le fait que le produit d'hydrogénation partielle est observé pour **5.16** indique que ce substrat pourrait être libéré de la surface des nanoparticules et coordonner dans un autre mode offrant le stéréoisomère *trans*. Toutefois, dans les essais tentés, aucune énantiosélectivité n'a été obtenue.

Lorsque l'hydrogénation du substrat **5.17** a été tentée sous 20 bars de H₂ pendant 64 heures, 78% de conversion a été obtenue et 6 % dans le cas de **5.18**. Néanmoins, aucune énantiosélectivité n'a pu être détectée.

Puis, dans le but de comparer le comportement des nanoparticules préparées dans ce chapitre avec celui de celles préparées dans les chapitres précédents et pour vérifier si un degré d'énantiosélectivité pourrait être observée dans la réduction de cétones, nous avons testé la réduction de certains dérivés de l'acétophénone. L'acétophénone et le trifluoroacétophénone ont été réduites à l'aide de toutes les nanoparticules chirales mais aucune énantiosélectivité n'a été observée.

À ce stade et après les résultats négatifs d'énantiosélectivité obtenue dans l'hydrogénation des différentes arènes, il a été décidé d'étudier l'interaction et la façon dont les ligands sont coordonnés sur la surface des nanoparticules afin d'essayer de comprendre quelles mesures devraient être prises pour atteindre notre objectif ambitieux: l'énantiosélectivité.

- Etudes de Deuteration

Récemment, Chaudret *et al.* ont rapporté un échange H/D qui permet la deutération de pyridines, quinoléines, indoles, alkylamines et composés biologiquement actifs avec D₂ en présence de nanoparticules de ruthenium stabilisées par PVP.³⁸ Cette technique permet la deutération exclusive des positions voisines à l'atome d'azote dans les différents substrats, même en présence d'autres éléments électronégatifs tels que des atomes d'oxygène.

Pour cette raison, cette méthode pourrait également être utilisée pour mieux comprendre comment les différents ligands interagissent avec la surface et pour savoir quels atomes sont coordonnés ou quels postes pourraient être proches de la surface métallique. De plus, cette technique pourrait être utile pour deutérer non seulement les postes voisins aux atomes d'azote, mais aussi aux autres centres, par exemple, aux atomes de phosphore.

La cinchonidine et le ligand **5.13** sont très complexes et pour cette raison, nous pensons qu'il serait plus facile de commencer l'étude de deutération avec des ligands plus simples. Ainsi, la triphénylphosphine, l'oxyde de triphénylphosphine et le triphénylphosphite ont été deutérés.

La triphénylphosphine a pu être monodeutérée, dideutérée ou polydeutérée en modifiant la température et le temps de réaction. Dans le cas de l'oxyde de triphénylphosphine, moins de temps était nécessaire pour monodeutérer les positions vicinales à l'atome de phosphore. Toutefois, la réduction des groupes phényles n'a pas pu être évitée. Enfin, la deutération du triphénylphosphite a été essayée dans les conditions de réaction standard utilisées précédemment et, étonnamment, aucune deutération n'a été observée.

Tous les résultats obtenus dans l'étude préliminaire de deutération nous amènent à déduire que dans le cas de la phosphine, il semble que le ligand est coordonné à travers l'atome de phosphore. Les arènes doivent être positionnés orthogonalement à la surface des nanoparticules et, par conséquent, les positions vicinales à l'atome de phosphore peuvent être facilement deutérées. Le cas de l'oxyde de phosphine est différent, le ligand ne peut pas se coordonner par l'atome de phosphore et par conséquent, l'interaction avec la surface des nanoparticules se produit par les arènes. Ce fait a pour conséquence une réduction plus facile des arènes.

Enfin, en ce qui concerne le triphénylphosphite, l'atome d'oxygène pourrait coordonner à la surface et, par conséquent, les phényles devraient être situés à proximité de la nanoparticule et donc être facilement deutérés. Mais puisqu'aucune deutération n'est observée, sans doute la coordination a lieu par l'atome de phosphore, de telle sorte que les phényles se positionnent loin de la surface des nanoparticules.

REFERENCES

1. Shylesh, S.; Schünemann, V.; Thiel, W. R. *Angew. Chem. Int. Ed.* **2010**, *49*, 3428–3459.
2. Wassersheid, P.; Keim, W. *Angew. Chem. Int. Ed.* **2000**, *39*, 3772–3789.
3. Widegren, J. A.; Finke, R. G. *J. Mol. Catal. A: Chem.* **2003**, *102*, 187–207.
4. (a) Chaudret, B. *C. R. Physique* **2005**, *6*, 117–131. (b) Philippot, K.; Chaudret, B. *C. R. Chimie* **2003**, *6*, 1019–1034.
5. Chaudret B.; Philippot, K. *Oil Gas Sci. Technol.* **2007**, *62*, 799–817.
6. (a) Lara, P.; Philippot, K.; Chaudret, B. *ChemCatChem* **2013**, *5*, 28–45. (b) Scholten, J. D.; Leal, B. C.; Dupont, J. *ACS Catal.* **2012**, *2*, 184–200. (c) Ott, L. S.; G. Finke, R. G. *Coord. Chem. Rev.* **2007**, *251*, 1075–1100.
7. Roucoux, A.; Schulz, J.; Patin, H. *Chem Rev.* **2002**, *102*, 3757–3778.
8. Roucoux, A. *Top. Organomet. Chem.* **2005**, *16*, 261–279.
9. Astruc, D.; Lu, F.; Aranzaes, J. R. *Angew. Chem., Int. Ed.* **2005**, *44*, 7852–7872.
10. Bennett, M. A.; Smith, A. K. *Dalton Trans.* **1974**, 233–241.

11. Gual, A.; Godard, C.; Castellón, S.; Claver, C. *Dalton Trans.* **2010**, 39, 11499–11512.
12. Van Hove, M. A.; Lin, R. F.; Somorjai, G. A. *J. Am. Chem. Soc.* **1986**, 108, 2532–2537.
13. (a) Dyson, P. J. *Dalton Trans.* **2003**, 2964–2974. (b) Novio, F.; Monahan, D.; Coppel, Y.; Antorrena, G.; Lecante, P.; Philippot, K.; Chaudret, B. *Chem. Eur. J.* **2014**, 20, 1287–1297.
14. Van der Steen, P. J.; Scholten, J. J. F. *Appl. Catal.* **1990**, 58, 291–304.
15. (a) Zhao, C.; Wang, H-Z.; Yan, N.; Xiao, C-X.; Mu, X-D.; Dyson, P. J.; Kou, Y. *J. Catal.* **2007**, 250, 33–40. (b) Silveira, E. T.; Umpierre, A. P.; Rossi, L. M.; Machado, G.; Morais, J.; Soares, G. V.; Baumvol, I. J. R.; Teixeira, S. R.; Fichtner, P. F. P.; Dupont, J. *Chem. Eur. J.* **2004**, 10, 3734–3740. (c) Rossi, L. M.; Machado, G. *J. Mol. Catal. A: Chem.* **2009**, 298, 69–73. (d) Escárcega-Bobadilla, M. V.; Tortosa, C.; Teuma, E.; Pradel, C.; Orejón, A.; Gómez, M.; Masdeu-Bultó, A. M. *Catalysis Today* **2009**, 148, 398–404. (e) Castelbou, J. L.; Gual, A.; Mercadé, E.; Claver, C.; Godard, C. *Catal. Sci. Technol.* **2013**, 3, 2828–2833.
16. Gonzalez-Galvez, D.; Lara, P.; Rivada-Wheelaghan, O.; Conejero, S.; Chaudret, B.; Philippot, K.; van Leeuwen, P. W. N. M. *Catal. Sci. Technol.* **2013**, 3, 99–105.
17. (a) Januszklewicz, K. R.; Alper, H. *Organometallics* **1983**, 2, 1055–1057. (b) Nasar, K.; Fache, F.; Lemaire, M.; Béziat, J.; Besson, M.; Galezot, P. *J. Mol. Catal.* **1994**, 87, 107–115.
18. Jansat, S.; Picurelli, D.; Pelzer, K.; Philippot, K.; Gómez, M.; Muller, G.; Lecante, P.; Chaudret, B. *New J. Chem.* **2006**, 30, 115–122.
19. (a) Kogan, V.; Aizenshtat, Z.; Neumann, R. *New J. Chem.* **2002**, 26, 272–274. (b) Lenarda, M.; Casagrande, M.; Moretti, E.; Storaro, L.; Frattini, R.; Polizzi, S. *Catal. Lett.* **2007**, 114, 79–84. (c) Janusklewicz, K. R.; Alper, H. *Organometallics* **1983**, 2, 1055–1057. (d) Bergault, I.; Fouilloux, P.; Joly-Vuillemin, C.; Delmas, H. *J. Catal.* **1998**, 175, 328–337. (e) Gelman, F.; Avnir, D.; Schumann, H.; Blum, J. *J. Mol. Catal. A: Chem.* **2001**, 171, 191–194. (f) Casagrande, M.; Storaro, L.; Talon, A.; Lenarda, M.; Frattini, R.; Rodriguez-Castellon, E.; Maireles-Torres, P. *J. Mol. Catal. A: Chem.* **2002**, 188, 133–139. (g) Ito, M.; Endo, Y.; Ikariya, T. *Organometallics* **2008**, 27, 6053–6055. (h) Duraczynska, D.; Drelinkiewicz, A.; Bielanska, E.; Serwicka, E. M.; Litynska-Dobrzynska, L. *Catal. Lett.* **2011**, 141, 83–94.
20. (a) Anderson, J. A.; Athawale, A.; Imrie, F. E.; Kenna, F. –M. M.; Cue, A. M.; Molyneux, D.; Power, K. *J. Catal.* **2010**, 270, 9–15. (b) Song, L.; Li, X.; Wang, H.; Wu, H.; Wu, P. *Catal. Lett.* **2009**, 133, 63–69. (c) Motoyama, Y.; Takasaki, M.; Yoon, S. H.; Mochida, I.; Nagashima, H. *Org. Lett.* **2009**, 11, 5042–5045. (d) Guerrero, M.; Roucoux, A.; Denicourt-Nowicki, A.; Bricout, H.; Monflier, E.; Collière, V.; Fajerweg, K.; Philippot, K. *Catal. Today* **2012**, 183, 34–41. (e) Chau, N. T. T.; Handjani, S.; Guegan, J.-P.; Guerrero, M.; Monflier, E.; Philippot, K.; Denicourt-Nowicki, A.; Roucoux, A. *ChemCatChem* **2013**, 5, 1497–1503. (f) Rafter, E.; Gutmann, T.; Löw, F.; Buntkowsky, G.; Philippot,

- K.; Chaudret, B.; van Leeuwen, P. W. N. M. *Catal. Sci. Technol.* **2013**, *3*, 595–599. (g) Denicourt-Nowicki, A.; Leger, B.; Roucoux, A. *Phys. Chem. Chem. Phys.* **2011**, *13*, 13510–13517. (h) Park, I. S.; Kwon, M. S.; Kang, K. Y.; Lee, J. S.; Park, J. *Adv. Synth. Catal.* **2007**, *349*, 2039–2047.
21. Fonseca, G. S.; Scholten, J. D.; Dupont, J. *Synlett* **2004**, *9*, 1525–1528.
 22. Bamforth, S. M.; Singleton, I. *J. Chem. Technol. Biotechnol.* **2005**, *80*, 723–736.
 23. *Benzo[*a*]pyrene, Polynuclear aromatic compounds, Part 1, Chemical, environmental and experimental data, Monographs on the evaluation of the carcinogenic risk of chemicals to humans*, vol. 32. International agency for research on cancer, 1983, 211–224.
 24. (a) Pawelec, B.; Campos-Martin, J. M.; Cano-Serrano, E.; Navarro, R. M.; Thomas, S.; Fierro, J. L. G. *Environ. Sci. Technol.* **2005**, *39*, 3374–3381. (b) García-Martínez, M. J.; Riva, I. D.; Canoira, L.; Llamas, J. F.; Alcántara, R.; Gallego, J. L. R. *Appl. Catal. B: Environ.* **2006**, *67*, 279–289. (c) Rivas, F. J. *Hazard. Mater.* **2006**, *138*, 234–251. (d) Ferrarese, E.; Andreottola, G.; Oprea, I. A. *J. Hazard. Mater.* **2008**, *152*, 128–139.
 25. Beckers, N. A.; Huynh, S.; Zhang, X.; Luber, E. J.; Buriak, J. M. *ACS Catal.* **2012**, *2*, 1524–1534.
 26. (a) Huang, T.; Kang, B. *Chem. Eng. J.* **1996**, *63*, 27–36. (b) Deshmukh, R. R.; Lee, J. W.; Shin, U. S.; Lee, J. Y.; Song, C. E. *Angew. Chem. Int. Ed.* **2008**, *47*, 8615–8617. (c) He, T.; Wang, Y.; Miao, P.; Li, J.; Wua, J.; Fang, Y. *Fuel* **2013**, *106*, 365–371.
 27. Ohde, M.; Ohde, H.; Wai, C. M. *Chem. Commun.* **2002**, 2388–2389.
 28. (a) Larock, R. C. *Comprehensive Organic Transformations*. New York: Wiley, 1999, 6–7, and references cited therein. (b) Lin, Q.; Shimizu, K.; Satsuma, A. *Appl. Catal. A. Gen.* **2010**, *387*, 166–172. (c) Borowski, A. F.; Vendier, L.; Sabo-Etienne, S.; Rozycka-Sokolowski, E.; Gaudyn, A. V. *Dalton Trans.* **2012**, *41*, 14117–14125.
 29. (a) Jacinto, M. J.; Santos, O. H. C. F.; Landers, R.; Kiyohara, P. K.; Rossi, L. M. *Appl. Catal. B. Environ.* **2009**, *90*, 688–692. (b) Deng, J.; Shih, W.; Mou, C. *ChemPhysChem* **2005**, *6*, 2021–2025. (c) Deng, J.; Shih, W.; Mou, C. *J. Phys. Chem. C* **2007**, *111*, 9723–9728. (d) Yoon, B.; Wai, C. M. *J. Am. Chem. Soc.* **2005**, *127*, 17174–17175. (e) Park, K. H.; Jang, K.; Kim, H. J.; Son, S. U. *Angew. Chem. Int. Ed.* **2007**, *46*, 1152–1155. (g) Pan, H.; Wai, C. M. *J. Phys. Chem. C* **2009**, *113*, 19782–19788. (h) Chen, H.-J.; Liu, H.-W.; Liao, W.; Pan, H. B.; Wai, C. M.; Chiu, K.-H.; Jen, J.-F. *Appl. Catal. B* **2012**, *111–112*, 402–408.
 30. Nador, F.; Moglie, Y.; Vitale, C.; Yus, M.; Alonso, F.; Radivoy, G. *Tetrahedron* **2010**, *66*, 4318–4325.
 31. Mallat, T.; Orglmeister, E.; Baiker, A. *Chem. Rev.* **2007**, *107*, 4863–4890.
 32. (a) Bönemann, H.; Braun, G. A. *Angew. Chem. Int. Ed.* **1996**, *35*, 1992–1995. (b) Bönemann, H.; Braun, G. A. *Chem. Eur. J.* **1997**, *3*, 1200–1202. (c) Diezi,

- S.; Reimann, S.; Bonalumi, N.; Mallat, T.; Baiker, A. *J. Catal.* **2006**, *239*, 255–262. (d) Sutyinszki, M.; Szöri, K.; Felföldi, K.; Bartók, M. *Catal. Commun.* **2002**, *3*, 125–127. (e) Zuo, X.; Liu, H. *Tetrahedron* **1999**, *55*, 7787–7804. (f) Bilé, E. G.; Cortelazzo-Polisini, E.; Denicourt-Nowicki, A.; Sassine, R.; Launay, F.; Roucoux, A. *ChemSusChem* **2012**, *5*, 91–101. (g) Beier, M. J.; Andanson, J.; Mallat, T.; Krumeich, F.; Baiker, A. *ACS Catal.* **2012**, *2*, 337–340. (h) Studer, M.; Blaser, H.; Exner, C. *Adv. Synth. Catal.* **2003**, *345*, 45–65. (i) Blaser, H.; Jalett, H.; Müller, M.; Studer, M. *Catal. Today*, **1997**, *37*, 441–467.
33. (a) LeBlond, C.; Wang, J.; Liu, Andrews, A. T.; Sun, Y. K. *J. Am. Chem. Soc.* **1999**, *121*, 4920–4921. (b) Balázsik, K.; Bartók, M. *J. Mol. Catal. A: Chem.* **2004**, *219*, 383–389.
34. Yan, N.; Yuan, Y.; Dyson, P. J. *Dalton. Trans.* **2013**, *42*, 13294–13304.
35. (a) Hu, A.; Gordon, T.; Lin, W. *J. Am. Chem. Soc.* **2005**, *127*, 12486–12487. (b) Hu, A.; Liu, S.; Lin, W. *RSC Adv.* **2012**, *2*, 2576–2580. (c) Sonnenberg, J. F.; Coombs, N.; Dube, P. A.; Morris, R. H. *J. Am. Chem. Soc.* **2012**, *134*, 5893–5899.
36. Fache, F.; Lehuede, S.; Lemaire, M. *Tetrahedron Lett.* **1995**, *36*, 885–888.
37. Gual, A.; Godard, C.; Philippot, K.; Chaudret, B.; Denicourt-Nowicki, A.; Roucoux, A.; Claver, C. *ChemSusChem* **2009**, *2*, 769–779.
38. Pieters, G.; Taglang, C.; Bonnefille, E.; Gutmann, T.; Puente, C.; Berthet, J.; Dugave, C.; Chaudret, B.; Rousseau, B. *Angew. Chem. Int. Ed.* **2014**, *53*, 230–234.

CHAPTER 1

INTRODUCTION

1.1. INTRODUCTION TO NANOPARTICLES

Nanochemistry is an exponentially growing research field in science and it involves the synthesis and application of nanoparticles with different sizes, shapes, activity and selectivity.¹

The word colloid² was introduced for the first time in 1861 and implied the suspension of a phase (solid or liquid) into a second phase, and was used for suspensions, which were neither settled nor deposited spontaneously.³

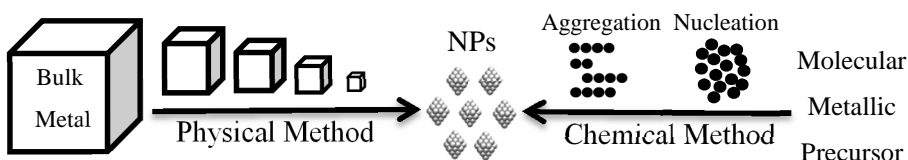
Modern transition-metal nanoclusters also called nanoparticles (NPs), are in the 1-10 nm range in diameter, smaller than classical colloids (typically >10 nm in diameter). They are isolable and redispersible, soluble in organic solvents (classical colloid were usually used in aqueous systems), and are well defined compositionally (unlike classical colloids). Nanoparticles have narrow size distributions, clean surfaces and reproducible synthesis and activities.

Soluble metal nanoparticles are at the frontier between homogeneous and heterogeneous catalysis and combine the advantages of both. They are active under mild reaction conditions, more selective than heterogeneous systems and due to their solubility and different analytical techniques can be used to study their behaviour. These systems are freely rotational and three-dimensional in reaction systems which enhance the accessibility towards the surface active sites.⁴ However, there are some drawbacks like their tendency to agglomeration and the relatively poor thermal stability.⁵

1.2. SYNTHESIS AND STABILIZATION OF METAL NANOPARTICLES

The formation of zerovalent nanoparticles can be obtained following two main methods operating in various media (aqueous, organic or a solvent mixture): the physical method and the chemical method (Scheme 1.1).⁶

The physical method also commonly named as “top-down” uses various methods of lithography to pattern nanoscale structures. It yields broad particle size dispersion, larger nanoparticles (>10nm) and bad reproducibility. On the contrary, the chemical method or the “bottom-up” approach uses interactions between colloidal particles to assemble discrete nanoscale structures in two and three dimensions. It is the most convenient way to obtain smaller isolable nanoparticles with a well-defined surface composition and with high level of reproducibility.^{3,7}



Scheme 1.1. Methods for the synthesis of metal nanoparticles (NPs).

In general, these suspensions have to be stabilized by protective agents to prevent aggregation or agglomeration to the bulk. At short interparticle distance and in the absence of repulsive forces, the van der Waals forces will attract two metallic particles to each other. For that reason, two different types of nanoparticles stabilization can be envisaged: charge stabilization and steric stabilization.

On the one hand, ionic compounds like halides, carboxylates or polyoxoanions in solution (aqueous media in general) can generate electrostatic stabilization. These compounds can create an electrical double-

layer that prevents agglomeration due to the coulombic repulsion generated between the particles (Figure 1.1). Colloidal systems stabilized by electrostatic repulsion are very sensitive to ionic strength or thermal motion which could disrupt the double layer formed.

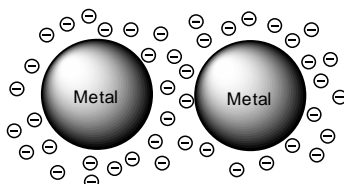


Figure 1.1. Schematic representation of electrostatic stabilization of two nanoparticles.

On the other hand, polymers, oligomers, ligands, solvents or an organic molecule containing coordination groups can be adsorbed on the particles surface providing a protective layer. These molecules will be restricted in motion in the interparticle space and the increasing of concentration will favour the interpenetration of the two protective layers. This results in an osmotic repulsion and, therefore, the media restores the equilibrium by separating the particles (Figure 1.2). The steric stabilization can be used both in organic or in aqueous phase.⁸

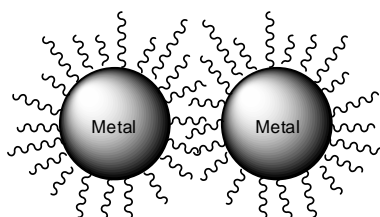


Figure 1.2. Schematic representation of steric stabilization of two nanoparticles.

The properties of nanoparticles are size dependent and it is important to control the size and the shape to reach a monodisperse assembly and to tune their activity and selectivity.¹ For this reason, the reduction methods

display limitations and, for example, the presence of salts and water can produce oxides or hydroxides that can consequently passivize the nanoparticle surface.

Chaudret *et al.*⁹ developed the use of an organometallic precursor which can be decomposed in the presence of a reducing gas (H_2 or CO) obtaining a net reduction of the metal. The ideal precursor is a zerovalent olefinic complex in which the organic ligands (olefinic or polyolefinic) can be displaced easily in mild conditions obtaining a non-contaminated surface.¹⁰ Different precursors such as $[Ru(C_8H_{10})(C_8H_{12})]$ also named as $[Ru(COD)(COT)]$ (COD: 1,5-cyclooctadiene, COT: 1,3,5-cyclooctatriene)¹¹, $[Ni(C_8H_{12})]$ ¹², $[Rh(\eta^3-C_3H_5)_3]$ ¹³ and complexes like $[Pd_2(dba)_3]$ ¹⁴, $[Pt(dba)_2]$ ¹⁵ or $[Rh(acac)(\mu^4-C_8H_{12})]$ ¹⁶ have been used. Moreover, the nanoparticles obtained by this procedure have a high degree of control on the size, shape and surface environment.

Concerning to the stabilizing agent, solvents, polymers, ionic surfactants, ionic agents and ligands can be used to stabilize nanoparticles by this approach.^{8,10,17}

1.3. CHARACTERIZATION OF NANOPARTICLES

Before studying the reactivity of nanoparticles, it is necessary to establish the surface composition in order to know how the reaction will evolve. Several techniques generally used in the field of nanomaterials such as transmission electron microscopy (TEM), high-resolution transmission electron microscopy (HRTEM), scanning electron microscope (SEM), X-ray diffraction (XRD), wide-angle X-ray scattering (WAXS), elemental analysis (EA), X-ray photoelectron spectroscopy (XPS), etc. can be used to characterize nanoparticles. Moreover techniques derived from molecular

chemistry like infrared spectroscopy (IR), UV, nuclear magnetic resonance spectroscopy in solid state or in solution (NMR) and magnetic measurements are useful to characterize the nanoparticles surface.¹⁸ The most commonly used techniques are briefly described below:

- Transition electronic microscopy (TEM) is the most commonly used technique to characterize metal nanoparticles. It can yield information such as particle size, size distribution, shape, dispersity, structure and morphology of the nanoparticles. TEM permits the visualization of thin slices of material with nanometer resolution.¹⁹ TEM has a resolution of $\pm 4 \text{ \AA}$ and HRTEM has a resolution of $\pm 2 \text{ \AA}$. The disadvantages of these techniques are: 1) electron beam induces structural rearrangement, aggregation or decomposition of the nanoparticles; 2) three dimensional samples have to be interpreted from two-dimensional images and 3) the samples are dried under high-vacuum condition, so no direct information of nanoparticles in solution is obtained.¹⁸
- X-ray diffraction (XRD) is a non-destructive technique which allows determining the composition of crystallized compounds for particles larger than 4 nm.²⁰ When the NPs are smaller, the acquisition of structural information is more difficult and broad diffractograms are expected.²¹ The peak position of X-ray diffractogram is related to the crystallographic symmetry and the peak intensity is related to the unit cell composition.
- Wide-angle X-ray scattering (WAXS) consists in the diffraction of X-rays on atoms from nanocrystals and it reveals the internal structure of the average nanocrystal core and permits an approximate assumption of nanoparticle dimensions.²² The samples are analysed in solid state, sealed in 1mm Lindemann glass capillaries. The WAXS provides a distribution

of the metal-metal bonds inside a homogeneous assembly of nanoparticles and a well-defined RDF is related to crystallised nanoparticles. Using a model is then possible to have an access to the structure and coherence length of the particle, assuming that all particles adopt the same size and structure.

- X-ray photoelectron spectroscopy (XPS) is a technique that gives information about the composition and chemical status of the elements present on the solid surface. It provides data *via* expulsion and analysis of the related energies of the electrons that come from the solid when are irradiated by X-rays. The exciting beam does not usually damage the surface.²³ The peak intensities measured indicate how much of a material is at the surface and the peak position is related to the elemental and chemical composition.
- Infrared spectroscopy (IR) is used to study the surface of nanoparticles and the adsorption of different molecules on the surface. In general, it demonstrates the clean and unoxidized nature of the nanoparticle surfaces by adding CO and the surface dynamic at room temperature. Carbon monoxide has been widely used due to its characteristic vibrational frequencies around 1800-2100 cm^{-1} . The detection of bridging CO is in general associated to the absorption on the NPs faces, the germinal ones on the edges. Furthermore, the presence of some surface oxidation leads to an important shift towards high frequencies of the typical CO bands.^{18,9}
- Nuclear magnetic resonance (NMR) spectroscopy in solid state or in solution permits the study of the intra-core metallic atoms and the ligands surrounding the metal core. This technique can give useful information on the dynamics of the surface ligands.²⁴ However, the study of the metal

core is more difficult because the nuclear-spin lattice relaxation time is really sensitive to any metallic property that the cluster can have.²⁵

1.4. GENERAL APPLICATIONS OF METAL NANOPARTICLES IN CATALYSIS

As it was commented before, transition metal colloids have generated great interest over the last decade due to their potential catalytic activity and selectivity. Nevertheless, it is important to elucidate whether if the true active catalyst is homogeneous or heterogeneous. For that reason, several studies have been performed to identify the real active species in different reactions.

The most commonly method used to identify the true catalyst in a general reaction is the poisoning of the surface by the addition of reagents that could bind to the heterogeneous catalyst inhibiting the reaction. If the activity of the catalyst remains unchanged after the addition of the poisoning (mercury or CO), then the reaction would be most likely homogeneous.²⁶ However, mercury may react with certain complexes or ligands deactivating the catalyst in homogeneous systems too and, consequently, the results obtained using this test are not conclusive.

Ligands like CS₂, PPh₃ or thiols can also be used as poisons. When less than one equivalent of ligand for surface atoms stops the activity, then it can be deduced the presence of an heterogeneous catalyst.^{5,27}

In some cases, the type of reactivity observed permits the determination of the real catalyst. For instance, Dupont *et al.* reported the used of Rh and Ir NPs stabilised by ionic liquids for the hydrogenation of arenes. In this study, hydrogenolysis products which are related to surface

metal catalysis were observed and, consequently, the presence of homogeneous systems was discarded.²⁸

Furthermore, the study of the kinetics of a reaction can also be useful to determine the nature of the catalyst. When nanoparticles are the real catalyst, no induction period is expected and an exponential decay kinetic curve should be observed.²⁹ However, in some examples an incubation period has been observed while the real heterogeneous catalyst is formed from a homogeneous compound.³⁰

All these techniques help to obtain information about the system although an unambiguous and conclusive distinction between homogeneous and heterogeneous catalysis is very difficult to achieve.

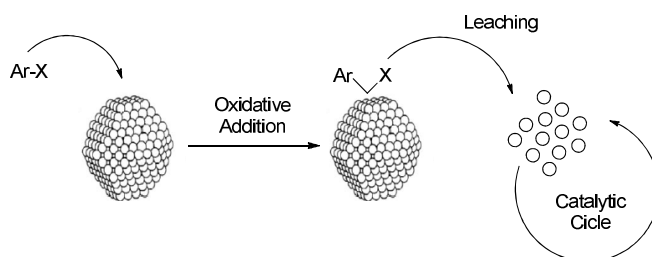
Nanoparticles have been widely used as catalysis in several reactions such as oxidation, cross coupling, hydroformylation and hydrogenation reactions among others.³ An overview of the uses of nanoparticles in catalysis will be described in the following section.

1.4.1. NANOPARTICLES IN C-C COUPLING REACTIONS

Coupling reactions like Suzuki, Heck and Sonogashira reactions have been widely described with Pd catalysts providing large turn over numbers.³¹

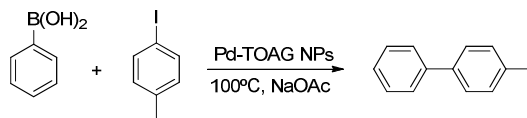
Herrmann was the first one to describe the use of Pd nanoparticles in a Heck coupling reaction.³² Several examples have been reported³³ and, in general, a higher activity was observed when the arenes are substituted with an electron-withdrawing groups such as a nitro or a carbonyl. However, more investigations are required to determine the real catalyst.³ Palladium nanoparticles, either preformed or generated *in situ*, can act as a reservoir of molecular complexes becoming the true catalytically active species. The

accepted mechanism involves an oxidative addition of the aryl halide substrate to the colloid surface, then a leaching of Pd(II) molecular species takes place that enter in the catalytic cycle and reform the nanoparticles at the end of the reaction (Scheme 1.2).³⁴



Scheme 1.2. Representation of the accepted mechanism for Heck reaction with Pd NPs as catalytic precursors.³⁴

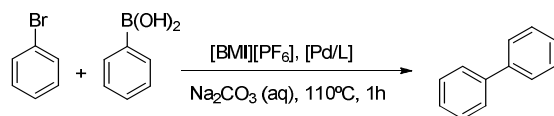
A similar behaviour was observed in Suzuki coupling reactions. For instance, Rothenberg and co-workers used a membrane reactor and concluded that the molecular species leached from palladium nanoparticles were the responsible of catalysis (Scheme 1.3).³⁵ Dyson *et al.* used nitrile-functionalized ionic liquids as solvent, forming nanoparticles *in situ* from PdCl₂ for Suzuki and Stille reactions. Nevertheless, the catalyst in this case could also be the Pd molecular species and the nanoparticles were considered to act as reservoirs.³⁶



Scheme 1.3. Pd nanocolloids stabilized by tetraoctylammonium glycolate (TOAG) in a Suzuki cross-coupling reaction.³⁵

It has also been demonstrated the influence of the solvent and the decisive role of nanoparticles for Suzuki reactions. While in organic solvents, good donor ligands lead to the formation of stable complexes, in ionic liquids,

palladium systems are only active when nanoparticles are generated (probably acting as reservoir).³⁷ However, Chang *et al.* reported a ruthenium-catalysed olefination and Suzuki cross-coupling reactions in which they proposed that the real catalytic species were Ru nanoparticles even when a homogeneous complex precursor such as $[\text{RuCl}_2(p\text{-cymene})]_2$ was employed.³⁸ Similar trend was observed by Gómez *et al.* that performed Suzuki C-C coupling reactions using Pd nanoparticles. The inactivity detected for the molecular precursor and for the palladium powder confirmed the colloidal nature of the catalyst.³⁹



Scheme 1.4. C-C coupling between bromobenzene and phenylboronic acid using Pd NPs.^{37, 39}

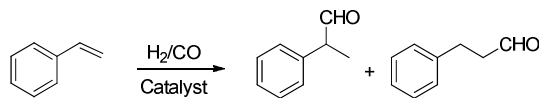
The carbonylation of methanol is another C-C coupling reaction with a lot of importance in industrial processes. Rh nanoparticles stabilized by PVP have been used in this reaction obtaining lower activities than the homogeneous system already described. The catalysis was due to Rh(I) species formed by oxidation of nanoparticles by the methyl iodide present in the media.⁴⁰

Other C-C coupling reaction like cycloaddition,⁴¹ allylation,⁴² aldol and Mannich-type⁴³ reactions have also been described by using nanocolloids.

1.4.2. NANOPARTICLES IN HYDROFORMYLATION REACTIONS

The hydroformylation using nanoparticles (Scheme 1.5) is a reaction in which the role of the metal is not clear. Some results point out that the

nature of the catalysts are nanoparticles⁴⁴ but other studies⁴⁵ show that the real catalyst is homogeneous.



Scheme 1.5. Hydroformylation reaction.

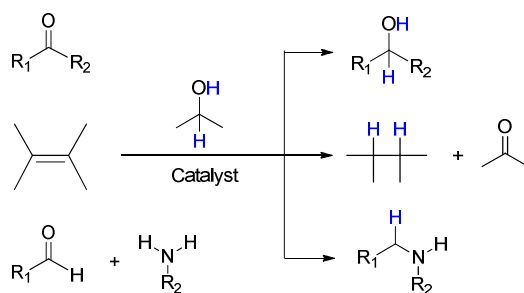
Hydroformylation of olefins in neat condition using unmodified or Xantphos-modified Rh nanoparticles have been reported. The hydroformylation of 1-alkenes has a strong influence on the nanoparticle size and linear/branched selectivities up to 25% were achieved. Moreover, TEM, XRD, IR and NMR experiments indicated that Rh (0) NPs were probably degraded into soluble mononuclear Rh-carbonyl catalytically active species.⁴⁶

Then Chaudret *et al.* used rhodium nanoparticles stabilized by a chiral diphosphite ligand in the hydroformylation of styrene. Although the diluted experiments and the poisoning test were not conclusive, the *in situ* HP NMR revealed the formation of molecular species which could act as the true catalyst.⁴⁷

Recently, it has been reported a Rh nanoparticle system formed in a HPS matrix for the hydroformylation reactions in scCO₂.⁴⁸

1.4.3. NANOPARTICLES IN HYDROGEN TRANSFER REACTIONS

The transfer hydrogenation process is safer and more environmentally benign process than other reduction processes. In general, 2-propanol is used as source of hydrogen because it is cheap and easy to remove (Scheme 1.6).⁴⁹



Scheme 1.6. Transfer hydrogenation reactions.

Nickel (0) nanoparticles have been used in the transfer hydrogenation of olefins⁵⁰, carbonyl compounds⁵¹ and in the reductive amination of aldehydes⁵².

Zeolite supported copper nanoparticles were used in reduction of aromatic and aliphatic carbonyl compounds by transfer hydrogenation in high yields.⁵³

Moreover, magnetic silica-supported ruthenium nanocatalyst was developed for the transfer hydrogenation of carbonyl compounds. Due to the magnetic nature of the nanoparticles it can be separated by an external magnet and, therefore, the filtration of the catalyst is avoided.⁵⁴

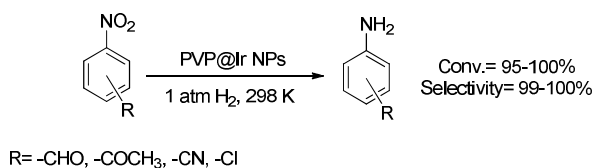
Finally, it is important to highlight that iron nanoparticles have been used in the asymmetric transfer hydrogenation of ketones. Although several methods like poisoning with PMe_3 , kinetic analysis and image techniques have been used, it is difficult to rule out completely the fact that small amount of homogeneous catalyst is generated during the reaction.⁵⁵

1.4.4. NANOPARTICLES IN HYDROGENATION REACTIONS

Metal nanoparticles have been widely used in hydrogenation reactions of different functional groups. For instance, reduction of substrates bearing terminal, internal or cyclic olefins have been investigated. In general, good results in terms of activities and selectivities were obtained.³ An important substrate which has been hydrogenated by several types of metal nanoparticles is styrene. This substrate is of great interest due to the fact that it cannot be hydrogenated by classical homogeneous systems like Wilkinson's catalyst and in the case of heterogeneous catalysts, the hydrogenation does not only take place in the alkene but also in the arene

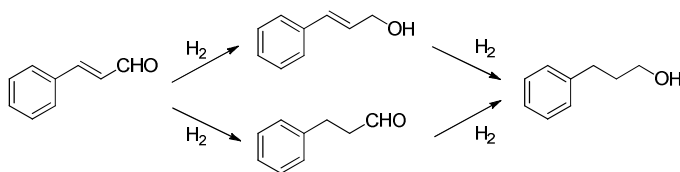
In general, ruthenium,⁵⁶ rhodium⁵⁷ and, in less proportion, palladium⁵⁸ nanoparticles have been used. As an example, Philippot *et al.* reported the synthesis of water soluble ruthenium nanoparticles stabilised by alkyl sulphonated diphosphines for the hydrogenation of styrene. Different proportion of ligand were used to stabilise the nanoparticles and the ones with higher L/Ru ratio provided an increase towards the formation of ethylbenzene by restricting the approach of the aromatic ring to the more hindered nanoparticle surface.⁵⁹

The reduction of other functionalities like nitro groups has been also performed using nanoparticles. Contrary to what occurs when heterogeneous systems are used, by-products like azo and azoxy derivatives and hydroxylamines are not formed in notable proportions. Several examples have been reported,^{3,60} for instance, iridium nanoparticles stabilised by PVP has been used in the hydrogenation of nitroaromatics containing aldehydes, ketones, nitriles and chlorides.⁶¹ Really good results in terms of chemoselectivity were achieved and the corresponding aniline compounds were obtained leaving the other functional groups intact (Scheme 1.7).



Scheme 1.7. Selective hydrogenation of nitroaromatics by iridium nanoparticles.⁶¹

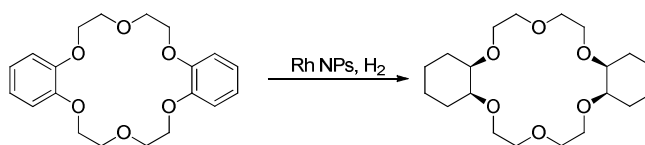
Another example of selective reduction of a substrate containing more than one reducible functional groups is the hydrogenation of unsaturated carbonyls into unsaturated alcohols.⁶² One of the first examples reported was the chemoselective hydrogenation of cinnamaldehyde into cinnamic alcohol using several bimetallic colloids such as Pt, Pt/Co in PVP or Pt immobilized in supports like polystyrene or alumina. Selectivity up to 99 % at 84% of conversion towards the selective hydrogenation of the alkene was obtained when PVP-Pt-FeCl₃ was used as catalytic system (Scheme 1.8).⁶³



Scheme 1.8. Pathways for the cinnamaldehyde hydrogenation.⁶³

Regioselective hydrogenations using transition metal colloids such as hydrogenation of conjugated dienes to monoolefins⁶⁴ and hydrogenation of conjugated alkyne-alkene compounds to dienes, have been reported.⁶⁵

Stereoselective hydrogenations have also been performed. As an example, Lemaire developed the stereoselective hydrogenation of dibenzo-18-crown-6-ether (DB18C6) using Rh nanoparticles obtaining as the major product the *cis-syn-cis* compound (Scheme 1.9).⁶⁶



Scheme 1.9. Reduction of DB18C6 using rhodium nanoparticles stabilized by trioctylamine.⁶⁶

Finally, it is important to put the accent on the use of nanoparticles for arene hydrogenation. Nanoparticles have emerged as the solution for reducing aromatic rings under mild reaction conditions. Ruthenium, rhodium, iridium and platinum nanoparticles are the metals of choice for this purpose and a general overview will be presented in the following section.

1.5. ARENE HYDROGENATION

Nowadays, the hydrogenation of arenes is an important area of research owing to the interesting industrial application. The most important application of the arene hydrogenation reaction is the hydrogenation of benzene to cyclohexene for the adipic acid production (nylon precursor).^{3,5,8,67}

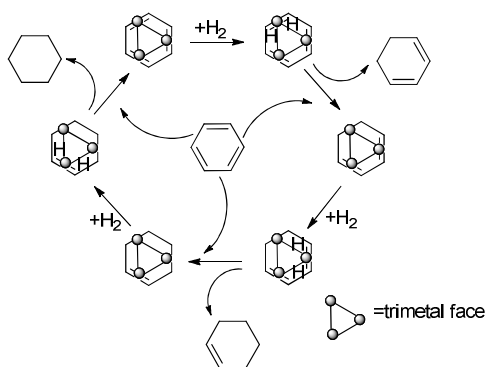
The generally accepted mechanism for the hydrogenation of arenes was proposed in 1974.⁶⁸ This mechanism can be applied for arenes that interact with more than one metal centre like in clusters, nanoparticles or bulk metal surfaces.⁶⁹ Furthermore, other interesting reactions like the partial arene hydrogenation for the synthesis of cyclohexenes, the treatment of diesel to obtain low-aromatic-content diesel fuels and the hydrogenation of aromatic polymers to produce new materials are reactions with a high industrial interest.

The hydrogenation of arenes is much more difficult than the hydrogenation of simple olefins due to the resonance stabilization energy that

is lost during the hydrogenation. Traditionally, Rh/Al₂O₃, metal sulfides and Raney NickelTM have been the catalysts of choice for the hydrogenation of monocyclic arenes. Nevertheless, drastic conditions in terms of pressure and/or temperature were required.⁷⁰

Regarding the homogeneous catalysis, some examples have been reported although, in some cases, the true catalyst was concluded to be colloidal systems formed under the reaction conditions.⁷¹ For instance, bulk ruthenium metal has been demonstrated to be the true catalyst in the benzene hydrogenation using as precatalyst the molecular complex Ru(II)(η^6 -C₆Me₆)(OAc)₂.⁷²

The coordination modes of arenes (η^6), cyclohexadiene (η^4) and cyclohexene (η^2) to several metallic centres have been crystallographically characterized.^{26a,73} A common coordination mode in cluster chemistry and on metal surfaces is the μ_3 - η^2 : η^2 : η^2 (Scheme 1.10).

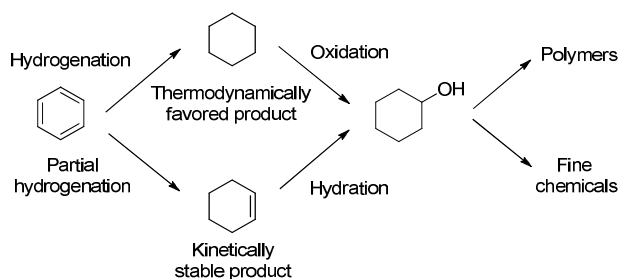


Scheme 1.10. Proposed arene-exchange mechanism on a metal face in a homogeneous cluster or heterogeneous catalyst.⁶⁹

The addition of hydrogen across one double bond leads to a μ_3 - η^2 : η^2 -diene and further hydrogenation results in a monoene.⁷⁴ The release of the diene and monoene products can take place by replacement of the partially hydrogenated product by a new arene substrate.⁶⁹

1.5.1. PARTIAL ARENE HYDROGENATION

Partial reduction of arenes to cyclic dienes or monoenes represents a synthetically useful reaction due to the straightforward formation of cyclohexanol *via* hydration (Scheme 1.11). This reduction is generally conducted with stoichiometric reagents like in the Birch reduction.²⁶

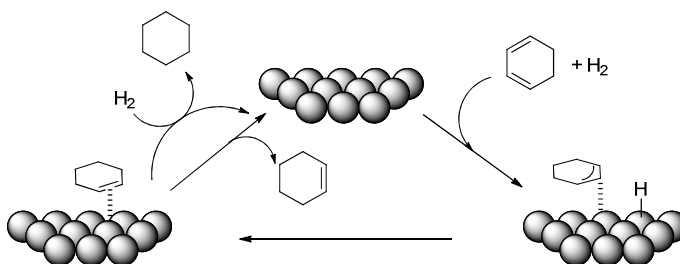


Scheme 1.11. Industrial application of partially hydrogenated arenes.⁷⁵

The most effective catalyst for the hydrogenation of benzene to cyclohexene used on an industrial scale employs a selective bilayer catalytic system using ruthenium metal catalyst, ZrO_2 and $ZnSO_4$. The process affords 60% of selectivity and 90% of conversion.⁷⁶

Nanoparticles represent a new opportunity for the partial hydrogenation of arenes. However, there are some obstacles to overcome due to the easy reduction of the double bonds once the aromaticity is lost. Moreover, the elimination of a diene coordinated or chemisorbed to the metal is a difficult task.⁷⁷

It is assumed that in the case of nanoparticles, the arene reduction occurs through a Horiuti-Polanyi mechanism and the product selectivity depends on the affinity of the partially hydrogenated product with the surface (Scheme 1.12).⁷⁸



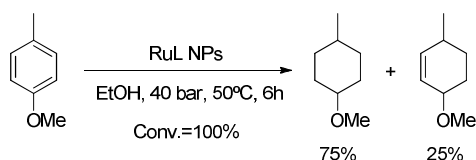
Scheme 1.12. Full and partial hydrogenation of 1,3-cyclohexadiene mechanism by surface atoms.⁷⁸

In general, palladium nanoparticles are the most common catalysts used in the partial hydrogenation of 1,3-dienes. Nevertheless, the specific case of partial hydrogenation of benzene is limited to the use of aqueous reaction media⁷⁹ or the use of ionic liquids where the solubility of the substrate is higher than that of the cyclohexene product. Furthermore, the best selectivity obtained is lower than 39% at very low benzene conversion (<1%) using ruthenium nanoparticles stabilized by imidazolium ionic liquids.⁸⁰ The same type of ionic liquids were used by Machado *et al.* obtaining 65% of selectivity towards cyclohexene product at 0.3% of benzene conversion.⁸¹

In relation to the partial hydrogenation of substituted arenes, the higher steric hindrance generated by the presence of the substituents affects the selectivity since the bulky groups favour the dissociation of the partially hydrogenated product from the catalyst surface and disfavour the re-adsorption.

Some example of partial hydrogenation of substituted arenes have been reported using nanoparticles.^{79,80b} For instance, Masdeu-Bultó, Gómez and co-workers reported the use of rhodium and ruthenium nanoparticles stabilized by phosphines containing fluorinated groups (PPh_3 and $\text{P}[3,5-(\text{CF}_3)_2\text{C}_6\text{H}_3]_3$) in the partial hydrogenation of methylanisoles obtaining selectivity up to 15% at 21% of conversion in a scCO_2 media.⁸² The same

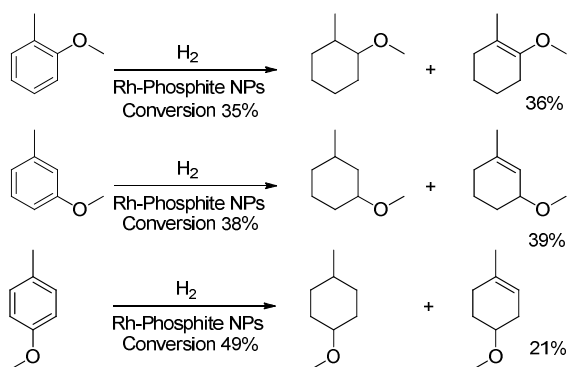
group reported the use of ruthenium nanoparticles stabilized by 4-(3-phenylpropyl)-pyridine in the hydrogenation of different substrates and obtaining 25% of selectivity for the partial hydrogenation product of *p*-methylanisole (Scheme 1.13).^{56b}



Scheme 1.13. Hydrogenation of *p*-methylanisole using Ru NPs stabilised by 4-(3-phenylpropyl)-pyridine.^{56b}

Chaudret and van Leeuwen reported the use of NHC carbenes to stabilize ruthenium nanoparticles in the hydrogenation of different arenes. At 393 K and 20% of conversion, approximately 60% of the partial hydrogenation of *o*-methylanisole was obtained.⁸³

Recently, a series of P-donor stabilized Rh-NPs have also been used in the partial hydrogenation of xylenes and methylanisoles with selectivity up to 39% at relatively high conversions (Scheme 1.14).⁷⁵

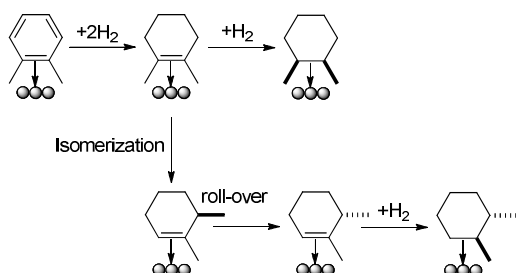


Scheme 1.14. Hydrogenation of *o*-, *m*-, *p*-methylanisole with Rh-phosphite NPs.⁷⁵

1.5.2. *CIS/TRANS* SELECTIVITY IN ARENE HYDROGENATION

The substituents on disubstituted aromatic compounds have an important effect not only on the reaction rate, but also in the *cis/trans* selectivity. The *cis* isomer is the only product expected if the aromatic substrate is adsorbed in a flat fashion on the surface. However, in some arene hydrogenations, the *trans* product is also obtained as a minor product. For that reason, the *cis* stereoisomer is considered as the kinetically favoured product whereas the *trans* isomer as the thermodynamically favoured.

The selectivity towards the *cis* stereoisomer is rationalized by a continuous addition of hydrogen to only one face of the arene and the *trans* stereoisomer is formed when a partially hydrogenated intermediate dissociates from the nanoparticle surface and re-associates with the opposite face before further hydrogenation (Scheme 1.15).⁵



Scheme 1.15. Proposed mechanism for the hydrogenation of disubstituted arenes on metal surfaces.⁶⁹

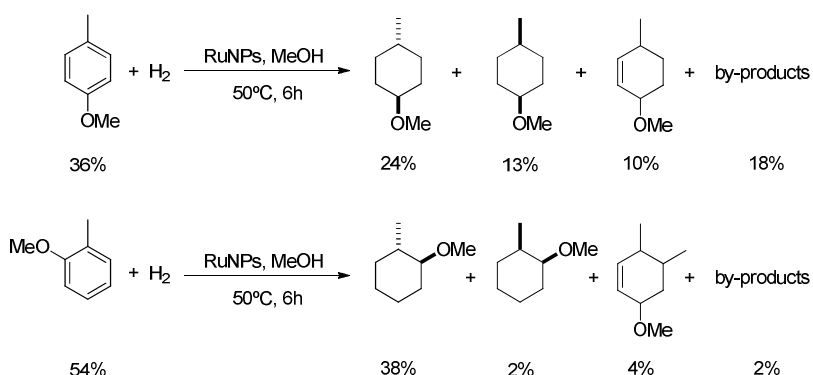
Di-substituted arenes like methylanisoles or xylenes have been typically used to study the *cis/trans* selectivity in hydrogenation reactions by NPs. Alper and co-workers hydrogenate the *p*-methylanisole obtaining just the *cis*-product using Rh nanoparticles (92% yield)⁸⁴ and Lemaire, Gallezot *et al.* found *cis*-selectivities up to 97% in the hydrogenation of *o*-

methylanisole using Rh- and Ru-nanocatalyst (higher *cis* selectivities were observed for arenes bearing electron-withdrawing substituents).⁸⁵

Furthermore, nanoparticles stabilized by carbohydrate-derived 1,3-diphosphite ligands,⁸⁶ chiral ammonium-capped rhodium nanoparticles⁸⁷ and ruthenium nanoparticles stabilized by carbenes⁸³ have been used to hydrogenate methylanisoles obtaining always the *cis*-stereoisomer as the major one.

The temperature and the hydrogen pressure can have an important influence on the *cis/trans* selectivity. Schuetz and Siegel reported higher *cis* selectivities in the hydrogenation of xylenes when the pressure was increased and the temperature decreased. Under this reaction conditions, the substrate was rapidly hydrogenated avoiding the desorption during the catalysis.⁸⁸

Finally, it is interesting to highlight the fact that using Ru-NPs stabilized by chiral mono-oxazolines, the *trans* product was obtained as the major one in a *trans:cis* ratio of 19:1 (Scheme 1.16).⁸⁹

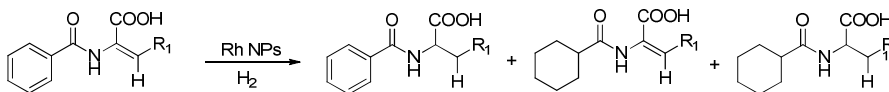


Scheme 1.16. Hydrogenation of *ortho*- and *para*-methylanisole catalysed Ru NPs stabilised by mono-oxazolines.⁸⁹

1.5.3. ARENE HYDROGENATION VS. OTHER FUNCTIONAL GROUPS. CHEMOSELECTIVITY.

Contrary to what it generally happens with heterogeneous catalysts, nanoparticles can act as selective system for the chemoselective reduction of an arene in the presence of other reducible functional groups.

Arenes containing imide groups have been hydrogenated using nanoparticles.⁹⁰ For instance, rhodium nanoparticles stabilised by solid ammonium salts which formed ionic liquids in solution have been used. Selectivities up to 96% at 60% of conversion towards the hydrogenation of the arene in the presence of an alkene was achieved at 100 bar of H₂ and 60°C when the R₁ group was 2,4,5,6-tetramethylpyrimidine (Scheme 1.17).⁹¹



Scheme 1.17. Hydrogenation of (*E*)-2-(benzoylamino)-2-propenoic acids.

Fewer examples of aromatic rings hydrogenation by nanoparticles in the presence of esters⁹² and amides⁹³ have been reported. Concerning esters, rhodium nanoparticles on charcoal have been used to reduce methyl benzoate obtaining 100% of selectivity towards the hydrogenation of the arene under 1 atm of H₂.⁹⁴

Finally, the chemoselective hydrogenation of an aromatic arene in the presence of a ketone has also been studied using different metallic nanoparticles. A more detailed review of the literature related to this topic is presented in Chapter 3 of this thesis.

1.6. REFERENCES

1. Shylesh, S.; Schünemann, V.; Thiel, W. R. *Angew. Chem. Int. Ed.* **2010**, *49*, 3428–3459.
2. Graham, T. *Philos. Trans. R. Soc.* **1861**, *151*, 183–224.
3. Roucoux, A.; Schulz, J.; Patin, H. *Chem Rev.* **2002**, *102*, 3757–3778.
4. Wassersheid, P.; Keim, W. *Angew. Chem. Int. Ed.* **2000**, *39*, 3772–3789.
5. Widegren, J. A.; Finke, R. G. *J. Mol. Catal. A: Chem.* **2003**, *102*, 187–207.
6. Roucoux, A.; Nowicki, A.; Philippot, K. Rhodium and Ruthenium Nanoparticles in Catalysis. In *Nanoparticles and Catalysis Volume 1*; Astruc, D., Ed.; Wiley-VCH: Weinheim, 2008; pp 349–386.
7. Gates, B.; Xuo, Q.; Stewart, M.; Ryan, D.; Willson, C. G.; Whitesides, G.M. *Chem. Rev.* **2005**, *105*, 1171–1196.
8. Roucoux, A. *Top. Organomet. Chem.* **2005**, *16*, 261–279.
9. (a) Chaudret, B. *C. R. Physique* **2005**, *6*, 117–131. (b) Philippot, K.; Chaudret, B. *C. R. Chimie* **2003**, *6*, 1019–1034.
10. Chaudret B.; Philippot, K. *Oil Gas Sci. Technol.* **2007**, *62*, 799–817.
11. Vidoni, O.; Philippot, K.; Amiens, C.; Chaudret, B.; Balmes, O.; Malm, J.; Bovin, J.; Senocq, F.; Casanove, M. *Angew. Chem. Int. Ed.* **1999**, *38*, 3736–3738.
12. Ely, T. O.; Amiens, C.; Chaudret, B.; Snoeck, E.; Verelst, M.; Respaud, M.; Broto, J. *Chem. Mater.* **1999**, *11*, 526–529.
13. Wostek-Wojciechowska, D.; Jeszka, J. K.; Amiens, C.; Chaudret, B.; Lecante, P. *J. Colloid Interface Sci.* **2005**, *287*, 107–113.
14. Ramirez, E.; Jansat, S.; Philippot, K.; Lecante, P.; Gómez, M.; Masdeu-Bultó, A. M.; Chaudret, B. *J. Organomet. Chem.* **2004**, *689*, 4601–4610.
15. Ramirez, E.; Eradès, L.; Philippot, K.; Lecante, P.; Chaudret, B. *Adv. Funct. Mater.* **2007**, *17*, 2219–222.
16. Zitoun, D.; Respaud, M.; Fromen, M.; Casanove, M. J.; Lecante, P.; Amiens, C.; Chaudret, B. *Phys. Rev. Lett.* **2002**, *89*, 037203/1–037203/4.
17. (a) Lara, P.; Philippot, K.; Chaudret, B. *ChemCatChem* **2013**, *5*, 28–45. (b) Scholten, J. D.; Leal, B. C.; Dupont, J. *ACS Catal.* **2012**, *2*, 184–200. (c) Ott, L. S.; G. Finke, R. G. *Coord. Chem. Rev.* **2007**, *251*, 1075–1100.
18. Chaudret, B. *Top. Organomet. Chem.* **2005**, *16*, 233–259.
19. Akbari, B.; Tavandashti, M. P.; Zandrahimi, M. *Iran. J. Mater. Sci. Eng.* **2011**, *8*, 48–56.
20. Epron, F.; Especel, C.; Lafaye, G.; Marécot, P. Multimetallic Nanoparticles Prepared by Redox Processes Applied in Catalysis. In *Nanoparticles and Catalysis Volume 1*; Astruc, D., Ed.; Wiley-VCH: Weinheim, 2008; pp 279–302.

21. Reetz, M. T.; Winter, M.; Breinbauer, R.; Thurn-Albrecht, T.; Vogel, W. *Chem. Eur. J.* **2001**, *7*, 1084–1094.
22. Arici, E. Inorganic nanoparticles for photovoltaic applications. In *Inorganic Nanoparticles: Synthesis, Applications and Perspectives*; Altavilla, C.; Ciliberto, E., Ed.; CRC Press: U.S.A., 2011; pp 197–198.
23. Leofanti, G.; Tozzola, G.; Padovan, M.; Petrini, G.; Bordiga, S.; Zecchina, A. *Catalysis Today* **1997**, *34*, 307–327.
24. (a) Pan, C.; Pelzer, K.; Philippot, K.; Chaudret, B.; Dassenoy, F.; Lecante, P.; Casanove, M. *J. Am. Chem. Soc.* **2001**, *123*, 7584–7593. (b) Novio, F.; Philippot, K.; Chaudret, B. *Catal. Lett.* **2010**, *140*, 1–7. (c) González-Galvez, D.; Nolis, P.; Philippot, K.; Chaudret, B.; van Leeuwen, P. W. N. M. *ACS Catal.* **2012**, *2*, 317–321. (d) Bronger, R.; Le, T. D.; Bastin, S.; Carcía-Antón, J.; Citadelle, C.; Chaudret, B.; Lecante, P.; Igau, A.; Philippot, K. *New J. Chem.* **2011**, *42*, 2653–2660.
25. Aiken III, J. D.; Finke, R. G. *J. Mol. Catal. A:Chem.* **1999**, *145*, 1–44.
26. (a) Dyson, P. J. *Dalton. Trans.* **2003**, 2964–2974. (b) Novio, F.; Monahan, D.; Coppel, Y.; Antorrena, G.; Lecante, P.; Philippot, K.; Chaudret, B. *Chem. Eur. J.* **2014**, *20*, 1287–1297.
27. Gómez, M.; Favier, I. Chapter 31 in *Metal Nanoclusters in Catalysis and Material Science: The issue of size control*. Amsterdam: Elsevier, 2008.
28. Fonseca, G. S.; Umpierre, A. P.; Fichtner, P. F. P.; Teixeira, S. R.; Dupont, J. *Chem. Eur. J.* **2003**, *9*, 3263–3269.
29. Watzky, M. A.; Finke, R. G. *J. Am. Chem. Soc.* **1997**, *119*, 10382–10400.
30. Weedle, K. S.; Aiken III, J. D.; Finke, R. G. *J. Am. Chem. Soc.* **1998**, *120*, 5653–5666.
31. Taladriz-Blanco, P.; Hervés, P. *Top Catal.* **2013**, *56*, 1154–1170.
32. Beller, M.; Fischer, H.; Kühlein, K.; Reisinger, C. P.; Herrmann, W. A. *J. Organomet. Chem.* **1996**, *520*, 257–259.
33. (a) Consorti, C. S.; Zanini, M. L.; Leal, S.; Ebeling, G.; Dupont, J. *Org. Lett.* **2003**, *5*, 983–986. (b) de Vries, A. H. M.; Mulder, J. M. C. A.; Mommers, J. H. M.; Henderickx, H. J. W.; de Vries, J. G. *Org. Lett.* **2003**, *5*, 3285–3288. (c) Trzeciak, A. M.; Ziólkowski, J. *J. Coord. Chem. Rev.* **2005**, *249*, 2308–2322. (d) Phan, N. T. S.; Van Der Sluys, M.; Jones, C. W. *Adv. Synth. Catal.* **2006**, *348*, 609–679. (e) Trzeciak, A. M.; Ziólkowski, J. *J. Coord. Chem. Rev.* **2007**, *251*, 1281–1293. (f) Reetz, M. T.; Westermann, E. *Angew. Chem. Int. Ed.* **2000**, *39*, 165–168. (g) Reetz, M. T.; de Vries, J. G. *Chem. Commun.* **2004**, 1559–1563.
34. Durand, J.; Teuma, E.; Gómez, M. *Eur. J. Inorg. Chem.* **2008**, 3577–3586.
35. Gaikwad, A. V.; Holuigue, A.; Thathagar, M. B.; ten Elshof, J. E.; Rothenberg, G. *Chem. Eur. J.* **2007**, *13*, 6908–6913.
36. (a) Zhao, D.; Fei, Z.; Geldbach, T. J.; Scopelliti, R.; Dyson, P. J. *J. Am. Chem. Soc.* **2004**, *126*, 15876–15882. (b) Fei, Z.; Zhao, D.; Pieraccini, D.; Ang, W. H.;

- Geldbach, T. J.; Scopelliti, R.; Chiappe, C.; Dyson, P. J. *Organometallics* **2007**, *26*, 1588–1598.
37. Fernández, F.; Cordero, B.; Durand, J.; Muller, G.; Malbosc, F.; Kihn, Y.; Teuma, E.; Gómez, M. *Dalton Trans.* **2007**, 5572–5581.
38. Na, Y.; Park, S.; Han, S. B.; Han, H.; Ko, S.; Chang, S. *J. Am. Chem. Soc.* **2004**, *126*, 250–258.
39. Durand, J.; Teuma, E.; Malbosc, F.; Kihn, Y.; Gómez, M. *Catal. Commun.* **2008**, *9*, 273–275.
40. Wang, Q.; Liu, H.; Han, M.; Li, X.; Jiang, D. *J. Mol. Catal. A: Chem.* **1997**, *118*, 145–151.
41. (a) Reetz, M. T.; Breinbauer, R.; Wedemann, P.; Binger, P. *Tetrahedron* **1998**, *54*, 1233–1240. (b) Chahdoura, F.; Pradel, C.; Gómez, M. *ChemCatChem* **2014**, *6*, 2929–2936.
42. (a) Akiyama, R.; Kobayashi, S. *Angew. Chem., Int. Ed.* **2001**, *40*, 3469–3471. (b) Jansat, S.; Gómez, M.; Philippot, K.; Muller, G.; Guiu, E.; Claver, C.; Castellón, S.; Chaudret, B. *J. Am. Chem. Soc.* **2004**, *126*, 1592–1593. (c) Favier, I.; Gómez, M.; Muller, G.; Axet, M. R.; Castellón, S.; Claver, C.; Jansat, S.; Chaudret, B.; Philippot, K. *Adv. Synth. Catal.* **2007**, *349*, 2459–2469. (d) Diéguez, M.; Pàmies, O.; Mata, Y.; Teuma, E.; Gómez, M.; Ribaudó, F.; van Leeuwen, P. W. N. M. *Adv. Synth. Catal.* **2008**, *350*, 2583–2598. (e) Reimann, S.; Mallat, T.; Baiker, A. *J. Catal.* **2008**, *254*, 79–83.
43. Manabe, K.; Mori, Y.; Wakabayashi, T.; Nagayama, S.; Kobayashi, S. *J. Am. Chem. Soc.* **2000**, *122*, 7202–7207.
44. Han, D.; Li, X.; Zhang, H.; Liu, Z.; Li, J.; Li, C. *J. Catal.* **2006**, *243*, 318–328.
45. Tuchbreiter, T.; Mecking, S. *Macromol. Chem. Phys.* **2007**, *208*, 1688–1693.
46. Bruss, A. J.; Gelesky, M. A.; Machado, G.; Dupont, J. *J. Mol. Catal. A: Chem.* **2006**, *252*, 212–218.
47. Axet, R. M.; Castellón, S.; Claver, C.; Philippot, K.; Lecante, P.; Chaudret, B. *Eur. J. Inorg. Chem.* **2008**, 3460–3466.
48. Lyubimov, S. E.; Rastorguev, E. A.; Lubentsova, K. I.; Korlyukov, A. A.; Davankov, V. A. *Tetrahedron Lett.* **2013**, *54*, 1116–1119.
49. Alonso, F.; Riente, P.; Yus, M. *Acc. Chem. Res.* **2011**, *44*, 379–391.
50. Dhakshinamoorthy, A.; Pitchumani, K. *Tetrahedron Lett.* **2008**, *49*, 1818–1823.
51. (a) Alonso, F.; Riente, P.; Yus, M. *Tetrahedron Lett.* **2008**, *49*, 1939–1942. (b) Alonso, F.; Riente, P.; Yus, M. *Tetrahedron* **2008**, *64*, 1847–1852.
52. Alonso, F.; Riente, P.; Yus, M. *Synlett* **2008**, 1289–1292.
53. Subramanian, T.; Pitchumani, K. *Catal. Sci. Technol.* **2012**, *2*, 296–300.
54. Baig, R. B. N.; Varma, R. S. *ACS Sustainable Chem. Eng.* **2013**, *1*, 805–809.
55. Sonnenberg, J. F.; Coombs, N.; Dube, P. A.; Morris, R. H. *J. Am. Chem. Soc.* **2012**, *134*, 5893–5899.

56. (a) Nowicki, A.; Zhang, Y.; Léger, B.; Rolland, J.; Bricout, H.; Monflier, E.; Roucoux, A. *Chem. Commun.* **2006**, 296–298. (b) Jahjah, M.; Kihn, Y.; Teuma, E.; Gomez, M. *J. Mol. Catal. A: Chem.* **2010**, 332, 106–112. (c) Denicourt-Nowicki, A.; Ponchel, A.; Monflier, E.; Roucoux, A. *Dalton Trans.* **2007**, 5714–5719.
57. (a) Mervellec, V.; Leger, B.; Mauduit, M.; Roucoux, A. *Chem. Commun.* **2005**, 2838–2839. (b) Léger, B.; Denicourt-Nowicki, A.; Olivier-Bourbigou, H.; Roucoux, A. *Inorg. Chem.* **2008**, 47, 9090–9096. (c) Yang, X.; Yan, N.; Fei, Z.; Crespo-Quesada, R. M.; Laurency, G.; Kiwi-Misker, L.; Kou, Y.; Li, Y.; Dyson, P. *J. Inorg. Chem.* **2008**, 47, 7444–7446. (d) Léger, B.; Denicourt-Nowicki, A.; Roucoux, A.; Olivier-Bourbigou, H. *Adv. Synth. Catal.* **2008**, 350, 153–159. (e) Léger, B.; Denicourt-Nowicki, A.; Olivier-Bourbigou, H.; Roucoux, A. *Tetrahedron Lett.* **2009**, 50, 6531–6533.
58. Yen, C. H.; Wei, H-H.; Lin, H-W. Tan, C-S. *Appl. Organometal. Chem.* **2012**, 26, 736–742.
59. Guerrero, M.; Roucoux, A.; Denicourt-Nowicki, A.; Bricout, H.; Monflier, E.; Collière, V.; Fajerweg, K.; Philippot, K. *Catal. Today* **2012**, 183, 34–41.
60. (a) Yuan, X.; Yan, N.; Xiao, C.; Li, C.; Fei, Z.; Cai, Z.; Kou, Y.; Dyson, P. J. *Green Chem.* **2010**, 12, 228–233. (b) Lara, P.; Suárez, A.; Collière, V.; Philippot, K.; Chaudret, B. *ChemCatChem* **2014**, 6, 87–90. (c) Liu, M.; Zhang, J.; Liu, J.; Yu, W. *J. Catal.* **2011**, 278, 1–7. (d) Cai, S.; Duan, H.; Rong, H.; Wang, D.; Li, L.; He, W.; Li, Y. *ACS Catal.* **2013**, 3, 608–612. (e) Harrad, M. A.; Boualy, B.; Firdoussi, L. E.; Mehdi, A.; Santi, C.; Giovagnoli, S.; Nocchetti, M.; Ali, M. A. *Catal. Commun.* **2013**, 32, 92–100. (f) Gkizis, P. L.; Stratakis, M.; Lykakis, I. N. *Catal. Commun.* **2013**, 36, 48–51. (g) Li, G.; Zeng, C.; Jin, R. *J. Am. Chem. Soc.* **2014**, 136, 3673–3679. (h) Liu, M.; Yu, W.; Liu, H.; Zheng, J. *J. Colloid Interface Sci.* **1999**, 214, 231–237.
61. Sharif, Md. J.; Maity, P.; Yamazoe, S.; Tsukuda, T. *Chem. Lett.* **2013**, 42, 1023–1025.
62. (a) Yu, W.; Liu, H.; An, X.; Ma, X.; Liu, Z.; Qiang, L. *J. Mol. Catal. A: Chem.* **1999**, 147, 73–81. (b) Yu, W.; Liu, M.; Liu, H.; An, X.; Liu, Z.; Ma, X. *J. Mol. Catal. A: Chem.* **1999**, 142, 201–211. (c) Yu, W.; Liu, H.; Liu, M.; Liu, Z. *React. Funct. Polym.* **2000**, 44, 21–29. (d) Fonseca, G. S.; Scholten, J. D.; Dupont, J. *Synlett* **2004**, 1525–1528. (e) Mitsudomea, T.; Kaneda, K. *Green Chem.* **2013**, 15, 2636–2654. (f) Yu, W.; Liu, M.; Liu, H.; Ma, X.; Liu, Z. *J. Colloid Interface Sci.* **1998**, 208, 439–444.
63. Yu, W.; Liu, H.; Tao, Q. *Chem. Commun.* **1996**, 1773–1774.
64. (a) Hirai, H.; Chawanya, H.; Toshima, H. *React. Polym.* **1985**, 3, 127–141. (b) Wang, Q.; Liu, H.; Wang, H. *J. Colloid Interface Sci.* **1997**, 190, 380–386.
65. (a) Yu, Z.; Liao, S.; Xu, Y.; Yang, B.; Yu, D. *J. Mol. Catal. A: Chem.* **1997**, 120, 247–255. (b) Silvert, P. Y.; Vijayakrishnan, V.; Vibert, P.; Herrera-Urbina, R.; Elhsissen, K. T. *Nanostruct. Mater.* **1996**, 7, 611–618.

66. (a) Landré, P. D.; Lemaire, M.; Richard, D.; Gallezot, P. *J. Mol. Catal.* **1993**, *78*, 257–261. (b) Landré, P. D.; Richard, D.; Draye, M.; Gallezot, P.; Lemaire, M. *J. Catal.* **1994**, *147*, 214–222.
67. Stanislaus, A.; Cooper, B. H. *Catal. Rev. Sci. Eng.* **1994**, *36*, 75–123.
68. Bennett, M. A.; Smith, A. K. *Dalton Trans.* **1974**, 233–241.
69. Gual, A.; Godard, C.; Castellón, S.; Claver, C. *Dalton Trans.* **2010**, *39*, 11499–11512.
70. Astruc, D.; Lu, F.; Aranzas, J. R. *Angew. Chem., Int. Ed.* **2005**, *44*, 7852–7872.
71. (a) Hagen, C. M.; Widegren, J. A.; Maitlis, P. M.; Finke, R. G. *J. Am. Chem. Soc.* **2005**, *127*, 4423–4432. (b) Hagen, C. M.; Vieille-Petit, L.; Laurenzy, G.; Süß-Fink, G.; Finke, R. G. *Organometallics* **2005**, *24*, 1819–1831.
72. Widegren, J. A.; Bennet, M. A.; Finke, R. G. *J. Am. Chem. Soc.* **2003**, *125*, 10301–10310.
73. (a) Stamp, L.; Dieck, H. T. *Inor. Chim. Acta* **1987**, *129*, 107–114. (b) Geldbach, T. J.; Dyson, P. J. *J. Organomet. Chem.* **2005**, *690*, 3552–3557. (c) Widegren, J. A.; Finke, R. G. *J. Mol. Catal. A: Chem.* **2003**, *198*, 317–341.
74. Van Hove, M. A.; Lin, R. F.; Somorjai, G. A. *J. Am. Chem. Soc.* **1986**, *108*, 2532–2537.
75. Castebou, J. L.; Gual, A.; Mercadé, E.; Claver, C.; Godard, C. *Catal. Sci. Technol.* **2013**, *3*, 2828–2833.
76. Kuniyuki, Y.; Hideaki, O.; Issei, K. Method for partially hydrogenating a monocyclic aromatic hydrocarbon. US5457251, January 21, 1993.
77. Van der Steen, P. J.; Scholten, J. J. F. *Appl. Catal.* **1990**, *58*, 291–304.
78. Luza, L.; Gual, A.; Dupont, J. *ChemCatChem* **2014**, *6*, 702–710.
79. Widegren, J. A.; Finke, R. G. *Inorg. Chem.* **2012**, *41*, 1558–1572.
80. (a) Silveira, E. T.; Umpierre, A. P.; Rossi, L. M.; Machado, G.; Morais, J.; Soares, G. V.; Baumvol, I. J. R.; Teixeira, S. R.; Fichtner, P. F. P.; Dupont, J. *Chem. Eur. J.* **2004**, *10*, 3734–3740. (b) Zhao, C.; Wang, H.; Yana, N.; Xiao, C.; Mua, X.; Dyson, P. J.; Kou, Y. *J. Catal.* **2007**, *250*, 33–40.
81. Rossi, L. M.; Machado, G. *J. Mol. Catal. A: Chem.* **2009**, *298*, 69–73.
82. Escárcega-Bobadilla, M. V.; Tortosa, C.; Teuma, E.; Pradel, C.; Orejón, A.; Gómez, M.; Masdeu-Bultó, A. M. *Catalysis Today* **2009**, *148*, 398–404.
83. Gonzalez-Galvez, D.; Lara, P.; Rivada-Wheelaghan, O.; Conejero, S.; Chaudret, B.; Philippot, K.; van Leeuwen, P. W. N. M. *Catal. Sci. Technol.* **2013**, *3*, 99–105.
84. Januszkiewicz, K. R.; Alper, H. *Organometallics* **1983**, *2*, 1055–1057.
85. Nasar, K.; Fache, F.; Lemaire, M.; Béziat, J.; Besson, M.; Gallezot, P. *J. Mol. Catal.* **1994**, *87*, 107–115.
86. Gual, A.; Godard, C.; Philippot, K.; Chaudret, B.; Denicourt-Nowicki, A.; Roucoux, A.; Claver, C. *ChemSusChem* **2009**, *2*, 769–779.

87. Bilé, E. G.; Cortelazzo-Polisini, E.; Denicourt-Nowicki, A.; Sassine, R.; Launay, F.; Roucoux, A. *ChemSusChem* **2012**, *5*, 91–101.
88. (a) Schuetz, R. D.; Caswell, L. R. *J. Org. Chem.* **1962**, *27*, 486–489. (b) Siegel, S.; Smith, G. V.; Dmuchovsky, B.; Dubbel, D.; Halpern, W. *J. Am. Chem. Soc.* **1962**, *84*, 3136–3139.
89. Jansat, S.; Picurelli, D.; Pelzer, K.; Philippot, K.; Gómez, M.; Muller, G.; Lecante, P.; Chaudret, B. *New. J. Chem.* **2006**, *30*, 115–122.
90. Poreddy, R.; García-Suárez, E. J.; Riisager, A.; Kegnæs, S. *Dalton Trans.* **2014**, *43*, 4255–4259.
91. Cimpeanu, V.; Kočevár, M.; Parvulescu, V. I.; Leitner, W. *Angew. Chem. Int. Ed.* **2009**, *48*, 1085–1088.
92. (a) Bonilla, R. J.; James, B. R.; Jessop, P. G. *Chem. Commun.* **2000**, 941–942. (b) Zheng, J.; Lin, H.; Wang, Y.; Zheng, X.; Duan, X.; Yuan, Y. *J. Catal.* **2013**, *297*, 110–118. (c) Yoon, B.; Wai, C. M. *J. Am. Chem. Soc.* **2005**, *127*, 17174–17175. (d) Lu, F.; Liu, J.; Xu, J. *J. Mol. Catal. A: Chem.* **2007**, *271*, 6–13. (d) Takasaki, M.; Motoyama, Y.; Higashi, K.; Yoon, S-H.; Mochida, I.; Nagashima, H. *Chem. Asian J.* **2007**, *2*, 1524–1533.
93. Anderson, J. A.; Athawale, A.; Imrie, F. E.; Mc Kenna, F.-M.; Mc Cue, A.; Molyneux, D.; Power, K.; Shand, M.; Wells, R. P. K. *J. Catal.* **2010**, *270*, 9–15.
94. Park, K. H.; Jang, K.; Kim, H. J.; Son, S. U. *Angew. Chem. Int. Ed.* **2007**, *46*, 1152–1155.

C *HAPTER* *2*



OBJECTIVES

The final goal of this thesis is the synthesis and characterization of ruthenium nanoparticles stabilised by different ligands and their application as effective and selective catalysts for arene hydrogenation reactions.

The research presented in Chapter 3 aims to synthesize ruthenium nanoparticles stabilized by triphenylphosphine and 1,4-bis(diphenylphosphino) and their application in the hydrogenation of aromatic ketones. In particular, the specific objectives of this chapter are:

- To synthesize and fully characterise ruthenium and rhodium nanoparticles stabilized by phosphine-donor ligands (PPh₃ and dppb).
- Study the structural factors in substrate and nanoparticles that can influence the selectivity on the hydrogenation of the arene vs. the ketone function.
- To perform selective hydrogenation of various substituted phenyl, benzyl and phenethyl ketones.

The work presented in this chapter has been carried out in collaboration with the group of Prof. Carmen Claver and Dr. Cyril Godard.

The research described in Chapter 4 aims to use ruthenium nanoparticles stabilized by triphenylphosphine in the hydrogenation of polycyclic aromatic hydrocarbons. In particular, the specific objectives of this chapter are:

- To perform selective hydrogenation of various polycyclic arenes under mild reaction conditions.

- To compare the catalytic behaviour of the nanoparticles on the hydrogenation of substrates containing two, three or more fused aromatic rings.
- To obtain high selectivities towards the hydrogenation of one arene over others presented on the substrate.
- To study the influence on the selectivity of naphthalenes containing substituents in different positions of the aromatic ring.

The research described in Chapter 5 aims to develop an approach to the enantoselective hydrogenation of arenes using chiral nanoparticles. In particular, the specific objectives of this chapter are:

- To design and synthesize a chiral phosphine ligand to be applied as stabilizer for ruthenium nanoparticles.
- To prepare nanoparticles stabilized by different proportions of cinchonidine.
- To use all the nanoparticles prepared in the asymmetric hydrogenation of different substituted arenes.
- To investigate coordination and interaction aspects of the different ligands with the nanoparticle surface by using isotopic labelling with deuterium.

CHAPTER 3

SELECTIVE HYDROGENATION OF AROMATIC KETONES

This work has been carried out in collaboration with the group of Prof. Carmen Claver and Cyril Godard. The work developed using rhodium nanoparticles has been entirely carried out by Dr. Jessica Llop in the context of her PhD work.

3.1. INTRODUCTION TO THE SELECTIVE HYDROGENATION OF AROMATIC KETONES

The reduction of ketones to alcohols is a very straightforward reaction which has been accomplished by a legion of reagents and catalysts like boron- and aluminium-based hydride reagents, zero-valent metals or by the use of hydrogen and transition metal catalysts.¹ Nevertheless, from an ecological and economical point of view, the use of catalytic hydrogenation methods is more desirable than traditional stoichiometric reduction systems.²

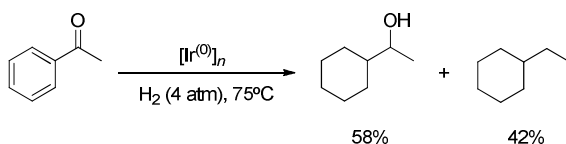
However, the chemoselective hydrogenation of aromatic rings in substrates containing other reducible functional groups like ketones is still a challenge. Few examples of chemoselective hydrogenation of arenes have been reported using heterogeneous catalysts and, in general, mixtures of products are obtained.³ For that reason, nanoparticles have appeared as a promising way to overcome this problem.

3.1.1. Acetophenone Hydrogenation

Acetophenone is, in general, the benchmark substrate used in the study of the selective hydrogenation of an arene *vs.* a carbonyl group using nanoparticles. Different examples have been reported and, here we will comment in more detail those targeting the selectivity.⁴

One of the first examples was reported by Dupont *et al.* in 2003 in which iridium and rhodium nanoparticles stabilized by imidazolium ionic liquids were used in the hydrogenation of acetophenone among other aromatic substrates.⁵ Nanoparticles with a diameter around 2.0-2.5 nm were prepared and used in solventless conditions at 75°C and 4 atm of H₂ pressure in the hydrogenation of acetophenone. Both arene and ketone were reduced

under these conditions. Noteworthy, 42% of the hydrogenolysis product ethylcyclohexane was obtained using iridium nanoparticles (Scheme 3.1). Although the hydrogenolysis of PhC-X bonds is a well-known reaction, using nanoparticles it is in general much slower compared with the aromatic ring reduction and the hydrogenolysis products are only formed in small quantities.⁶ Interestingly, when rhodium nanoparticles were used, no hydrogenolysis products were observed in this case.



Scheme 3.1. Hydrogenation of acetophenone using Ir NPs stabilized by imidazolium ionic liquids.⁵

In 2010, Gómez and co-workers reported a comparative study on the use of ruthenium nanoparticles unsupported and supported on multi-walled carbon nanotubes as catalyst for hydrogenation processes.⁷ In the particular case of acetophenone, total conversion towards the fully hydrogenated product (1-cyclohexylethanol) was obtained at 40 bar and 50°C for 16 h using the supported catalyst.

Then, van Leeuwen *et al.* reported the use of N-heterocyclic carbenes (tBu and IPr) stabilized Ru NPs in the hydrogenation of different aromatic substrates.⁸ Concerning acetophenone, a deep study was performed in which the solvent, pressure, temperature and catalyst loading was optimized. THF was the solvent of choice due to the low activity of other solvents like pentane or MeOH. The pressure did not affect the ketone hydrogenation rate but it did affect the arene hydrogenation and the increase of temperature had a positive effect on the activity but not on the selectivity. In relation to the catalyst loading, better results were obtained when lower quantities of ruthenium were used, obtaining the best results in terms of activity and selectivity using 0.3%

of Ru. As it is shown in Figure 3.1, selectivities up to almost 60% towards the hydrogenation of the arene was obtained using the nanoparticles stabilized by IPr.

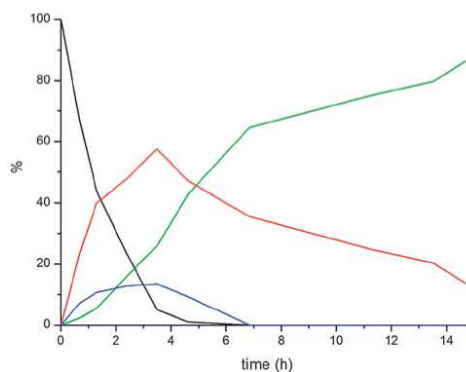
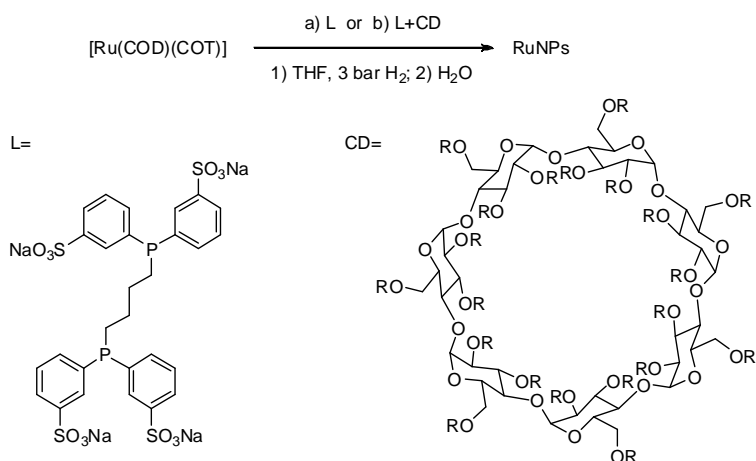


Figure 3.1. Hydrogenation of acetophenone at 40 bar of H₂, 298 K and 0.3% of Ru using RuIPr0.2 NPs. Acetophenone (black), cyclohexylmethylketone (red), 1-phenylethanol (blue), 1-cyclohexylethanol (green).⁸

Water-soluble ruthenium nanoparticles stabilized by sulfonated diphosphines or by a sulfonated-diphosphine-cyclodextrin system with a diameter range 1.2-1.5 nm have also been used in biphasic liquid-liquid conditions in the hydrogenation of unsaturated model substrates like styrene, acetophenone and *m*-methylanisole (Scheme 3.2).⁹ When cyclodextrin was also used to stabilize the nanoparticles, it acted as a phase-transfer reagent that promoted an increase on activity and affected the selectivity. In the particular case of acetophenone, the presence of cyclodextrin pushed the selectivity towards 1-phenylethanol up to 91% when 0.5 equivalents of the ligand were used at only 1 bar of pressure for 20 hours.

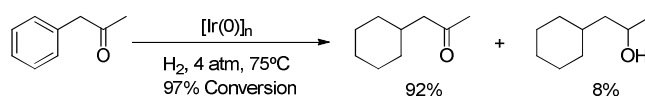


Scheme 3.2. Synthesis of the Ru NPs stabilized by sulfonated diphosphine and cyclodextrin (R=H or CH₃, degree of substitution=1.8).⁹

3.1.2. Hydrogenation of non-Conjugated Aromatic Ketones

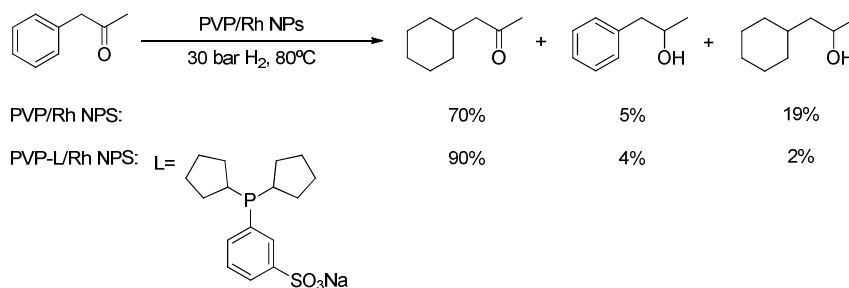
The reduction of acetophenone towards the formation of cyclohexylmethylketone with selectivities higher than 60% is still a challenge due to the no preferential coordination mode of the arene *vs.* the carbonyl group. However, better selectivity results have been obtained in the reduction of non-conjugated aromatic ketones using nanoparticles.

Thus, for instance, in 2004, Dupont *et al.* reduced phenylacetone using iridium nanoparticles stabilized by 1-*n*-butyl-3-methylimidazolium hexafluorophosphate (BMI·PF₆). A 92% of selectivity towards the hydrogenation of the arene under mild reaction conditions (4 atm and 75°C) at 97% of conversion was achieved (Scheme 3.3).²



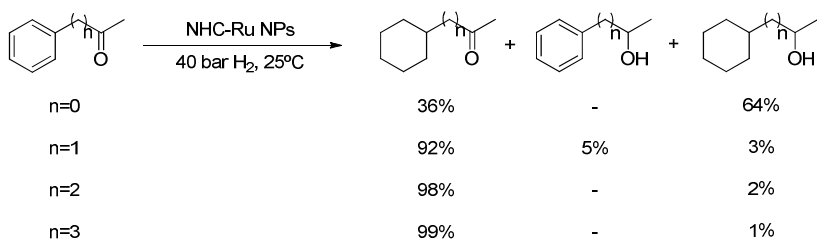
Scheme 3.3. Selective hydrogenation of phenylacetone using Ir Nps stabilized by ILs.²

In 2012, Dyson and co-workers reported the use of PVP Rh nanoparticles in the hydrogenation of phenylacetone obtaining 70% of selectivity towards the hydrogenation of the arene. The chemoselectivity was increased up to 90% at 80% of conversion when a phosphine ligand was added as poisoning (site blocking) (Scheme 3.4).¹⁰



Scheme 3.4. Hydrogenation of phenylacetone using PVP/Rh and PVP-L/Rh NPs.¹⁰

As it was commented on the previous section, recently NHC-stabilized ruthenium nanoparticles have been successfully used in the hydrogenation of acetophenone.⁸ Moreover, the influence of the alkyl chain length on the chemoselectivity was studied. It was concluded that, as more distance there was between the arene and the ketone, better were the selectivities (up to 98% in 4-phenyl-2-butanone, Scheme 3.5). For this reason, it could be concluded that there is a preference for coordination of the arene over the ketone on the nanoparticle surface.



Scheme 3.5. Hydrogenation of aromatic ketones using Ru NPs stabilized by NHC ligands.⁸

3.2. OUTLOOK AND OBJECTIVES OF THIS CHAPTER

As previously outlined, nanoparticles are a very versatile class of catalyst which have been used with great success in several catalytic transformations. In particular, arene hydrogenation is a reaction in which nanoparticles have been successful catalysts, allowing the reaction to be performed under really mild reaction conditions. However, in terms of selectivity, the ability to hydrogenate an aromatic ring in the presence of another more easily reducible functional group still remains a challenge.

As it was commented in the introduction, different studies of selective reduction of arenes in the presence of keto groups using different metals and different stabilizers have been performed. However, most of these studies are limited to one type of metal, stabilizer or substrate. For that reason, we decided to perform a general study of reduction of arene *vs.* ketone using Ru and Rh nanoparticles stabilized by phosphine-donor ligands. Ruthenium and rhodium were selected because they were the most promising metals for arene reduction. Phosphines were selected as stabilizers because they offer the possibility of modulate the surface of the nanoparticle by selecting mono or bidentate ligands besides of using different metal/ligand ratio. Moreover, phosphines showed interesting results of selectivity in the few studies carried out. Thus, the aim of this chapter is the comparison of the catalytic behavior

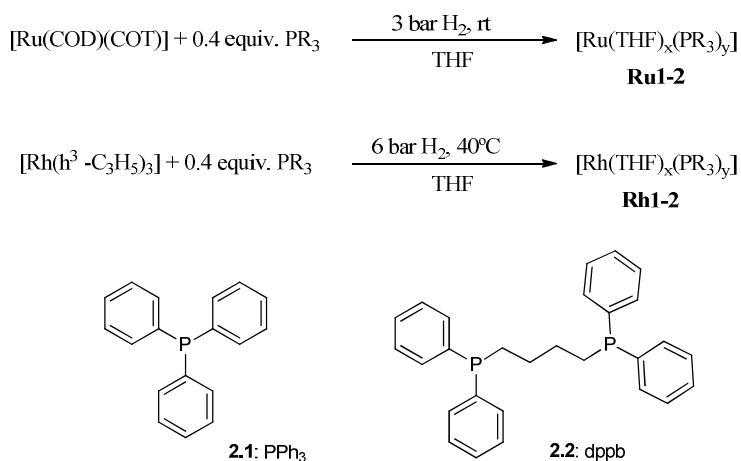
of Ru and Rh nanoparticles in the hydrogenation of the arene *vs.* the ketone function. The effect of the nature of the metal, the stabilizing agent and the influence of the substrate structure will be studied.

As it was stated before, this work was performed in collaboration with the group of Prof. Carmen Claver and Cyril Godard and the study of rhodium nanoparticles was supervised by them and carried out by Jessica Llop in the frame of her Doctoral Thesis. The work was programmed by both groups together, the nanoparticles were synthesized using the same batch of ligands, and the catalysis was performed in the same reactor and using the same batch of substrates and solvents in order to get really comparable results. For this reason, and in order to understand the general conclusions derived from this study, the results obtained by Jessica Llop with rhodium nanoparticles, have also been included in the Results and Discussion section.

3.3. RESULTS AND DISCUSSION

3.3.1. SYNTHESIS, STABILIZATION AND CHARACTERIZATION OF RUTHENIUM AND RHODIUM NANOPARTICLES

Soluble Ru- and Rh-NPs stabilised by the phosphorus donor ligands PPh₃ and dppb (P:Ru/Rh= 0.4) were synthesised by decomposition of the organometallic precursors [Ru(COD)(COT)] and [Rh(η^3 -C₃H₅)₃], respectively, in THF under H₂ pressure (Scheme 3.6). The NPs were isolated as black powders after precipitation with pentane and characterised by transmission electron microscopy (TEM), X-ray diffraction (XRD), X-ray photoelectron spectroscopy (XPS), wide-angle X-ray scattering (WAXS), elemental analysis (EA) and thermogravimetric analysis (TGA) (see Experimental Part).



Scheme 3.6. Synthesis of Ru and Rh-NPs stabilized by PPh₃ and dppb.

- **Ru1 nanoparticles:**

Initially, 0.4 equivalents of the monodentate ligand triphenylphosphine **2.1** were used to synthesize **Ru1** nanoparticles. TEM micrographs permitted to observe the formation of small and spherical shaped nanoparticles, narrow size distribution and a diameter of 1.32 ± 0.28 nm. Moreover, the high-resolution transmission electron microscopy (HRTEM) confirmed the formation and dispersion of the nanoparticles (Figure 3.2).

Then, the proportion of ligand present on the nanoparticle surface was determined not only by elemental analysis but also by thermogravimetric analysis (TGA). By elemental analysis, 6% of phosphorus and 54% of Ru was determined. These results were confirmed by TGA in which 69% of Ru, 29% of PPh₃ and 2% of THF was observed (Figure 3.3).

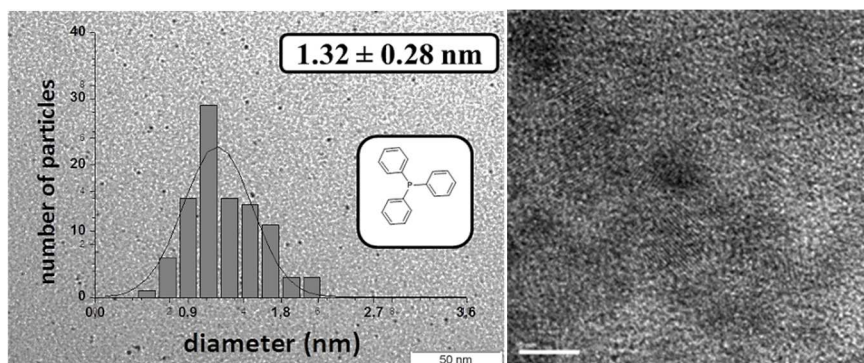


Figure 3.2. TEM and HRTEM micrographs of **Ru1** NPs.

To help to clarify the TGA graphic (Figure 3.3) it is important to highlight that the sample of nanoparticles was heated from 30°C to 900°C under a flow of N₂, while the weight was continuously recorded. Triphenylphosphine was used as reference and a unique loss at around 340°C was observed. Then **Ru1** nanoparticles were heated and two main weight losses were observed between 70°C and 100°C corresponding to the solvent (THF) and between 200°C and 450°C corresponding to the ligand (PPh₃). No free ligand at around 340°C was observed and the weight measured at the end of the experiment (900°C) was referred to the remaining ruthenium.

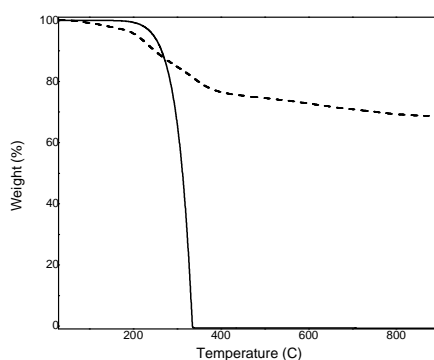


Figure 3.3. TGA of **Ru1** nanoparticles. Free ligand PPh₃ (solid line) and the corresponding nanoparticle (dashed line).

From the experimental data obtained by TEM and by TGA and using the *Van Hardevel Hartog* model, the approximate quantity of ruthenium atoms present on the **Ru1** nanoparticles surface can be calculated. In Table 3.1 are presented the values referring to the total number of atoms (Nt) and the atoms on the surface (Ns) related to the diameters obtained by TEM. A P/Ru_s ratio between 0.2-0.3 that represents approximately 1 phosphorus ligand for 6-8 ruthenium surface atoms is obtained. The ratio of surface atoms per total atoms in the nanoparticle remains similar in all the cases.

Table 3.1. Approximate quantity of ruthenium atoms on the **Ru1** surface.

Size of NPs	1.04 nm	1.32 nm	1.60 nm
Nt	43	89	158
Ns	35	63	99
Ns/Nt	0.810	0.709	0.628
P/Ru _s	0.25	0.23	0.26

The structure of the nanoparticles **Ru1** was determined by X-Ray diffraction (XRD). The diffraction pattern is shown in Figure 3.4 in which Bragg's diffraction corresponding to the planes (010), (002), (011), (012), (110), (013) and (020) are related to the hexagonal close packing lattice of Ru-NPs and coherence length of 1.01 ± 0.02 nm was determined.

Moreover, Wide Angle X-Ray Scattering (WAXS) was performed revealing crystalline ruthenium nanoparticles displaying hcp structure with a coherence length of 1.5 nm and a bond length of 0.265 nm (Figure 3.5). Then mean size is slightly higher than the ones determined by TEM and XRD and this fact could be due to the different approximation used for the calculations.¹¹

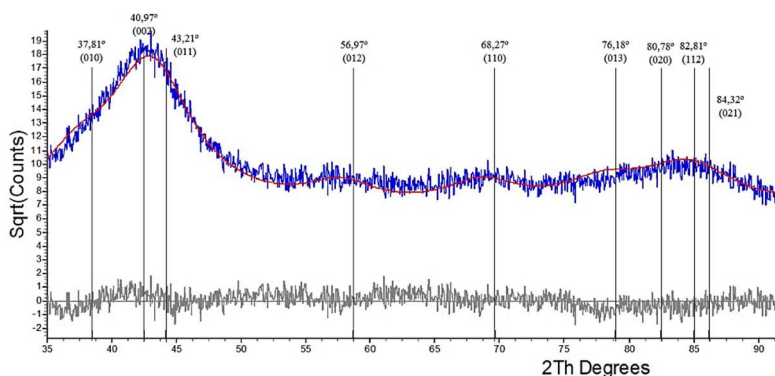


Figure 3.4. XRD of hcp crystalline **Ru1** nanoparticles.

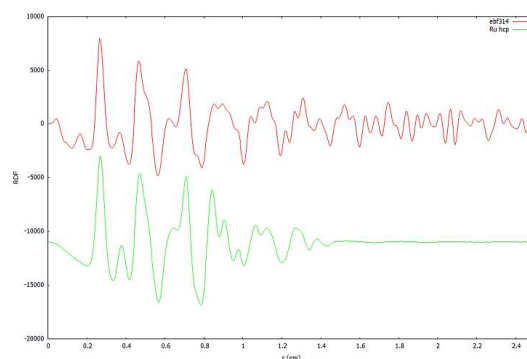


Figure 3.5. Experimental RDF of **Ru1** nanoparticles (red line) and theoretical RDF for Ru hcp (green line).

Finally, the oxidation state of the atoms situated on the **Ru1** nanoparticles surface was determined by X-ray Photoelectron Spectroscopy (XPS) (Figure 3.6). Two peaks are expected for Ru^0 nanoparticles although the Ru 3d region shows highly overlapping between Ru 3d and C 1s peaks. Six component peaks are necessary to fit the experimental peaks: 3d_{5/2} and 3d_{3/2} for Ru(0), 3d_{5/2} and 3d_{3/2} for Ru(IV) and C 1s peaks. Using the Monte-Carlo approximation¹² and taking into account the parameters optimized for Ru systems, the analysis revealed a 100% of Ru(0) atoms at the surface of the NPs.

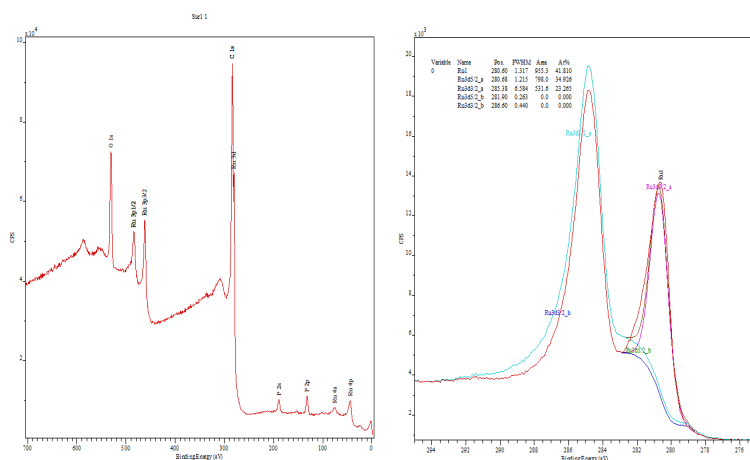


Figure 3.6. XPS spectra of **Ru1** nanoparticles.

To summarise, the **Ru1** NPs exhibit a diameter of 1.32 ± 0.28 nm, are highly crystalline with hcp packing and no oxidation is detected. Quantitatively, they contain 70% Ru and 30% PPh_3 .

- **Ru2 nanoparticles:**

Initially, 0.2 equivalents of the bidentate ligand 1,4-bis(diphenylphosphino)butane (dppb) **2.2** were used to synthesize **Ru2** nanoparticles. Small nanoparticles with a diameter of 1.49 ± 0.35 nm, narrow distribution and spherical shape were observed by TEM. The high-resolution transmission electron microscopy (HRTEM) confirmed the formation and dispersion of the nanoparticles (Figure 3.7).

The proportion of ligand present on the nanoparticle surface was determined by elemental analysis and by thermogravimetric analysis (TGA). By elemental analysis, 3.35% of phosphorus and 74.99% of Ru was determined. These results were confirmed by TGA and 72% of Ru, 25% of PPh_3 and 3% of THF was observed (Figure 3.8).

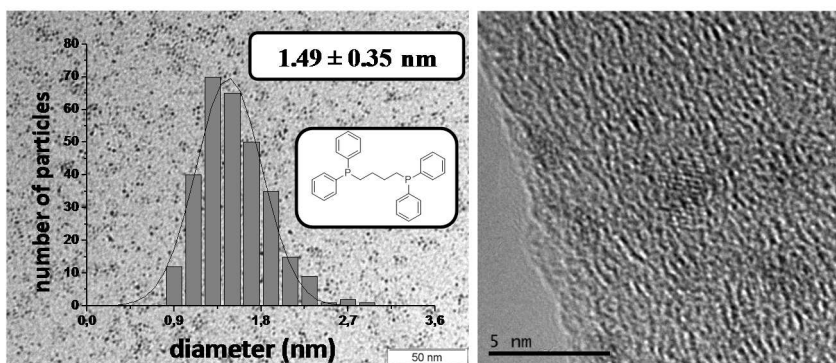


Figure 3.7. TEM and HRTEM micrographs of **Ru₂** NPs.

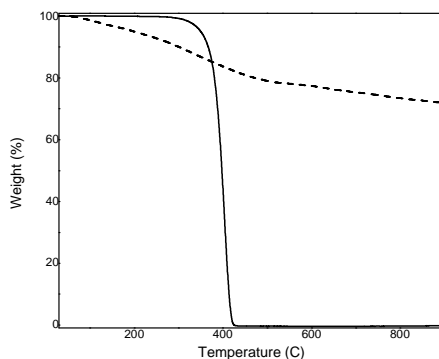


Figure 3.8. TGA of **Ru₂** nanoparticles. Free ligand PPh₃ (solid line) and the corresponding nanoparticle (dashed line).

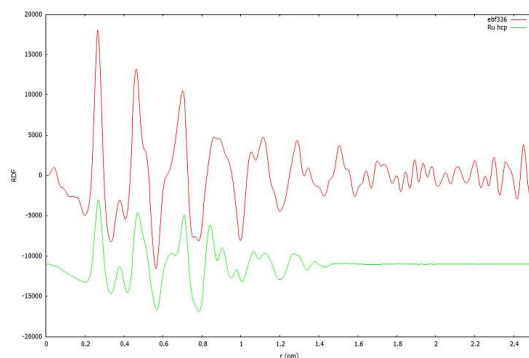
From the experimental data obtained by TEM and by TGA and using the *Van Hardevel Hartog* model, the approximate quantity of ruthenium atoms contained on the **Ru₂** nanoparticles surface can be calculated. In Table 3.2 are presented the values related to the total number of atoms (N_t) and the atoms on the surface (N_s) related to the diameters obtained by TEM. A P/Ru_s ratio between 0.1-0.32 which represents approximately 1 phosphorus ligand for 11-14 ruthenium surface atoms is obtained. The ratio of surface atoms per total atoms in the nanoparticle remains similar in all the cases.

Table 3.2. Approximate quantity of ruthenium atoms on the **Ru2** surface.

Size of NPs	1.14 nm	1.49 nm	1.84 nm
Nt	57	127	240
Ns	44	84	137
Ns/Nt	0.771	0.658	0.572
P/Ru _s	0.11	0.13	0.15

The structure of the nanoparticles **Ru2** was determined by X-Ray diffraction (XRD). Bragg's diffraction are related to the hexagonal close packing lattice of ruthenium nanoparticles and coherence length of 1.12 ± 0.05 nm was determined.

Wide Angle X-Ray Scattering (WAXS) was performed revealing crystalline ruthenium nanoparticles displaying hcp structure with a coherence length of around 1.8 nm (Figure 3.9).

**Figure 3.9.** Experimental RDF of **Ru2** nanoparticles (red line) and theoretical RDF for Ru hcp (green line).

Finally, the oxidation state of the atoms situated on the **Ru2** nanoparticles surface was also determined by X-Ray Photoelectron Spectroscopy (XPS) (Figure 3.10) After the optimization of the parameters and using the Monte-Carlo approximation, 6% of Ru^{δ+} was observed on the

NPs surface (oxidation of the samples during the manipulation and the measurements cannot be discarded).

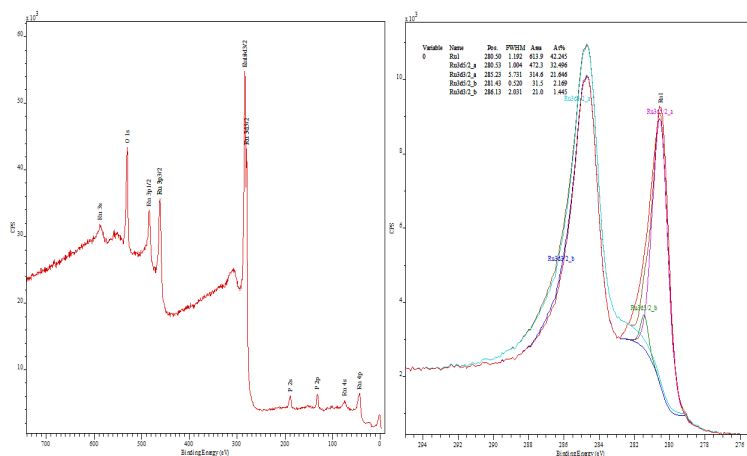


Figure 3.10. XPS spectra of Ru2 nanoparticles.

To conclude, the TEM micrographs of these NPs revealed in all cases the formation of small nanoparticles with spherical shape, narrow size distribution and similar diameter (*ca.* 1.5 nm diameter, Figure 3.2 and Figure 3.7). The mean diameter and size distribution of the Ru1-2 NPs are in agreement with the size of Ru-NPs stabilised with these ligands previously reported at lower L/M ratios (0.1 equivalent of triphenylphosphine¹³ and dppb¹⁴). It was therefore concluded that for these systems, the amount of ligand used to stabilise the nanoparticles does not affect significantly their size.

Diffuse peaks were observed in the XRD pattern of these NPs, as expected for an homogeneous distribution of very small particles with a hexagonal close-packing (hcp) lattice structure. Thermogravimetric analysis of Ru1-2 systems showed that these NPs contained *ca.* 2% of solvent, 25% of phosphine ligands and 70% of Ru, in agreement with previous reports.¹³⁻¹⁴

Similar results were already reported for the Rh systems.¹⁵ In the case of Rh nanoparticles, TEM micrographs revealed the formation of small nanoparticles with spherical shape and narrow size distribution (*ca.* 1.6 nm diameter, Figure 3.11). Diffuse peaks were observed in the XRD pattern of these NPs, as expected for an homogeneous distribution of very small particles with a face-centred cubic (fcc) lattice structure. No reflections due to rhodium oxide were observed. Thermogravimetric analysis of **Rh1-2** systems showed that these NPs contained *ca.* 1% of solvent, 29% of phosphine ligands and 70% of Rh (see Experimental Part for more details).

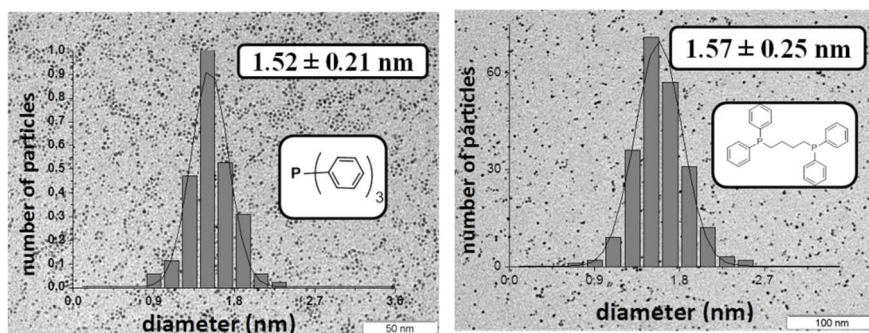
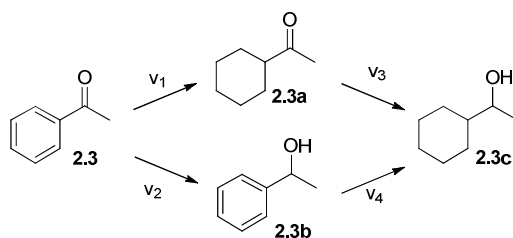


Figure 3.11. TEM micrographs and the corresponding size histograms of **Rh1-2** NPs.

3.3.2. Acetophenone Hydrogenation

As it was mentioned in the introduction, acetophenone was used as benchmark substrate in the studies of competitive reduction of arene and keto group. Thus, acetophenone **2.3** was first used to evaluate the selectivity of the hydrogenation (aryl group *vs.* ketone group) using **Ru1-2** and **Rh1-2** nanoparticles. Three main products are expected in this reaction (Scheme 3.7): cyclohexylmethylketone **2.3a** resulting from the selective reduction of the aromatic ring, phenylethanol **2.3b** resulting from selective reduction of the ketone group and cyclohexylethanol **2.3c**, the total hydrogenated product.



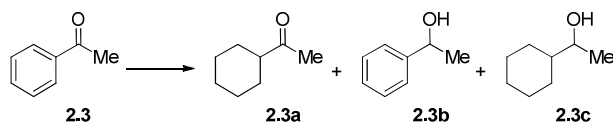
Scheme 3.7. Expected products formed in the hydrogenation of acetophenone.

Initially, **Ru1** nanoparticles stabilised by triphenylphosphine (**2.1**) were used to optimize conditions. Initially, as it is shown in Table 3.3, it was decided to use the pressure and temperature conditions already reported for acetophenone hydrogenation by ruthenium nanoparticles.⁸ Therefore, **2.3** was reduced at 40 bar of pressure and at 30°C and total conversion was achieved and 74% of the total hydrogenated product **2.3c** was detected (Table 3.3, Entry 1). Then the reaction pressure was reduced to 20 bar and the time was increased to 5 hours in order to see if more selectivity towards the hydrogenation of the arene could be obtained (Table 3.3, Entry 2). Under these reaction conditions, full conversion and 87% of the total hydrogenated product **2.3c** was achieved.

At this point, different solvents were tested conducting the reaction at 30 °C and at 20 bar of H₂. When the reaction was performed in pentane for 5 hours (Table 3.3, Entry 3), the reaction was slower than in THF and in contrast with the previous experiment, the major product was **2.3b** (53%). This result was attributed to the poor solubility of the ruthenium nanoparticles in this solvent although, in general, the activity of this type of heterogeneous catalysts depends on the competitive coordination of the substrate *vs.* the solvent. Then, as it was expected, the reaction did not proceed using acetonitrile as solvent (Table 3.4, Entry 4). This result was in agreement with previous reports¹⁶ and indicated that competitive coordination of acetonitrile at the surface blocks the active sites of the catalyst. From this screening, it

was deduced that the best results in terms of activity and selectivity were obtained using THF as solvent and subsequent experiments were carried out in this solvent.

Table 3.3. Optimization of the conditions for the hydrogenation of acetophenone **2.3** using **Ru1** NPs.^a



E.	Solvent	P (bar)	T (°C)	Time (h)	Conv. (%) ^b	2.3a ^b	2.3b ^b	2.3c ^b
1	THF	40	30	2.5	100	26	-	74
2	THF	20	30	5	100	13	-	87
3	Pentane	20	30	5	24	23	53	24
4	CH ₃ CN	20	30	5	-	-	-	-
5	THF	20	30	2.5	90	57	4	39
6	THF	10	30	2.5	50	61	21	18
7	THF	20	50	2.5	100	7	-	93

^aGeneral conditions: 2mol% **Ru1** NPs (2mol%), substrate (1.24 mmol), solvent (10 ml).

^bDetermined by GC.

When the reaction using THF was repeated during 2.5h under the same reaction conditions, 90% conversion was reached with a selectivity up to 57% of the arene reduction **2.3a** (Table 3.3, Entry 5), 39% of the totally hydrogenated product **2.3c** and, curiously, of only 4% of phenylethanol **2.3b**.

Finally, it was decided to optimize the pressure and the temperature. When the pressure was reduced to 10 bar and the temperature was maintained at 30°C, the conversion decreased to 50% although the selectivity remained practically unchanged and 61% of product **2.3a** was obtained (Table 3.4, Entry 6). Therefore, it was decided to maintain the pressure to 20 bar and increase the temperature to 50°C in order to see if the conversion could be improved and the selectivity maintained (Table 3.3, Entry 7). However, the

total hydrogenated product was obtained in 93% of selectivity and only 7% of product **2.3a** was achieved.

Therefore, the best results are obtained using THF as solvent, 20 bar of pressure and 30°C and the subsequent experiments were carried out under these reaction conditions.

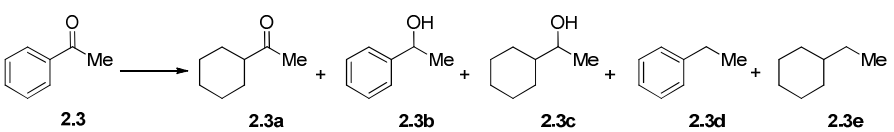
Then the reaction was performed using **Ru2** nanoparticles for 5h (Table 3.4, Entry 2), a conversion of 70% was obtained with selectivities of 43% and 41% for **2.3a** and **2.3b**, respectively. The **Ru2** nanoparticles are therefore apparently less active than **Ru1**, which could be attributed to the more facile dissociation of the monodentate PPh₃ from the surface of **Ru1**. From these results, it can be concluded that the ligand used to stabilise the nanoparticles has an effect on the activity and the selectivity. It is noteworthy that bidentate phosphine stabilised Ru-NPs are usually more active than their monodentate counterparts.¹⁷

Then, the rhodium nanoparticles **Rh1,2** were used as catalysts in the hydrogenation of acetophenone **2.3** under the same reaction conditions. **Rh1** nanoparticles provided high conversions when the reaction was driven in THF during 5h (Table 3.4, Entries 5-7). However, using this catalyst, in addition to the expected products **2.3a-c** obtained in 15, 23 and 33%, respectively, the hydrogenolysis products ethylbenzene (**2.3d**) and ethylcyclohexane (**2.3e**) were detected in 13% and 17%, respectively. In previous reports on hydrogenation of acetophenone by soluble Rh-NPs, these products were only observed as traces.^{5,18}

As it was mentioned before and in the frame of a collaboration, **Rh2** nanoparticles, which bear dppb as stabilising ligand, also afforded full conversion under the same reaction conditions (Table 3.4, Entry 8). Relevant differences between the two rhodium systems were observed in terms of

selectivity. Indeed, using **Rh2** system as catalyst, the hydrogenolysis products **2.3d** and **2.3e** were not detected while 1-phenylethanol **2.3b** (46%) was the main product, and **2.3a** and **2.3c** were obtained in similar percentages, 28% and 26%, respectively.

Table 3.4. Ru-NPs (**Ru1,2**) and Rh-NPs (**Rh1,2**) catalysed hydrogenation of acetophenone **2.3**.^a



E.	Subs.	NPs	Solvent	Time (h)	Conv. (%) ^b	2.3a ^b	2.3b ^b	2.3c ^b
1	2.3	Ru1	THF	2.5	90	57	4	39
2	2.3	Ru2	THF	5	70	43	41	16
3	2.3a	Ru1	THF	16	100	-	-	100
4	2.3b	Ru1	THF	16	5	-	95	5
5 ^c	2.3	Rh1	THF	5	90	15	23	33
6 ^d	2.3	Rh1	Pentane	5	100	6	1	8
7	2.3	Rh1	CH ₃ CN	5	-	-	-	-
8	2.3	Rh2	THF	5	100	28	46	26
9	2.3a	Rh1	THF	16	-	-	-	-
10	2.3a	Rh1	Pentane	5	-	-	-	-
11 ^e	2.3b	Rh1	THF	16	100	1	-	26
12	2.3c	Rh1	THF	16	-	-	-	-

^aGeneral conditions: NPs= Ru, Rh (2 mol%), substrate (1.24 mmol), T = 30 °C, P= 20 bar H₂.

^bDetermined by GC. ^c13% of **2.3d** and 17% of **2.3e** were also obtained. ^d57% of **2.3d** and 27% of **2.3e** were also obtained. ^e63% of **2.3e** was obtained.

These results therefore indicated strong differences depending on the metal and stabilising agents used. In terms of activities, no important changes were observed, although the system **Ru2** was slightly less active than the other NPs. However, large differences were observed in terms of selectivity. With the ruthenium systems, the selectivity towards the cyclohexylmethylketone (**2.3a**) varied from 13% with **Ru1** (Table 3.3, 57% at shorter reaction times) to 43% using **Ru2**. With the rhodium systems, the

same trend was observed, although in this case the main difference in selectivity was the formation or not of hydrogenolysis products, since products **1e** and **1f** were only detected using the system **Rh1**. This therefore suggests that the stabilising ligand dppb in **Rh2** blocks the active sites of the NPs responsible for the hydrogenolysis process.

Interesting results were obtained for both metal nanoparticles and, at this point and to further investigate the evolution of the selectivity with time, the hydrogenation of acetophenone **2.3** catalysed by **Ru1** and **Rh1** systems were monitored by GC-MS under the optimized reaction conditions (30°C, 20 bar of H₂ pressure and THF as solvent).

Using the **Ru1** system, full conversion was obtained after *ca.* 4h (Figure 3.12). During the first 30 min, the conversion reached *ca.* 20% and products **2.3a**, **2.3b** and **2.3c** were rapidly formed, with **2.3a** as the major product (*ca.* 60%). Comparing the initial rates of formation of **2.3a** and **2.3b**, the hydrogenation of the arene ring revealed to be 3 times faster. The concentration of **2.3a** remained constant for *ca.* 1h before decreasing to 15% after 5h of reaction. At 20% of conversion, the product **2.3b** reached a maximum of *ca.* 20% of selectivity, progressively decreasing at longer reaction times, until full disappearance after 5 h. During the reaction, 2-cyclohexylethanol **2.3c** became the main product *via* the hydrogenation of **2.3a** and **2.3b**.

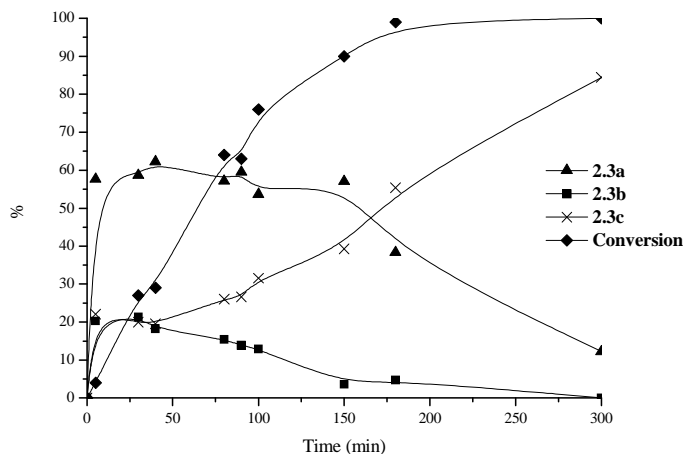


Figure 3.12. Monitoring the hydrogenation of acetophenone **2.3** using **Ru1** NPs (Conditions: substrate (1.24 mmol), **Ru1** (2 mol%), THF, 30°C, 20 bar H₂).

Then to compare the reactivity of the intermediates, **2.3a** and **2.3b** were used as substrates under the same reaction conditions than **2.3**. Surprisingly, when the reaction was performed with 1-phenylethanol **2.3b** as substrate, only 5% conversion into the total hydrogenated product **2.3c** was obtained, even after 16h (Table 3.4, Entry 4).

This result is in contrast with the kinetic study where **2.3b** fully disappeared after 5h, although in this case, conversion in **2.3b** was very low. It was deduced that the relative concentration of phenylethanol **2.3b** in solution could explain the difference observed. Kühn and co-workers have recently reported that alcohols like **2.3b** can deactivate the catalyst by forming stable adducts with the active species.¹⁹

As expected, when cyclohexylmethylketone **2.3a** was used as substrate, total conversion was observed (Table 3.4, Entry 3) indicating that **2.3c** is mainly formed through **2.3a**.

The same study was monitored using the rhodium system **Rh1** (Figure 3.13) and, at early stages of the reaction, the product **2.3b** was rapidly formed and reached a maximum selectivity of *ca.* 60%. Comparing the initial rates of formation of **2.3a** and **2.3b**, the hydrogenation of the arene ring revealed to be 4 times slower than that of the ketone function. At longer reaction times, the concentration of **2.3b** was observed to steadily decrease. The selectivity towards **2.3a** reached 20% after 40 min and practically remained unchanged at higher conversion. As expected, the formation of the product **2.3c** progressively increased until the end of the reaction. The hydrogenolysis product **2.3d** was rapidly formed at the beginning of the reaction and its concentration was maintained constant during the rest of the hydrogenation process. The concentration in product **2.3d** was also practically constant throughout the experiment, suggesting that this product is formed at a similar rate than that at which it is converted into **2.3e**.

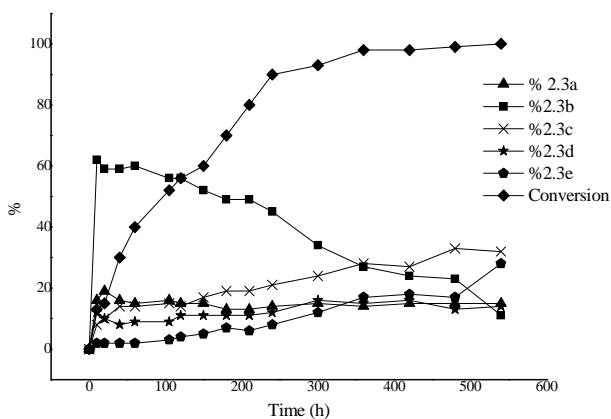
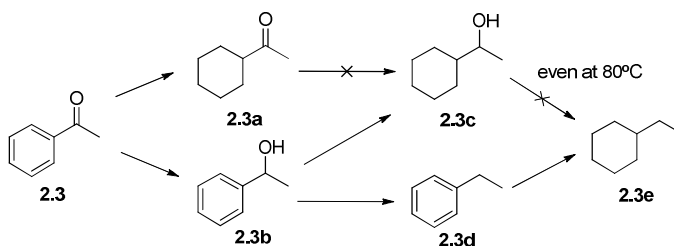


Figure 3.13. Monitoring the hydrogenation of acetophenone **2.3** using **Rh1** as catalyst (Conditions: substrate (1.24 mmol), **Rh1** (2 mol%), THF, 30°C, 20 bar H₂).

Then, products **2.3a-2.3c** were again used as substrates in order to elucidate the reaction pathway (Figure 3.13). Interestingly, when cyclohexylketone **2.3a** or cyclohexylethanol **2.3c** were reacted, no conversion

was achieved even at 80°C (Table 3.4, Entries 9-10, 12). In contrast, when 1-phenylethanol **2.3b** was used as substrate, complete conversion was achieved with up to 63% selectivity for the hydrogenolysed product **2.3e**, and 26% of **2.3c** (Table 3.4, Entry 11).

These results therefore showed that during the hydrogenation of **2.3**, the formation of product **2.3c** only arises from the hydrogenation of the aryl group of **2.3b**, and not from the hydrogenation of the ketone group of **2.3a**. Furthermore, the formation of the hydrogenolysis product **2.3e** necessarily involves the product **2.3b** as intermediate while the transformation of **2.3a** and **2.3c** into **2.3e** were shown not to proceed under these conditions (Scheme 3.8).



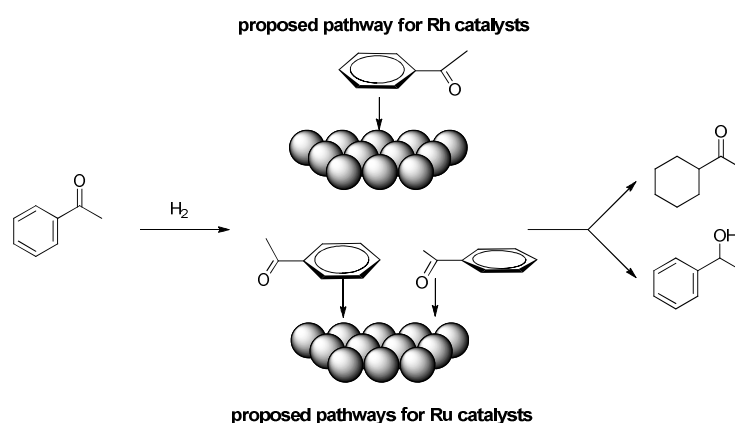
Scheme 3.8. Reaction pathway for the hydrogenation of acetophenone **2.3** using **Rh1** nanoparticles.

To summarize, the results obtained in the hydrogenation of acetophenone **2.3** show that, very surprisingly, distinct reaction pathways are employed depending on the metal and ligand used:

- Ru NPs favour the reduction of the aromatic ring over the reduction of the keto group, and are also able to reduce **2.3a** to produce **2.3c**. However, with these catalysts, **2.3b** is reduced very slowly. Moreover, the selectivity is influenced by the stabilising ligand.

- Rh NPs favour the reduction of the keto group over that of the aromatic ring to produce 1-phenylethanol **2.3b**, which is then further hydrogenated to form **2.3c** or hydrogenolysed to **2.3d** exclusively when **Rh1** is used as catalysts. Interestingly, the Rh-NPs do not reduce the cyclohexylketone **2.3a**.

The selectivity trends observed for the hydrogenation of acetophenone **2.3** are summarized in Scheme 3.9.



Scheme 3.9. Schematic representation of the selectivity trends observed in the hydrogenation of acetophenone **2.3**.

Based on these results, the **Ru1** nanoparticles appeared to be more active than **Ru2** and **Rh1-2**. Therefore, in order to obtain similar conversions and to facilitate the comparisons in terms of selectivity, the hydrogenation of the other substrates **2.4-2.11** was carried out during 2.5h using **Ru1** as catalyst and 5h when **Ru2** and **Rh1-2** were employed.

3.3.3. Hydrogenation of Acetophenone using Ru/C and Rh/C

Ru/C and Rh/C, conventional heterogeneous catalysts, were used in blank experiments, in order to know if the presence of stabilizing ligands had

influence in the activity and selectivity. Surprisingly, the reaction did not proceed when Ru/C was used as catalyst.

However, when the reaction was monitored and performed under the optimized reaction conditions (20 bar of H₂ and 30°C) using Rh/C, full conversion was achieved after 90 min and 1-cyclohexylethanol **2.3c**, was principally obtained (Figure 3.14).

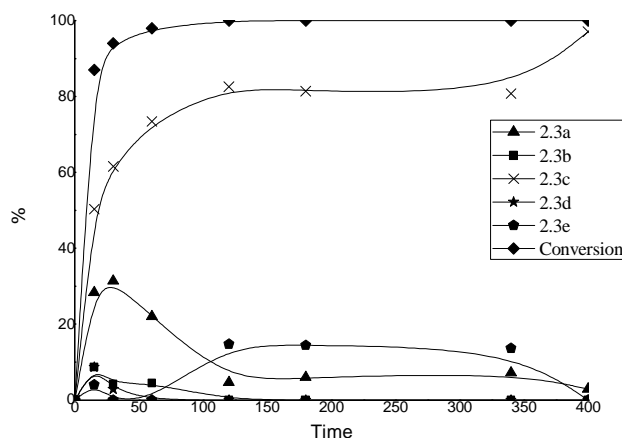


Figure 3.14. Monitoring the hydrogenation of acetophenone **2.3** using Rh/C as catalyst. (Conditions: substrate (1.24 mmol), Rh/C (1 mol%), THF, 30°C, 20 bar H₂).

In this case, hydrogenation was faster than using nanoparticles and the total hydrogenation product was observed as the major one from the beginning. Product **2.3b** is observed as a minor product which is rapidly hydrogenated to form **2.3c** and the hydrogenolysis product **2.3d** and **2.3e** are only observed as traces.

These results justify the use of nanoparticles as selective catalyst for the hydrogenation of an arene in the presence of a ketone. Using the Rh/C system only *ca.* 30% of cyclohexylketone **2.3a** was detected whereas using Ru NPS almost 60% of selectivity could be achieved.

3.3.4. Hydrogenation of non-Conjugated Aryl Ketones

As it was commented before, concerning selectivity, the behaviour of Ru and Rh NPs seems to be complementary: Ru NPs mainly reduce the arene ring while Rh NPs reduce first the keto group. On the other hand, Ru NPs reduce the keto group of cyclohexyl methyl ketone (**2.3a**), while Rh NPs do not. These results prompted us to explore the behaviour of these nanocatalysts in the hydrogenation of non-conjugated aryl ketones.

The reduction of non-conjugated aryl ketones and the influence of the alkyl chain length between the phenyl and the ketone (substrates **2.4** and **2.5**) groups was studied using **Ru1-2** and **Rh1-2** as catalysts (Table 3.5). Using the ruthenium systems **Ru1-2**, similar activities were obtained (conversions around 65%) for both substrates (Table 3.5, Entries 1-2 and 3-4). For substrate **2.4**, 58% selectivity for the arene-hydrogenated product **2.4a** was obtained (Table 3.5, Entry 1) using **Ru1**, while only 30% was achieved using **Ru2** system (Table 3.5, Entry 2). For substrate **2.5** using **Ru1** to give **2.5a** is higher than in the reduction of **2.4** to give **2.4a**. A similar trend was observed when **Ru2** were used.

When the reaction was performed using **Rh1-2** as catalysts, good activities (conversions up to 80) were obtained in all the cases. In these reactions, high to excellent selectivities for the arene hydrogenated products were achieved, obtaining up to *ca.* 75% of the cyclohexylketone derivative **2.4a** and up to 94% of product **2.5a** (Table 3.5, Entries 5-8). The selectivities obtained for both substrates were similar using both systems **Rh1** and **Rh2**. It should be noted that low selectivity for the fully hydrogenated products was obtained in these experiments.

Table 3.5. Hydrogenation of ketones **2.4**, **2.5** catalysed by Ru (**Ru1-2**) and Rh NPs (**Rh1-2**).^a

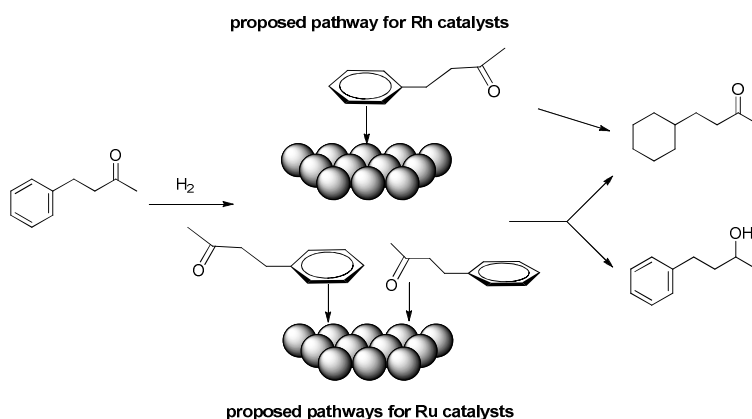
Entry	Substrate	NPs	Conv. (%) ^b	2.4a ^b	2.4b ^b	2.4c ^b
1 ^b	2.4	Ru1	67	58	39	3
2	2.4	Ru2	66	30	70	-
3 ^b	2.5	Ru1	66	74	17	9
4	2.5	Ru2	67	47	37	16
5	2.4	Rh1	78	76	24	-
6	2.4	Rh2	64	74	26	-
7	2.5	Rh1	73	93	3	4
8	2.5	Rh2	80	94	2	4

^aGeneral conditions: NPs=Ru, Rh (2 mol%), substrate (1.24 mmol), THF (10 ml), T = 30 °C, P= 20 bar H₂, t=5h. ^bt=2.5h. ^b% determined by GC.

For substrates **2.4** and **2.5** the nature of the metal affects significantly the catalytic results. Indeed, with Rh NPs, the selectivity for arene reduction increases when the separation between arene and carbonyl group increases until reaching practically total selectivity for arene reduction. Moreover, the stabilizing ligand shows neither influence on the conversion nor on the selectivity. This suggests that substrate coordination takes place through the aromatic ring while the carbonyl group is progressively pushed away from the nanoparticle. The fact that the ligand does not affect the activity and selectivity of the catalysts indicates that both ligands leave enough space at the surface of these nanoparticles for the arene coordination.

In the case of the Ru catalysts, the stabilizing ligand does not influence the activity but affects the selectivity of the catalysts, increasing the percentage of ketone reduction when dppb is the stabilizer (**Ru2**). It is relevant that even for compound **2.5**, 37% of ketone reduction was obtained. However, this is not surprising since we observed earlier that ruthenium is able to reduce alkyl ketones like **2.2a** (see Table 3.4). These results suggest that the stronger coordination and higher steric hindrance of the dppb ligand limits more efficiently the coordination of the arene than the coordination of ketone. This may be due to a higher bonding energy of phosphines towards ruthenium than towards rhodium and/or to the different geometries of these small polyhedral NPs as a result of their different crystal structure, namely hcp and fcc.²⁰

Comparing the results from Table 3.4 and Table 3.5, it can be observed that the rhodium NPs reduce selectively the arene in compounds **2.4** and **2.5**, since these catalysts do not reduce alkyl ketones such as **2.3a**. However, in the case of acetophenone **2.3** the reduction of the ketone group is preferred. Concerning, ruthenium NPs the situation is different since reduction of arene and carbonyl groups are competitive for all substrates, including for non-conjugated aryl ketones. Although the selectivity towards arene reduction also increases when aryl and keto groups become more and more separated (Scheme 3.10).

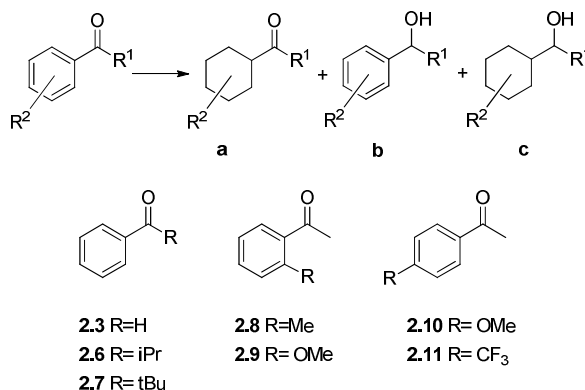


Scheme 3.10. Schematic representation of the selectivity trends observed in the hydrogenation of aryl ketones **2.4**, **2.5**.

3.3.5. Hydrogenation of Substituted Acetophenones Using Ruthenium Nanoparticles

All the results presented suggest that acetophenone **2.3**, which is often selected for testing the competition between reduction of arene and carbonyl group, is in fact a particular case that deserves additional attention. In this context, it was decided to enlarge the study to the reduction of the acetophenone derivatives. Compounds **2.6-2.11** containing different substituents in the alkyl and phenyl moieties were hydrogenated and the results obtained are summarized in Table 3.6.

In general, low to moderate activities were observed using **Ru1-2** nanoparticles. Lower conversion were obtained when there was an increase of the substitution in the alkyl chain (Table 3.6, Entries 3-6) or in the aromatic ring (Table 3.6, Entries 7-14), particularly when the substituents are located in *ortho* position (Table 3.6, Entries 7-10).

Table 3.6. Ru-NPs (**Ru1,2**) catalysed hydrogenation of ketones **2.6-2.11**.^a


Entry	Substrate	NPs	Conv. (%) ^b	a ^b	b ^b	c ^b
1 ^d	2.3	Ru1	90	57(96) ^c	4	39
2	2.3	Ru2	70	43(56) ^c	41	16
3 ^d	2.6	Ru1	39	54(67) ^c	33	13
4	2.6	Ru2	35	47(59) ^c	41	12
5 ^d	2.7	Ru1	35	38(46) ^c	54	8
6	2.7	Ru2	36	35(41) ^c	59	6
7 ^d	2.8	Ru1	44	64	36	-
8	2.8	Ru2	25	36	64	-
9 ^d	2.9	Ru1	39	39	61	-
10	2.9	Ru2	20	22	78	-
11 ^d	2.10	Ru1	60	34(50) ^c	50	16
12	2.10	Ru2	42	18(37) ^c	63	19
13 ^d	2.11	Ru1	62	16	84	-
14	2.11	Ru2	49	14	86	-

^aGeneral conditions: Ru-NPs (2 mol%), substrate (1.24 mmol), THF (10 ml), T = 30 °C, P= 20 bar H₂, t=5h. ^bDetermined by GC. ^cSelectivity in arene reduction considering that compound **c** it has been generated from **a**. ^dt= 2.5 h.

For substrates **2.8**, **2.9** and **2.11**, the products resulting from the total reduction were not observed (Table 3.6, Entries 7-10, 13-14). The stabilizing ligand also affected significantly the activity of these catalysts and, in general, when **Ru1** NPs were used, higher or similar activity than with **Ru2** NPs was obtained (take into account the different reaction times for both nanoparticles

systems). This indicates that in this case, the coordination of both aromatic ring and keto groups are strongly affected by steric factors in the substrate or in the ligand. Consequently, low conversions were achieved for substrates **2.8** and **2.9**, respectively (Table 3.6, Entries 8 and 10).

The selectivity was shifted towards ketone reduction when the steric hindrance in the substrate was increased or when dppb was used as stabilizer indicating that the rate of arene reduction is more affected than that of ketone reduction. Furthermore, using ruthenium nanoparticles, the substrate **2.11** has a particular behaviour, since the reaction affords high percentages of carbonyl group reduction. This fact probably confirms the slow arene reduction in the 1-arylethanol derivative, since in this case, product **2.11c** was not observed.

Comparing the results obtained with substrates **2.3** and **2.6-2.11**, the reduction of the arene group is largely preferred in compound **2.3** as a consequence of the affinity of the arene for the NPs. However, the results obtained with the substituted compounds indicate that small variations in the steric properties of the substituents of the aromatic ring and of the alkyl keto group cause important shifts in selectivity.

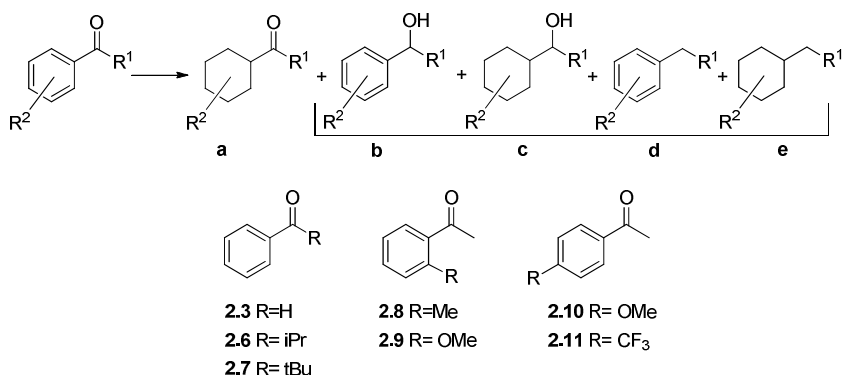
3.3.6. Hydrogenation of Substituted Acetophenones Using Rhodium Nanoparticles

The same substrates **2.6-2.11** were hydrogenated using **Rh1-2** nanoparticles. The results are presented in Table 3.7 (results obtained in the reduction of acetophenone **2.3**, under the same reaction conditions are also included for comparison). It is important to highlight that, since it was demonstrated in Table 3.4, **Rh1-2** do not reduce cyclohexyl alkyl ketones it can be considered that compounds **c**, **d**, **e**, are generated from **b**, and a new value resulting from the addition of the percentages of all these compounds was included in the table.

As it can be observed in Table 3.7, the activity of the catalysts is significantly affected by the steric hindrance of the alkyl substituent of the ketone (compounds **2.6-2.7**, Entries 3-6) but the ratio of products a: b+c+d+e remains practically unchanged when the substituent varies from a *iso*-propyl to a *tert*-butyl group.

However, when the substituents are on the aromatic ring, they have little influence and high activities are obtained in all cases (Table 3.7, Entry 7-11). It is worth noting that, in contrast with previous studies which determined that substrates with electron donating groups are hydrogenated faster than substrates with electron-withdrawing groups,⁸ no clear effect of the substituents on the aromatic ring on the activity was observed in this study (Table 3.7, Entries 11-14).

Concerning the selectivity, products obtained from reduction of the ketone group were preferably obtained in all cases (>70%), in agreement with the results observed for compound **2.3**. In general, ketone reduction slightly decreases when **Rh2** (dppb stabilizer) is used. The selectivity is not influenced by the modification of the alkyl moiety, but is more significantly affected when substituents are present on the arene moiety. This is particularly true when the substituent is located in *para* position, since arene reduction decreases notably (Table 3.7, Entries 10-14). Interestingly, using **Rh2** nanoparticles as catalysts, exclusive reduction of the carbonyl group was obtained in the reduction of compound **2.11**, which incorporates the electron withdrawing group CF₃. Nevertheless, a general trend concerning the influence of the stabilizing ligand on the selectivity cannot be established.

Table 3.7. Rh-NPs (**Rh1-2**) catalysed hydrogenation of ketones **2.6-2.11**.^a

Entry	Substrate	NPs	Conv. (%) ^b	a (%) ^b	(b+c+d+e) ^b
1	2.3	Rh1	90	15	85 ^c (23,33,12,17)
2	2.3	Rh2	100	28	72 ^c (46,26,-,-)
3	2.6	Rh1	90	13	87 ^c (69,18,-,-)
4	2.6	Rh2	91	21	79 ^c (63,16,-,-)
5	2.7	Rh1	50	18	82 ^c (71,11,-,-)
6	2.7	Rh2	54	27	79 ^c (66,7,-,-)
7	2.8	Rh1	85	24	76 ^c (59,-,14,3)
8	2.8	Rh2	81	32	68 ^c (59,9,-,-)
9	2.9	Rh1	100	20	80 ^c (50,-,26,4)
10	2.9	Rh2	75	11	89 ^c (73,16,-,-)
11	2.10	Rh1	96	17	83 ^c (43,9,24,7)
12	2.10	Rh2	98	16	84 ^c (48,36,-,-)
13	2.11	Rh1	100	8	92 ^c (57,-,23,12)
14	2.11	Rh2	100	0	100 ^c (87,13,-,-)

^aGeneral conditions: Rh-NPs (2 mol%), substrate (1.24 mmol), THF (10 ml), T = 30 °C, P= 20 bar H₂, t=5h. ^b% determined by GC. ^cAddition of percentage of compounds **b-e**.

Moreover, similarly to the results obtained for substrate **2.3**, hydrogenolysis of 1-phenylethanol derivatives, produced by the reduction of the carbonyl group of the substrates to provide ethyl benzene and then ethylcyclohexane was only observed with the **Rh1** nanoparticles stabilized with PPh₃. These results can be related with the lability of the monophosphine in contrast with the stronger coordinating diphosphine. Indeed, PPh₃ can

dissociate from the particle and therefore liberate the sites responsible for the hydrogenolysis reaction. These sites are therefore expected to be the apex and edge sites which are left undercoordinated.

It is noteworthy that the hydrogenolysis process was stopped when the steric hindrance of the alkyl side chain increases, but not when the substituents are present in *ortho* or *para* position of the aromatic ring.

To summarize, in the case of rhodium nanoparticles, the coordination of the arene group dominates the interaction of the substrate with the catalyst surface, while the coordination of carbonyl group with the nanoparticle is not evidenced by the results of this study since for substrates such as aromatic compounds containing a carbonyl group far from the ring, the aromatic ring is mainly reduced. The case of acetophenone derivatives is singular, since despite coordination to the nanoparticle takes place through the aromatic ring, the carbonyl group remains in a position very favourable for its reduction, in such a way that it takes place faster than the arene reduction. The selectivity of this process is scarcely affected by substitution in the alkyl or arene sides, and only the substitution in *para* completely drives the reaction towards the reduction of ketone. No significant electronic effect was observed (Table 3.7, Entries 11, 12 vs. 13, 14).

Interestingly, once the carbonyl group is reduced, further aromatic ring reduction can take place and hydrogenolysis is also observed when the reaction is catalysed by **Rh1** (PPh₃ stabilizer).

3.4. CONCLUSIONS

A series of Ru and Rh nanoparticles stabilized by P-based ligands were successfully synthesized and characterized. Comparable results in terms

of size and stabiliser content were obtained when similar metal/ligand ratios were used. In a comparative study, these nanoparticles were used as catalysts in the reduction of various substituted phenyl, benzyl and phenethyl ketones.

In the case of arylketones, acetophenone **2.3** was used as model substrate and it can be concluded that:

- i) Ruthenium nanoparticles are more selective than rhodium nanoparticles for the reduction of the aryl group.
- ii) The stabilizing ligand PPh₃ (**Ru1**) provides higher selectivities towards the arene hydrogenation rather than dppb (**Ru2**).
- iii) The selectivity towards the arene hydrogenation is negatively affected by the presence of substituents on the aromatic ring.
- iv) The presence of electron-withdrawing substituents in **2.11** and the steric hindrance induced by substituents in the keto group were also shown to affect the selectivity in favour of the keto group reduction.
- v) Rhodium nanoparticles have a clear tendency to preferentially reduce the keto group of arylketones and this trend was enhanced by the same factors than in the case of ruthenium. Interestingly, only **Rh1** nanoparticles provided hydrogenolysis products under the conditions used.

Concerning the non-conjugated aryl ketones (**2.4-2.5**), it can be concluded that:

- vi) For both metals, arene reduction was mainly observed although higher selectivities were observed when Rh catalysts were used. In the case of the reduction of substrate **2.5** with rhodium, this process is practically exclusive.
- vii) Selectivity to arene reduction increases when the distance between the arene and the ketone group increases.

viii) The influence of the ligand on the selectivity was distinct for ruthenium and rhodium. For both rhodium systems, similar selectivities were obtained, while in the case of ruthenium higher value for arene reduction were obtained with **Ru1**.

3.5. EXPERIMENTAL PART

General Methods

All syntheses were performed using standard Schlenk techniques under argon atmosphere. Chemicals were purchased from Aldrich Chemical Co and Alfa Aesar and used without further purification. All solvents were purified by distillation following standard procedures and were deoxygenated before use. The precursor [Ru(COD)(COT)] was purchased from Nanomeps. The precursor $\text{Rh}(\eta^3\text{-C}_3\text{H}_5)_3$, was prepared following previously described methods.²¹ The synthesis of the nanoparticles was performed using 1L Fisher Porter and pressurized to 3 bar on a high pressure line.

All reactions temperatures were kept electronically controlled by heating baths.

Characterization Techniques

Transmission Electron Microscopy (TEM)

TEM experiments were performed at the “Unitat de Microscopia dels Serveis Científicotècnics de la Universitat Rovira i Virgili” (TEM-SCAN) in Tarragona with a Zeiss 10 CA electron microscope operating at 100 kV with resolution of 3 Å. The particles size distributions were determined by a manual analysis of enlarged images. At least 300 particles on a given grid were measured in order to obtain a statistical size distribution and a mean diameter.

High Resolution TEM (HRTEM)

HRTEM experiments were performed at the Unitat de Microscopia dels Serveis Científics i Tecnològics de la Universitat de Barcelona with a JEOL 1010 electron microscope working at 200kV with a resolution of 2.5 Å. The particles size distributions were determined by a manual analysis of enlarged images.

Thermo Gravimetric Analysis (TGA)

TGA experiments were carried out in the oven of a Mettler Toledo TGA/SDTA851 instrument.

1-2 mg of the nanoparticles were placed in the sample holder in the oven and it was heated up at a rate of $10^{\circ}\text{Cmin}^{-1}$ in N_2 , while the weight was recorded continuously from 30°C to 900°C . The weight loss of the organic part and metal were used to calculate the approximate number of ligands coordinated on the metal surface.

X-Ray Diffraction (XRD)

XRD measurements were performed using a Siemens D5000 diffractometer (Bragg- Brentano parafocusing geometry and vertical θ - θ goniometer) fitted with a curved graphite diffracted- beam monochromator, incident and diffracted- beam Soller slits, a 0.06° receiving slit and scintillation counter as a detector. The angular 2θ diffraction range was between 26 and 95° . The data were collected with an angular step of 0.05° at 16s per step and sample rotation. A low background Si(510) wafer was used as sample holder. $\text{CuK}\alpha$ radiation was obtained from a copper X- ray tube operated at 40 kV and 30 mA .

Wide Angle X-ray Scattering (WAXS)

WAXS analyses were performed at CEMES-CNRS. Samples were sealed in 1 mm diameter Lindemann glass capillaries. The samples were irradiated with graphite-monochromatized $\text{Mo}_{\text{K}\alpha}$ (0.071069 nm) radiation and the X-ray intensity scattered measurements were performed using a dedicated two-axis diffractometer. Radial distribution functions (RDF) were obtained after Fourier transform of the reduced intensity functions.

X-Ray Photoelectron Spectroscopy (XPS)

XPS measurement were performed using a PHI 5500 Multitechnique System (from Physical Electronics) with a monochromatic X-ray source (Aluminium Kalfa line of 1486.6 eV energy and 350 W), placed perpendicular to the analyser axis and calibrated using the 3d5/2 line of Ag with a full width at half maximum (FWHM) of 0.8 eV. The analysed area was a circle of 0.8 mm diameter, and the selected resolution for the spectra was 187.5eV of Pass Energy and 0.8 eV/ step for the general spectra and 23.5 eV of Pass Energy and 0.1 eV/step for the spectra of the different elements in the depth profile spectra. A low energy electron gun (<10 eV) was used in order to discharge the surface when necessary. All measurements were performed in an ultra-high vacuum (UHV) chamber pressure between 5×10^{-9} and 2×10^{-8} torr. The data processing was carried out using the CasaXPS program.

General procedure for the synthesis of ruthenium nanoparticles

In a typical procedure, the $[\text{Ru}(\text{COD})(\text{COT})]$ (400 mg, 1.268 mmol) was placed into a Fischer-Porter reactor in 400 mL of dry and deoxygenated THF by freeze-pump-thaw cycles in the presence of the ligand (0.2 eq. for dppb and 0.4 eq. for PPh_3). The Fischer-Porter reactor was pressurised under 3 bar of H_2 and stirred for 24 h at room temperature. Then the solution was

concentrated under reduced pressure to 40 ml. Precipitation and washing with pentane (3x15 ml) was then carried out, obtaining a black precipitate.

General procedure for the synthesis of rhodium nanoparticles

In a typical procedure, the $[\text{Rh}(\eta^3\text{-C}_3\text{H}_5)_3]$ (400 mg, 1.746 mmol) was placed into a Fischer-Porter reactor at $-110\text{ }^\circ\text{C}$ (acetone/ N_2 bath) in 64 mL of dry and deoxygenated THF by freeze-pump-thaw cycles in the presence of the appropriate ligand (0.2 equiv. for dppb and 0.4 equiv. for PPh_3). The Fischer-Porter reactor was pressurised under 6 bar of H_2 and stirred for 30 minutes at room temperature. After that time, the solution was then heated to 40°C and stirred at this temperature during 24 h. Then the solution was concentrated under reduced pressure. Precipitation and washing with pentane (3 x 15mL) was then carried out, obtaining a black precipitate.

Ru1 nanoparticles stabilized by 0.4 eq of PPh_3 :

- *TEM*: mean size 1.32 ± 0.28 nm.
- *XRD*: hcp crystalline Ru nanoparticles, coherence length 1.01 ± 0.02 nm.
- *XPS*: $3d_{5/2}$ (280.68 eV) and $3d_{3/2}$ (285.38 eV), 100% Ru (0) at the nanoparticles surface.
- *TGA*: 69% Ru, 29% PPh_3 , 2% THF.
Approximate formula: $[\text{Ru}_{89}\text{THF}_5\text{L}_{15}]$.

Ru2 nanoparticles stabilized by 0.2 eq dppb:

- *TEM*: mean size 1.49 ± 0.35 nm.
- *XRD*: hcp crystalline Ru nanoparticles, coherence length 1.12 ± 0.05 nm.
- *XPS*: $3d_{5/2}$ (280.53 eV) and $3d_{3/2}$ (285.23 eV), 6% $\text{Ru}^{\delta+}$ at the nanoparticles surface.
- *TGA*: 72% Ru, 25% dppb, 3% THF.
Approximate formula: $[\text{Ru}_{127}\text{THF}_9\text{L}_{11}]$.

Rh1 nanoparticles stabilized by 0.4 eq of PPh₃:

- *TEM*: mean size 1.52±0.21 nm.
- *XRD*: fcc crystalline Rh nanoparticles, coherence length 1.49±0.03 nm.
- *XPS*: 3d_{5/2} (308.32 eV) and 3d_{3/2} (313.02 eV), 40% Rh^{δ+} at the nanoparticles surface.
- *TGA*: 72% Rh, 27% PPh₃, 1% THF.

Approximate formula: [Rh₁₃₂ THF₂ L₂₀].

Rh2 nanoparticles stabilized by 0.2 eq dppb:

- *TEM*: mean size 1.57±0.25 nm.
- *XRD*: fcc crystalline Rh nanoparticles, coherence length 1.49±0.07 nm.
- *XPS*: 3d_{5/2} (307.43 eV) and 3d_{3/2} (312.13 eV), 100% Rh (0) at the nanoparticles surface.
- *TGA*: 69% Rh, 29% dppb, 2% THF.

Approximate formula: [Rh₁₄₆ THF₈ L₁₅].

General procedure for the hydrogenation reactions

Autoclave Par 477 equipped with PID control temperature and reservoir for kinetic measurements and HEL 24 Cat reactor for substrate scope were used as reactors for the hydrogenation reactions. In a typical experiment, the autoclave was charged in the glove-box with Ru or Rh nanoparticles (3 mg for Ru-NPs; 3.5 mg of Rh-NPs; the catalyst concentration was calculated based on the total number of metallic atoms in the NPs) and the substrate (1.24 mmol, approx. substrate to metal ratio=55) in 10 mL of THF. Molecular hydrogen was then introduced until the desired pressure was reached. The reaction was stirred during the corresponding time at 30°C. The autoclave was then depressurised. The solution was filtered over silica and analysed by gas chromatography. The conversion and the selectivities of the

product were determined using a Fisons instrument (GC 9000 series) equipped with a HP-5MS column.

Conversion and selectivity was determined by GC-M spectroscopy. GC-MS spectroscopy was carried out on a HP 6890A spectrometer, with an achiral HP-5 column (0.25mm x 30m x 0.25 μ m). The method used consist in an initial isotherm period at 40°C for 3 min followed by a 3°C min⁻¹ temperature ramp to 120°C and a hold time of 12 min, flow 1.3 ml/min.

Substrate **3.1**: $tr_{3,1}$ = 16.70 min, $tr_{3,1a}$ = 15.0 min, $tr_{3,1b}$ = 1.58 min, $tr_{3,1c}$ = 15.82 min, $tr_{3,1e}$ = 6.30 min.

Substrate **3.2**: $tr_{3,2}$ = 19.80 min, $tr_{3,2a}$ = 19.07 min, $tr_{3,2b}$ = 20.01 min, $tr_{3,2c}$ = 20.14 min, $tr_{3,2d}$ = 10.71 min, $tr_{3,2e}$ = 12.77 min, $tr_{3,2f}$ = 8.36 min.

Substrate **3.3**: $tr_{3,3}$ = 25.24 min, $tr_{3,3a}$ = 24.79 min, $tr_{3,3b}$ = 25.87 min, $tr_{3,3c}$ = 25.05 min.

Substrate **3.4**: $tr_{3,4}$ = 23.44 min, $tr_{3,4a}$ = 21.4 min, $tr_{3,4b}$ = 23.65 min, $tr_{3,4c}$ = 23.06 min, $tr_{3,4d}$ = 24.61 min.

Substrate **3.5**: $tr_{3,5}$ = 24.82 min, $tr_{3,5a}$ = 23.04 min, $tr_{3,5b}$ = 26.28 min, $tr_{3,5c}$ = 25.36 min, $tr_{3,5d}$ = 25.71 min.

Substrate **3.6**: $tr_{3,6}$ = 20.18 min, $tr_{3,6a}$ = 18.20 min, $tr_{3,6b}$ = 22.14 min, $tr_{3,6c}$ = 19.70 min, $tr_{3,6d}$ = 12.51 min, $tr_{3,6e}$ = 10.11 min.

Substrate **3.7**: $tr_{3,7}$ = 27.54 min, $tr_{3,7a}$ = 22.80 min, $tr_{3,7b}$ = 27.09 min, $tr_{3,7c}$ = 23.06 min, $tr_{3,7d}$ = 17.60 min, $tr_{3,7e}$ = 13.70 min.

Substrate **3.8**: $tr_{3,8}$ = 30.21 min, $tr_{3,8a}$ = 24.72 min, $tr_{3,8b}$ = 28.33 min, $tr_{3,8c}$ = 24.85 min, $tr_{3,8d}$ = 15.53 min, $tr_{3,8e}$ = 14.72 min.

Substrate **3.9**: $tr_{3,9}$ = 16.65 min, $tr_{3,9a}$ = 17.89 min, $tr_{3,9b}$ = 19.16 min, $tr_{3,9c}$ = 18.30 min, $tr_{3,9d}$ = 9.45 min, $tr_{3,9e}$ = 9.62 min.

3.6. REFERENCES

1. (a) Abdel-Magid, A. F. *Reductions in Organic Synthesis*. ACS Symposium Series 641. Washington DC: American Chemical Society, 1996. (b) Hudlick, M. *Reductions in Organic Chemistry*. ACS Monograph 188, 2nd ed.; Washington DC: American Chemical Society, 1996.
2. Fonseca, G. S.; Scholten, J. D.; Dupont, J. *Synlett* **2004**, *9*, 1525–1528.
3. (a) Kogan, V.; Aizenshtat, Z.; Neumann, R. *New J. Chem.* **2002**, *26*, 272–274. (b) Lenarda, M.; Casagrande, M.; Moretti, E.; Storaro, L.; Frattini, R.; Polizzi, S. *Catal. Lett.* **2007**, *114*, 79–84. (c) Janusklewick, K. R.; Alper, H. *Organometallics* **1983**, *2*, 1055–1057. (d) Bergault, I.; Fouilloux, P.; Joly-Vuillemin, C.; Delmas, H. *J. Catal.* **1998**, *175*, 328–337. (e) Gelman, F.; Avnir, D.; Schumann, H.; Blum, J. *J. Mol. Catal. A: Chem.* **2001**, *171*, 191–194. (f) Casagrande, M.; Storaro, L.; Talon, A.; Lenarda, M.; Frattini, R.; Rodriguez-Castellon, E.; Maireles-Torres, P. *J. Mol. Catal. A: Chem.* **2002**, *188*, 133–139. (g) Ito, M.; Endo, Y.; Ikariya, T. *Organometallics* **2008**, *27*, 6053–6055. (h) Duraczynska, D.; Drelinkiewicz, A.; Bielanska, E.; Serwicka, E. M.; Litynska-Dobrzynska, L. *Catal. Lett.* **2011**, *141*, 83–94.
4. (a) Anderson, J. A.; Athawale, A.; Imrie, F. E.; Kenna, F. –M. M.; Cue, A. M.; Molyneux, D.; Power, K. *J. Catal.* **2010**, *270*, 9–15. (b) Song, L.; Li, X.; Wang, H.; Wu, H.; Wu, P. *Catal. Lett.* **2009**, *133*, 63–69. (c) Motoyama, Y.; Takasaki, M.; Yoon, S. H.; Mochida, I.; Nagashima, H. *Org. Lett.* **2009**, *11*, 5042–5045. (d) Guerrero, M.; Roucoux, A.; Denicourt-Nowicki, A.; Bricout, H.; Monflier, E.; Collière, V.; Fajerweg, K.; Philippot, K. *Catal. Today* **2012**, *183*, 34–41. (e) Chau, N. T. T.; Handjani, S.; Guegan, J.-P.; Guerrero, M.; Monflier, E.; Philippot, K.; Denicourt-Nowicki, A.; Roucoux, A. *ChemCatChem* **2013**, *5*, 1497–1503. (f) Rafter, E.; Gutmann, T.; Löw, F.; Buntkowsky, G.; Philippot, K.; Chaudret, B.; van Leeuwen, P. W. N. M. *Catal. Sci. Technol.* **2013**, *3*, 595–599. (g) Denicourt-Nowicki, A.; Leger, B.; Roucoux, A. *Phys. Chem. Chem. Phys.* **2011**, *13*, 13510–13517. (h) Park, I. S.; Kwon, M. S.; Kang, K. Y.; Lee, J. S.; Park, J. *Adv. Synth. Catal.* **2007**, *349*, 2039–2047.
5. Fonseca, G. S.; Umpierre, A. P.; Fichtner, P. F. P.; Teixeira, S. R.; Dupont, J. *Chem. Eur. J.* **2003**, *9*, 3263–3269.
6. (a) Widegren, J. A.; Finke, R. G. *Inor. Chem.* **2002**, *41*, 1558–1572. (b) Gual, A.; Godard, C.; Castellón, S.; Claver, C. *Dalton Trans.* **2010**, *39*, 11499–11512.
7. Jahjah, M.; Kihn, Y.; Teuma, E.; Gómez, M. *J. Mol. Catal. A: Chem.* **2010**, *332*, 106–112.

8. Gonzalez-Galvez, D.; Lara, P.; Rivada-Wheelaghan, O.; Conejero, S.; Chaudret, B.; Philippot, K.; van Leeuwen, P. W. N. M. *Catal. Sci. Technol.* **2013**, *3*, 99–105.
9. Guerrero, M.; Coppel, Y.; Chau, N. T. T.; Roucoux, A.; Denicourt-Nowicki, A.; Monflier, E.; Bricout, H.; Collière, V.; Lecante, P.; Philippot, K. *ChemCatChem* **2013**, *5*, 1–11.
10. Snelders, D. J. M.; Yan, N.; Gan, W.; Laurenczy, G.; Dyson, P. J. *ACS Catal.* **2012**, *2*, 201–207.
11. Pelzer, K.; Laleu, B.; Lefebvre, K.; Philippot, K.; Chaudret, B.; Candy, J. P.; Basset, J. M. *Chem. Mater.* **2004**, *16*, 4937–4941.
12. Austin, B. M.; Zubarev, D. Y.; Lester, W. A. J. *Chem. Rev.* **2012**, *112*, 263–288.
13. Escárcega-Bobadilla, M. V.; Tortosa, C.; Teuma, E.; Pradel, C.; Orejón, A.; Gómez, M.; Masdeu-Bultó, A. M. *Catal. Today* **2009**, *148*, 398–404.
14. García-Antón, J.; Axet, M. R.; Jansat, S.; Philippot, K.; Chaudret, B.; Pery, T.; Buntkowsky, G.; Limbach, H. *Angew. Chem. Int. Ed.* **2008**, *47*, 2074–2078.
15. Llop-Castelbou, J.; Gual, A.; Mercadé, E.; Claver, C.; Godard, C. *Catal. Sci. Technol.* **2013**, *3*, 2828–2833.
16. Gual, A.; Godard, C.; Philippot, K.; Chaudret, B.; Denicourt-Nowicki, A.; Roucoux, A.; Castellón, S.; Claver, C. *ChemSusChem* **2009**, *2*, 769–779.
17. Lara, P.; Philippot, K.; Chaudret, B. *ChemCatChem* **2013**, *5*, 28–45.
18. Jutz, F.; Andanson, J. –M.; Baiker, A. *J. Catal.* **2009**, *268*, 356–366.
19. Jantke, D.; Cokoja, M.; Drees, M.; Herrmann, W. A.; Kühn, F. E. *ChemCatChem* **2013**, *5*, 3241–3248.
20. Xia, Y.; Xiong, Y.; Lim, B.; Skrabalak, S. E. *Angew. Chem. Int. Ed.* **2009**, *48*, 60–103.
21. (a) Fryzuk, M. D.; Piers, W. E. *Organometallic Syntheses*. Eds.: King, R. B.; Eisch, J. J. Amsterdam: Elsevier, 1986, vol. 3, 128. (b) Herrmann, W. A. *Synthetic Methods of Organometallic and Inorganic Chemistry*. Ed.: Herrmann, W. A. Stuttgart: Thieme, 1996, 38.

*C*HAPTER 4

SELECTIVE HYDROGENATION OF POLYCYCLIC ARENES USING RUTHENIUM NANOPARTICLES

4.1. INTRODUCTION TO THE HYDROGENATION OF POLYCYCLIC AROMATIC HYDROCARBONS

Polycyclic aromatic hydrocarbons (PAHs) are a class of organic compounds comprising two or more fused benzene rings with different structural arrangements.¹ PAHs have earned considerable attention due to their toxic, carcinogenic and teratogenic effects.² Their hydrophobicity permits a high resistance to natural degradation processes and the developing of removing methods is getting much relevance for environmental and human health reasons. Different methods have been proposed for remediation of PAHs like thermal treatment, bio-remediation, photo-degradation, chemical oxidation, etc. but these processes are slow and that imply complex techniques with high energy consumption.³

As it was commented in Chapter 1, in the last few years, metal nanoparticles have been widely used in different domains such as medicine, sensors or catalysis. Particularly in catalysis, nanoparticles are advantageous for the moderate reaction conditions needed, the high selectivity and activity obtained due to their small particle size (high surface area), their unique electronic effects and their potentially low cost.

Nanoparticles have been used in a wide assortment of reactions. In particular, several studies have been focused on the hydrogenation of aromatic compounds due to their usefulness for preparing key intermediates in organic chemistry and for the production of aromatic-content-free-fuels.⁴ However, there have been only few studies concerning the hydrogenation of polyaromatics substrates under ambient or mild reaction conditions using nanoparticles.⁵

It is important to highlight the fact that the hydrogenation of arenes is much more difficult than the reduction of simple olefins due to the resonance stabilization. Moreover, at least under mild conditions, monocyclic arenes are more difficult to hydrogenate than polycyclic arenes.⁶ Marshall *et al.* concluded that the partial hydrogenation of PAHs does not suffer a dramatic loss of resonance compared to mono-ring compounds but longer reaction times are needed to obtain complete hydrogenation (a greater number of fused benzene rings implies longer reaction times).⁷

In addition, several factors should be considered in order to understand the decrease in reaction rates when the hydrogenation of PAHs proceeds:

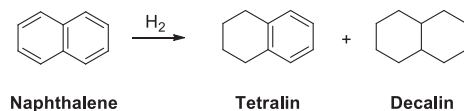
- Adsorption constant: for heterogeneous catalysis, the adsorption of reactants on catalyst surfaces is a crucial step before the surface reaction and, in general, it increases with the number of fused benzene rings. For example, the adsorption constant of phenanthrene is approximately 1.5 times higher than the constant of naphthalene.⁸
- Superdelocalizability (S_r): index to measure the hydrogen-accepting abilities of an atom in aromatic rings. The higher S_r value, the easier an atom can accept a hydrogen atom.⁹
- Loss of resonance energy: as it was commented before, the hydrogenation of monocyclic arenes implies a higher loss of resonance energy than polycyclic arenes. For instance, the resonance energy of benzene and naphthalene is approximately 151 and 255 $\text{kJ}\cdot\text{mol}^{-1}$, respectively. When benzene is

hydrogenated to cyclohexane, it loses all its resonance energy, ($151 \text{ kJ}\cdot\text{mol}^{-1}$) but, in the case of naphthalene, it only loses $104 \text{ kJ}\cdot\text{mol}^{-1}$ when is hydrogenated to tetralin.⁶

- Hydrogen accessibility: the access of the adsorbed hydrogen atoms to the adsorbed PAHs substrates on catalyst surface will be influenced by the extruding hydrogen atoms and by the hindrance generated by the polyaromatic substrates.¹⁰

4.1.1. HYDROGENATION OF NAPHTHALENE

Naphthalene has probably been the polyaromatic system the most studied in hydrogenation reactions (Scheme 4.1).



Scheme 4.1. Products formed in the hydrogenation of naphthalene.

Initially, in 1996, Huand and Kang investigated the hydrogenation of naphthalene on some noble metals such as platinum and palladium obtaining decalins rather than tetralins.¹¹

In 2008, Song *et al.* reduced naphthalene to tetralin at 1 atm of hydrogen pressure using a Pd/C catalyst in the presence of an ionic liquid but the hydrogenation to decalin is still a challenge under mild reaction conditions.¹²

One of the first examples related to the use of nanoparticles in the naphthalene hydrogenation was reported in 2002. In this paper, naphthalene was reduced using rhodium nanoparticles in a water-supercritical CO₂

microemulsion and after one hour 96% of conversion was achieved and tetralin was obtained as unique product.¹³

Finally, in 2013, Fang *et al.* studied a new platinum supported catalyst in the reduction of naphthalene. In some experiments, dibenzothiophene (DBT) was added to test the sulfur tolerance of the catalyst. The platinum supported catalyst showed better sulfur resistance than that of Pt/Alumina. The excellent catalytic performance and sulfur tolerance was attributed to the combination of high acidity and mesoporous structure of the catalyst.¹⁴

4.1.2. HYDROGENATION OF POLYCYCLIC AROMATIC HYDROCARBONS CONTAINING MORE THAN TWO FUSED ARENES

The hydrogenation of naphthalenes is known to take place under mild reaction conditions using a variety of catalysts. Nonetheless, the reduction of polycyclic arenes requires higher temperatures and pressures and mixture of products are in general obtained (low selectivity).¹⁵

In 1995, Quann *et al.* studied the catalytic hydrogenation of some PAHs like naphthalene, anthracene, pyrene, etc. over presulfided CoMo/Al₂O₃ catalysts in cyclohexane at 350°C and 68 atm of H₂ pressure and it was deduced the fact that the reactivity decreased with the number of aromatic rings. This fact was justified by different adsorption parameters that clearly increased with the increasing aromatic rings number.¹⁶

Then in 2002, Blum and co-workers hydrogenated anthracene, phenanthrene, triphenylene, pyrene and perylene (Figure 4.1) using a palladium-rhodium system embedded in a silica sol-gel matrix at 80°C and 400 psi (30 bar approx.). Mixtures of products and low selectivities in all the cases were obtained.¹⁷ For instance, in the case of anthracene 60% of

selectivity towards 1,2,3,4,5,6,7,8-octahydroanthracene was observed, 37% towards 9,10-dihydrophenanthrene in the case of phenanthrene or 27% of selectivity towards 1,2,3,4,5,6,7,8-octahydrotriphenylene in the case of triphenylene.

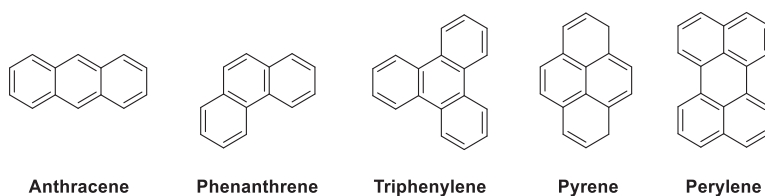


Figure 4.1. Structures of selected polycyclic aromatic hydrocarbons.

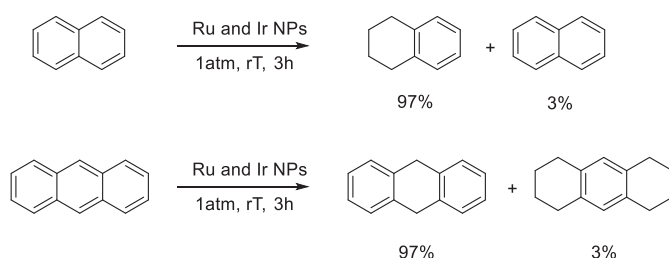
Different polycyclic arenes were hydrogenated over activated carbon at 300°C and it was concluded that the hydrogenation was dependent on the hydrogen-accepting abilities of the arenes (S_r value, Table 4.1) and on the adsorption strengths to the catalyst.⁹ In addition, the hydrogen transfer was also studied.⁴

Table 4.1. S_r values of different polycyclic arenes.¹⁸

Position				
1	0.833	0.994	0.978	1.073
2		0.873	0.859	0.922
3			0.892	
4			0.940	
9		0.703	0.998	1.314

Nanoparticles have also been used as catalyst for the hydrogenation of polycyclic aromatic hydrocarbons with more than two fused rings. Nevertheless, totally hydrogenated products are rarely obtained.¹⁹ For instance, in 2007, Park and co-workers, synthesized Rh and Ir nanoparticles

entrapped in aluminium oxyhydroxide nanofibers which were applied in arene hydrogenation reactions. High yields and selectivities in the hydrogenation of bicyclic and tricyclic aromatic compounds were obtained by controlling the reaction conditions. Naphthalene was reduced to tetralin and anthracene to 9,10-dihydroanthracene at room temperature with a hydrogen balloon (1 atm, Scheme 4.2). However, long reactions times were needed for obtaining the total hydrogenated products and high catalyst loading in the case of anthracene.²⁰



Scheme 4.2. Hydrogenation of naphthalene and anthracene at 1 atm and room temperature.²⁰

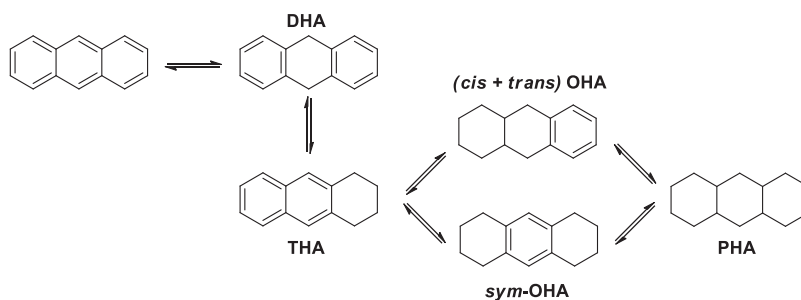
Supported Pd, Rh and Rh/Pd nanoparticles on CNT have also been used to hydrogenate arenes and anthracene showing an unusually high catalytic activity.²¹ In all the cases, moderate to high selectivities towards the partial hydrogenation of anthracene (major product 1,2,3,4,5,6,7,8-octahydroanthracene) were obtained and the total hydrogenated product could not be achieved even under 10 bar of H₂ pressure.

Concerning triphenylene, it is important to highlight that the central ring is very difficult to saturate.^{7,17} Few examples are reported in which the total hydrogenated product is observed.²² With rhodium nanoparticles supported on carbon nanotubes, high selectivities towards 1,2,3,4,5,6,7,8,9,10,11,12-dodecahydrotriphenylene were obtained under mild reaction conditions (10 atm H₂ and room temperature) after 3 hours of

reaction. Rh/C and other commercial Rh nanocatalyst were not useful for this purpose.^{22b}

Finally, the hydrogenation of other polycyclic aromatic hydrocarbon compounds like pyrene or phenanthrene has also been attempted in the presence of supercritical carbon dioxide.²³ For instance, Pd nanoparticles stabilized in polydimethylsiloxane (PDMS) have been used to hydrogenate polychlorinated biphenyls (PCBs) and polycyclic aromatic hydrocarbons (200 atm of CO₂, 10 atm of H₂ and 1 hour).²⁴ Affording total hydrogenated products for naphthalene, anthracene, phenanthrene and pyrene.

The last study reported on the hydrogenation of polycyclic aromatic compounds describes the use of carbon-supported Pd nanoparticles in the hydrogenation of anthracene. A study of the dependence of the selectivity on the temperature and the reaction time was performed and a hydrogenation mechanism is proposed (Scheme 4.3).²⁵



Scheme 4.3. Proposed mechanism for the anthracene hydrogenation using carbon-supported Pd nanoparticles as catalyst.²⁵

4.1.3. HYDROGENATION OF HETEROAROMATIC COMPOUNDS AND SUBSTITUTED NAPHTHALENES

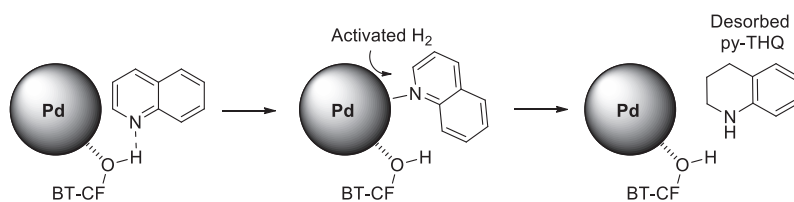
The hydrogenation of substituted aromatic rings is important for the release of aniline and alkyanilines from coal²⁶ and the upgrading of coal-derived oil and heavy fractions from petroleum.²⁷

In industry, polycyclic hydrocarbons and N- and S-heteroaromatics compounds are substrates needed to be removed from fuel²⁸ because, in general, nitrogen- or sulfur- species act as poison of the catalyst surface.²⁹ Heterogeneous processes like hydrodenitrogenation and hydrodesulfurization require the use of high temperatures and pressures. However, there are limited examples in the literature in which these compounds are hydrogenated using metal NPs as catalysts under mild reaction conditions.

In 2011, Sánchez-Delgado *et al.* prepared Ru NPs of 3.1 nm stabilized by poly(4-vinylpyridine) (PVPy) which were used in the hydrogenation of a wide variety of aromatic hydrocarbons and N- and S-heteroaromatic compounds. They concluded that two different hydrogenation pathways were performed in two distinct active site of the nanosurface: a conventional homolytic hydrogen splitting of the simple aromatic substrates and a novel heterolytic hydrogenation for the N-heteroaromatics. Nevertheless, 120 or 150°C and pressures of 10-50 atm of H₂ were needed.^{28a} Recently, the same group reported the use of ruthenium nanoparticles supported on magnesium oxide for the same purpose including the hydrogenation of S-heteroaromatics compounds. Selectivities around 80% towards the hydrogenation of one arene in naphthalene and anthracene (1,2,3,4-tetrahydroanthracene as major product) were achieved. Furthermore, comparable selectivities towards the partial hydrogenation of

N-heterocyclic compounds and selectivities up to 60% in S-heteroaromatics were achieved.²⁹

Roucoux and co-workers also used Rh NPs stabilized by N,N-dimethyl-N-cetyl-N-(2-hydroxyethyl)ammonium salts to hydrogenate different substrates such as pyridine to piperidine and quinoline to 1,2,3,4-tetrahydroquinoline at 1 atm of H₂ pressure and 20 °C. However, no catalytic activities were observed when sulfur compounds like thiophene were used.³⁰ Shi *et al.* used Pd NPs on black tannin grafted collagen fibers to hydrogenate quinoline to 1,2,3,4-tetrahydroquinoline between 20 and 80 °C and 10–40 atm H₂. They proposed a mechanism in which the coordination of the nitrogen to the palladium surface took place initially (Scheme 4.4). The catalyst could be recycled at least 6 times without significant loss of activity.³¹



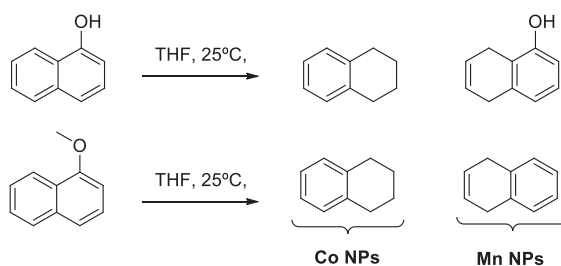
Scheme 4.4. Proposed mechanism for the hydrogenation of quinoline over Pd-BT-CF catalyst.³¹

Bimetallic systems have also been used to enhance activity, selectivity and tolerance to nitrogen and sulfur substrates. For instance, as commented before, Wai *et al.* demonstrated that a bimetallic RhPd/CNT system, driving the reaction at 10 atm H₂ and 25 °C, showed higher catalytic activity for the hydrogenation of anthracene towards 1,2,3,4,5,6,7,8-octahydroanthracene than the monometallic catalysts.^{21a} Then, in 2012 Buriak and co-workers synthesized a series of mono-, bi-, and trimetallic NPs catalysts supported on metal oxides (72 catalyst in total). They were applied in the hydrogenation of mono, poly- and heteroaromatic substrates

(naphthalene, pyridine, indole, quinoline, thiophene and benzothiophene) under mild reaction conditions obtaining good to excellent selectivities towards the partial hydrogenation or the hydrogenation of the arene containing the heteroatom. Kinetic studies were also performed.⁵

One example of the hydrogenation of polyarenes containing nitro or amine functionalities using silica sol-gel entrapped palladium-[Rh(COD)Cl]₂ catalyst, has been reported. High temperatures (140°C) and long reaction times (from 3 to 21 days) were needed to obtain total hydrogenated products due to the presence of the NH₂ moiety which extremely slowed down the reaction.³² In general, the major product formed was the one in which the non-substituted ring was hydrogenated. Nonetheless, deamination products were also observed in proportions around 10%.

There is only one study of the hydrogenation of naphthalenes in the presence of different functional groups using nanoparticles under mild reaction conditions. In this case, the substrates are reduced using non-stabilized manganese and cobalt nanoparticles and when the naphthalenes bear oxygenated functionalities, hydrogenolysis of the C-O bond takes place. In general, the tetralin derivate and hydrogenolysed products are observed. (Scheme 4.5).³³



Scheme 4.5. Reduction of 1-naphthol and 1-methoxynaphthalene promoted by Co or Mn NPs.³³

4.2. OUTLOOK AND OBJECTIVES OF THIS CHAPTER

As it was commented in the introduction, different studies have been reported for the hydrogenation of polyaromatic substrates. However, few of them are performed using well-defined nanoparticles under mild reaction conditions (especially ruthenium nanoparticles) and no attention has been focused on more hindered substrates or in competitive studies between different functional groups. In this context, the goals of this chapter are:

- i) To carry out a study of the hydrogenation of different polycyclic arenes under mild reaction conditions using well defined ruthenium nanoparticles. The study is focused on the selectivity towards the partial hydrogenation of polyarenes, but, at the same time, it also aims to know if it is possible to achieve the total reduction of polyarenes under mild reaction conditions.
- ii) To study the hydrogenation of naphthalenes containing substituents in different positions of the aromatic ring (Figure 4.2). The competition between the hydrogenation of the substituent (for instance in the case of ketones) and the naphthalenic system will be also studied.



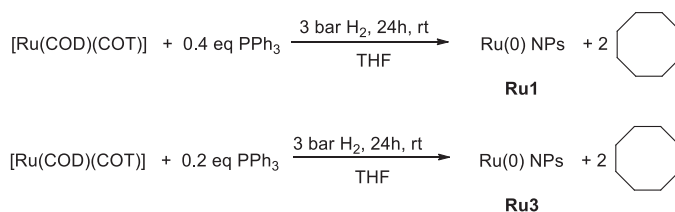
Figure 4.2. Naphthalene containing a functional group in position 1 or 2.

4.3. RESULTS AND DISCUSSION

4.3.1. SYNTHESIS, STABILIZATION AND CHARACTERIZATION OF RUTHENIUM NANOPARTICLES

In the previous chapter, we concluded that ruthenium nanoparticles stabilized by triphenylphosphine were active catalysts for the reduction of substituted arenes. Our purpose is to know the behaviour of these nanoparticles in the reduction of polyarenes. In that chapter nanoparticles stabilized with 0.4 equiv. of PPh_3 (**Ru1**) were prepared and characterized. We will also study the catalytic performance of nanoparticles stabilized with 0.2 equiv. of PPh_3 in order to analyse the effect of the stabilising agent on the nanoparticles activity.

For this purpose, soluble Ru nanoparticles stabilised by the phosphorus donor ligand PPh_3 (0.2 and 0.4 equiv.), **Ru3** and **Ru1** respectively, were synthesised by decomposition of the organometallic precursors $[\text{Ru}(\text{COD})(\text{COT})]$ in THF under H_2 pressure following reported methods (Scheme 4.6, see also Chapter 3).³⁴ The non-reported ruthenium nanoparticles **Ru3** were characterised by transmission electron microscopy (TEM), X-ray diffraction (XRD), elemental analysis (EA), thermogravimetric analysis (TGA) and X-ray photoelectron spectroscopy (XPS) (see spectra data in the Experimental Section).



Scheme 4.6. Synthesis of ruthenium nanoparticles by decomposition of [Ru(COD)(COT)] in the presence of PPh₃.

- Ru3 nanoparticles stabilized by 0.2 eq of PPh₃:

TEM micrographs showed the formation of small and spherical shaped nanoparticles, with a narrow size distribution and a diameter of 1.57 ± 0.37 nm. Moreover, the high resolution transmission electron microscopy (HRTEM) confirmed the formation and dispersion of the nanoparticles.

The proportion of ligand present on the nanoparticle surface was determined by thermogravimetric analysis (TGA) and 70% of Ru and 30% of PPh₃ were observed.

From the experimental data obtained by TEM and by TGA and using the *Van Hardevel Hartog* model, the approximate quantity of ruthenium atoms contained on the **Ru3** nanoparticles surface was calculated. In Table 4.2 are presented the values referring to the total number of atoms (N_t) and the atoms on the surface (N_s) related to the diameters obtained by TEM. A P/Ru_s ratio between 0.21-0.30 that represents approximately 1 phosphorus ligand for 6-7 ruthenium surface atoms is obtained. The ratio of surface atoms per total atoms in the nanoparticle remains similar in all the cases.

Table 4.2. Approximate quantity of ruthenium atoms on the **Ru3** surface.

Size of NPs	1.20 nm	1.57 nm	1.94 nm
Nt	67	149	281
Ns	50	95	155
Ns/Nt	0.750	0.636	0.553
P/Ru _s	0.21	0.26	0.30

The structure of the nanoparticles **Ru3** was determined by X-Ray diffraction (XRD) in which an hexagonal close packing lattice and a coherence length of 1.36 ± 0.09 nm were determined.

Finally, the oxidation state of the atoms situated on the **Ru3** nanoparticles surface was determined by X-ray Photoelectron Spectroscopy (XPS). Using the Monte-Carlo approximation³⁵ and taking into account the parameters optimized for Ru systems, the analysis revealed a 100% of Ru(0) atoms at the surface of the NPs.

To summarise, the **Ru3** NPs exhibit a diameter of 1.57 ± 0.37 nm, are highly crystalline with hcp packing and no oxidation is detected. Quantitatively, they contain 70% Ru and 30% PPh₃.

Comparing **Ru3** and **Ru1** nanoparticles, it can be concluded that **Ru3** NPs are slightly bigger than **Ru1** (1.32 ± 0.28 nm). Both nanoparticles present hexagonal close packing lattice and no oxidation is detected. Quantitatively, they both contain 70% of Ru and 30% of PPh₃ approximately.

4.3.2. HYDROGENATION OF NAPHTHALENES AND POLYAROMATIC SUBSTRATES

The different PAHs studies are presented in Figure 4.3.

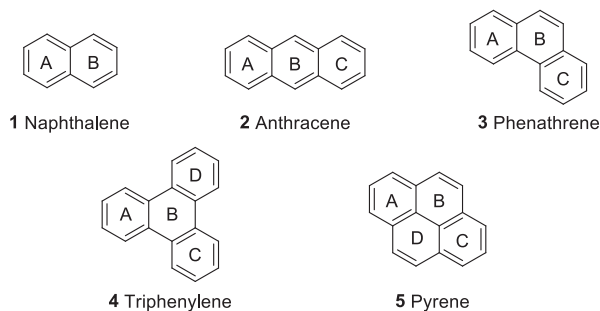


Figure 4.3. PAHs of 2, 3 and 4 fused aromatic rings.

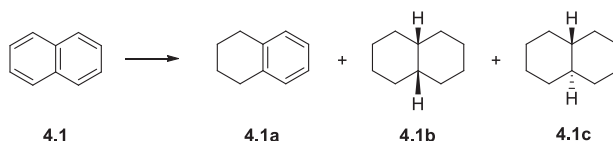
Naphthalene was initially used as model substrate to evaluate the selectivity towards the partial and the total hydrogenation. The pressure and temperature initially selected were the ones previously optimized for the reduction of aromatic ketones.³⁴ THF was the solvent of choice due to the better activities and selectivities obtained in comparison to heptane, pentane or acetonitrile. Low conversion were achieved when the reaction was conducted in these solvents. As it is shown in Table 4.3, hydrogenation with ruthenium nanoparticles stabilized by 0.4 equivalents of triphenylphosphine was carried out at 30°C and 20 bar of H₂ for 16 h affording quantitative conversion toward the total hydrogenated product with a proportion of *cis*-**4.1b**/*trans*-**4.1c** of 84/16 (Table 4.3, Entry 1). The products were detected by GC-MS and the *cis/trans* selectivity was determined by NOE experiments.

Next, the pressure was reduced to 3 bar in order to know the influence on the selectivity. Total conversion was also obtained but, in this case, product **4.1a**, which has only one arene hydrogenated, was the major

product with a selectivity of 74% and together with compounds **4.1b** and **4.1c** in a 24:2 ratio (Table 4.3, Entry 2). Then, the reaction time was reduced in order to increase the selectivity towards product **4.1a**. When the reaction was performed at only 3 bar of pressure for 10 hours (Table 4.3, Entry 3), excellent selectivity of 93% towards the partial hydrogenated product **4.1a** was obtained at 70% of conversion. Using these conditions, no product **4.1c** was observed.

The reaction was also performed using ruthenium nanoparticles stabilized by 0.2 equivalents of triphenylphosphine (**Ru3**) under the same conditions but in this case, only 9% of conversion and total selectivity towards product **4.1a** was achieved after 10 h (Table 4.3, Entry 4).

Table 4.3. Hydrogenation of naphthalene using **Ru1** and **Ru3** as catalyst.^a



E.	NPs	P (bar)	Time (h)	Conv. (%) ^b	%a ^b	%b ^b	%c ^b
1	Ru1	20	16	100	-	84	16
2	Ru1	3	16	100	74	24	2
3	Ru1	3	10	70	93	7	-
4	Ru3	3	10	9	100	-	-
5	Ru3	3	16	20	97	3	-

^aGeneral conditions: Ru NPs (2 mol %), substrate (0.62 mmol), THF (10 ml), T= 30°C. ^bDetermined by GC.

At this point, it was decided to increase the reaction time to 16 h in order to increase the conversion but only 20% was achieved maintaining a high selectivity (97%) towards product **4.1a** (Table 4.3, Entry 5). These results indicated relevant differences between the two ruthenium systems.

Contrary to the expected, less proportion of ligand implied lower activities but more selectivity towards the partial hydrogenated product **4.1a**.

From these results it can be concluded that the selectivity is highly dependent on the pressure and the obtaining of the partial or total hydrogenated naphthalene can be easily tuned.

As far as we are concerned, only in two cases similar selectivities have been reported using supported nanoparticles. In 2007, Rh and Pd nanoparticles were used in the hydrogenation of naphthalene and a yield up to 97% towards product **4.1a** was obtained.²⁰ In 2011 selectivity up to 91 towards product **4.1b** was described using rhodium nanoparticles supported on TiO₂.³⁶ In both cases only 1 bar of pressure was used. Some of the best results in terms of selectivity reported in the bibliography for naphthalene are presented in Table 4.4 for comparison.

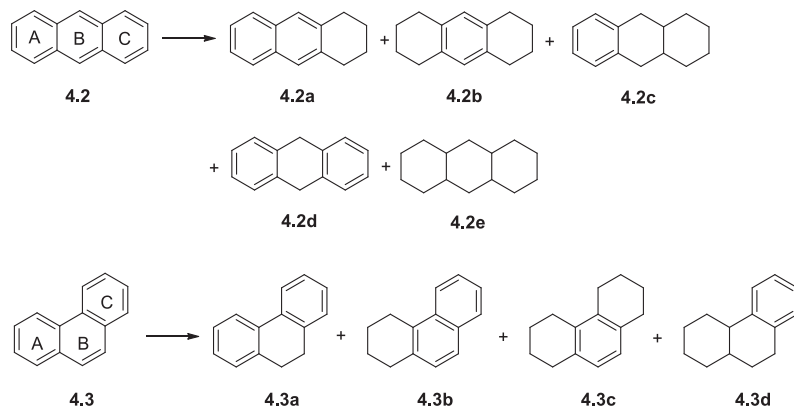
Table 4.4. Selected results reported for naphthalene hydrogenation.

E.	Catalyst	P (bar)	T (°C)	Time (h)	Conv. (%)	%a	%b	%c	Reference
1	Rh@TiO₂	1	rT	24	100	-	91	16	[36]
2	Supported Rh NPs	1	rT	16	100	-	88	12	[20]
3	Supported Rh NPs	1	rT	10	70	97	3	-	[20]
4	Supported Ru NPs	50	150	1	97	80	15	-	[29]

Then, polyaromatic systems containing three conjugated arenes were hydrogenated (Table 4.5). The aim of this part was the selective reduction of one arene. Using the same conditions in which good activity and selectivity was obtained in the naphthalene system, moderate conversion (41%) and excellent selectivity towards the hydrogenation of only one aromatic ring (91% of **4.2a**) was obtained (Table 4.5, Entry 1). These results indicated that a more hindered substrate needed more drastic conditions in order to improve the activity. Therefore the pressure was

increased to 20 bar (Table 4.5, Entry 2) and 44% of conversion was achieved after only 30 minutes with total selectivity towards product **4.2a**.

Table 4.5. Hydrogenation of anthracene and phenanthrene using **Ru1** nanoparticles as catalyst.^a



E.	Subs.	P (bar)	T (°C)	Time (h)	Conv. (%) ^b	%a ^b	%b ^b	%c ^b	%d ^b	%e ^b
1	4.2	3	30	16	41	91	6	-	3	-
2	4.2	20	30	0.5	44	100	-	-	-	-
3	4.2	20	30	9	100	-	96	-	-	4
4	4.2	20	30	16	100	-	90	-	-	10
5	4.3	20	30	16	6	42	35	23	-	-
6	4.3	20	50	16	24	42	28	30	-	-

^aGeneral conditions: **Ru1** NPs (2 mol%), substrate (0.62 mmol), THF (10 ml).

^bDetermined by GC.

When the reaction time was increased to 9h, conversion was complete and compound **4.2b** was obtained in a 96% of selectivity (Table 4.5, Entry 3). If the reaction time is increased to 16 h (Table 4.5, Entry 4), 10% of the total hydrogenated product **4.2e** is observed, which indicates the difficulty to achieve the total reductions under this reaction conditions.

With these results in hands and looking for additional insights in the hydrogenation of polycyclic aromatic hydrocarbons, a study of the

evolution of the hydrogenation of anthracene **4.2** with time was monitored by GC-MS (Figure 4.4).

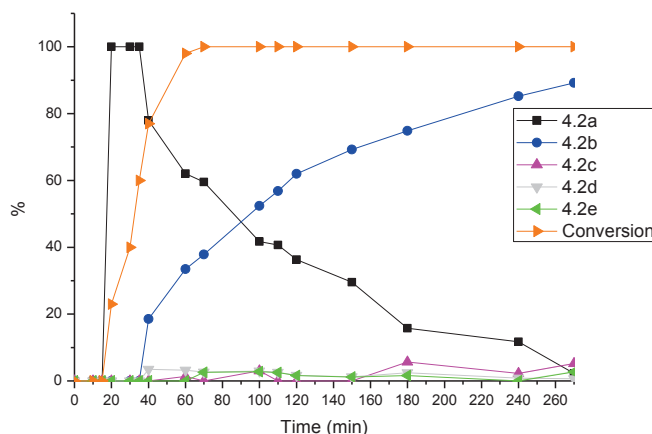


Figure 4.4. Monitoring of the catalytic hydrogenation of anthracene (**4.2**). (Conditions: **Ru1** (2 mol%), substrate (0.62 mmol), solvent= THF, T= 30 °C, P= 20 bar H₂).

Using the nanoparticles stabilized by 0.4 equiv. of triphenylphosphine, full conversion was obtained after *ca.* 1h. During the first 30 min, the conversion reached *ca.* 50% and total selectivity towards the formation of product **4.2a** as a result of the hydrogenation of ring A of anthracene was obtained. Then, after 40 min, the selectivity towards product **4.2a** started to decrease as a consequence of the progressively formation of product **4.2b**. However, selectivity up to *ca.* 80% towards product **4.2a** was achieved at a *ca.* 80% of conversion. After *ca.* 5 hours, selectivity up to 95% of product **4.2b** was achieved. During the reaction, products **4.2c** and **4.2d** were also detected as traces (maximum of 5%). As expected for longer reaction times, the formation of the product **4.2e** progressively increased but, only a maximum of 10% of selectivity was achieved after 16 hours indicating the difficulty in obtaining the total hydrogenated product.

Compared to the recent mechanistic proposal reported for anthracene hydrogenation using palladium nanoparticles,²⁵ in our case, total

conversion was achieved at room temperature and 20 bar of H₂ after only 30 minutes whereas 60 min and at least 260°C were needed in the reported work. The main difference was that total different selectivity was achieved. In our case, as it was commented before, the major product initially formed was **4.2a** while in the reported work, product **4.2d** was initially observed as the major product at 250°C. Then, when the temperature was increased to 300°C, mainly products **4.2b** and **4.2c** were detected. However, lower selectivities were reported and a maximum of 80% approx. of **4.2b** was achieved. Surprisingly, product **4.2d** was only observed in really low proportions in our monitored study (<5%) and, in the reported work, even at 300°C, low proportion (<10%) of the total hydrogenated product was observed.

Comparing these results using Ru NPs with those reported using Pd catalytic systems, it suggests a difference in the hydrogenation mechanisms. With palladium, reduction of ring B is initially observed while using ruthenium catalysts, ring A is clearly reduced first and only traces of compound **4.2d**, coming from ring B reduction, were observed along the reaction. The fact that reduction of ring B of anthracene to afford compound **4.2d**, which will preserve more the aromaticity, is not observed can suggest that that in the ruthenium case the reaction proceeds under kinetic control, probably determined by accessibility of the arene to the nanoparticle surface. It can also suggest a different hydrogen transfer mechanism in the case of palladium.

Next, phenanthrene **4.3** was also reduced under the same reaction conditions and, unexpectedly, really different results in terms of conversion were obtained compared to anthracene **4.2** despite the really similar structure of both substrates. Thus, when the reaction was performed at 20 bar for 16 hours (Table 4.5, Entry 5), only 6% of conversion was achieved

and 42% of product **4.3a**, with the middle arene hydrogenated, 35% of product **4.3b** with one external arene hydrogenated and 23% of product **4.3c** with two arenes hydrogenated were obtained. Consequently, it was decided to increase the temperature to 50°C to push the activity. Curiously, the conversion was only increased to 24% remaining the selectivity practically unchanged (Table 4.5, Entry 6).

Despite having the same number of fused benzene rings, really different behaviour was observed in substrate **4.2** and **4.3**. Surprisingly, in the case of anthracene, the first ring hydrogenated was the ring A despite the *Sr* value (the hydrogen accepting ability) in C-9 is 1.314, much higher than in C-1 or C-2 (1.073 and 0.922).³⁷ Consequently, it could be expected that **4.2d**, resulting from the reduction of ring B, should be preferably formed.

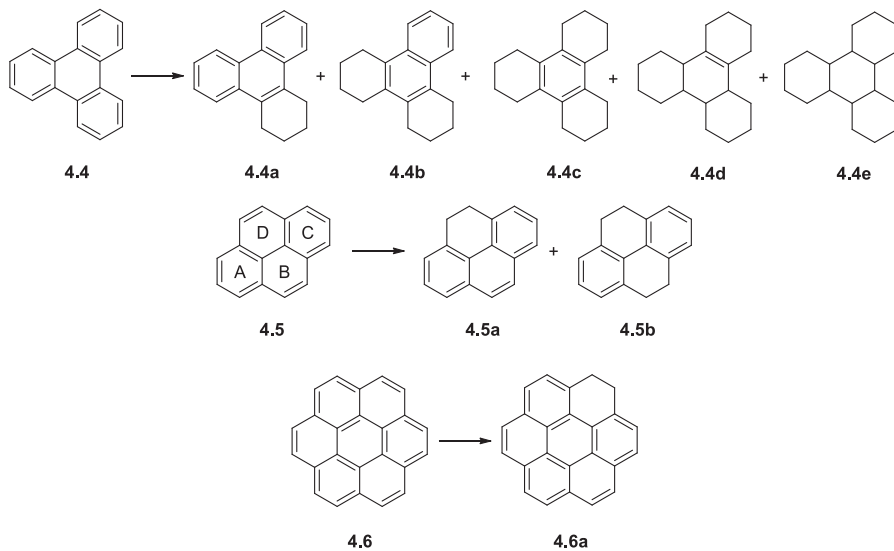
Nevertheless, hydrogenation of phenanthrene, afforded mixtures of products from the beginning of the reaction and the total hydrogenated product was not observed. However, also in this case, terminal rings A and C are reduced faster than the central ring B, although the selectivity is lower than for anthracene. In spite of the higher preservation of aromaticity that would suppose the obtaining of **4.3b**, the reduction of the terminal ring to afford **4.3a** is still preferably. Moreover, it seems that the hydrogenation of the second terminal ring is quite fast. Compound **4.3d** is not observed. This observed low selectivity is in agreement with previous results dealing with phenanthrene reduction.^{17, 38} There are only two cases in which using PtO₂³⁹ or a niobium catalyst under higher pressures and temperatures (80 bar and 80°C)⁴⁰ selectivities of ~70% towards compound **4.3a** were obtained. Some of the best results in terms of selectivity reported in the bibliography for phenanthrene are presented in Table 4.6 for comparison.

Table 4.6. Selected results reported for phenanthrene hydrogenation.

E.	Catalyst	P (bar)	T (°C)	Time (h)	Conv. (%)	%a	%b	%c	%d	Reference
1	PtO ₂	1	rT	120	70	70	-	-	-	[39]
2	Nb Catalyst	82	80	24	100	22	-	78	-	[40]
3	Pd-Rh	30	80	40	62	37	20	2	5	[17]

Finally, the hydrogenation of polyaromatics containing 4 or more conjugated arenes was attempted (Table 4.7). Triphenylene **4.4** was reduced under the optimized conditions (Table 4.7, Entry 1) for 16 hours, to afford 61% of conversion. Product **4.4a**, which has only one arene hydrogenated, was obtained with a selectivity up to 53%, compound **4.4b** (2 external rings hydrogenated) in a 12%, and product **4.4c** (3 external rings hydrogenated) in 35%. It is clear that the reduction of the external rings is easily performed.

Under the conditions tested, the fully hydrogenated product was not observed. This result indicates that the central ring of triphenylene is very difficult to hydrogenate probably due to the sterical hindrance of compound **4.4c** when the three saturated side rings interact with the catalyst surface. At this point, it was decided to increase the temperature to 80°C and, after 16 hours, full conversion and exclusive formation of **4.4c** was achieved (Table 4.7, Entry 2). Then the reaction time was increased to 60 hours but compound **4.4c** was still the major one and only traces of the total hydrogenated product **4.4e** were detected (Table 4.7, Entry 3). Therefore, it can be concluded that **4.4c** is really difficult to be hydrogenated using these nanoparticles and more drastic conditions would be needed to obtain the total hydrogenated product. Moreover, it is important to highlight the fact that 10% of product **4.4d** containing one double bond bridging two arenes rings is observed. This double bond is of course, the most difficult to hydrogenate.

Table 4.7. Hydrogenation of triphenylene, pyrene and coronene.^a


E.	Subs.	NPs	T (°C)	Time (h)	Conv. (%) ^b	%a ^b	%b ^b	%c ^b	%d ^b	%e ^b
1	4.4	Ru1	30	16	61	53	12	35	-	-
2	4.4	Ru1	80	16	100	-	-	100	-	-
3	4.4	Ru1	80	60	100	-	-	88	10	2
4	4.5	Ru1	50	16	17	93	7	-	-	-
5	4.5	Ru1	80	16	25	90	10	-	-	-
6	4.5	Ru1	80	60	44	86	14	-	-	-
7	4.5	Ru3	80	60	7	100	-	-	-	-
8	4.6	Ru1	80	60	0	-	-	-	-	-

^aGeneral conditions: **Ru1** NPs (2 mol%), substrate (0.62 mmol), P=20 bar H₂, THF (10 ml). ^bDetermined by GC.

The results obtained in the hydrogenation of triphenylene advised, similarly to the case of anthracene, to further investigate the hydrogenation of triphenylene **4.4** by monitoring the catalysis by GC-MS (Figure 4.5), looking for information about the evolution of the reaction and the selectivity.

Using **Ru1** nanoparticles, *ca.* 65% of conversion was obtained after 8 h. From the beginning of the reaction products **4.4a**, **4.4b** and **4.4c** were detected. During the first 2 hours, the conversion reached *ca.* 20% and selectivity up to 70% towards the formation of product **4.4a** in which the hydrogenation of ring A was produced. Then, the selectivity towards this product started to decrease and product **4.4c** with three hydrogenated external arenes started to be formed progressively in a major proportion. It is important to highlight the fact that the selectivity towards product **4.4b** was practically maintained during the reaction indicating that it is rapidly hydrogenated to **4.4c**. Therefore, the hydrogenation of the external arenes in **4.4a** becomes faster after the hydrogenation of the first aromatic ring in the starting material **4.4**. The fully hydrogenated product was not observed showing, as previously commented, the difficulty in reducing product **4.4c**.

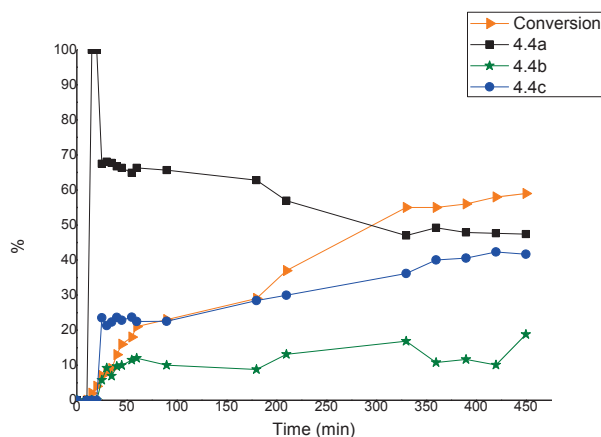


Figure 4.5. Monitoring of the catalytic hydrogenation of triphenylene **4.4**. (Conditions: **Ru1** NPs (2 mol%), substrate (0.62 mmol), solvent= THF, T= 80°C, P= 20 bar H₂).

In the case of pyrene **4.5**, the temperature has an important effect on the activity but not on the selectivity. Initially, the substrate was hydrogenated at 20 bar and 50°C obtaining only 17% of conversion but with

high selectivity towards product **4.5a** (93%), which has only one arene reduced (Table 4.7, Entry 4). Increasing the temperature to 80°C, the conversion was slightly increased to 25% without a substantial change in the selectivity (Table 4.7, Entry 5). Finally, when the reaction was performed under these reaction conditions for 60 hours, the conversion was raised to 44% and the selectivity towards product **4.5a** was maintained at 86% (Table 4.7, Entry 6). Pyrene can be considered as a phenanthrene derivative, with an additional internal ring. However, in this case, there are not disubstituted terminal rings such as in the case of anthracene (**4.2**) and phenanthrene (**4.3**). All rings are trisubstituted (A,C) or tetrasubstituted (B, D). In this case, although the higher substitution of rings B and D, the higher preservation of aromaticity seems to determine the selectivity.

Next, it was decided to try the same hydrogenation but using **Ru3** nanoparticles in order to improve the activity and/or the selectivity. However, as it happened in the case of naphthalene (Table 4.3, Entry 5), the conversion was very low (7% after 60 hours) and total selectivity towards the formation of **4.5a** was achieved (Table 4.7, Entry 7).

Then coronene **4.6** hydrogenation was studied. Initially it was tested quite drastic reaction conditions (20 bar and 80°C) but no conversion was obtained (Table 4.7, Entry 8). Coronene is a really complex and hindered molecule which could have difficulties to coordinate on the nanoparticle surface. Moreover, it is only partially soluble in THF and this fact could also prevent the reaction.

As it has been demonstrated, substrates containing 4 or more fused rings are more hindered and the approach to the nanoparticle could be limited. For that reason, harsher reaction conditions are needed to obtain moderate conversions and selectivities. In the case of triphenylene **4.4**, good selectivities towards product **4.4c**, which can be exclusively obtained, are

achieved after 16 hours. These results are comparable to those reported using supported Rh and Pt nanoparticles.^{22a} Nevertheless, to the best of our knowledge, it the first time that compound **4.4a** is obtained in such a selectivity (~50%) at similar conversion values. Some of the best results in terms of selectivity reported in the bibliography for triphenylene are presented in Table 4.8 for comparison.

Table 4.8. Selected reported results for triphenylene hydrogenation.

E.	Catalyst	P (bar)	T (°C)	Time (h)	Conv. (%)	%a	%b	%c	%e	Reference
1	Supported Rh	10	rT	3	100	-	-	100	-	[22a]
2	Rh/MWNTs	10	20	3	100	-	-	95	5	[22b]
3	Pd-Rh	30	80	40	71	15	27	28	1	[17]

In the case of pyrene, excellent selectivities towards product **4.5a** were detected at moderate conversions. Different publications have focused on the hydrogenation of pyrene obtaining mixtures of products and high temperatures were required in order to obtain good conversions.^{15b, 16, 17} Using Pt nanoparticles supported on carbon nanotubes, total selectivity towards product **5a** was achieved but the conversion was only 7%.^{22a}

The results obtained in the hydrogenation of all these polyaromatic hydrocarbons show that high selectivities towards different partial hydrogenated products can be obtained in all the cases except for phenanthrene, and forcing the reaction conditions or increasing the reaction times, the fully hydrogenated product can also be obtained in some of the substrates, namely naphthalene **4.1** and anthracene **4.2**. When the number of fused benzene rings increases, the hydrogenation becomes more difficult. The proportion of ligand used to stabilize the nanoparticles has an important effect not only on the activity but also on the selectivity. Based on these

results, the nanoparticles stabilized by 0.4 equiv. of triphenylphosphine appeared more active than the ones stabilized by 0.2 equiv.

Good results in terms of activity and selectivity were obtained in the reduction of naphthalene using **Ru1** NPs (Table 4.1). For that reason, it was considered that it would be interesting to study the effect of the presence of different substituents on a naphthalenic system, considering the nature of the substituent and the position.

4.3.3. CHEMOSELECTIVITY. HYDROGENATION OF SUBSTITUTED NAPHTHALENES *VS.* OTHER FUNCTIONALITIES

As it was commented in the introduction and to the best of our knowledge, few examples are reported related to the effect of substitution on the selectivity of polyarene hydrogenation, as well as the selective reduction of polyarenes *vs.* other functional groups.³²⁻³³ In order to gain information about these two aspects, reduction of substituted naphthalenes was studied. Different substitutions were considered: substitution at positions α (position 1) and β (position 2), donor and acceptor substituents, and substituents that could be competitively reduced.

4.3.3.1. HYDROGENATION OF SUBSTITUTED NAPHTHALENES

We began the study with 2-methoxynaphthalene **4.7** which was used as model substrate (Table 4.9). Considering the results obtained in the previous studies of this Thesis, it was thought that as the substrate is sterically more hindered compared to naphthalene, harder reaction conditions would be needed in order to have high conversions. We decided to maintain the temperature but we initially worked at 20 bar of hydrogen. Remember that only 3 bar were required for naphthalene hydrogenation (see

Table 4.3). Initially the effect of the solvent on the selectivity was studied. When the hydrogenation of **4.7** was carried out for 2.5 h using THF as solvent, a conversion of 31% and a selectivity of 83% towards the hydrogenation of the less substituted ring (**4.7a**) was obtained (Table 4.9, Entry 1). A 11% of compound **4.7b**, resulting from the reduction of the most substituted ring, and a 6% of the fully reduced compound **4.7c** was also obtained. Then, pentane and ethanol were used leading to excellent selectivities (up to 93%) towards product **4.7a** although really low conversions were achieved (Table 4.9, Entries 2 and 3). Interestingly, when MTBE was used as solvent (Table 4.9, Entry 4), conversion up to 35% and 91% of selectivity towards **4.7a** were obtained. In order to increase the conversion, the reaction was performed for 16 h but the conversion was still moderate (52%) and the selectivities were comparable to the ones obtained using THF as solvent (Table 4.9, Entry 5).

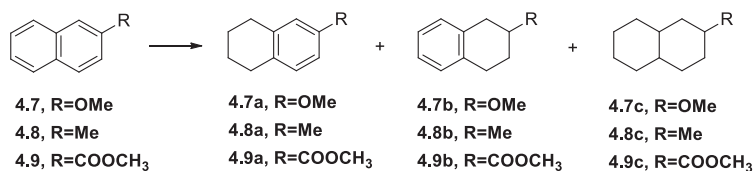
When the reaction was performed using MTBE as solvent and a more diluted solution (0.62 mmol substrate), the selectivity was still good (81%) and full conversion was achieved (Table 4.9, Entry 6). In the case of THF and in the same conditions (Table 4.9, Entry 7), the selectivity remained unchanged and 83% of **4.7a** was obtained at 91% of conversion performing the reaction for only 2.5 hours (6 times shorter than using MTBE). In MTBE there are not significant changes in the reaction rate (compare Entries 5 and 6). For the same reaction conditions, when there is double amount of substrate only 50% conversion was achieved (Table 4.9, Entry 5). However, in THF a significant increase in the reaction rate (approx. 50%) was observed when a more diluted solution of substrate was used (compare Entries 1 and 7). From these assays it was concluded that the best option was again to use THF as solvent due to the higher conversion at lower reaction times.

Then, the reaction was performed under the same reaction conditions using **Ru3** nanoparticles in order to see if the selectivity could be improved. Comparable results were obtained although the conversion (75%) was slightly decreased (Table 4.9, Entry 8). Contrary to what was observed in the case of naphthalene (Table 4.3, Entry 4 and 5), in this case, the conversion was not dramatically affected and the selectivity remained practically unmodified.

Next, we reduced the pressure in order to see if the selectivity could be enhanced. Using the same reaction conditions but under 10 bar for 2.5 hours, similar results in terms of selectivity were obtained but the conversion dropped to 11% (Table 4.9, Entry 9).

Unexpectedly, when substrate **4.8** containing a methyl group instead of a methoxy group was hydrogenated, a very low conversion (6%) was achieved after 16 h, although selectivity (79%) towards product **4.8a** was similar to the obtained in the previous examples (Table 4.9, Entry 10). We repeated this experiment several times, even using recrystallized substrate, with similar results.

Hydrogenation of substrate **4.9**, which contains an ester group, using **Ru1** nanoparticles (Table 4.9, Entry 11), was also unsuccessful and no conversion was obtained. Surprisingly, when **Ru3** NPs were applied under the same reaction conditions (Table 4.9, Entry 12), 12% of conversion was obtained after 16 hours with total selectivity towards product **4.9a**.

Table 4.9. Hydrogenation of 2-substituted naphthalenes.^a

E.	Subs.	NPs	mmol Subs.	Solvent (ml)	P (bar)	Time (h)	Conv. (%) ^b	%a ^b	%b ^b	%c ^b
1	4.7	Ru1	1.24	THF (10)	20	2.5	31	83	11	6
2	4.7	Ru1	1.24	Pentane	20	2.5	14	93	3	4
3	4.7	Ru1	1.24	EtOH (10)	20	2.5	18	91	6	3
4	4.7	Ru1	1.24	MTBE(10)	20	2.5	35	91	5	4
5	4.7	Ru1	1.24	MTBE (10)	20	16	52	89	6	5
6	4.7	Ru1	0.62	MTBE (10)	20	16	100	81	6	13
7	4.7	Ru1	0.62	THF (10)	20	2.5	91	83	11	6
8	4.7	Ru3	0.62	THF (10)	20	2.5	75	81	12	7
9	4.7	Ru1	0.62	THF (10)	10	2.5	11	83	12	5
10	4.8	Ru1	0.62	THF (10)	20	16	6	79	14	7
11	4.9	Ru1	0.62	THF (10)	20	16	0	-	-	-
12	4.9	Ru3	0.62	THF (10)	20	16	12	100	-	-

^aGeneral conditions: Ru NPs (2 mol%), T= 30°C. ^bDetermined by GC.

In conclusion, when the steric hindrance is increased compared to naphthalene, the reaction becomes slower although good results in terms of selectivity, towards the hydrogenation of the non-substituted ring, are obtained using different solvents. The good selectivity and high conversions in low reaction times, obtained using THF, makes it the solvent of choice for reducing naphthalene derivatives.

The selectivity results obtained in the hydrogenation of naphthalenes with different substituents in position 2 cannot be strictly related to the donor or acceptor abilities of the substituents, since when a weak donor substituent such as Me is present conversion is really low, as well as when there is an acceptor group such as an ester. A possible

explanation can be related with the coordination of the heteroatoms to the nanoparticle surface. Thus, while the oxygen of the substituted arene may interact with the metal surface upon approaching the nanoparticle, this interaction through the carbonyl group in the case of the ester function will leave the arene far away from the surface. The methyl group will only provide steric hindrance in the approach of the arene to the surface. Anyway, there is a clear different reaction rate in the reduction of both arenes, which can be determined by the substitution level and by the different electron density on each ring.

Then, the study was continued by reducing naphthalenes containing a substituent in position 1 (Table 4.10). When substrate **4.10** containing a methoxy group was reduced using the optimized reaction conditions for **4.7** (Table 4.9, Entry 7), 85% of product **4.10a** was obtained at a 40% of conversion (Table 4.10, Entry 1). Selectivity was similar to the obtained for compound **4.7**, since also similar amounts of compounds **4.10b** and **4.10c**, were obtained.

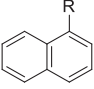
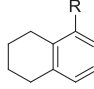
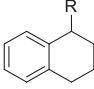
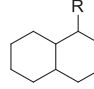
The use of **Ru3** nanoparticles, which contains less proportion of stabilizing ligand, afforded similar selectivities and slightly higher conversion (49%) (Table 4.10, Entry 2), contrary to what happened in naphthalene and in other polyarenes.

At this point, it was decided to run the reaction using **Ru1** nanoparticles for 16 hours in order to try to increase the conversion (Table 4.10, Entry 3). In this case, full conversion was achieved but the selectivity was shifted towards the totally reduced product *cis*-**4.10c**, which was present in a 65%. No product **4.10b** was observed in this case.

Interestingly, when an electron withdrawing group like $-\text{CF}_3$ is present in position 1 (substrate **4.11**), the selectivity towards the

hydrogenation of the more substituted ring increases, comparatively, and compound **4.11b** was obtained with a selectivity of 31% although the conversion was still moderate (Table 4.10, Entry 4). Changing the solvent to MTBE (Table 4.10, Entry 5), the conversion decreased to 15% although the selectivity towards product **4.11a** increased to 85%.

Table 4.10. Hydrogenation of 1-substituted naphthalenes.^a

	→		+		+	
4.10 , R=OMe 4.11 , R=CF ₃ 4.12 , R=NH ₂		4.10a , R=OMe 4.11a , R=CF ₃ 4.12a , R=NH ₂		4.10b , R=OMe 4.11b , R=CF ₃ 4.12b , R=NH ₂		4.10c , R=OMe 4.11c , R=CF ₃ 4.12c , R=NH ₂

E.	Subs.	NPs	Solvent (ml)	Time (h)	Conv. (%) ^b	%a ^b	%b ^b	%c ^b
1	4.10	Ru1	THF (10)	2.5	40	85	11	4
2	4.10	Ru3	THF (10)	2.5	49	86	10	4
3	4.10	Ru1	THF (10)	16	100	35	-	65
4	4.11	Ru1	THF (10)	2.5	45	63	31	6
5	4.11	Ru1	MTBE (10)	2.5	15	85	15	-
6	4.11	Ru3	THF (10)	16	34	68	27	5
7	4.12	Ru1	THF (10)	16	16	100	-	-

^aGeneral conditions: Ru NPs (2 mol%), substrate (0.62 mmol), P= 20 bar, T=30°C. ^bDetermined by GC.

When the reaction was performed using **Ru3** nanoparticles, a conversion of 34% was obtained after 16 h of reaction (Table 4.10, Entry 6). Selectivity was comparable to that obtained with **Ru1** under similar reaction conditions.

Finally, substrate **4.12** containing an amine was reduced for 16 h at 20 bar leading to a conversion of only 16%. Despite the long reaction time, only the product **4.12a** was obtained (Table 4.10, Entry 7).

In conclusion, the selectivity is affected when an electron donating groups or an electron withdrawing group is present. The presence of an electronwithdrawing group, slightly favours the reduction of the more substituted ring. When an amine is present in the substrate (**4.12**), the conversion decreases considerably (even after several hours) and only the arene that do not contain the amino group is reduced. The low reactivity of anilines and in general of aminoarenes has been already reported in the bibliography.³²

Comparing tables Table 4.9 and Table 4.10, it can be concluded that the position of the substituent has more influence on the conversion than on the selectivity. When the substituent is in position 1, conversions are lower probably due to the higher steric hindrance and to the consequent difficulty of the substrate for approaching the surface. Nonetheless, the selectivity is not significantly affected and the arene which does not contain substituents is still the one which is favourably hydrogenated. These results agree with the necessity for the arene ring to approach and coordinate to the nanoparticle's surface in order to be reduced.

4.3.3.2. HYDROGENATION OF AROMATIC RING VS. KETONE

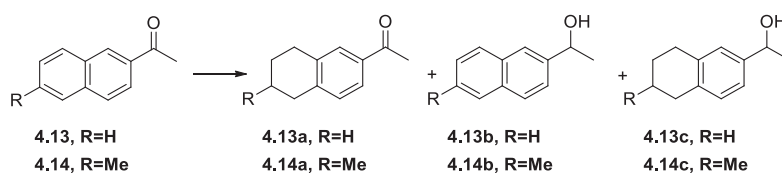
As a last objective of this chapter, and in connexion with the previous chapter, we were interested in studying the competitive reduction of arenes vs. ketones in polyarene substrates. Thus, naphthalenes containing keto groups directly linked to the aromatic ring, which presented a more interesting behaviour in the study carried out in the previous chapter, were also hydrogenated (Table 4.11 and Table 4.12).

In the previous section we have observed that the substituents present in one of the rings of naphthalene have a strong influence on the selectivity. In general the less substituted ring is preferably hydrogenated,

but the coordination of heteroatoms to the surface of the nanoparticle and the donor or withdrawing nature of substituents has also an influence. In the case of ketones, all this factors must be also taken into account, plus the possibility to compete with the arene for the reduction.⁴¹

Initially we studied the hydrogenation of naphthalene with an acetyl group located on position 2, compound **4.13**, under the standard reaction conditions leading to full conversion in 2.5h (Table 4.11, Entry 1). Three products **4.13a-4.13c**, resulting from the reduction of the less substituted ring (**4.13a**), the keto group (**4.13b**) and both the less substituted are and the keto group (**4.13c**) were obtained. The less substituted arene was mainly reduced (52%) in agreement with that observed in the Chapter 3 for acetophenone. However, the difference in selectivity cannot be pointed out since compound **4.13c** can proceed from **4.13a** and **4.13b**. When the reaction is performed using **Ru3** NPs (Table 4.11, Entry 2) the conversion drastically decreases achieving only 10% of compound **4.13b**.

Table 4.11. Hydrogenation of 2-ketonaphthalenes.^a



E.	Subs.	NPs	Time (h)	Conv. (%) ^b	% ^a	% ^b	% ^c
1	4.13	Ru1	2.5	100	52	26	22
2	4.13	Ru3	2.5	10	-	100	-
3	4.14	Ru1	2.5	44	16	84	-

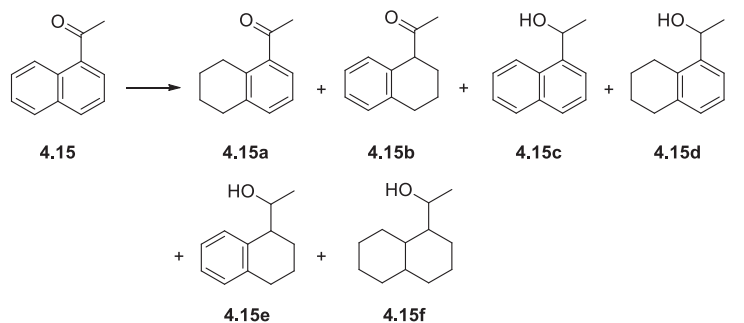
^aGeneral conditions: Ru NPs (2 mol%), substrate (0.62 mmol), THF (10 ml), P= 20 bar, T=30°C. ^bDetermined by GC.

The presence of a methyl group in position 6 in compound **4.14** place both rings with the same substitution pattern. The increase of

substitution in **4.14** has as a consequence a decrease in conversion and in the hydrogenation of the A ring and hence a preferred reduction of the acetyl group (Table 4.11, Entry 3).

Next, we studied compound **4.15** where the acetyl group is moved to position 1. Hydrogenation of compound **4.15** was carried out under the standard conditions. Full conversion was observed and a complex mixture was produced (Table 4.12, Entry 1). The previous observation that the substitution at position 1 has a negative effect on the arene reduction, translated in this case in the higher relative percentage of ketone reduction, compared with compound **4.13**. However, in this case it is also noteworthy that small percentages of reduction of the more substituted ring (B), affording product **4.15e**, or the presence of the fully reduced product **4.15f**. These facts indicate that the presence of the keto group at position 1 of ring B increase the hydrogenation ability of this ring.

Table 4.12. Hydrogenation of 1-acetonaphthone.^a



E.	P (bar)	Time (h)	Conv. (%) ^b	%a ^b	%b ^b	%c ^b	%d ^b	%e ^b	%f ^b
1	20	2.5	100	38	-	24	25	9	4
2	10	16	100	24	8	8	36	14	10

^aGeneral conditions: **Ru1** NPs (2 mol%), substrate (0.62 mmol), THF (10 ml), T= 30°C. ^bDetermined by GC.

This fact was confirmed upon driving the reaction at 10 bar of hydrogen pressure. After 16 hours of reaction a similar mixture of products was observed. However, now even the product **4.15b** resulting from the exclusive hydrogenation of ring B, the more substituted, was detected (Table 4.12, Entry 2).

From the results observed in Table 4.11 and Table 4.12, it can be concluded that also in this case, reduction involves important competition between the reduction of the arene and the ketone groups and it is influenced by the position of the keto group. Thus, when the keto group is at position 2 (**4.13**) reduction of the less substituted aromatic ring takes place principally, although significant reduction of the carbonyl group is also observed. If the keto group is at position 1, the most relevant observation is the fact that the most substituted ring is also reduced. The fact that electron-withdrawing groups activates the hydrogenation of the neighbouring ring was already observed in the case of trifluoromethyl derivative, compound **4.11**, but now we can conclude that this effect is more important when the substituent is at position 1.

4.4. CONCLUSIONS

In conclusion, ruthenium nanoparticles stabilized by triphenylphosphine are good catalysts for the hydrogenation of PAHs in mild conditions leading to good activities and interesting selectivities. In general, the reaction rate decreases when the number of aromatic rings increases. The disposition of the rings has also an influence on the reaction rate and, for instance, phenanthrene reacts much slower than anthracene in agreement with its more difficult approach to the nanoparticle's surface. Figure 4.6 shows the main results of conversion and selectivity achieved.

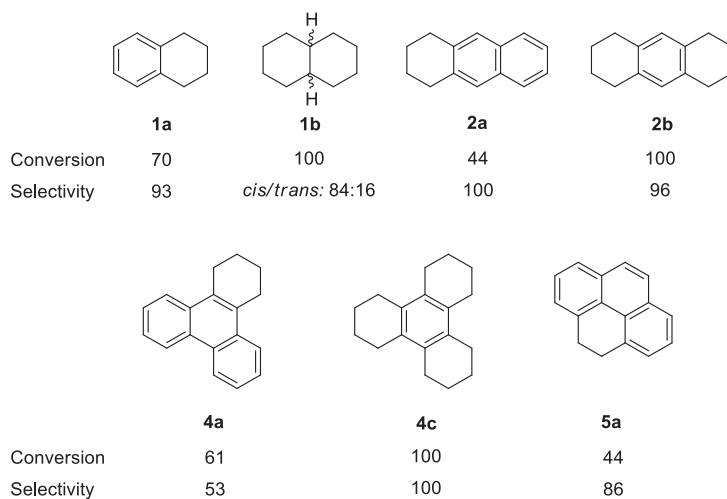


Figure 4.6. Main results of conversion and selectivity in PAHs reduction.

From the study of the hydrogenation of polycyclic aromatic hydrocarbons, the following conclusions can be extracted:

- i) Naphthalene is hydrogenated to tetralin (**4.1a**) or decalin (**4.1b**), *cis/trans*= 86:14, by just adjusting the hydrogen pressure.
- ii) Anthracene can be selectively hydrogenated to **4.2a** or **4.3b**. The total hydrogenated product **4.2d** might be obtained under the reaction conditions used, but really long reaction times would be required.
- iii) The hydrogenation of phenanthrene is more difficult and long reaction times are required to obtain low conversions. In all the cases, mixtures of products were obtained and the total hydrogenated product was not observed in any of the assays attempted.
- iv) Triphenylene has 3 equivalent external rings and it is difficult to achieve partial selectivity in hydrogenation. Thus, compound **4.4a** was obtained with a selectivity of 53% at 61% of conversion, which in spite of being quite low is one of the best reported in the bibliography.

The selective reduction of 3 rings to give compound **4.4c** was achieved in 88% of selectivity and full conversion.

- v) Pyrene, as well as phenanthrene, was difficult to hydrogenate and a 88% of selectivity in compound **4.5a** was obtained at 44% of conversion.
- vi) There are only few mechanisms proposed for PAHs hydrogenation. In general, we have observed, that there is a competition between kinetic and thermodynamic control, which affects the reduction of the less substituted ring in front to preservation of aromaticity. The hydrogenation of the less substituted ring predominates in compound **4.2**, but not in compound **4.3** and in compound **4.5**.

From the study of the chemoselective reduction of polyarenes *vs.* other functional groups, the following conclusions can be extracted:

- i) Substitution has an important effect on the reactivity and selectivity. The reactions are slower than in the unsubstituted naphthalene, and hydrogenation takes place in the ring that does not contain substituents.
- ii) Selectivity is influenced by the nature of substituents. Electron donating substituents deactivate the ring to which they are attached and, consequently, the neighbouring ring is preferably reduced. The more relevant example is the case of compound **4.12**. Electronwithdrawing substituents activate the ring. Then, although the effect of substitution predominates, reduction of the less substituted ring is mainly observed and appreciable amounts of reduction of the more substituted ring are achieved. See for instance, compounds **4.11** and **4.15**.
- iii) The position of the substituent (position 1 or 2) influences the conversion more than the selectivity. When the substituent is at position 1, the conversion decreases probably due to the higher steric

hindrance which hampers the approaching of the substrate to the surface.

- iv) Comparing the results obtained with compounds **4.7-4.9** it can be observed that the best results are obtained with compound **4.7**, which has an electrodonor substituent, while the presence of a carboxymethyl group in **4.9** clearly deactivates the reaction. Probably, it is necessary to consider the effect of the coordination to the nanoparticle of the oxygen atom of the methyl ether that will approach the arene to the NPs surface, while the interaction with the carbonylic oxygen of the ester group will put the aromatic ring away from the NP. The case of the ketone derivatives deserves then a comment, since in this case carbonyl group is also reduced. The difference should be the less electronegativity in the carbonylic oxygen that will allow different interaction modes.
- v) When a ketone is present in the substrate like in **4.13**, **4.14**, **4.15**, there is a competition between the reduction of the naphthalenic system and the ketone. If the ketone is placed in position 1 like in **4.15**, its reduction is favoured probably because the ketone coordinates preferably to the metal surface rather than the naphthalenic system.
- vi) Regarding the differences between the nanoparticles stabilized by 0.2 or 0.4 equivalents of triphenylphosphine, more proportion of ligand implies more activity and slightly less selectivity.

4.5. EXPERIMENTAL PART

General Methods

All syntheses were performed using standard Schlenk techniques under argon atmosphere. Chemicals were purchased from Aldrich Chemical

Co and Alfa Aesar and used without further purification. All solvents were purified by distillation following standard procedures and were deoxygenated before use. The precursor [Ru(COD)(COT)] was purchased from Nanomeps. The synthesis of the nanoparticles was performed using 1L Fisher Porter and pressurized on a high pressure line.

All reactions temperatures were kept electronically controlled by heating baths.

Characterization Techniques

Transmission Electron Microscopy (TEM)

TEM experiments were performed at the “Unitat de Microscopia dels Serveis Científicotècnics de la Universitat Rovira I Virgili” (TEM-SCAN) in Tarragona with a Zeiss 10 CA electron microscope operating at 100 kV with resolution of 3 Å. The particles size distributions were determined by a manual analysis of enlarged images. At least 300 particles on a given grid were measured in order to obtain a statistical size distribution and a mean diameter.

High Resolution TEM (HRTEM)

HRTEM experiments were performed at the Unitat de Microscopia dels Serveis Científics i Tecnològics de la Universitat de Barcelona with a JEOL 1010 electron microscope working at 200kV with a resolution of 2.5 Å. The particles size distributions were determined by a manual analysis of enlarged images.

Thermo Gravimetric Analysis (TGA)

TGA experiments were carried out in the oven of a Mettler Toledo TGA/SDTA851 instrument.

1-2 mg of the nanoparticles were placed in the sample holder in the oven and it was heated up at a rate of $10^{\circ}\text{Cmin}^{-1}$ in N_2 , while the weight was recorded continuously from 30°C to 900°C . The weight loss of the organic part and metal were used to calculate the approximate number of ligands coordinated on the metal surface.

X-Ray Diffraction (XRD)

XRD measurements were performed using a Siemens D5000 diffractometer (Bragg- Brentano parafocusing geometry and vertical θ - θ goniometer) fitted with a curved graphite diffracted- beam monochromator, incident and diffracted- beam Soller slits, a 0.06° receiving slit and scintillation counter as a detector. The angular 2θ diffraction range was between 26 and 95° . The data were collected with an angular step of 0.05° at 16s per step and sample rotation. A low background Si(510) wafer was used as sample holder. $\text{CuK}\alpha$ radiation was obtained from a copper X- ray tube operated at 40kV and 30mA.

X-Ray Photoelectron Spectroscopy (XPS)

XPS measurement were performed using a PHI 5500 Multitechnique System (from Physical Electronics) with a monochromatic X-ray source (Aluminium Kalfa line of 1486.6 eV energy and 350 W), placed perpendicular to the analyser axis and calibrated using the 3d5/2 line of Ag with a full width at half maximum (FWHM) of 0.8 eV. The analysed area was a circle of 0.8 mm diameter, and the selected resolution for the spectra was 187.5eV of Pass Energy and 0.8 eV/ step for the general spectra and 23.5 eV of Pass Energy and 0.1 eV/step for the spectra of the different elements in the depth profile spectra. A low energy electron gun (<10 eV) was used in order to discharge the surface when necessary. All measurements were performed in an ultra-high vacuum (UHV) chamber

pressure between 5×10^{-9} and 2×10^{-8} torr. The data processing was carried out using the CasaXPS program.

General procedure for the synthesis of ruthenium nanoparticles stabilized by triphenylphosphine³⁴

In a typical procedure, the [Ru(COD)(COT)] (400 mg, 1.268 mmol) was placed into a Fischer-Porter reactor in 400 mL of dry and deoxygenated THF by freeze-pump-thaw cycles in the presence of triphenylphosphine (0.2 eq. or 0.4 eq.) The Fischer-Porter reactor was pressurised under 3 bar of H₂ and stirred for 24 h at room temperature. Then the solution was concentrated under reduced pressure to 40 ml. Precipitation and washing with pentane (3x15 ml) was then carried out, obtaining a black precipitate.

Ru₃ nanoparticles stabilized by 0.2 eq of PPh₃:

- *TEM*: mean size 1.57 ± 0.37 nm.
- *XRD*: hcp crystalline Ru nanoparticles, coherence length 1.36 ± 0.09 nm.
- *XPS*: 3d_{5/2} (280.46 eV) and 3d_{3/2} (285.16 eV), 100% Ru (0) at the nanoparticles surface.
- *TGA*: 70% Ru, 30% PPh₃. Approximate formula: [Ru₁₄₉ L₂₄].

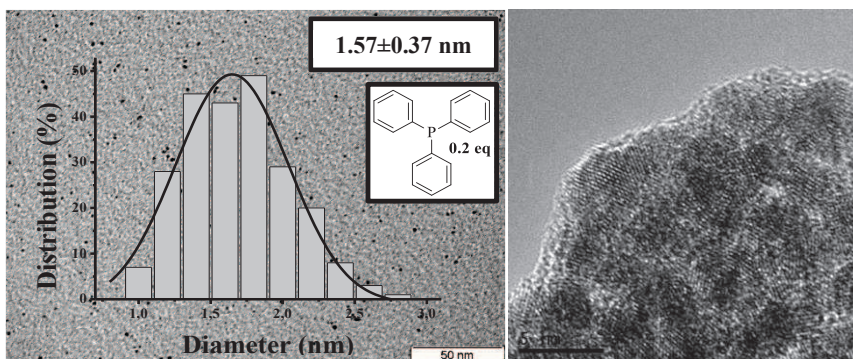


Figure 4.7. TEM and HRTEM micrographs of Ru₃ NPs.

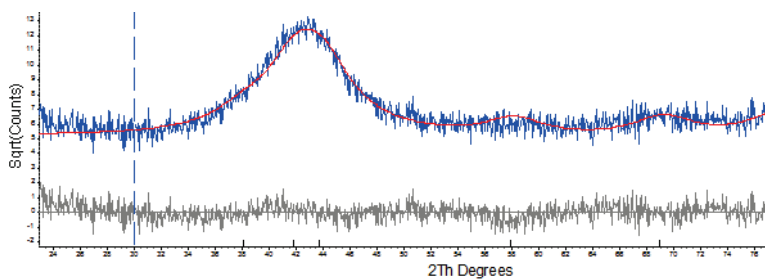


Figure 4.8. XRD of hep crystalline Ru₃ nanoparticles.

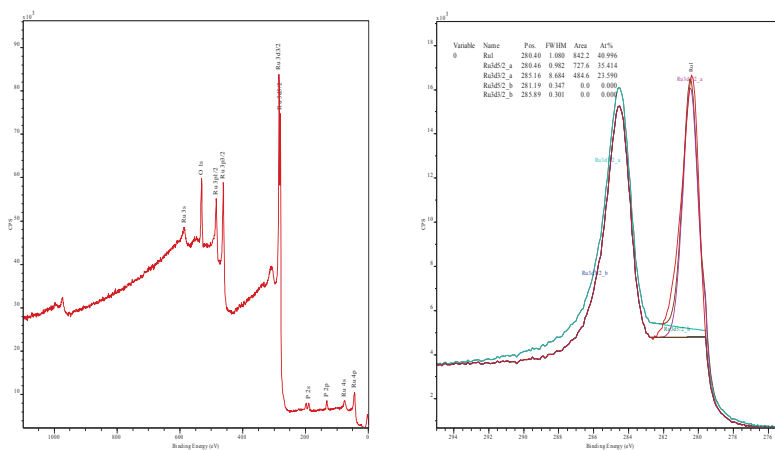


Figure 4.9. XPS spectra of Ru₃ nanoparticles.

General procedure for the hydrogenation reactions

In a typical experiment, a 5 entries autoclave or an autoclave Par 477 equipped with PID control temperature and reservoir for kinetic measurements were charged in the glove-box with 3 mg of Ru nanoparticles (the catalyst concentration was calculated based on the total number of metallic atoms in the NPs) and the substrate in 10 mL of solvent. Molecular hydrogen was then introduced until the desired pressure was reached. The reaction was stirred during the corresponding time at the desired temperature. The autoclave was then depressurised. The solution was filtered over silica and analysed by gas chromatography.

Conversion and selectivity was determined by GC-MS and *cis/trans* selectivity was confirmed by NOE experiments in NMR. GC-MS spectroscopy was carried out on a HP 6890A spectrometer, with an HP-5 column (0.25mm x 30m x 0.25 μ m). The method used for the polyaromatic systems consist in an initial isotherm period at 130°C for 10 min followed by a 10°C min⁻¹ temperature ramp to 180°C and a hold time of 35 min, flow 3.5 ml/min.

The method used for the substituted naphthalenes consist in an initial isotherm period at 40°C for 3 min followed by a 3°C min⁻¹ temperature ramp to 120°C and a hold time of 12 min, flow 1.3 ml/min.

Substrate **4.1**: $tr_{4.1} = 2.03$ min, $tr_{4.1a} = 1.83$ min, $tr_{4.1b} = 1.58$ min, $tr_{4.1c} = 1.41$ min.

Substrate **4.2**: $tr_{4.2} = 14.91$ min, $tr_{4.2a} = 14.22$ min, $tr_{4.2b} = 13.15$ min, $tr_{4.2c} = 10.73$ min, $tr_{4.2d} = 12.76$ min, $tr_{4.2e} = 8.37$ min.

Substrate **4.3**: $tr_{4.3} = 14.72$ min, $tr_{4.3a} = 13.04$ min, $tr_{4.3b} = 14.31$ min, $tr_{4.3c} = 13.71$ min.

Substrate **4.4**: $tr_{4.4} = 46.46$ min, $tr_{4.4a} = 44.62$ min, $tr_{4.4b} = 41.16$ min, $tr_{4.4c} = 36.74$ min, $tr_{4.4d} = 20.58$ min, $tr_{4.4e} = 21.90$ min.

Substrate **4.5**: $tr_{4.5} = 22.80$ min, $tr_{4.5a} = 20.80$ min, $tr_{4.5b} = 18.27$ min.

Substrate **4.7**: $tr_{4.7} = 5.56$ min, $tr_{4.7a} = 4.91$ min, $tr_{4.7b} = 3.68$ min, $tr_{4.7c} = 3.02$ min.

Substrate **4.8**: $tr_{4.8} = 27.39$ min, $tr_{4.8a} = 25.96$ min, $tr_{4.8b} = 23.70$ min, $tr_{4.8c} = 20.51$ min.

Substrate **4.9**: $tr_{4.9} = 11.93$ min, $tr_{4.9a} = 12.01$ min.

Substrate **4.10**: $tr_{4.10} = 5.46$ min, $tr_{4.10a} = 4.55$ min, $tr_{4.10b} = 3.39$ min, $tr_{4.10c} = 2.90$ min.

Substrate **4.11**: $tr_{4.11} = 2.11$ min, $tr_{4.11a} = 2.04$ min, $tr_{4.11b} = 1.96$ min, $tr_{4.11c} = 1.86$ min.

Substrate **4.12**: $tr_{4.12} = 7.94$ min, $tr_{4.12a} = 6.41$ min.

Substrate **4.13**: $tr_{4.13a} = 11.56$ min, $tr_{4.13b} = 10.79$ min, $tr_{4.13c} = 9.21$ min.

Substrate **4.14**: $tr_{4.14} = 14.06$ min, $tr_{4.14a} = 12.55$ min, $tr_{4.14b} = 13.61$ min.

4.6. REFERENCES

1. Bamforth, S. M.; Singleton, I. *J. Chem. Technol. Biotechnol.* **2005**, *80*, 723–736.
2. (a) *Benzo[α]pyrene, Polynuclear aromatic compounds, Part 1, Chemical, environmental and experimental data, Monographs on the evaluation of the carcinogenic risk of chemicals to humans*, vol. 32. International agency for research on cancer, 1983, 211–224. (b) Keith, L. H.; Telliard, W. A. *Environ. Sci. Technol.* **1979**, *13*, 416–423.
3. (a) Pawelec, B.; Campos-Martin, J. M.; Cano-Serrano, E.; Navarro, R. M.; Thomas, S.; Fierro, J. L. G. *Environ. Sci. Technol.* **2005**, *39*, 3374–3381. (b) García-Martínez, M. J.; Riva, I. D.; Canoira, L.; Llamas, J. F.; Alcántara, R.;

- Gallego, J. L. R. *Appl. Catal. B: Environ.* **2006**, *67*, 279–289. (c) Rivas, F. J. *J. Hazard. Mater.* **2006**, *138*, 234–251. (d) Ferrarese, E.; Andreottola, G.; Oprea, I. A. *J. Hazard. Mater.* **2008**, *152*, 128–139.
4. Stanislaus, A.; Cooper, B. H. *Catal. Rev. Sci. Eng.* **1994**, *36*, 75–123.
 5. Beckers, N. A.; Huynh, S.; Zhang, X.; Lubber, E. J.; Buriak, J. M. *ACS Catal.* **2012**, *2*, 1524–1534.
 6. Widegren, J. A.; Finke, R. G. *J. Mol. Catal. A: Chem.* **2003**, *191*, 187–207.
 7. Yuan, T.; Marshall, W. D. *J. Hazard. Mater.* **2005**, *126*, 149–157.
 8. Beltramone, A. R.; Resasco, D. E.; Alvarez, W. E.; Choudhary, T. V. *Ind. Eng. Chem. Res.* **2008**, *47*, 7161–7166.
 9. Sun, L.; Zong, Z.; Kou, J.; Zhang, L.; Ni, Z.; Yu, G.; Chen, H.; Wei, X.; Lee, C. W. *Energy Fuels* **2004**, *18*, 1500–1504.
 10. Mitsui, T.; Rose, M. K.; Fomin, E.; Ogletree, D. F.; Salmeron, M. *Nature* **2003**, *422*, 705–707.
 11. Huang, T.; Kang, B. *Chem. Eng. J.* **1996**, *63*, 27–36.
 12. Deshmukh, R. R.; Lee, J. W.; Shin, U. S.; Lee, J. Y.; Song, C. E. *Angew. Chem. Int. Ed.* **2008**, *47*, 8615–8617.
 13. Ohde, M.; Ohde, H.; Wai, C. M. *Chem. Commun.* **2002**, 2388–2389.
 14. He, T.; Wang, Y.; Miao, P.; Li, J.; Wua, J.; Fang, Y. *Fuel* **2013**, *106*, 365–371.
 15. (a) Larock, R. C. *Comprehensive Organic Transformations*. New York: Wiley, 1999, 6–7, and references cited therein. (b) Lin, Q.; Shimizu, K.; Satsuma, A. *Appl. Catal. A: Gen.* **2010**, *387*, 166–172. (c) Borowski, A. F.; Vendier, L.; Sabo-Etienne, S.; Rozycka-Sokolowski, E.; Gaudyn, A. V. *Dalton Trans.* **2012**, *41*, 14117–14125.
 16. Korre, S. C.; Klein, M. T.; Quann, R. J. *Ind. Eng. Chem. Res.* **1995**, *34*, 101–117.
 17. Abu-Reziq, R.; Avnir, D.; Miloslavski, I.; Schumann, H.; Blum, J. *J. Mol. Catal. A: Chem.* **2002**, *185*, 179–185.
 18. Yonezawa, T.; Nagata, C.; Koto, H.; Imamura, A.; Morakuma, K. *Guide to Quantum Chemistry*. Kyoto: Kagaku-Dojin Press, 1990, 232.
 19. (a) Jacinto, M. J.; Santos, O. H. C. F.; Landers, R.; Kiyohara, P. K.; Rossi, L. M. *Appl. Catal. B: Environ.* **2009**, *90*, 688–692. (b) Deng, J.; Shih, W.; Mou, C. *ChemPhysChem* **2005**, *6*, 2021–2025. (c) Deng, J.; Shih, W.; Mou, C. *J. Phys. Chem. C* **2007**, *111*, 9723–9728.

20. Park, I. S.; Kwon, M. S.; Kang, K.Y.; Lee, J. S.; Park, J. *Adv. Synth. Catal.* **2007**, *349*, 2039–2047.
21. (a) Yoon, B.; Wai, C. M. *J. Am. Chem. Soc.* **2005**, *127*, 17174–17175. (b) Park, K. H.; Jang, K.; Kim, H. J.; Son, S. U. *Angew. Chem. Int. Ed.* **2007**, *46*, 1152–1155.
22. (a) Pan, H.; Wai, C. M. *New. J. Chem.* **2011**, *35*, 1649–1660. (b) Pan, H.; Wai, C. M. *J. Phys. Chem. C* **2009**, *113*, 19782–19788.
23. (a) Yuan, T.; Marshall, W. D. *J. Environ. Monit.* **2007**, *9*, 1344–1351. (b) Liao, W.; Liu, H.; Chen, H.; Chang, W.; Chiu, K.; Wai, C. M. *Chemosphere* **2011**, *82*, 573–580. (c) Sahle-Demessie, E.; Devulapelli, V. G.; Hassan, A. A. *Catalysts* **2012**, *2*, 85–100.
24. Chen, H.-J.; Liu, H.-W.; Liao, W.; Pan, H. B.; Wai, C. M.; Chiu, K.-H.; Jen, J.-F. *Appl. Catal. B* **2012**, *111–112*, 402–408.
25. Pinilla, J. L.; García A. B.; Philippot, K.; Lara, P.; García-Suárez, E. J.; Millan, M. *Fuel* **2014**, *116*, 729–735.
26. Wei, X.; Ni, Z.; Xiong, Y.; Zong, Z.; Wang, X.; Cai, C.; Ji, Y.; Xie, K. *Energy Fuels* **2002**, *16*, 527–528.
27. (a) Girgis, M. J.; Gates, B. C. *Ind. Eng. Chem. Res.* **1991**, *30*, 2021–2058. (b) Mochida, I.; Sakanishi, K.; Korai, Y.; Fujitsu, H. *Fuel* **1986**, *65*, 1090–1093.
28. (a) Fang, M.; Machalaba, N.; Sánchez-Delgado, R.A. *Dalton Trans.* **2011**, *40*, 10621–10632. (b) Sánchez-Delgado, R. A.; Machalaba, N.; Ng-a-qui, N. *Catal. Commun.* **2007**, *8*, 2115–2118. (c) Furimsky, E.; Massoth, F. E. *Catal. Rev. Sci. Eng.* **2005**, *47*, 297–489.
29. Fang, M.; Sánchez-Delgado, R. A. *J. Catal.* **2014**, *311*, 357–368.
30. Mévellec, V.; Roucoux, A. *Inorg. Chim. Acta* **2004**, *357*, 3099–3103.
31. Mao, H.; Chen, C.; Liao, X.; Shi, B. *J. Mol. Catal. A: Chem.* **2011**, *341*, 51–56.
32. Bovkun, T. T.; Grayevsky, M.; Sasson, Y.; Blum, J. *J. Mol. Catal. A: Chem.* **2007**, *270*, 171–176.
33. Nador, F.; Moglie, Y.; Vitale, C.; Yus, M.; Alonso, F.; Radivoy, G. *Tetrahedron* **2010**, *66*, 4318–4325.
34. Llop-Castelbou, J.; Bresó-Femenia, E.; Blondeau, P.; Chaudret, B.; Castellón, S.; Claver, C.; Godard, C. *ChemCatChem.* **2014**, *6*, 3160–3168.
35. Austin, B. M.; Zubarev, D. Y.; Lester, W. A. *J. Chem. Rev.* **2012**, *112*, 263–288.

36. Hubert, C.; Bilé, E. B.; Denicourt-Nowicki, A.; Roucoux, A. *Green Chem.* **2011**, *13*, 1766–1771.
37. Ma, Y-M.; Wei, X-Y.; Zhou, X.; Cai, K-Y.; Peng, Y-L.; Xie, R-L.; Zong, Y.; Wei, Y-B.; Zong, Z-M. *Energy Fuels* **2009**, *23*, 638–645.
38. Suzuki, T.; Yamada, H.; Sears, P. L.; Watanabe, Y. *Energy Fuels* **1989**, *3*, 707–713.
39. Fu, P. P.; Lee, H. M.; Harvey, R. G. *J. Org. Chem.* **1980**, *45*, 2797–2803.
40. Yu, J. S.; Ankaniec, B. C.; Rothwell, I. P.; Nguyen, M. T. *J. Am. Chem. Soc.* **1992**, *114*, 1927–1929.
41. (a) Gonzalez-Galvez, D.; Lara, P.; Rivada-Wheelaghan, O.; Conejero, S.; Chaudret, B.; Philippot, K.; van Leeuwen, P. W. N. M. *Catal. Sci. Technol.* **2013**, *3*, 99–105. (b) Gonzalez-Galvez, D.; Nolis, P.; Philippot, K.; Chaudret, B.; van Leeuwen, P. W. N. M. *ACS Catal.* **2012**, *2*, 317–321. (c) Guerrero, M.; Coppel, Y.; Chau, N. T. T.; Roucoux, A.; Denicourt-Nowicki, A.; Monflier, E.; Bricout, H.; Lecante, P.; Philippot, K. *ChemCatChem* **2013**, *5*, 1–11. (d) Snelders, D. J. M.; Yan, N.; Gan, W.; Laurenczy, G.; Dyson, P. J. *ACS Catal.* **2012**, *2*, 201–207.

*C*HAPTER 5

APPROACH TO THE ENANTIOSELECTIVE HYDROGENATION OF ARENES USING CHIRAL RUTHENIUM NANOPARTICLES

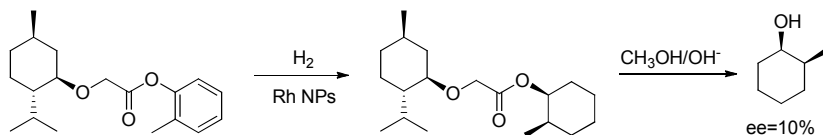
5.1. INTRODUCTION TO THE ASYMMETRIC HYDROGENATION OF ARENES

The significant development of homogeneous enantioselective catalysis has triggered the interest for the development of chiral surfaces and their application as recyclable catalysts. Homogeneous systems have typically a single active site while the surface geometry of heterogeneous systems implies various types of substrate sites with different coordination (terrace, step, edge, kink, vacancy, etc.) and, consequently, different adsorption properties.

Nowadays, the adsorption mode of the substrate and the modifier on the metal surface is only speculated based on ex-situ measurements and theoretical calculations.¹ For this reason, several mechanistic and coordinative modes have been proposed for the most studied reactions. However, it is generally accepted that enantioselection is generated by the direct interactions between modifier and substrate at the metal surface.

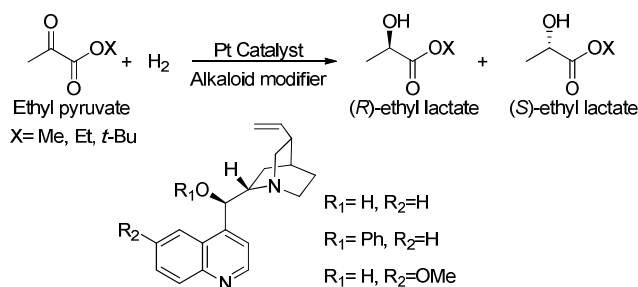
The first example of enantioselective catalysis (in fact it was diastereoselective) by metal nanoparticles was reported in 1994 by Lemaire, Gallezot *et al.* in which hydrogenation of a disubstituted aromatic ring linked to a chiral auxiliary was attempted using Rh nanoparticles and the chiral amine (*R*)-dioctylcyclohexyl-1-ethylamine (DOCEA) as stabilizer. However, only a very modest enantiomeric excess (10%) was achieved (Scheme 5.1).²

Thereafter, several asymmetric reactions using nanoparticles have been attempted. The most studied reaction has been the hydrogenation of α -ketoesters, typically ethyl pyruvate, using cinchona alkaloid derivatives as ligands.



Scheme 5.1. Diastereoselective hydrogenation using Rh NPs and DOCEA.²

In general, in all these examples, aliquots of the chiral ligands must be added during the catalysis in order to obtain high ee's. This requirement is attributed to the depletion of the modifier from the metal surface due to the hydrogenation.³ A very successful example was reported using Pt nanoparticles where enantioselectivities up to 98% at full conversion were obtained (Scheme 5.2).⁴



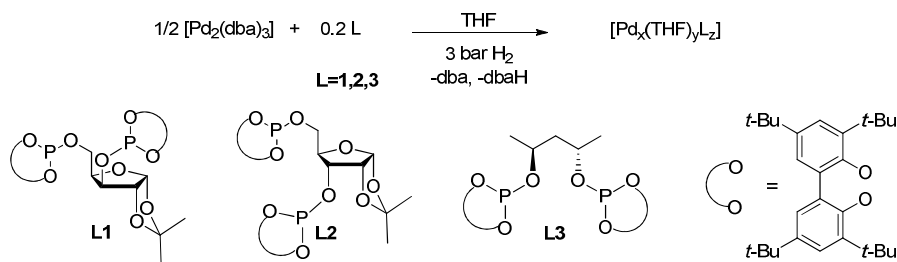
Scheme 5.2. Enantioselective hydrogenation of pyruvates using Pt NPs.⁵

Baiker *et al.* revealed that the enantioselective hydrogenation on chiral modified Pt NPs was shape-dependent and the reaction rate and the enantioselectivity increased with an increase in the Pt{111}/Pt{100} ratio.⁶ In some cases, it is supposed that there is a depletion of ligands from the surface of the nanoparticles and chiral homogeneous complexes can be formed *in situ* becoming the real catalytic species.

Nanoparticles stabilized by chiral ligands have also been used in C-C coupling asymmetric reactions catalysed by Pd NPs stabilized by chiral

phosphines.⁷ In the asymmetric Suzuki-Miyaura cross coupling reaction, enantioselectivity up to 69% was achieved and it depended on the dihedral angle of the backbone axes of the bis-phosphine ligands and on the application of a strong base. Therefore, these effects are consistent with the formation of molecular palladium(II) species.⁸ Glorius and co-workers developed immobilized Pd catalysts modified by chiral N-heterocyclic carbenes (NHC) in the asymmetric α -arylation of ketones with aryl halides. The heterogeneous nature of the active species was evidenced by several experiments such as hot filtration test, mercury-poisoning test and trace metal analysis.⁹

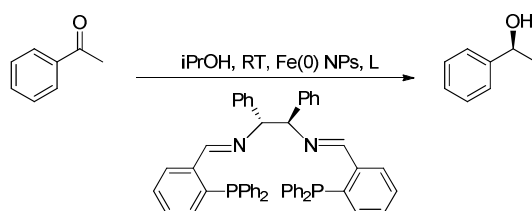
The asymmetric allylic alkylation catalysed by Pd NPs stabilized by chiral diphosphite ligands with *xylo*- or *ribo*- furanoside backbone has also been reported (Scheme 5.3), although the molecular nature of the catalysts cannot be excluded. The nanoparticles stabilized by L1 behaved differently from the corresponding molecular systems. However, in the case of the colloids stabilized by L2 and L3, no differences in terms of activity and selectivity were detected compared with the molecular species.¹⁰



Scheme 5.3. Pd NPs stabilized by chiral diphosphite ligands used in the discrimination between molecular and colloidal catalysts.^{10b}

Furthermore, several examples of asymmetric hydrogenation of different functional groups and transfer hydrogenation using NPs coated with chiral ligand have been reported.¹¹ For instance, Lin *et al.* synthesized metal

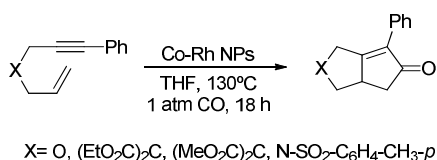
NPs-supported chiral catalysts containing BINAP-Ru-DPEN moieties in the asymmetric hydrogenation of aromatic ketones with high activity and enantioselectivity (up to 98% ee)¹² and, as it was commented in Chapter 1, Morris *et al.* reported the use of iron nanoparticles stabilized by PNNP-type tetradentate ligands for the transfer hydrogenation of ketones obtaining 64% of enantioselectivity (Scheme 5.4). However, the formation of homogeneous species during the reaction could be the responsible of enantioselectivity.¹³



Scheme 5.4. PNNP-Fe NPs used in the asymmetric transfer hydrogenation of acetophenone.¹³

In some reactions, the low selectivities are attributed to a dynamic behaviour of the ligands at the nanoparticle surface but further studies are required to elucidate the nature of the true catalyst.¹⁴

Moreover, a bimetallic Co-Rh system immobilized on charcoal and decorated with a chiral bis-phosphine ligand has reached 87% of enantioselectivity in the Pauson-Khand reaction (Scheme 5.5). The debate on whether the reaction was catalysed by homogeneous or heterogeneous species was not solved by the addition of mercury since poisoning of the system indicating that the active catalyst could involve NPs but Co and Rh species were detected by ICP-AES analysis.¹⁵



Scheme 5.5. Pauson-Khand reaction catalysed by Co-Rh NPs immobilized on charcoal.¹⁵

Nevertheless, in general, obtaining enantioselectivity in arene hydrogenation reactions is still a really challenging task. Thus, Rh nanoparticles stabilized by chiral amines, which combine the properties of a phase transfer agent and a chiral inductor, were used in the hydrogenation of *o*-methylanisole and *o*-methyl-*O*-trimethylsilyl-phenol. Good *cis/trans* selectivity were obtained but the enantiomeric excesses did not exceed the 6%.^{2, 16}

In 2009, Claver and co-workers reported the synthesis of Ru, Rh and Ir nanoparticles stabilized by chiral diphosphite ligands with furanoside backbone for the hydrogenation of prochiral disubstituted monocyclic arenes. Good activities under mild conditions and interesting results in terms of *cis*-selectivity were obtained. However, very low ee's were achieved (up to 6%).¹⁷

Chiral auxiliaries that covalently bind to the substrates were also used in order to obtain asymmetric induction (Figure 5.1).¹⁸ Covalent bonding should induce stronger interactions and enantioselectivity could be obtained with the help of a chiral auxiliary temporarily linked to the substrate. Therefore, the sterically hindrance will block the reaction at one face of the substrate.¹⁹

Using such systems, the catalyst does not need to be chiral but the scope of substrates is still limited and, in general, 2-methylbenzoic acid derivatives have been used.

For instance, Ranade *et al.* described the diastereoselective hydrogenation of anthranilic acid and *o*-toluidine covalently bonded to (*S*)-proline obtaining diastereoselectivities up to 96%.^{18a,18e}

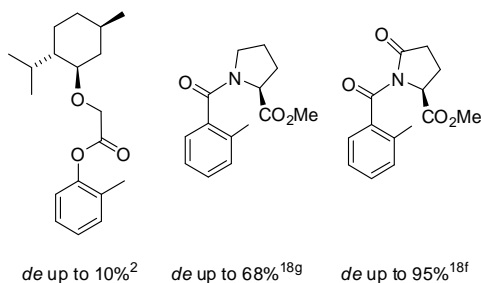


Figure 5.1. Arene derivatives bound to a chiral auxiliary and the corresponding diastereoselectivities.

5.2. OUTLOOK AND OBJECTIVES OF THIS CHAPTER

As commented above, only a few studies have been reported on the enantioselective hydrogenation of arenes using nanoparticles stabilized by chiral ligands and even more limited studies are focused on the supramolecular interaction of the chiral ligand with the substrate.

In the previous chapters, nanoparticles stabilized by PPh_3 revealed to be good catalysts for arene reduction. In this context, the aim of this work was to synthesize chiral phosphine ligands to stabilize ruthenium nanoparticles for the asymmetric hydrogenation of arenes. Our hypothesis was based on the idea that supramolecular interaction between the ligand and the substrate could direct the approach of the substrate to the catalyst surface and could eventually induce enantioselectivity.

As supramolecular interaction, we selected a double acid-base interaction. Thus, we planned to prepare a phosphine ligand with an acid and

a basic functional group that could interact with similar functions present in the substrate (Figure 5.2).

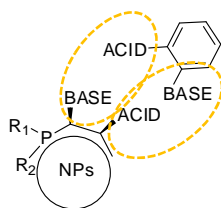


Figure 5.2. Supramolecular interaction proposed for a phosphine ligand and a general substrate.

On the other hand, cinchona alkaloids, which contain a basic and an acidic function, have been widely used in the asymmetric hydrogenation of ethyl pyruvate with really good results in terms of enantioselectivity using platinum catalyst.³ Since cinchonidine has not been used as stabiliser for nanoparticles applied in the asymmetric hydrogenation of arenes, nanoparticles stabilized by cinchonidine will also be synthesized and applied in the hydrogenation of substituted aromatic rings containing basic and acidic sites.

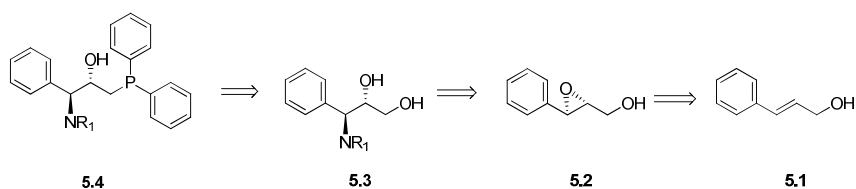
In the course of this study, we realized that we needed information about the interaction of the ligand and the nanoparticle to design the appropriate ligands. In this area, deuteration studies using Ru@PVP NPs have recently been used for the selective deuteration of pyridines, quinolines and alkyl amines, which informs about the possible coordination of heteroatoms at the surface.²⁰ Since this technique could be also useful to understand how the stabilizers can interact with the nanoparticle surface, preliminary deuteration studies of simple ligands have been performed.

5.3. RESULTS AND DISCUSSION

5.3.1. DESIGN AND SYNTHESIS OF THE TARGET CHIRAL PHOSPHINE LIGAND

As was previously commented, the design of the stabilizing agents for nanoparticles is an important aspect in order to obtain good results in terms of selectivity and activity in nanocatalysis. Several examples of phosphine ligands used as stabilizers have been reported and small and well dispersed nanoparticles have been obtained (see previous chapters).²¹ However, as far as we are concerned, no examples of chiral phosphine ligands have been used to stabilize Ru NPs for arene hydrogenation.

As it was previously mentioned, our hypothesis was to synthesise a phosphine with additional functional groups with acid and base properties. Phosphine **5.4** was selected as it is closely related to triphenylphosphine and incorporates a basic (NR_2) and an acid function (OH) and eventually the aromatic ring can provide an additional interaction with the surface.²² Scheme 5.6 shows the retrosynthetic analysis of the target phosphine. We envisage the synthesis of the phosphine **5.4** by a substitution reaction of the primary alcohol in compound **5.3**. This aminodiol can be obtained by regioselective opening of epoxide **5.2**, which in turn can be prepared from cinnammyl alcohol using Sharpless epoxidation. Using this methodology, modifying the nucleophile and the position attack in the oxirane ring *via* variation on the catalyst, should provide a series of different ligands.



Scheme 5.6. Retrosynthetic scheme for the synthesis of chiral amino-hydroxyl-phosphines based on Sharpless epoxidation.

In 1980 T. Katsuki and K. B Sharpless reported the first enantioselective epoxidation reaction from allylic alcohols with up to 90% of enantiomeric excess.²³ This classical asymmetric transformation uses *tert*-butyl hydroperoxide (TBHP) as terminal oxidant and the titanium tartrate catalyst is readily accessible from dialkyl tartrate and titanium alkoxide (most commonly diethyl tartrate (DET) and titanium isopropoxide). It was reported that the addition of molecular sieves to the reaction mixture had a beneficial effect on the process and the reaction can be performed with 5-10 mol% of the readily available Ti catalyst whereas in the absence of molecular sieves, a stoichiometric amount of this complex is needed.

The catalyst is considered to be the [Ti(tartrate)(OR)₂]₂ dimer **5.5** and will generate the structure **5.6** after the addition of the allylic alcohol and the oxidant (TBHP). The coordination of the oxygen atom from TBHP to the titanium activates the peroxide and facilitates the intramolecular oxygen delivery (Figure 5.3). This reaction is applicable to a wide range of substrates: (*E*)-allylic alcohols give high enantioselectivities while (*Z*)-allylic alcohols are more dependent on the substrate structure.

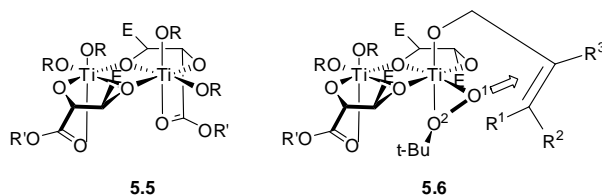
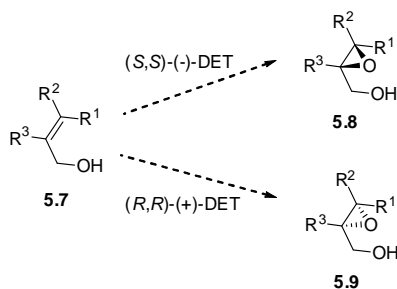


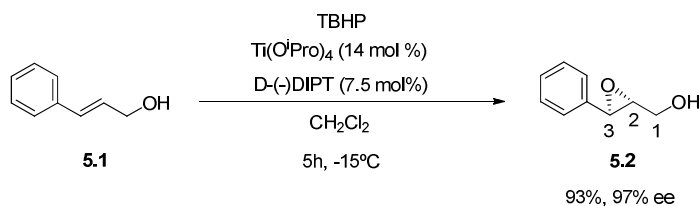
Figure 5.3. Proposed structure for the titanium tartrate complex (**5.5**) and its transformation after the addition of reagents (**5.6**).

With regard to enantioselectivity, the oxygen transfer from the coordinated alkyl peroxide to an allylic alcohol (represented as **5.7** in Scheme 5.7) will take place from “above” when (*S,S*)-(-)-DET is employed as chiral ligand, and from “below” when the (*R,R*)-(+)-DET is used.²⁴



Scheme 5.7. Enantiofacial differentiation depending on the configuration of the diethyl tartrate ligand in the titanium complex.

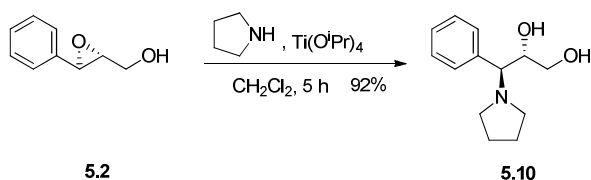
Therefore, cinnamyl alcohol **5.1** was selected as substrate for the Sharpless epoxidation (Scheme 5.8). Thus, when **5.1** was reacted under Sharpless epoxidation conditions using diethyl D-tartrate as chiral ligand the reaction proceeded with a 61% yield and a 32% of enantiomeric excess. However, when (-)-diisopropyl D-tartrate (DIPT) was used, the reaction was quantitative in conversion and enantiomeric excess achieved 97%.



Scheme 5.8. Sharpless epoxidation of allylic alcohol **5.1**.

The formation of product **5.2** was confirmed by $^1\text{H-NMR}$ in which the protons from the alkene disappeared and two new signals at 3.91 ppm (doublet) and a multiplet at 3.23 ppm corresponding to the protons from the epoxide were detected.

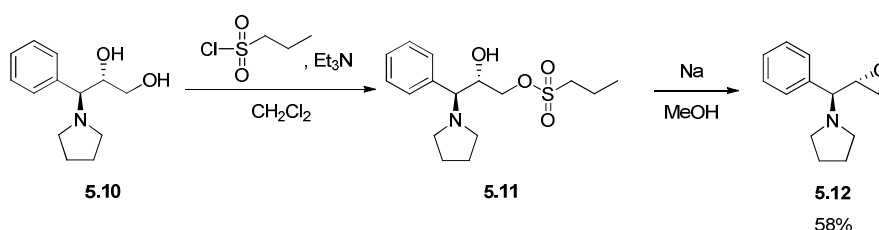
The following step was a regioselective epoxide opening by a secondary amine (Scheme 5.9). We selected pyrrolidine as secondary amine and the reaction with **5.2** in the presence of titanium(IV) isopropoxide afforded compound **5.10** in 92% yield.²⁵ Titanium coordinates the hydroxyl and the epoxidic oxygens directing the attack to position 3, which in addition, is a benzylic position. The incorporation of the pyrrolidine was confirmed by the corresponding multiplets at 2.43-2.53 and 1.66-1.72 ppm in the $^1\text{H-NMR}$ spectra. The incorporation at position 3 was indicated by the coupling of signals at 4.16 ppm (ddd, position 2) and 3.24 ppm (d, position 3) with the typical signals of CH_2OH at 3.42 and 3.28 ppm.



Scheme 5.9. Epoxide ring opening with pyrrolidine.

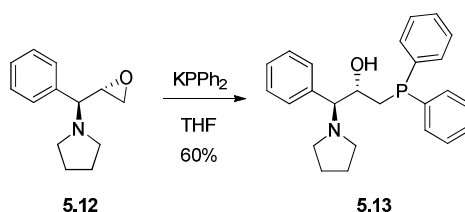
We initially attempted the selective tosylation of diol **5.10** but conversions were low and purification issues were encountered.

Consequently, the introduction of the phosphine moiety by an epoxide ring opening was considered. The primary alcohol of compound **5.10** was treated with propylsulphonyl chloride following a reported procedure²⁶ to afford the sulphonate **5.11** that was then treated in a one-pot manner with NaOMe yielding epoxide **5.12** in 58% overall yield (Scheme 5.10). The formation of the epoxide was confirmed by the corresponding characteristic signals at 3.11, 2.82 and 2.61 ppm for protons bonded to carbons of an epoxide.



Scheme 5.10. Synthesis of epoxide **5.12**.

Finally, the desired phosphine **5.13** was obtained by treating **5.12** with a solution of potassium diphenylphosphide (Scheme 5.11).



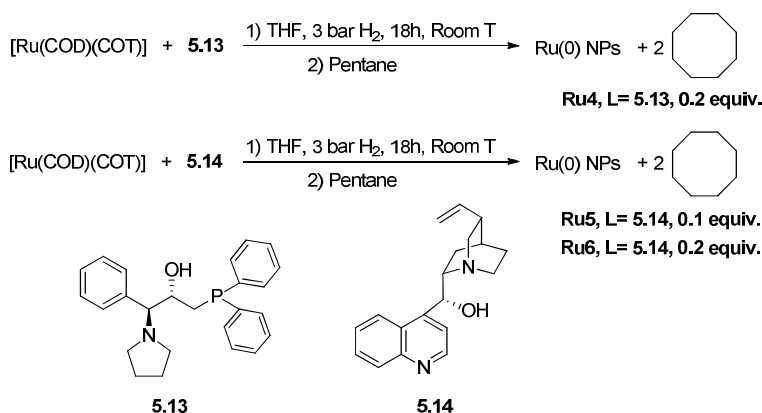
Scheme 5.11. Obtaining of the target ligand **5.13**.

The presence of the phosphine in the reaction product was confirmed by the signal at -22.9 ppm in the $^{31}\text{P}\{^1\text{H}\}$ NMR spectrum. Regarding the ^1H -NMR, the H-3 proton was located as a doublet at 3.35 ppm, the H-2 as a multiplet at 4.10 ppm (higher chemical shift) and the H-1 protons appeared at 2.03 and 1.78 ppm as multiplets due to the coupling with the phosphorus.

Moreover, 15 aromatic protons were detected. In ^{13}C the three carbons of the alkyl linear chain appeared as doublets due the coupling with the phosphorus.

5.3.2. SYNTHESIS AND STABILIZATION OF CHIRAL METAL NANOPARTICLES

The synthesis of the ruthenium nanoparticles was carried out following the method described in the previous chapters (see Experimental Section). The commercially available organometallic precursor $[\text{Ru}(\text{COD})(\text{COT})]$ was reduced in a Fischer-Porter bottle under H_2 atmosphere in the presence of the prepared chiral ligand **5.13** and cinchonidine **5.14** in sub-stoichiometric proportions and using THF as solvent. After 16 h, the nanoparticles were isolated as black powders after precipitation with pentane and they were characterized (Scheme 5.12, see spectroscopic data in the Experimental Part).



Scheme 5.12. Synthesis of ruthenium nanoparticles stabilised by chiral ligands.

- **Ru4** nanoparticles

Initially, 0.2 equivalents of the monodentate phosphine ligand **5.13** were used to synthesize **Ru4** nanoparticles. The formation of small and

spherical nanoparticles was observed by TEM, exhibiting a diameter of 1.61 ± 0.35 nm and a narrow size distribution.

Then, the amount of ligand present at the nanoparticle surface was determined by thermogravimetric analysis (TGA), which indicated the presence of 79 wt% of Ru and 21 wt% of ligand **5.13**.

From the experimental data obtained by TEM and by TGA and using the *Van Hardevel Hartog* model, the approximate quantity of ruthenium atoms present on the **Ru4** nanoparticles surface can be calculated. In Table 5.1 are presented the values referring to the total number of atoms (Nt) and the atoms on the surface (Ns) related to the diameters obtained by TEM are presented. The P/Ru_s ratio is between 0.10-0.13 that represents approximately 1 phosphorus ligand for 15 ruthenium surface atoms. The ratio of surface atoms per total atoms in the nanoparticle remains similar in all the cases.

Table 5.1. Approximate quantity of ruthenium atoms on the **Ru4** surface.

Size of NPs	1.26 nm	1.61 nm	1.96 nm
Nt	77	161	290
Ns	56	101	159
Ns/Nt	0.729	0.626	0.549
P/Ru _s	0.10	0.11	0.13

The structure of the nanoparticles **Ru4** was determined by X-Ray diffraction (XRD). The diffraction pattern is related to the hexagonal close packing lattice of Ru-NPs and coherence length of 1.47 ± 0.20 nm was determined. This value is in concordance with the size determined by TEM.

Finally, the oxidation state of the atoms situated on the **Ru4** nanoparticles surface was determined by X-ray Photoelectron Spectroscopy

(XPS). The analysis revealed a 100% of Ru(0) atoms at the surface of the NPs.

To summarise, the **Ru4** NPs exhibit a diameter of 1.61 ± 0.35 nm, are highly crystalline with hcp packing and no oxidation is detected. Quantitatively, they contain 79% of Ru and 21% of **5.13**.

- **Ru5 nanoparticles**

Ru5 nanoparticles were prepared using 0.1 equivalents of cinchonidine **5.14**. TEM micrographs permitted the observation of the formation of small and spherical shaped nanoparticles with a diameter of 1.85 ± 0.54 nm.

Then, the proportion of ligand present on the nanoparticle surface was determined by thermogravimetric analysis (TGA) resulting 72 wt% of Ru and 28 wt% of cinchonidine.

From the experimental data obtained by TEM and by TGA and using the *Van Hardevel Hartog* model, a L/Ru_s ratio between 0.18-0.27 that represents approximately 1 cinchonidine ligand for 7-8 ruthenium surface atoms was determined (Table 5.2).

The structure of the nanoparticles **Ru5** was again determined by X-Ray diffraction (XRD). A hexagonal close packing lattice and a coherence length of 1.35 ± 0.06 nm was determined.

The oxidation state of the atoms situated on the **Ru5** nanoparticles surface was determined by X-ray Photoelectron Spectroscopy (XPS), revealing 100% of Ru(0) atoms at the surface of the NPs.

Table 5.2. Approximate quantity of ruthenium atoms on the **Ru5** surface.

Size of NPs	1.31 nm	1.85 nm	2.39 nm
Nt	87	244	526
Ns	62	139	255
Ns/Nt	0.713	0.570	0.485
L/Ru _s	0.18	0.23	0.27

To summarise, the **Ru4** NPs exhibit a diameter of 1.85 ± 0.54 nm, are highly crystalline with hcp packing and no oxidation is detected. Quantitatively, they contain 72% of Ru and 28% of cinchonidine.

- **Ru6** nanoparticles

Ru6 nanoparticles were prepared using 0.2 equivalents of the cinchonidine **5.14**. The formation of small and spherical shaped nanoparticles with a diameter of 1.23 ± 0.40 nm was obtained from TEM micrographs. The amount of ligand present at the nanoparticle surface was determined by thermogravimetric analysis (TGA) and 67% of Ru and 33% of cinchonidine were measured.

From the experimental data obtained by TEM and by TGA and using the *Van Hardevel Hartog* model, it was determined a L/Ru_s ratio between 0.19-0.28 that represents approximately 1 cinchonidine ligand for 6-7 ruthenium surface atoms (Table 5.3).

Ru6 presented an hexagonal close packing lattice with a coherence length of 0.81 ± 0.04 nm and 100% of Ru(0) atoms were observed at the surface of the NPs

Table 5.3. Approximate quantity of ruthenium atoms on the **Ru6** surface.

Size of NPs	0.88 nm	1.27 nm	1.66 nm
Nt	26	79	176
Ns	23	57	108
Ns/Nt	0.877	0.726	0.613
L/Ru _s	0.19	0.23	0.28

To summarise, the **Ru6** NPs exhibit a diameter of 1.27 ± 0.39 nm, are highly crystalline with hcp packing and no oxidation is detected. Quantitatively, they contain 67% of Ru and 33% of cinchonidine.

Comparing both nanoparticles stabilised by cinchonidine, it can be deduced that smaller nanoparticles are obtained when more ligand is used as stabiliser (**Ru6** are smaller than **Ru5**). No relevant differences in the amount of ruthenium vs. ligand were observed. Table 5.4 collects the most relevant characterization data of nanoparticles **Ru4-6**.

Table 5.4. Summary of **Ru4-Ru6** characterization.

NPs	Diameter (nm)		Structure (XRD)	Oxidation State (%Ru ^{δ+}) (XPS)	%Ru (TGA)	%L
	(TEM)	(XRD)				
Ru4	1.61±0.35	1.47±0.20	hcp	0	79	21
Ru5	1.85±0.54	1.35±0.05	hcp	0	72	28
Ru6	1.23±0.40	0.81±0.04	hcp	0	67	33

5.3.3. HYDROGENATION OF DISUBSTITUTED AROMATIC COMPOUNDS USING CHIRAL NANOPARTICLES

As previously commented in the introduction of this chapter, an exploratory study of arene reduction was carried out using **Ru4-6** as catalysts, which were bearing two stabilizers, namely the phosphine **5.13** and

cinchonidine. Both stabilisers contained amino-alcohol moieties aiming to provide supramolecular interactions with the substrate.

For these reactions, substrates that should be able to provide acid-base interactions with the ligand were selected: the amides **5.15** and **5.16** since amides are usually not reduced under mild reaction conditions, 2-pyridinemethanol (**5.17**) and the 2-methoxyphenylmethanol (**5.18**). The configuration of the chiral centres bearing the acid-base functions in the ligand should determine the interaction orientation with the substrate. Subsequently, face discrimination should occur at the metal surface (Figure 5.4).

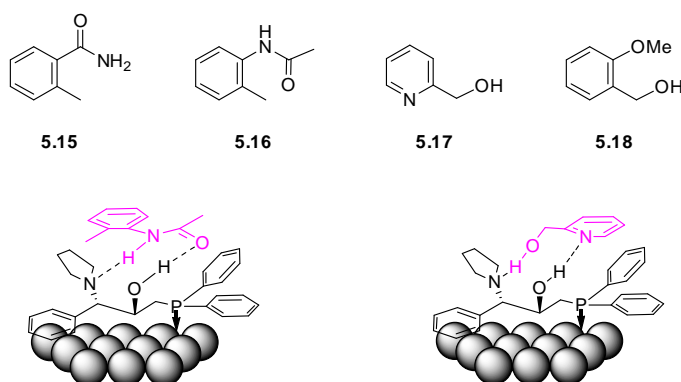


Figure 5.4. Proposed model of the interaction between the ligand **5.13** and disubstituted substrates.

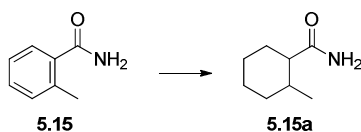
We initiated the study with the hydrogenation of 2-methylbenzamide (**5.15**) using **Ru4** and **Ru6** nanoparticles. As shown in Table 5.5 when the reaction was performed at 30°C and 40 bar of hydrogen pressure in THF for 64 h using **Ru4** nanoparticles as catalysts, 72% of conversion was obtained (Table 5.5, Entry 1) whereas when **Ru6** were used, the conversion decreased to 17% (Table 5.5, Entry 3). No conversion was obtained when the reaction was performed using heptane probably due to the low solubility of the

substrate in the solvent (Table 5.5, Entries 2 and 4). No enantioselectivity was observed in any case.

Alternatively, the reaction was tried using PVP nanoparticles (**Ru7**) modified by the addition of 0.5 equivalents of cinchonidine. In this case, the reaction was again slow and only 13% conversion was achieved after 64 hours. The steric bulk induce by cinchonidine that could fully cover the nanoparticle surface, can explain the low conversion achieved (Table 5.5, Entry 5).

Enantioselectivity was not achieved in these reactions and *cis*-hydrogenated product was always obtained as the unique product, as demonstrated by NOE experiments.

Table 5.5. Hydrogenation of 2-methylbenzamide **5.15**.



E.	NPs	Excess of ligand L/Ru	Solvent (ml)	Conv. (%) ^b	%a ^{b,c}	%ee ^d
1	Ru4	-	THF (4)	72	100	0
2	Ru4	-	Heptane (4)	0	-	0
3	Ru6	-	THF (4)	17	100	0
4	Ru6	-	Heptane (4)	0	-	0
5	Ru7	0.5 Cinch	THF (4)	13	100	0

^aGeneral conditions: Ru NPs (2 mol%), substrate (0.62 mmol), T= 30°C, P= 40 bar, 64 h.

^bDetermined by GC and NMR. ^cOnly the *cis* isomer was observed. ^dEnantiomeric excess was calculated by chiral GC.

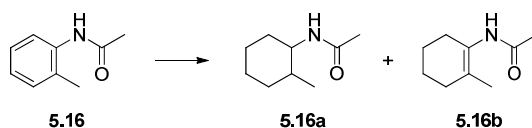
Then, N-(*o*-tolyl)acetamide **5.16** was hydrogenated using the same ruthenium nanoparticles (Table 5.6). When the reaction was carried out in heptane, the reaction did not evolve (Table 5.6, Entries 1 and 4). However, when the reaction was performed in THF, 69% conversion was achieved

using **Ru4** NPs, and 39% using **Ru6** (Table 5.6, Entries 2 and 5). This substrate was thus more easily hydrogenated than substrate **5.15**, but in this case a *cis/trans* mixture was obtained, with 42% of the *trans*-product using **Ru4** and 19% using **Ru6**. The *cis/trans* ratio configuration of products was determined by NMR-NOE experiments.

The reaction was also performed using **Ru4** NPs in methyl *tert*-butyl ether (MTBE) as solvent for 64 hours (Table 5.6, Entry 3). In this case, the conversion was significantly reduced to 25% and the *cis*-**5.16a** product was obtained in a 55% of selectivity showing again the crucial role of the solvent in the catalysis.

Next, the effect of the proportion of stabilizing agent used was studied, and **Ru5** NPs (stabilised by 0.1 equivalent of cinchonidine) were applied as catalyst in the hydrogenation of **5.16** (Table 5.6, Entry 6). After 24 hours, 57% of conversion was achieved and a *cis:trans* ratio of 51:18.

Table 5.6. Hydrogenation of N-(*o*-tolyl)acetamide **5.16**.^a



E.	NPs	Solvent (ml)	Time (h)	Conv. (%) ^b	% ^{a,b} <i>cis/trans</i>	% ^b	% ^{ee} ^c
1	Ru4	Heptane (4)	24	0	-	-	0
2	Ru4	THF (4)	24	69	48/42	10	0
3	Ru4	MTBE (4)	64	25	55/15	30	0
4	Ru6	Heptane (4)	24	0	-	-	0
5	Ru6	THF (4)	24	39	71/19	10	0
6	Ru5	THF (4)	24	57	51/18	31	0

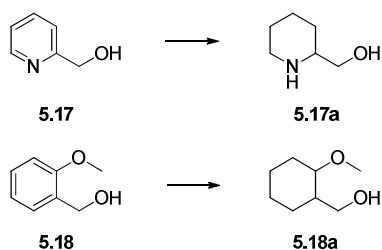
^aGeneral conditions: Ru NPs (2 mol%), substrate (0.62 mmol), T= 30°C, P= 40 bar. ^bDetermined by GC and NMR. ^cEnantiomeric excess was calculated by chiral HPLC.

Curiously, in all the cases, the partial hydrogenated product **5.16b** was obtained in selectivities up to 30%. Despite the similarities between substrate **5.15** and **5.16**, important differences were observed. Thus, hydrogenation of **5.15** affords only the fully hydrogenated *cis*-product, while hydrogenation of **5.16** affords *cis/trans* mixtures and the partially hydrogenated product **5.16b**. It should be noted that the percentage of *cis*-isomer suffers small variations and that the sum of the percentage of *trans*-isomer plus the percentage of compound **5.16b** is almost constant (Table 5.6, Entries 2 and 3). The isomer *trans* should be formed from the partially hydrogenated product **5.16b**.

Finally, **Ru4** nanoparticles were tested in the hydrogenation of **5.17** and **5.18**. For substrate **5.17**, stronger acid-base interactions between substrate and ligand were expected.

The hydrogenation of substrate **5.17** under 20 bar of H₂ for 64 hours, afforded compound **5.17a** in 78% conversion, but no enantioselectivity was obtained (Table 5.7, Entry 1). Substrate **5.18**, which was expected to interact weakly with the ligand, was hydrogenated but only 6% conversion was achieved after 64h. No enantioselectivity could be achieved (Table 5.7, Entry 2).

The low conversion even at long reaction times could be due to the presence of the nitrogen and/or the alcohol moiety in the substrate which could interact with the surface and could somehow limit the reaction.

Table 5.7. Hydrogenation of **5.17** and **5.18** using **Ru4** NPs.^a

E.	Subs.	P (bar)	Time (h)	Conv. (%) ^b	%a ^b	%ee ^c
1	5.17	20	64	78	100	0
2	5.18	20	64	6	100	0

^aGeneral conditions: Ru NPs (2 mol%), substrate (0.62 mmol), THF (10 ml), T= 30°C. ^bDetermined by GC and NMR. ^cEnantiomeric excess was calculated by chiral HPLC.

5.3.4. HYDROGENATION OF AROMATIC KETONES USING CHIRAL NANOPARTICLES

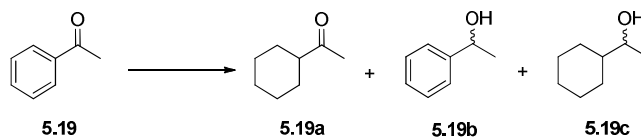
With the aim of comparing the behaviour of the nanoparticles prepared in this chapter with those prepared in the previous ones, and also aiming to check if some enantioselectivity could be observed in the reduction of ketones, we tested the reduction of some acetophenone derivatives (see Chapter 3 for comparison).

Therefore, **Ru4** nanoparticles were employed in the hydrogenation of aromatic ketones. Acetophenone was selected as model substrate and it was hydrogenated under the same reaction conditions used in Chapter 3 (Table 5.8, Entry 1). Total conversion and 56% of the totally hydrogenated product **5.19c** were obtained but no enantioselectivity was observed. When the reaction time was increased to 24 h (Table 5.8, Entry 2), the percentage of **5.19c** increased to 80% but no enantioselectivity was again detected.

It has been reported that, in some heterogeneous systems, catalyst deactivation and poor enantioselectivities are observed under high pressure conditions.^{6,27} Then, we decided to reduce the pressure to 3 bar of H₂ (Table 5.8, Entry 3). Under these conditions, and after 24 hours, 11% conversion and total selectivity towards product **5.19b** was obtained but enantioselectivity was neither observed.

Next, **Ru6** NPs were tested as catalysts in this reaction. When the reaction was performed at 3 bar, 31% of selectivity towards compound **5.19b** was achieved at 49% of conversion (Table 5.8, Entry 4). Increasing the pressure to 20 bar the selectivity towards the achiral product **5.19a** increased to 70% (Table 5.8, Entry 5).

Table 5.8. Acetophenone hydrogenation with **Ru4** and **Ru6** nanoparticles.^a



E.	NPs	P (atm)	Time (h)	Conv. (%) ^b	%a ^b	%b ^b	%c	%ee ^c
1	Ru4	20	5	100	44	-	56	0
2	Ru4	20	24	100	20	-	80	0
3	Ru4	3	24	11	-	100	-	0
4	Ru6	3	24	49	58	31	11	0
5	Ru6	20	24	89	70	11	19	0

^aGeneral conditions: Ru NPs (2 mol%), substrate (0.62 mmol), THF (10 ml), T= 30°C.

^bDetermined by GC. ^cEnantiomeric excess was calculated by chiral GC.

Regarding the selectivity, it is important to comment the influence of the pressure on the selectivity in the case of **Ru4** nanoparticles (Table 5.8, Entry 1-3). At lower pressures (Entry 3), only hydrogenation of the ketone was produced. When the reaction was conducted at higher pressures (Table 5.8, Entries 1-2), **5.19b** was not observed, indicating that this product is easily

hydrogenated to yield the totally hydrogenated product **5.19c**. In the case of **Ru6** nanoparticles, the H₂ pressure had an effect on both the selectivity and the conversion. It is important to highlight that up to 70% of selectivity towards the arene hydrogenation at *ca.* 90% of conversion was obtained. This selectivity is higher than that obtained using ruthenium nanoparticles stabilized by triphenylphosphine described in Chapter 3,²⁸ and is the best obtained in the reduction of the arene *vs.* a ketone in acetophenones.

At this point, we decided to study the hydrogenation of trifluoroacetophenone, which was successfully used in several asymmetric hydrogenations using cinchonidine-Modified Pt/Al₂O₃.²⁹ It was reported that when trifluoroacetophenone is reduced, the chiral alcohol obtained forms a diastereomeric complex with the cinchonidine at the surface *via* N-H-O type H bonding, which can induce enantioselectivity. However, this alcohol could also interact in a competitive manner at the surface slowing the reaction.

Initially the reaction was performed under 3 bar of hydrogen pressure, 30°C for 24 h using **Ru6** NPs. Under these conditions, 26% conversion and 100% selectivity towards product **5.20b** was obtained (Table 5.9, Entry 1). When the pressure was increased to 10 bar, product **5.20b** was obtained with 85% of selectivity at *ca.* 65% conversion (Table 5.9, Entry 2). Finally, under 20 bar of H₂ pressure total conversion and 63% of selectivity towards product **5.20b** was obtained (Table 5.9, Entry 3). It was therefore concluded that using **Ru6** NPs, the ketone is preferably hydrogenated rather than the arene under the conditions used in this study.

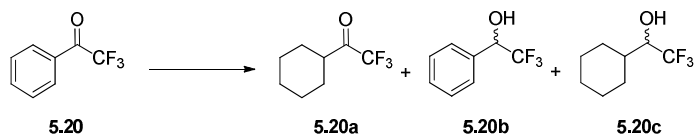
Ru5 NPs were more active catalysts since total conversion and approximately 60% of selectivity towards product **5.20c** was obtained when the reaction was performed under 3 bar of hydrogen pressure and similar reaction time (Table 5.9, Entry 4). The pressure was then increased to 10 bar,

however, comparable results in terms of conversion and selectivity were achieved (Table 5.9, Entry 5).

Comparing both nanoparticles, more activity is obtained with the nanoparticles synthesized with less proportion of ligand probably due to the easier accessibility of the substrate to the nanoparticle surface. Furthermore, it is important to highlight that distinct selectivities were obtained for both types of nanoparticles when the reaction was performed at 10 bar (Table 5.9, Entry 2 and 5). In the case of **Ru6**, high selectivity (85%) towards the hydrogenation of the ketone (**5.20b**) was observed whereas using **Ru5**, the major product was **5.20c** indicating that the arene is easily reduced.

Once more, no enantioselectivity was obtained using nanoparticles stabilized by cinchonidine.

Table 5.9. Trifluoroacetophenone hydrogenation with **Ru5** and **Ru6** nanoparticles.^a



E.	NPs	P (atm)	Time (h)	Conv. (%) ^b	%a ^b	%b ^b	%c	%ee ^c
1	Ru6	3	24	26	0	100	0	0
2	Ru6	10	24	64	4	85	11	0
3	Ru6	20	24	100	6	63	31	0
4	Ru5	3	24	100	15	22	63	0
5	Ru5	10	24	100	12	27	61	0

^aGeneral conditions: Ru NPs (2 mol%), substrate (0.62 mmol), THF (10 ml), T= 30°C.

^bDetermined by GC. ^cEnantiomeric excess was calculated by chiral GC.

At this point, after the negative results of enantioselectivity obtained in the hydrogenation of different arenes, it was decided to study the interaction of the ligands with the nanoparticle surface *via* deuteration.

5.3.5. DEUTERATION STUDIES

Recently, Chaudret *et al.* have reported an H/D exchange which allows the deuteration of pyridines, quinolines, indoles, alkyl amines and biologically active compounds with D₂ in the presence of Ru@PVP nanoparticles.²⁰ This technique permits the exclusive deuteration of the positions neighbouring to the nitrogen atoms in different substrates, even in the presence of other electronegative elements such as oxygen atoms. These results gave information about the direct coordination of the substrate to the nanoparticle surface by the nitrogen atom and that the affinity of other functional groups like ethers is much lower.

We thought that this method could also be used to understand how the different ligands interact with the surface and to know which atoms are coordinated or which positions could be close to the metal surface. Moreover, this technique could be useful to deuterate not only neighbouring positions to nitrogen atoms but also other atoms, for instance, phosphorus atoms.

Cinchonidine and ligand **5.13** are really complex stabilizing agents which could interact with the nanoparticles surface by different positions. On the one hand, cinchonidine has two different nitrogen atoms which could interact with the nanoparticle, an easy-reducible alkene and a quinoline moiety which can generate a η^6 -interaction with the metal surface. Therefore, many different positions can be mono- or polideuterated and really complex mixtures products would be expected.

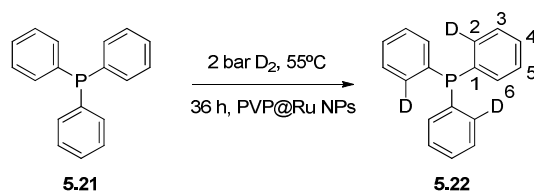
On the other hand, ligand **5.13** has, besides the phosphorus atom, a pyrrolidine moiety and three different aromatic systems that could also be deuterated. For this reason, it was thought that, initially, it would be easier to start the deuteration study with more simple ligands in order to understand

better the basis of the technique and the interpretation of the results before analysing more complicated compounds. Here we present the preliminary results of this study.

5.3.5.1 DEUTERATION OF TRIPHENYLPHOSPHINE

Triphenylphosphine ligand was chosen to perform the deuteration study because it was widely used as stabilizing agent in our work (see Chapters 3 and 4) and because phosphorus atoms are really prone to coordinate to the metal surface and it is supposed that its adjacent positions could be easily deuterated.

For that reason, PVP nanoparticles were synthesized^{22b} and triphenylphosphine was firstly used as model substrate. The reaction was initially carried out following the reported conditions in the presence of 2 bar of D₂ and 55°C for 36 hours.²⁰ An analysis of the NMR spectra indicated that the monodeuteration of each phenyl ring of triphenylphosphine was produced (Scheme 5.13).



Scheme 5.13. Deuteration of PPh₃ at 2 bar of D₂ and 55°C for 36 hours.

The monodeuteration of each phenyl ring was confirmed by ¹³C- and ³¹P-NMR. In the ¹³C-NMR spectrum, the signals of carbons that appeared as doublets in the starting material, now appeared unfolded. Particularly, the carbon containing the deuterium (C2) becomes a complex signal at 134.4 ppm while C6, which is not deuterated, is still observed as a doublet at 134.8 ppm

(Figure 5.5). Carbon C1 (137.3 ppm) becomes a pseudo-quadruplet, and carbons C3 and C5 appear as two doublets and are not coupled with the deuterium but they are coupled with the phosphorus atom. C4 remains as a singlet and, therefore, it is not coupled neither with phosphorus nor deuterium. The pseudo-quadruplet at 137.1 (C1), with relative intensities 1:2:2:1, can be justified by the coupling of C1 with P and D with similar coupling constant values of *ca.* 11 Hz ($^1J_{C,P} \approx ^2J_{C,D}$). The C2 signal is quite complex but it can be explained by the coupling with P and D with coupling constants of 18 Hz ($^2J_{C,P}$) and 26 Hz ($^1J_{C,D}$), respectively (Figure 5.6). No signals in the aliphatic region were observed.

By ^{31}P -NMR (Figure 5.7) a possible septuplet at -7.5 ppm was detected indicating the coupling with 3 atoms of deuterium. 10% of deuterated phosphine oxide is also observed at 29.1 ppm and, this fact is confirmed by the presence of a small peak corresponding to the oxide that is observed in ^2H -NMR (7.8 ppm) and it is also confirmed in the mass spectrum.

Mass spectrum showed a complex molecular ion with peaks between 262 and 270 (Figure 5.8). The molecular ion of PPh_3 is expected at 263 (262+1) and that of trideuterated phosphine should appear at 266 (265+1), while the most intense peak is at 267. All this indicates that the situation is more complex than that reflected by the NMR spectra and probably a mixture of different deuterated compounds could be present, where compound **5.22** is the major one. In fact the multiplet assigned to C1, in ^{13}C -NMR, consisting of 4 signals of relative intensities 1:2:2:1 match well with a monodeuteration at position C2 of each phenyl ring.

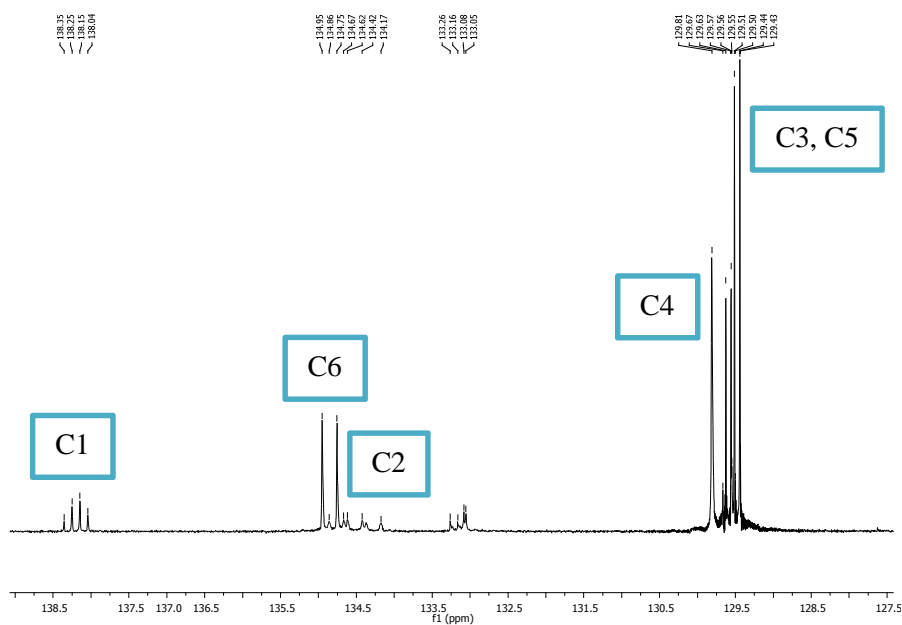


Figure 5.5. ^{13}C -NMR of monodeuterated PPh_3 5.22.

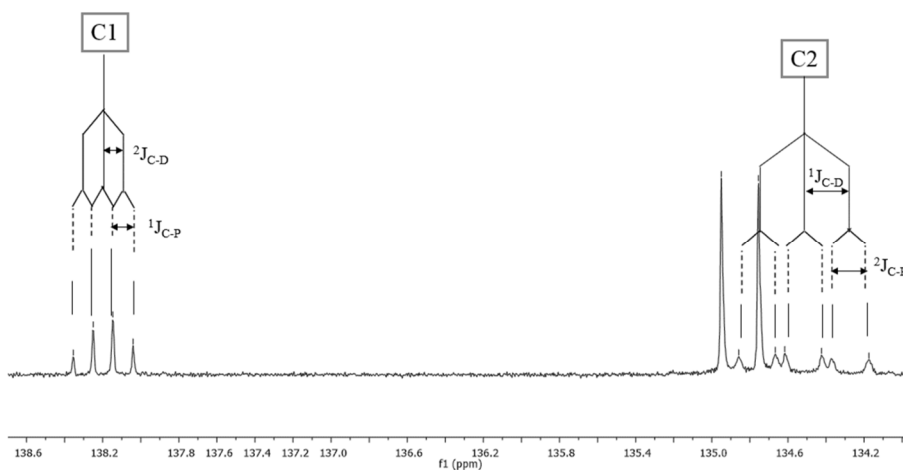


Figure 5.6. ^{13}C -NMR of monodeuterated PPh_3 5.22, signals C1, C2 and C6.

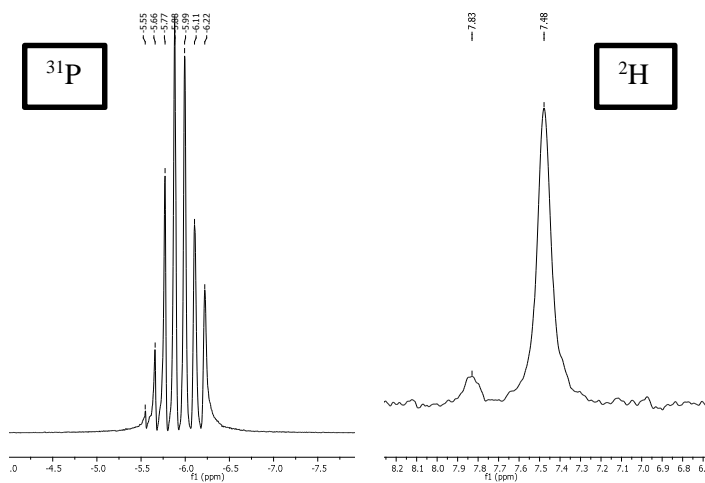


Figure 5.7. ^{31}P -NMR and ^2H -NMR of monodeuterated PPh_3 **5.22**.

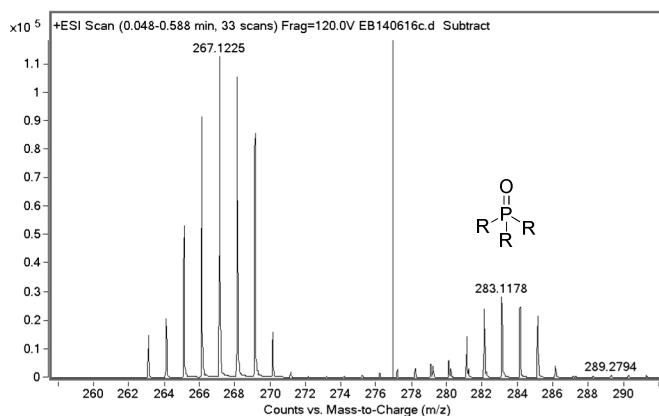
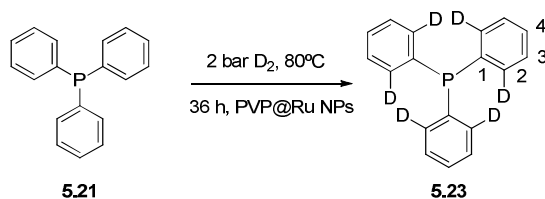


Figure 5.8. Detail of the mass spectrum **5.22**, molecular peak at 267 m/z.

Aiming to explore if a higher deuteration was possible, we performed the reaction at 2 bar of D_2 but at 80°C for 36 hours. In the ^{13}C -NMR spectrum of the obtained product, it was observed that the signal at 134.8 ppm corresponding to C6-H had completely disappeared, while it was still present the multiplet around 133 ppm, similar to that observed for C2-D in the

previous experiment (Figure 5.8). This fact suggests that dideuteration of positions *ortho* of all the phenyl rings has took place (Scheme 5.14).



Scheme 5.14. Deuteration of PPh₃ at 2 bar of D₂ and 80°C for 36 hours.

Surprisingly, the signal corresponding to C1 appeared as a doublet (maybe two singlets) although a sextuplet was expected. We have not for the moment a clear explanation for this fact, and further experiments will be necessary for elucidating the spectrum. The C3 and C4 signals remained quite simple and similar to the ones obtained for triphenylphosphine (doublet and singlet, respectively) indicating that no polydeuteration was produced (Figure 5.9).

By ³¹P-NMR two broad signals were observed one at 29.1 ppm (60% of oxide detected) and at -6.2 ppm. The presence of oxide was unexpected since all the manipulations were performed under inert conditions. The same information was obtained from the ²H-NMR spectrum (Figure 5.10).

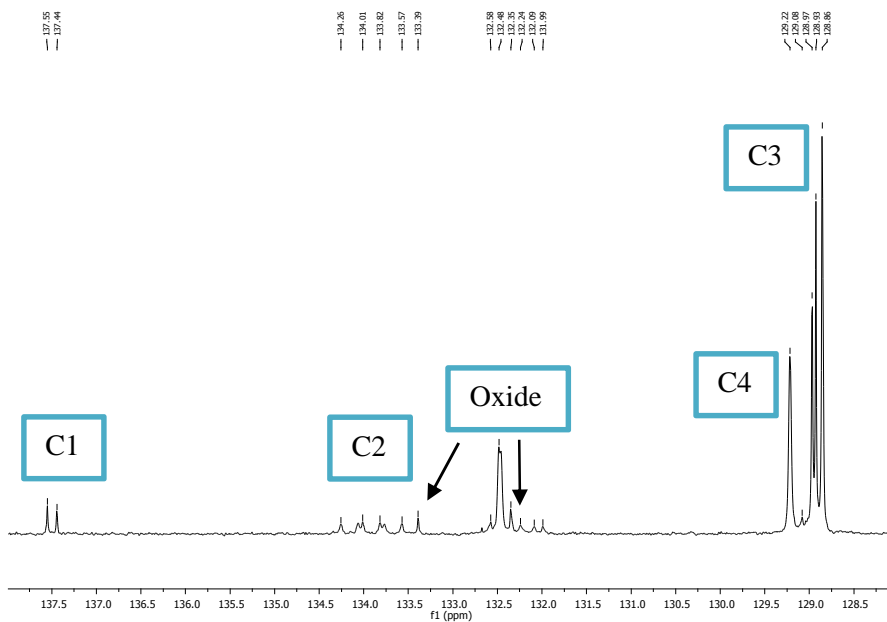


Figure 5.9. ^{13}C -NMR of dideuterated PPh_3 5.23.

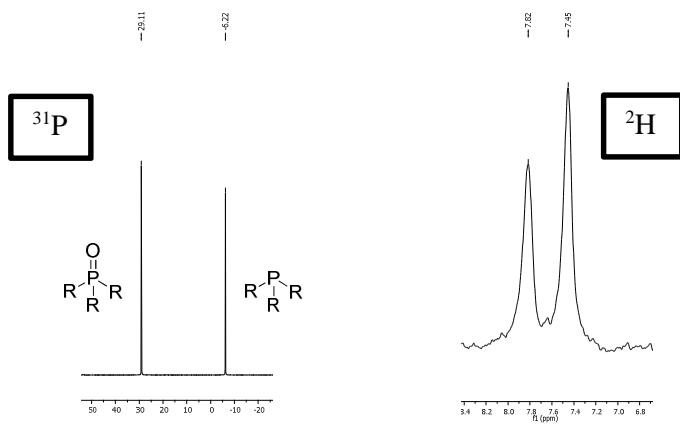


Figure 5.10. ^{31}P -NMR and ^2H -NMR of dideuterated PPh_3 , 5.23.

Mass spectrum showed a complex molecular ion with a main peak at 285 (Figure 5.11). The molecular ion of PPh₃ dideuterated (6D) is expected at 269 (268+1), but the peak at 285 (262+6+16+1) seems to indicate that the sample is oxidized, probably during the manipulations for performing the mass spectra. All these data are in agreement with a dideuteration at positions C2,6 of each phenyl ring.

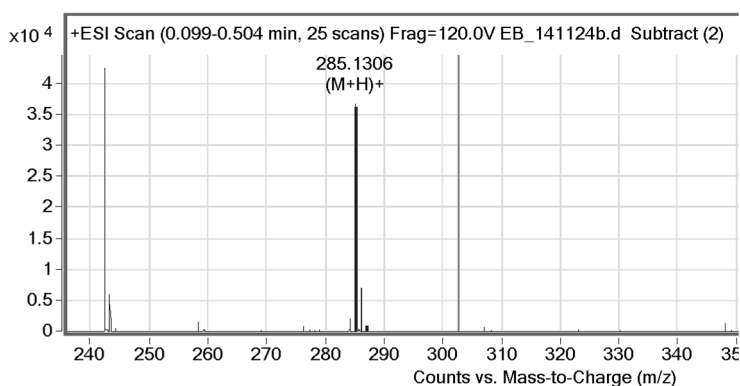
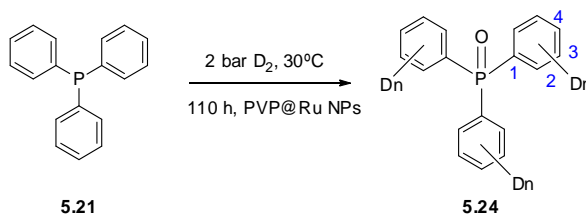


Figure 5.11. Detail of the mass spectrum **5.23**, molecular peak at 285 m/z.

Finally, the reaction was performed at 2 bar of D₂ and 30°C but during 110 hours in order to see if at lower temperature the oxidation could be avoided maintaining high deuteration. Nonetheless, the total oxidation of the phosphine was produced and, what is more, deuteration on different positions was detected (Scheme 5.16).



Scheme 5.15. Deuteration of PPh₃ at 2 bar of D₂ and 30°C for 110 hours.

It was thought that THF could be the responsible for the oxidation of the triphenylphosphine because the system is not in contact with the air atmosphere at any stage of the reaction. For that reason, different solvents which do not contain an oxygen atom were tested. Thus, the reaction was performed using heptane and pentane but in both cases no deuteration was observed and totally oxidation was produced indicating that THF is not the responsible of the phosphine oxide formation.

5.3.5.2 DEUTERATION OF TRIPHENYLPHOSPHINE OXIDE AND TRIPHENYLPHOSPHITE

At this point, we decided to explore the deuteration of triphenylphosphine oxide in order to see if the oxidation of triphenylphosphine hamper the reaction or if it could be deuterated in the same way. When triphenylphosphine oxide was deuterated under 2 bar of D_2 at $55^\circ C$ for 36 h, a really complex ^{13}C -NMR spectra was obtained and an important proportion of signals in the aliphatic zone were observed, which informs that the triphenylphosphine oxide had been reduced. This fact was confirmed by the presence of several broad signals in the aliphatic region of deuterium and proton spectra (Figure 5.12). The signal at 51.4 and 45.6 ppm in the ^{31}P -NMR spectrum corresponding to the fully reduced phosphine oxide and the dicyclohexylphenylphosphine oxide respectively, confirmed the previous observations.

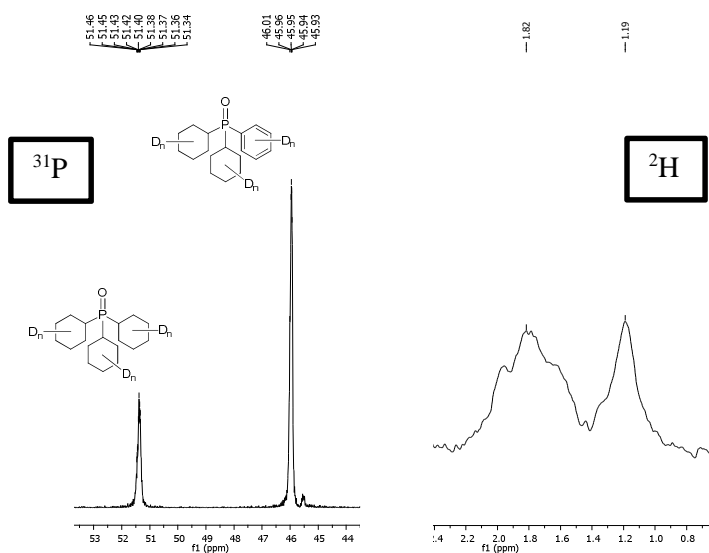
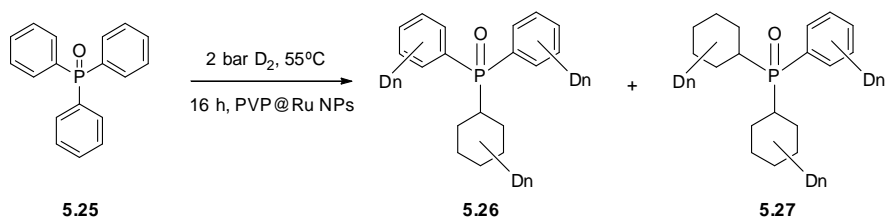


Figure 5.12. ^{31}P -NMR and ^2H -NMR of deuterated POPh_3 under 2 bar of D_2 and 55°C for 36 h.

Moreover, the complex molecular ion with peaks between 304 and 324 observed by mass spectrometry also support that reduction and polydeuteration took place.

In order to avoid the formation of reduced products we performed the reaction under the same reaction conditions but during 16 h (Scheme 5.16).



Scheme 5.16. Deuteration of POPh_3 at 2 bar of D_2 and 30°C for 16 hours.

However, the reaction was not completed and 3 different phosphorus signals were detected by ^{31}P -NMR (Figure 5.13). One corresponded to the unreacted substrate (peak at 29.2 ppm, 4%). The two other signals were assigned, the more intense to compound **5.26** (34.4 ppm), which has a ring reduced, and the third signal to compound **5.27** (45.2 ppm).

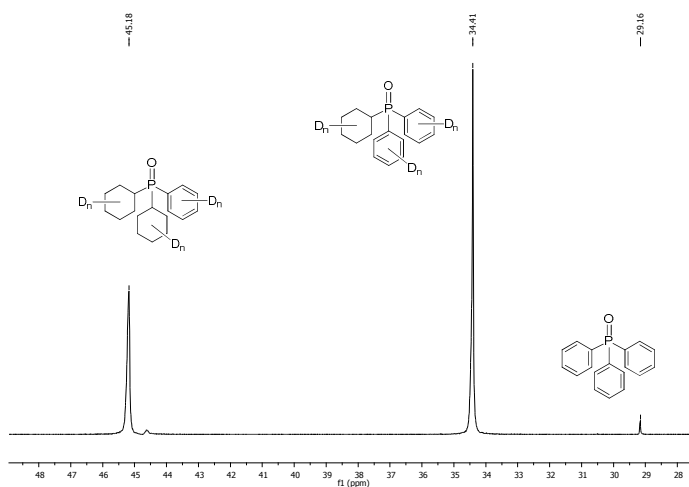


Figure 5.13. ^{31}P -NMR of deuterated POPh_3 under 2 bar of D_2 and 55°C for 16 h.

In the ^2H -NMR spectra (Figure 5.14), broad peaks are present in the aliphatic zone (1.0-2.3 ppm), in agreement with previous observation. In the aromatic region, 7.5 ppm, the signal was very weak indicating that the deuteration of aromatic rings took place, but that they were mostly reduced. This fact was also confirmed by the presence of signals in the aliphatic region of the ^1H NMR spectrum.

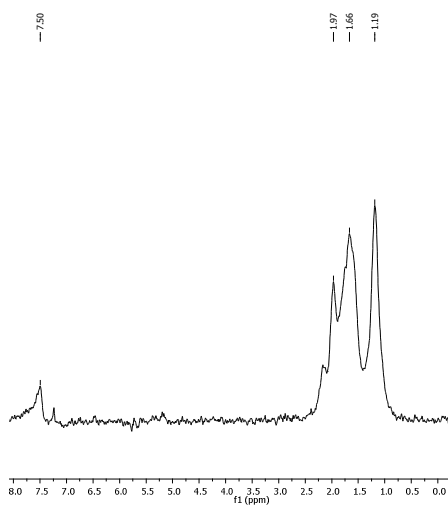


Figure 5.14. ^2H -NMR of deuterated POPh_3 under 2 bar of D_2 and 55°C for 16 h.

The reaction was then carried out at room temperature but no conversion was observed even after 36 hours of reaction. It is worthy to comment that we have observed that heating is necessary for a good dispersion of nanoparticles in the reaction medium.

Finally, we tried the deuteration of triphenylphosphite under the standard reaction conditions previously used and, surprisingly, no deuteration was observed.

The preliminary results obtained in the deuteration of phosphorus ligands allowed concluding that important differences are observed between phosphine, phosphine oxide or phosphite. In the case of phosphine, selective deuteration of carbons C2,6 indicates that the ligand is strongly coordinated through the phosphorus atom, which can make a pseudo-agostic interaction in a way similar to what is observed for H/D exchange on nitrogen donors.²⁰ The key intermediate must be a five membered ring Ru-P-C-C-Ru'.

The case of phosphine oxide is different and the arene is reduced under the same reaction conditions. In triphenylphosphine oxide the arenes are more activated for hydrogenation due to the electron withdrawing properties of the P=O group. Moreover, the coordination through the oxygen is unlikely, so the preferred coordination occurs through the arenes and leads to the reduction of the aromatic rings.

Finally, triphenylphosphite is not deuterated neither reduced. This fact can be explained considering that the five membered intermediate described for PPh₃ cannot be made because of the oxygen atom and the deuteration is disfavoured.

5.4. CONCLUSIONS

Ru nanoparticles stabilized by the chiral ligands cinchonidine and **5.13** were successfully synthesized and characterized. These nanoparticles have been applied in the hydrogenation of different substrates (arenes containing an acid and a basic group, aromatic amides and aromatic ketones) and the following conclusions can be extracted:

- i) In the reactions carried out with nanoparticles stabilized with chiral ligands no enantioselectivity was observed.
- ii) Reduction of compound **5.15** afforded only the *cis*-product, while in the reduction of **5.16** considerably proportions of *trans*-product were formed.
- iii) A preliminary study of deuteration of triphenylphosphine, triphenylphosphine oxide and triphenylphosphite has been developed using ruthenium nanoparticles stabilized by PVP, aiming to elucidate how the ligands are coordinated to the nanoparticles surface.

- iv) Mono-, di- and polideuteration of triphenylphosphine can be achieved by controlling the reaction conditions.
- v) In the case of triphenylphosphine oxide significant reduction of the aromatic ring was produced.
- vi) Triphenylphosphite was not deuterated.
- vii) These results inform about the coordination of the ligands on the nanoparticle surface. Thus, the triphenylphosphine must interact with the nanoparticle through the phosphorus atom, which would facilitate the deuteration at positions 2. That would be also the case of the triphenylphosphite, but the presence of the oxygen will prevent the deuteration. Concerning the triphenylphosphine oxide, the coordination with the nanoparticle surface takes probably place through the aromatic rings which favours the reduction of them.

5.5. EXPERIMENTAL PART

General Methods

All preparations and manipulations were carried out under an oxygen-free nitrogen atmosphere using conventional Schlenk techniques or inside a glovebox. The solvents were dried, distilled and degassed using standard procedure.³⁰ Reagents were purchased from Aldrich and Alfa-Aesar and were used as received.

The precursor [Ru(COD)(COT)] was purchased from Nanomeps. The synthesis of the nanoparticles was performed using 1L Fisher Porter and pressurized on a high pressure line.

All reactions temperatures were kept electronically controlled by heating baths.

Characterization Techniques

Transmission Electron Microscopy (TEM)

TEM experiments were performed at the “Unitat de Microscopia dels Serveis Científicotècnics de la Universitat Rovira I Virgili” (TEM-SCAN) in Tarragona with a Zeiss 10 CA electron microscope operating at 100 kV with resolution of 3 Å. The particles size distributions were determined by a manual analysis of enlarged images. At least 300 particles on a given grid were measured in order to obtain a statistical size distribution and a mean diameter.

Thermo Gravimetric Analysis (TGA)

TGA experiments were carried out in the furnace of a Mettler Toledo TGA/SDTA851 instrument.

1-2 mg of the nanoparticles were placed in the sample holder in the furnace and it was heated up at a rate of $10^{\circ}\text{Cmin}^{-1}$ in N_2 , while the weight was recorded continuously from 30°C to 900°C . The weight loss of the organic part and metal were used to calculate the approximate number of ligands coordinated on the metal surface.

X-Ray Diffraction (XRD)

XRD measurements were performed using a Siemens D5000 diffractometer (Bragg- Brentano parafocusing geometry and vertical θ - θ goniometer) fitted with a curved graphite diffracted- beam monochromator, incident and diffracted- beam Soller slits, a 0.06° receiving slit and scintillation counter as a detector. The angular 2θ diffraction range was between 26 and 95° . The data were collected with an angular step of 0.05° at

16s per step and sample rotation. A low background Si(510) wafer was used as sample holder. $\text{CuK}\alpha$ radiation was obtained from a copper X-ray tube operated at 40kV and 30mA.

Wide Angle X-ray Scattering (WAXS)

WAXS analyses were performed at CEMES-CNRS. Samples were sealed in 1 mm diameter Lindemann glass capillaries. The samples were irradiated with graphite-monochromatized $\text{MoK}\alpha$ (0.071069 nm) radiation and the X-ray intensity scattered measurements were performed using a dedicated two-axis diffractometer. Radial distribution functions (RDF) were obtained after Fourier transform of the reduced intensity functions.

X-Ray Photoelectron Spectroscopy (XPS)

XPS measurement were performed using a PHI 5500 Multitechnique System (from Physical Electronics) with a monochromatic X-ray source (Aluminium Kalfa line of 1486.6 eV energy and 350 W), placed perpendicular to the analyser axis and calibrated using the 3d5/2 line of Ag with a full width at half maximum (FWHM) of 0.8 eV. The analysed area was a circle of 0.8 mm diameter, and the selected resolution for the spectra was 187.5eV of Pass Energy and 0.8 eV/ step for the general spectra and 23.5 eV of Pass Energy and 0.1 eV/step for the spectra of the different elements in the depth profile spectra. A low energy electron gun (<10 eV) was used in order to discharge the surface when necessary. All measurements were performed in an ultra-high vacuum (UHV) chamber pressure between 5×10^{-9} and 2×10^{-8} torr. The data processing was carried out using the CasaXPS program.

Nuclear Magnetic Resonance (NMR)

^1H , ^{13}C and ^{31}P spectra were recorded on a Varian® Mercury VX 400 (400 MHz, 100.6 MHz, 162 MHz respectively). Chemical shift values for ^1H

and ^{13}C were referred to internal SiMe_4 (0.0 ppm) and for ^{31}P was referred to H_3PO_4 (85% solution in D_2O , 0 ppm). 2D correlation spectra (gCOSY, gHSQC and gHMBC) were visualized using VNMR program (Varian®).

Mass spectrometry (MS)

Apparatus: Finnigan MAT 900S (EB-Trap-Geometry) Syringes pump Model 22.

Specific rotation ($[\alpha]$)

Apparatus: Perkin Elmer 343plus Optical rotations were measured using a 1 mL cell with a 1 dm path length. Measurements were carried out in different wavelengths using sample solution in chloroform at 20 °C. The sample concentrations are given in g/100 mL unit.

General procedure for the synthesis of ruthenium nanoparticles stabilized by the chiral ligands

In a typical procedure, the $[\text{Ru}(\text{COD})(\text{COT})]$ (200 mg, 0.634 mmol) was placed into a Fischer-Porter reactor in 200 mL of dry and deoxygenated THF by freeze-pump-thaw cycles in the presence of the ligand (0.1 or 0.2 eq.). The Fischer-Porter reactor was pressurised under 3 bar of H_2 and stirred for 24 h at room temperature. Then the solution was concentrated under reduced pressure to 40 mL. Precipitation and washing with pentane (3x15 mL) was then carried out, obtaining a black precipitate.

General procedure for the synthesis of ruthenium nanoparticles stabilized by polyvinylpyrrolidone^{22b}

$[\text{Ru}(\text{COD})(\text{COT})]$ (158 mg, 0.50 mmol) was introduced in a Fischer-Porter bottle and left in vacuum for 30 min. Then, a solution of 1 g of PVP in

60 mL of THF (degassed by freeze-pump cycles) was added using a transfer tubing. The resulting yellow solution was stirred for 30 min at room temperature, after which the Fischer-Porter was pressurized under 3 bar of H₂ and the solution was stirred for 68 h, during which time a black precipitate formed. After elimination of excess dihydrogen, the solution was concentrated to 20 mL and filtrated by cannula. The black precipitate was washed three times with 20 mL of THF and dried in vacuo. The precipitate was then washed with pentane (30 mL) and dried in vacuum overnight leading to dark grey nanoparticles.

Ru5 nanoparticles stabilized by 0.2 eq of 5.13:

- TEM: mean size 1.61 ± 0.35 nm.
- XRD: hcp crystalline Ru nanoparticles, coherence length 1.47 ± 0.12 nm.
- XPS: 3d5/2 (279.50 eV) and 3d3/2 (284.20 eV), 100% Ru (0) at the nanoparticles surface.
- TGA: 79% Ru, 21% P.
- Approximate formula: [Ru₁₆₁L₁₁].

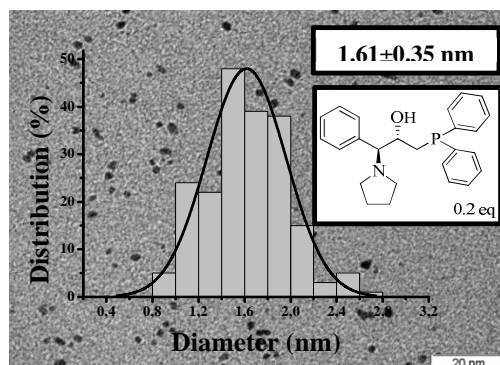


Figure 5.15. TEM micrographs and size distribution of **Ru5** NPs.

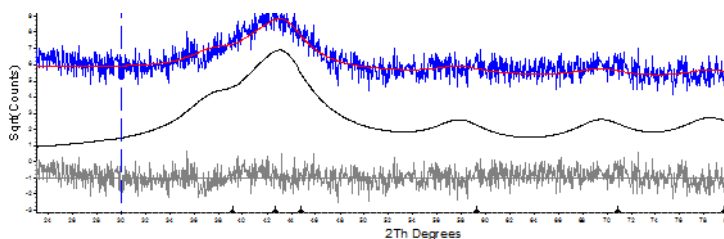


Figure 5.16. XRD of hcp crystalline **Ru5** nanoparticles.

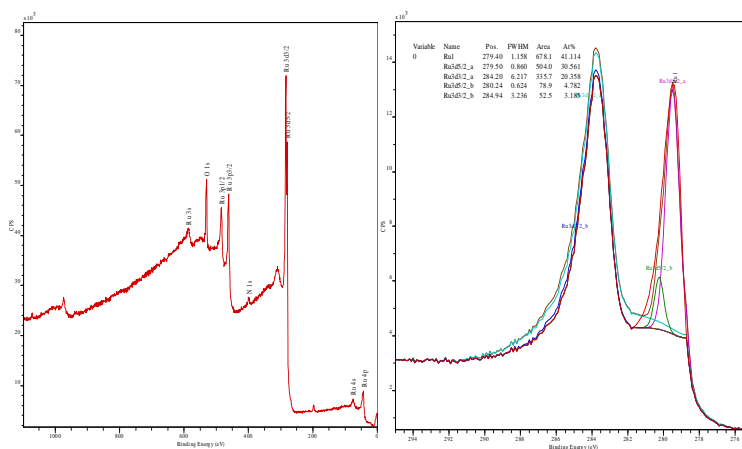


Figure 5.17. XPS spectra of **Ru5** NPs.

Ru4 nanoparticles stabilized by 0.1 eq of 5.14:

- *TEM*: mean size 1.85 ± 0.54 nm.
- *XRD*: hcp crystalline Ru nanoparticles, coherence length 1.35 ± 0.06 nm.
- *XPS*: 3d_{5/2} (278.84 eV) and 3d_{3/2} (283.54 eV), 100% Ru (0) at the nanoparticles surface.
- *TGA*: 72% Ru, 28% Cinchonidine.
Approximate formula: [Ru₂₃₄L₃₂].

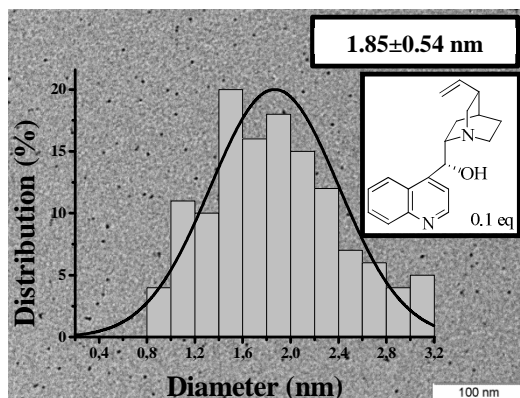


Figure 5.18. TEM micrographs and size distribution of **Ru4** NPs.

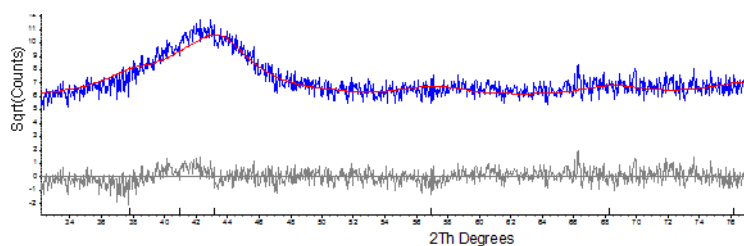


Figure 5.19. XRD of hcp crystalline **Ru4** nanoparticles.

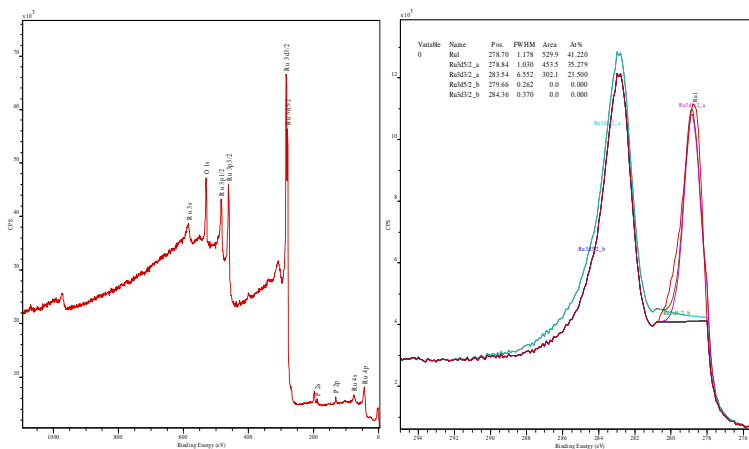


Figure 5.20. XPS spectra of **Ru4** NPs.

Ru6 nanoparticles stabilized by 0.2 eq of 5.14:

- *TEM*: mean size 1.27 ± 0.34 nm.
- *XRD*: hcp crystalline Ru nanoparticles, coherence length 0.81 ± 0.04 nm.
- *XPS*: 3d5/2 (279.97 eV) and 3d3/2 (284.45 eV), 100% Ru (0) at the nanoparticles surface.
- *TGA*: 67% Ru, 33% Cinchonidine.

Approximate formula: $[\text{Ru}_{79}\text{L}_{13}]$.

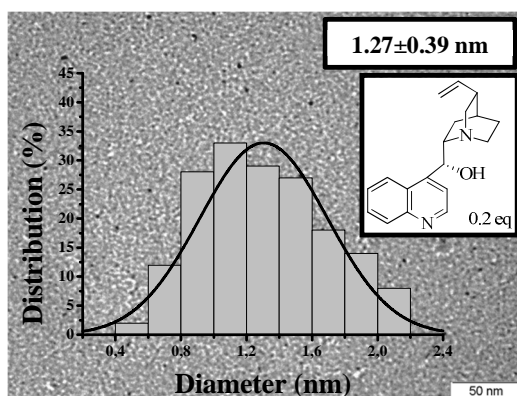


Figure 5.21. TEM micrographs and size distribution of **Ru6** NPs.

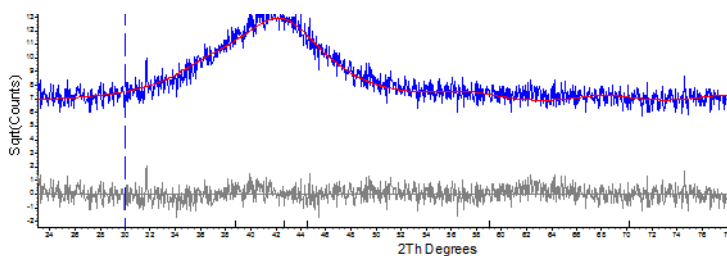


Figure 5.22. XRD of hcp crystalline **Ru6** nanoparticles.

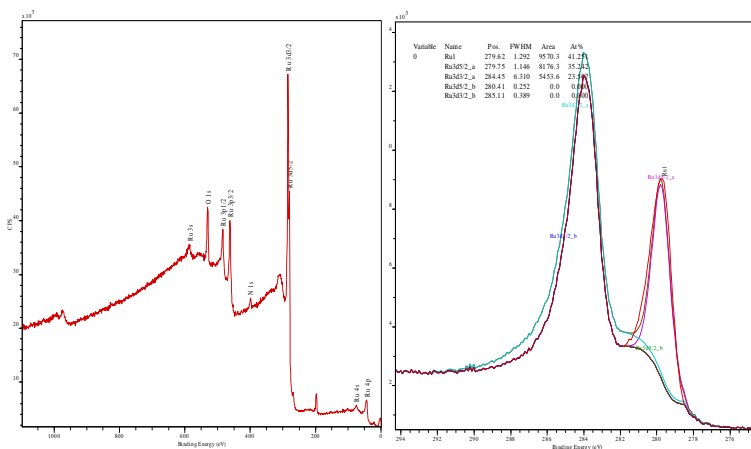


Figure 5.23. XPS spectra of Ru6 NPs.

General procedure for the hydrogenation reactions

Hydrogenation reactions were carried out in a Berghof 5 x 25mL stainless steel autoclave. In a typical experiment, the autoclave was charged inside the glove-box with the nanoparticles, the substrate and the corresponding solvent. The autoclave was then removed from the glove-box and immediately pressurized to the appropriate H₂ pressure and temperature. After the desired reaction time, the autoclave was depressurized. Conversion was calculated by GC-MS and confirmed by ¹H-NMR and the enantiomeric ratios were determined by GC or HPLC analysis.

Gas chromatography analyses were carried out in a Hewlett-Packard HP 6890 gas chromatograph, using the chiral column CP Chirasil-Dex CB. HPLC analyses were carried out in a Merck-Hitachi L-6200A liquid chromatograph, using the appropriate chiral column (Chiralpack AD-H, Chiralpack IA).

Method 1: Gas chromatography. CP Chirasil-Dex CB, 25 m column, internal diameter: 0.25 mm, film thickness: 0.25 μm , carrier gas: 120 kPa He, temperature: 80 $^{\circ}\text{C}$ for 15 min, rate 5 $^{\circ}\text{C}/\text{min}$ to 180 $^{\circ}\text{C}$ and hold for 3min.

Method 2: HPLC. Chiralpack AD-H column, hexanes:iPrOH = 95:5, flow: 1 mL/min, λ : 205 nm.

Method 3: HPLC. Chiralpack ID column, hexanes:iPrOH = 50:50, flow: 0.8 mL/min, λ : 240 nm.

Method 4: Gas chromatography. CP Chirasil-Dex CB, 25 m column, internal diameter: 0.25 mm, film thickness: 0.25 μm , carrier gas: 120 kPa He, temperature: 90 $^{\circ}\text{C}$, rate 0.5 $^{\circ}\text{C}/\text{min}$ to 120 $^{\circ}\text{C}$ and hold for 3min.

Method 5: Gas chromatography. CP Chirasil-Dex CB, 25 m column, internal diameter: 0.25 mm, film thickness: 0.25 μm , carrier gas: 120 kPa He, temperature: 130 $^{\circ}\text{C}$ for 10 min, rate 10 $^{\circ}\text{C}/\text{min}$ to 180 $^{\circ}\text{C}$ and hold for 3min.

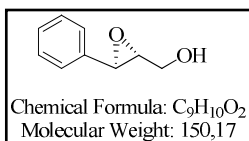
Product	Method	Ret. Time (min)	Product	Method	Ret. Time (min)
5.15a	1	30.32, 30.53	5.18a	3	4.70, 5.03
5.16a	2	8.59, 9.30	5.19b	4	14.59, 16.14
5.17a	3	5.61, 6.40	5.20b	5	4.70, 5.03

General procedure for H/D exchanges

A Fischer–Porter glassware was charged with Ru@PVP NPs (8 mg, 3.3%) and a magnetic stirrer in a glove box under argon. The Fischer–Porter glassware was then left under vacuum for 5 min and pressurized with 3 bars of D_2 gas during 2 hours. A solution of the substrate (0.15 mmol) in distilled and degassed solvent (1 mL) was added under argon. The reaction mixture was magnetically stirred at the desired temperature and pressure of D_2 during

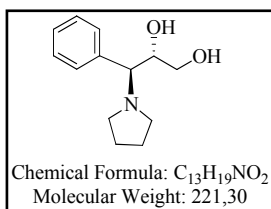
the corresponding hours. Finally, the solution was cooled down to room temperature and filtrated on a small neutral alumina pad (Pasteur pipette) using 10 mL of THF as elution solvent.

Synthesis of ((2R,3R)-2,3-Epoxy-3-phenylpropanol (5.2):



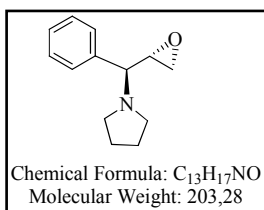
To a solution of diisopropyl D-tartrate (3 mL, 2.8 mmol) in methylene chloride (80 mL) at -10°C under argon was added 4 Å molecule sieve (1.5 g), titanium isopropoxide (0.6 mL, 20 mmol), and cinnamyl alcohol (2.7g, 200 mmol). The mixture was allowed to age for 40 minutes at -10°C, cooled to -20°C, and treated in a dropwise fashion with a solution of t-butyl hydroperoxide (TBHP, ~45 mmol) in decane. After 18 hours at -15°C, the reaction mixture was treated with 30% aqueous sodium hydroxide solution (0.5 mL) and diethyl ether (10 mL). The cold bath was removed and the mixture was allowed to warm to ~10°C. Magnesium Sulfate (anhydrous, 1.5 g) was added and the mixture was stirred for 20 minutes. After solid settled, the solution was filtered through a pad of Celite®, washing with ether (5 mL). The resulting mixture was concentrated and purified by flash chromatography (hexane:ethyl acetat 3:1), to afford 1.56 g of compound **5.2** (93 %) as a pale yellow solid. An enantiomeric excess of 97% ee was determined by chiral HPLC (chiralpack OD, heptane:*i*PrOH 96:4, 1 mlmin⁻¹, t_R(R) = 33.8 min and t_R(S) = 37.6 min).

¹H NMR (CDCl₃, 400 MHz, δ in ppm): 7.29 (m, 5H), 4.01 (m, 1H), 3.91 (d, 1H, *J* = 3.5 Hz), 3.76 (m, 1H), 3.60 (bs, 1H, OH), 3.23 (m, 1H). ¹³C NMR (CDCl₃, 100.6 MHz, δ in ppm): 136.8, 128.5, 128.3, 125.8, 62.8, 61.5, 55.8. All spectroscopy data matched with those described in the literature.³¹

Synthesis of (2S,3S)-3-Phenyl-3-(pyrrolidin-1-yl)propane-1,2-diol (5.10)

To a solution of **5.2** (0.38 g, 2.53 mmol) in CH₂Cl₂ (18 mL) were added pyrrolidine (0.32 mL, 3.84 mmol) and Ti(OⁱPr)₄ (1.14 mL, 3.83 mmol) under argon at room temperature. After 5 h of stirring at room temperature, a 10% solution of NaOH in brine (10 mL) was added, and vigorous stirring continued for another 24 h. The mixture was filtered through Celite[®] and the residue washed with CH₂Cl₂ (2 x 25 mL). The combined organic extracts were dried and concentrated in vacuum. 0.52 g of product **5.10** (92%) was afforded as a yellow oil.

¹H NMR (CDCl₃, 400 MHz, δ in ppm): 7.22-7.32 (m, 5H), 4.16 (ddd, 1H, *J* = 7.0, 5.0, 5.0 Hz), 3.63 (bs, 2H, OH), 3.42 (dd, 1H, *J* = 11.4, 5.0 Hz), 3.24 (d, 1H, *J* = 5.0 Hz), 3.28 (dd, 1H, *J* = 11.4, 7.0 Hz), 2.53 (m, 2H), 2.43 (m, 2H), 1.66-1.72 (m, 4H). ¹³C NMR (CDCl₃, 100.6 MHz, δ in ppm): 137.0, 129.6, 128.5, 128.1, 72.3, 71.2, 66.3, 51.8, 23.3. All spectroscopy data matched with those described in the literature.²⁵

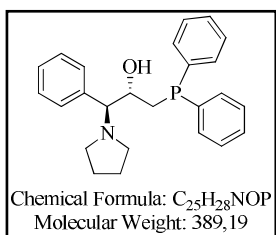
Synthesis of 1-((S)-((S)-Oxiran-2-yl)(phenyl)methyl)pyrrolidine (5.12)

To a stirred solution of **5.12** (7.00 mmol) in dry dichloromethane (50 ml) under argon atmosphere at -10°C was added triethylamine (2.05 ml, 14.7 mmol) in one portion followed by propanesulfonyl chloride (0.79 ml, 7.00 mmol) in dry dichloromethane (10 ml) dropwise. The mixture was stirred for 20 and treated dropwise with a solution of sodium (0.42 g, 18.3 mmol) in dry methanol (30 ml) and stirred below 0°C until TLC showed complete conversion to the epoxide. The reaction mixture was quenched with brine (200 ml) and extracted with

dichloromethane (3x 100ml). Concentration in vacuo of the combined, dried (MgSO₄) organic phases gave the crude product which was purified by column chromatography (3:7 ethyl acetate: hexane) and was **5.12** obtained in 58% yield.

¹H NMR (CDCl₃, 400 MHz, δ in ppm): 7.24-7.40 (m, 5H), 3.11-3.15 (m, 1H), 2.82 (dd, 1H, J = 5.3, 3.7 Hz), 2.56 (d, 1H, J = 7.6 Hz), 2.61 (dd, 1H, J = 5.3, 2.6 Hz), 2.55 (m, 2H), 2.40 (m, 2H), 1.71 (m, 4H). **¹³C NMR** (CDCl₃, 100.6 MHz, δ in ppm): 140.7, 128.3, 128.1, 127.5, 73.2, 55.1, 52.9, 48.5, 23.1. All spectroscopy data matched with those described in the literature.²⁶

Synthesis of (1*S*,2*S*)-3-(diphenylphosphino)-1-phenyl-1-(pyrrolidin-1-yl)propan-2-ol (**5.13**)



A solution of **5.12** (0.1 g, 0.7 mmol) in 2 ml of THF was added to another solution of potassium *tert*-butoxide in THF 0.5 M (1.4 ml, 0.7 mmol) and the mixture was stirred overnight. The solvent was evaporated in vacuum, then the mixture was redissolved in toluene, filtrate through Celite[®] and the solvent was evaporated in vacuum. The crude product was purified by column chromatography (1:1 ethyl acetate: hexane) and **5.13** was obtained in 60% yield.

¹H NMR (CDCl₃, 400 MHz, δ in ppm): 7.35-7.42 (m, 5H), 7.25-7.30 (m, 10H), 4.10 (m, 1H), 3.35 (d, 1H, J = 3.4 Hz), 2.56 (m, 2H), 2.34 (m, 2H), 2.03 (m, 1H), 1.78 (ddd, 1H, J = 13.6, 6.8, 1.1 Hz), 1.71 (m, 4H). **¹³C NMR** (CDCl₃, 100.6 MHz, δ in ppm): 133.3, 133.1, 133.0, 132.8, 130.0, 129.0, 128.7, 128.3, 74.6 (d, J = 7.7 Hz), 69.4 (d, J = 16.6 Hz), 53.0, 33.3 (d, J = 13.2 Hz), 23.6. **³¹P-NMR** (CDCl₃, 162 MHz, δ in ppm): δ = -22.9 (s). **ESI-TOF MS** for [M+H]⁺ C₂₅H₂₉NOP (m/z): calc. 390.1987; found: 390.2025. **[α]_D²⁵**: -11.25° (c 0.007, CHCl₃).

5.6. REFERENCES

1. Mallat, T.; Orglmeister, E.; Baiker, A. *Chem. Rev.* **2007**, *107*, 4863–4890.
2. Nasar, K.; Fache, F.; Lemaire, M.; Béziat, J.; Besson, M.; Gallezot, P. *J. Mol. Catal.* **1994**, *87*, 107–115.
3. (a) LeBlond, C.; Wang, J.; Liu, Andrews, A. T.; Sun, Y. K. *J. Am. Chem. Soc.* **1999**, *121*, 4920–4921. (b) Balázsik, K.; Bartók, M. *J. Mol. Catal. A: Chem.* **2004**, *219*, 383–389.
4. (a) Bönnemann, H.; Braun, G. A. *Angew. Chem. Int. Ed.* **1996**, *35*, 1992–1995. (b) Bönnemann, H.; Braun, G. A. *Chem. Eur. J.* **1997**, *3*, 1200–1202. (c) Diezi, S.; Reimann, S.; Bonalumi, N.; Mallat, T.; Baiker, A. *J. Catal.* **2006**, *239*, 255–262. (d) Sutyinszki, M.; Szöri, K.; Felföldi, K.; Bartók, M. *Catal. Commun.* **2002**, *3*, 125–127. (e) Zuo, X.; Liu, H. *Tetrahedron* **1999**, *55*, 7787–7804. (f) Bilé, E. G.; Cortelazzo-Polisini, E.; Denicourt-Nowicki, A.; Sassine, R.; Launay, F.; Roucoux, A. *ChemSusChem* **2012**, *5*, 91–101. (g) Beier, M. J.; Andanson, J.; Mallat, T.; Krumeich, F.; Baiker, A. *ACS Catal.* **2012**, *2*, 337–340. (h) Studer, M.; Blaser, H.; Exner, C. *Adv. Synth. Catal.* **2003**, *345*, 45–65. (i) Blaser, H.; Jalett, H.; Müller, M.; Studer, M. *Catal. Today*, **1997**, *37*, 441–467.
5. Yan, N.; Yuan, Y.; Dyson, P. J. *Dalton. Trans.* **2013**, *42*, 13294–13304.
6. Schmidt, E.; Vargas, A.; Mallat, T.; Baiker, A. *J. Am. Chem. Soc.* **2009**, *131*, 12358–12367
7. Mori, K.; Kondo, Y.; Yamashita, H. *Phys. Chem. Chem. Phys* **2009**, *11*, 8949–8954
8. (a) Sawai, K.; Tatum, R.; Nakahodo, T.; Fujihara, H. *Angew. Chem. Int. Ed.* **2008**, *47*, 6917–6919. (b) Tamura, M.; Fujihara, H. *J. Am. Chem. Soc.* **2003**, *125*, 15742–15743.
9. (a) Ranganath, K. V. S.; Kloesges, J.; Schäfer, A. H.; Glorius, F. *Angew. Chem., Int. Ed.* **2010**, *49*, 7786–7789. (b) Richter, C.; Ranganath, K. V. S.; Glorius, F. *Adv. Synth. Catal.* **2012**, *354*, 377–382. (c) Ranganath, K. V. S.; Schäfer, A. H.; Glorius, F. *ChemCatChem* **2011**, *3*, 1889–1891. (d) Ranganath, K. V. S.; Glorius, F. *Catal. Sci. Technol.* **2011**, *1*, 13–22.
10. (a) Jansat, S.; Gómez, M.; Philippot, K.; Muller, G.; Guiu, E.; Claver, C.; Castellón, S.; Chaudret, B. *J. Am. Chem. Soc.* **2004**, *126*, 1592–1593. (b) Favier, I.; Gómez, M.; Muller, G.; Axet, M. R.; Castellón, S.; Claver, C.; Jansat, S.; Chaudret, B.; Philippot, K. *Adv. Synth. Catal.* **2007**, *349*, 2459–2469. (c) Castellón, S.; Claver, C.; Díaz, Y. *Chem. Soc. Rev.* **2005**, *34*, 702–713.
11. Hu, A.; Gordon, T.; Lin, W. *J. Am. Chem. Soc.* **2005**, *127*, 12486–12487.
12. Hu, A.; Liu, S.; Lin, W. *RSC Adv.* **2012**, *2*, 2576–2580.
13. Sonnenberg, J. F.; Coombs, N.; Dube, P. A.; Morris, R. H. *J. Am. Chem. Soc.* **2012**, *134*, 5893–5899.

14. Jansat, S.; Picurelli, D.; Pelzer, K.; Philippot, K.; Gomez, M.; Muller, G.; Lecante, P.; Chaudret, B. *New J. Chem.* **2006**, *30*, 115–122.
15. Park, K. H.; Chung, Y. K. *Adv. Synth. Catal.* **2005**, *347*, 854–866.
16. Fache, F.; Lehuède, S.; Lemaire, M. *Tetrahedron Lett.* **1995**, *36*, 885–888.
17. Gual, A.; Godard, C.; Philippot, K.; Chaudret, B.; Denicourt-Nowicki, A.; Roucoux, A.; Claver, C. *ChemSusChem* **2009**, *2*, 769–779.
18. (a) Ranade, V. S.; Prins, R. *J. Catal.* **1999**, *185*, 479–486. (b) Ranade, V. S.; Consiglio, G.; R. Prins, R. *Catal. Lett.* **1999**, *58*, 71–74. (c) Barbosa, L. A. M. M.; Sautet, P. *J. Catal.* **2003**, *217*, 23–29. (d) Besson M.; Pinel, C. *Top. Catal.* **2003**, *25*, 43–61. (e) Ranade, V. S.; Consiglio, G.; Prins, R. *Catal. Lett.* **1999**, *58*, 71–74. (f) Besson, M.; Gallezot, P.; Neto, S.; Pinel, C. *Chem. Commun.* **1998**, 1431–1432. (g) Besson, M.; Blanc, B.; Champelet, M.; Gallezot, P.; K. Nasar, K.; Pinel, C. *J. Catal.* **1997**, *170*, 254–264.
19. Besson, M.; Delbecq, F.; Gallezot, P.; Neto, S.; Pinel, C. *Chem. Eur. J.* **2000**, *6*, 949–958.
20. Pieters, G.; Taglang, C.; Bonnefille, E.; Gutmann, T.; Puente, C.; Berthet, J.; Dugave, C.; Chaudret, B.; Rousseau, B. *Angew. Chem. Int. Ed.* **2014**, *53*, 230–234.
21. (a) Lara, P.; Philippot, K.; Chaudret, B. *ChemCatChem* **2013**, *5*, 28–45. (b) Scholten, J. D.; Leal, B. C.; Dupont, J. *ACS Catal.* **2012**, *2*, 184–200. (c) Ott, L. S.; G. Finke, R. G. *Coord. Chem. Rev.* **2007**, *251*, 1075–1100.
22. (a) Novio, F.; Monahan, D.; Coppel, Y.; Antorrena, G.; Lecante, P.; Philippot, K.; Chaudret, B. *Chem. Eur. J.* **2014**, *20*, 1287–1297. (b) Novio, F.; Philippot, K.; Chaudret, B. *Catal. Lett.* **2010**, *140*, 1–7.
23. Katsuki, T.; Sharpless, K. B. *J. Am. Chem. Soc.* **1980**, *102*, 5976–5978.
24. Kürti, L.; Czakó, B. *Strategic Applications of Named Reactions in Organic Synthesis*. San Diego: Elsevier, 2005. 408–409.
25. Vidal-Ferran, A.; Moyano, A.; Pericàs, M. A.; Riera, A. *J. Org. Chem.* **1997**, *62*, 4970–4982.
26. Harden, R. C.; Hodgkinson, T. J.; Mckillop, A.; Prowse, W. G.; Urquhart, M. W. *J. Tetrahedron*, **1997**, *53*, 21–36.
27. Meier, D. M.; Ferri, D.; Mallat, T.; Baiker, A. *J. Catal.* **2007**, *248*, 68–76.
28. Llop-Castelbou, J.; Bresó-Femenia, E.; Blondeau, P.; Chaudret, B.; Castellón, S.; Claver, C.; Godard, C. *ChemCatChem* **2014**, *6*, 3160–3168.
29. (a) Meemken, F.; Baiker, A.; Dupré, J.; Hungerbühler, K. *ACS Catal.* **2014**, *4*, 344–354. (b) Maeda, N.; Hungerbühler, K.; Baiker, A. *J. Am. Chem. Soc.* **2011**, *133*, 19567–19569. (c) Maeda, N.; Sano, S.; Mallat, T.; Hungerbühler, K.; Baiker, A. *J. Phys. Chem. C* **2012**, *116*, 4182–4188.
30. Perrin, D. D.; Armarego, W. L. F. *Purification of Laboratory Chemicals*, 3rd ed., Pergamon Press, Oxford, 1989.

31. Vidal, A. *Síntesi de Lligands per a Catàlisi Enantioselectiva a partir de 2-Amino-1,2-diols Homoquirals*. Doctoral Thesis, Universitat de Barcelona. Barcelona, 1996.

CHAPTER 6



GENERAL CONCLUSIONS

From the study on the selective hydrogenation of aromatic ketones carried out in Chapter 3, the following conclusions were extracted:

- Ruthenium and rhodium nanoparticles stabilized by P-donor ligands have been synthesized.
- These nanoparticles have been fully characterised and comparable results in terms of size and stabiliser content have been obtained.

This family of nanoparticles has been applied in the selective hydrogenation of aromatic ketones. From this study, the following conclusions can be extracted:

- Ruthenium nanoparticles are more selective than rhodium nanoparticles for the reduction of the aryl group in the case of arylketones.
- The selectivity towards the arene hydrogenation is negatively affected by the presence of substituents on the aromatic ring.
- Only **Rh1** nanoparticles provided hydrogenolysis products under the conditions used.
- In relation to non-conjugated aryl ketones (**2.4-2.5**), arene reduction was mainly observed for both metals although higher selectivities were observed when Rh catalysts were used.
- Selectivity to arene reduction increases when the distance between the arene and the ketone group increases.

From the study of the selective reduction of polycyclic aromatic hydrocarbons carried out in Chapter 4, the following conclusions can be drawn:

- Ruthenium nanoparticles stabilized by PPh_3 are good catalysts for the hydrogenation of PAHs with high activity and selectivity in mild reaction conditions.
- In the case of naphthalene, the obtaining of tetralin and/or decalin can be tuned by adjusting the hydrogen pressure.
- Anthracene can be selectively hydrogenated to **4.2a** or **4.3b**. The total hydrogenated product **4.2d** might be obtained under the reaction conditions used, but really long reaction times would be required.
- The hydrogenation of phenanthrene is more difficult and long reaction times are required to obtain low conversions. In all the cases, mixtures of products were obtained and the total hydrogenated product was not observed in any of the assays attempted.
- Triphenylene has 3 equivalent rings and it is difficult to achieve partial selectivity in hydrogenation. Thus, compound **4.4a** was obtained with a selectivity of 53% at 61% of conversion, which in spite of being quite low is one of the best reported in the bibliography. The selective reduction of 3 rings to give compound **4.4c** was achieved in 88% of selectivity and full conversion.
- Pyrene was difficult to hydrogenate and a 88% of selectivity in compound **4.5a** was obtained at 44% of conversion.

From the study of the chemoselective reduction of polyarenes vs. other functional groups, the following conclusions can be deduced:

- The reactions are slower than in the unsubstituted naphthalene, and hydrogenation takes place in the ring that does not contain substituents.
- Electron donating substituents deactivate the ring to which they are attached and, consequently, the neighbouring ring is preferably reduced. Electronwithdrawing substituents activate the ring. Then, although the effect of substitution predominates, reduction of the less substituted ring is mainly observed and appreciable amounts of reduction of the more substituted ring are achieved.
- The position of the substituent (position 1 or 2) influences the conversion more than the selectivity. When the substituent is at position 1, the conversion decreases probably due to the higher steric hindrance which hampers the approaching of the substrate to the surface.
- When a ketone is present in the substrate like in **4.13**, **4.14**, **4.15**, there is a competition between the reduction of the naphthalenic system vs. the ketone. If the ketone is placed in position 1 like in **4.15**, its reduction is favoured reduced probably because the ketone coordinates easily to the metal surface rather than the naphthalenic system.
- More proportion of stabilising ligand implies more activity and slightly less selectivity.

From the approach to the enantioselective hydrogenation of arenes carried out in Chapter 5, the following conclusions can be extracted:

- A novel enantiomerically enriched phosphine ligand has been synthesized and fully characterized.

- This phosphine ligand and the commercial cinchonidine have been used in different proportions as stabilising agents for ruthenium nanoparticles.
- These nanoparticles have been applied in the asymmetric hydrogenation of aromatic amides, arenes containing an acid and a basic group and aromatic ketones. However, no good results in terms of enantioselectivity have been obtained in any of the reactions.
- Attempts to elucidate how the ligands are coordinated to the nanoparticles surface have been performed by deuteration studies. Mono-, di- and polideuteration has been observed in the case of triphenylphosphine. Monodeuteration and mostly reduction of the arene has been achieved in the case of triphenylphosphine oxide and there has not been success in the attempt to deuterate triphenylphosphite.
- Triphenylphosphine must interact with the nanoparticle through the phosphorus atom, placing the rings orthogonal to the surface. The same trend is deduced for triphenylphosphite, but the presence of the oxygen push away the aromatic rings. In triphenylphosphine oxide, the coordination with the nanoparticle surface takes probably place through the aromatic ring.

